Università degli Studi di Palermo (UNIPA)
Dipartimento di Ingegneria (ID)
Université du Québec
Institut National de la Recherche Scientifique (INRS)

Characterizing and Protecting Quantum Resources in Composite Quantum Systems

Farzam Nosrati

Thesis submitted to obtain the double Degree of Philosophy Doctor (Ph.D.)
in Information and Communication Technologies (ICT)
and
in Energy and Material Sciences (EMT)

Directeur de recherche	Prof. Roberto Morandotti University of Palermo, Italy
Codirecteur de recherche	Prof. Roberto Morandotti INRS-EMT, Québec, Canada

To my father

Acknowledgements

First and foremost, I wish to express my deep gratitude to my supervisor, Rosario Lo Franco, at the University of Palermo. His invaluable guidance and unwavering support have been instrumental in shaping the direction and enhancing the quality of my research. His belief in my abilities has constantly inspired me to surpass my limits and strive for excellence. Beyond academia, Rosario has also been a mentor and a cherished friend, teaching me the joy of being.
I am indebted to my supervisor, Roberto Morandotti, at INRS-EMT. His expertise, insightful feedback, and continuous guidance have played a pivotal role in my academic journey. His mentorship has been truly transformative and has propelled me towards greater heights in my research endeavors.
I extend a heartfelt acknowledgment to Prof. Giuseppe Compagno, whose guidance has not only shaped my approach to physics but also instilled in me a deep joy for the subject. My sincere gratitude also goes to Dr. Alessia Castellini, who not only taught me many things about physics but also served as a constant source of inspiration in my life.
I want to express my gratitude to my colleagues and close friends, Kobra Mahdavipour and Mahshid Khazaei Shadfar. Your valuable input and feedback have taught me so much. I cannot measure the support, love, and companionship you have given me. Being part of the same group was an absolute pleasure. Also, I would like to thank my colleague Matteo Piccolini, whose interest regarding physics is inspirational. Also, I would like to thank Samira Ebrahimi for her kindness and support.
I would like to express my gratitude to Prof. Ilenia Tinnirello and her research group for providing me with a research home. Your support has been invaluable. I am also deeply grateful to Dr. Daniele Croce for his continued support, wisdom, and kindness, which have been incredibly helpful.
I would like to express my gratitude to my colleagues at INRS-EMT, particularly Dr. Stefania Sciara and Dr. Mario Chemnitz, for their unwavering support and kindness. Their invaluable guidance, productive discussions, and collaborative endeavors have greatly enhanced my research. It has been an honor to work with such accomplished experts, and I have gained a wealth of knowledge from our partnership.
I would like to express my gratitude to Prof. Ali Mortezapour, my esteemed colleague, who taught me about the importance of novelty and creativity in physics. Your kindness and trust in sharing your beautiful and unique ideas with me are greatly appreciated.
I would like to express my gratitude to Prof. Bruno Bellomo and Prof. Gabriele De Chiara for their valuable discussions throughout our recent project. Not only have I gained a great deal from their expertise in the field, but their passion for physics is truly inspiring.
To my dear friends from outside of academia, there are so many that I cannot name all. Thank you for standing by my side throughout this journey. Your unwavering support has kept me motivated and focused.
I want to dedicate this thesis to my beloved family: my mother, Roya; my father, Fares; and my brother, Perdram. Your love, support, and understanding have been my pillars of strength, especially during challenging times. Although my heart aches not to have my father, Fares, physically present to witness this achievement, I know he is with me in spirit, guiding me every step of the way. His unwavering belief in my abilities and his profound impact on my life inspire me to strive for greatness. I am grateful to have such a wonderful extended family with a fantastic uncle, Mostafa, lovely aunts, and many supportive

cousins.
Once again, thank you from the bottom of my heart for your invaluable contributions. I am truly honored and blessed to have had you as my supervisors, collaborators, friends, and family. I feel blessed, and I am on my way to trying to deserve it.

With profound gratitude,
Farzam Nosrati

Abstract

This ongoing Ph.D. thesis presents original research that revolves around the characterization and preservation of quantum resources in composite quantum systems. In Part I, the investigation centers on the concept of indistinguishability among identical particles – a crucial inherent resource for quantum information processing. In Part II, the thesis delves into the dynamic control of indistinguishable particles, with a specific focus on photons, as they propagate through various quantum photonic setups, which serve as potential photonic-based quantum information processors for advancing quantum technologies.

Part I focuses on the exploration of the indistinguishability of identical particles as a valuable quantum resource for information processing. It introduces a generalized entanglement measure applicable to arbitrary states of two identical qubits, highlighting the capability of quantum indistinguishability to generate noise-free entanglement. Additionally, it proposes a theoretical and experimental framework for remote entangling gates, enabling teleportation with fidelities that surpass classical thresholds by manipulating spatial indistinguishability. Furthermore, it investigates the resilience of entanglement in the presence of spatial indistinguishability during open system dynamics, showcasing its robustness against different environmental noise sources. The thesis also presents an entanglement distillation method that leverages spatial overlap, establishing conditions for maximum entanglement distillation and examining the impact of noise parameters and local temperatures.

Part II focuses on the photonic-based quantum model for quantum transport phenomena and quantum information tasks. The thesis introduces a probing protocol to detect disorder in quantum walks, offering valuable insights into anomalous transport phenomena and Anderson localization. Furthermore, it explores the role of controlled disorder in enhancing quantum correlations between indistinguishable photons, demonstrating the potential for improved quantum correlations between selected network modes through the careful adjustment of suitable disorder configurations. Lastly, the thesis presents a scalable quantum walk processor with temporal photonic lattices. This processor operates on a fiber-loop system and enables the generation and processing of high-dimensional time-bin entanglement. This novel approach establishes a proof-of-principle for preparing and harnessing entangled states in high-dimensional systems by controlling high-dimensional bi-photon quantum interference.

The contributions made in this thesis significantly advance the field of quantum information processing. They enhance our understanding of the importance of indistinguishability in various quantum phenomena and provide practical frameworks for utilizing indistinguishability as a valuable resource. These findings provide fundamental insights for quantum information processing and open up promising avenues for future research within the development of quantum technologies.

Résumé

Cette thèse de doctorat en cours présente des recherches originales qui tournent autour de la caractérisation et de la préservation des ressources quantiques dans les systèmes quantiques composites. Dans la Partie I, l'enquête se concentre sur le concept d'indiscernabilité entre particules identiques - une ressource inhérente cruciale pour le traitement de l'information quantique. Dans la Partie II, la thèse explore le contrôle dynamique des particules indiscernables, en mettant l'accent spécifique sur les photons, alors qu'ils se propagent à travers diverses configurations quantiques de photonique, lesquelles servent de potentiels processeurs quantiques basés sur le photon pour faire progresser les technologies quantiques.

La première partie met l'accent sur l'exploration de l'indiscernabilité des particules identiques en tant que ressource quantique précieuse pour le traitement de l'information. Elle introduit une mesure généralisée de l'entrelacement applicable à des états arbitraires de deux qubits identiques, mettant en évidence la capacité de l'indiscernabilité quantique à générer un entrelacement sans bruit. De plus, elle propose un cadre théorique et expérimental pour les portes d'entrelacement à distance, permettant la téléportation avec une fidélité dépassant le seuil classique en manipulant l'indiscernabilité spatiale. En outre, elle étudie la résilience de l'entrelacement en présence d'indiscernabilité spatiale pendant la dynamique des systèmes ouverts, démontrant sa robustesse face à différentes sources de bruit environnemental. La thèse présente également une méthode de distillation de l'entrelacement qui exploite le chevauchement spatial, établissant des conditions pour une distillation d'entrelacement maximale et examinant l'impact des paramètres de bruit et des températures locales.

La deuxième partie se concentre sur le modèle quantique basé sur la photonique pour les phénomènes de transport quantique et les tâches d'information quantique. Le mémoire présente un protocole d'investigation pour détecter le désordre dans les marches quantiques, offrant de précieuses perspectives sur les phénomènes de transport anormaux et la localisation d'Anderson. De plus, elle explore le rôle du désordre contrôlé dans l'amélioration des corrélations quantiques, démontrant le potentiel d'amélioration des corrélations quantiques entre des modes de réseau sélectionnés grâce au réglage minutieux de configurations de désordre appropriées. Enfin, la thèse présente un processeur de marches quantiques évolutif avec des réseaux photoniques temporels. Ce processeur fonctionne sur un système de boucle de fibre et permet la génération, la manipulation et le test d'entrelacements à plusieurs dimensions de boîtes de temps. Cette approche novatrice établit une preuve de principe pour la préparation et l'utilisation d'états intriqués dans des systèmes à haute dimension en contrôlant l'interférence quantique à deux photons à haute dimension.

Les contributions apportées par cette thèse font progresser considérablement le domaine du traitement de l'information quantique. Elles améliorent notre compréhension de l'importance de l'indiscernabilité dans divers phénomènes quantiques et fournissent des cadres pratiques pour utiliser l'indiscernabilité en tant que ressource précieuse. Ces découvertes offrent des perspectives fondamentales pour le traitement de l'information quantique et ouvrent des voies prometteuses pour la recherche future dans le développement des technologies quantiques.

Synopsis

Cette thèse de doctorat présente des résultats de recherche originales qui tournent autour de la caractérisation et de la préservation des ressources quantiques dans les systèmes quantiques composites. Dans la Partie I, la recherche se concentre sur le concept d'indiscernabilité entre particules identiques - une ressource inhérente cruciale pour le traitement de l'information quantique. Dans la Partie II, la thèse explore le contrôle dynamique des particules indiscernables, en mettant l'accent spécifique sur les photons, alors qu'ils se propagent à travers divers systèmes, qui servent de potentiels processeurs quantiques basés sur les photons pour réaliser des technologies quantiques avancées.

Partie I : Indiscernabilité des particules identiques en tant que ressource quantique pour le traitement de l'information

Dans **la première partie** de ma thèse de doctorat, j'étudie l'indiscernabilité des particules identiques en tant que véritable ressource quantique pour le traitement de l'information quantique. Elle est constituée de chapitres basés sur des articles précédemment publiés dans des revues scientifiques réputées. Avant de présenter les résultats, j'introduis brièvement le sujet en abordant les questions suivantes :

1. Quel est le concept physique derrière l'identité et la non-individualité des entités quantiques ?
2. Les états de deux particules identiques sous la forme $|\phi_1\rangle \otimes |\phi_2\rangle \pm |\phi_2\rangle \otimes |\phi_1\rangle$ présentent-ils un véritable entrelacement, comme leur forme le suggère ? Établir un concept d'entrelacement à la fois physiquement significatif et pratiquement applicable est d'une importance capitale.
3. Quels sont les cadres sous-jacents pour quantifier et caractériser l'entrelacement entre particules identiques ?
4. L'indiscernabilité des particules identiques peut-elle servir de ressource non classique pour effectuer des tâches de traitement de l'information quantique ?

Ces questions constituent la base d'une exploration approfondie et d'une meilleure compréhension des systèmes constitués de particules identiques (par exemple, qubits, atomes à deux niveaux, photons, électrons, quasi-particules), qui sont les éléments constitutifs fondamentaux (particules) des réseaux quantiques. Cette tâche revêt une importance particulière dans les architectures intégrées avec des opérations quantiques intrinsèquement significatives. Des progrès encourageants ont été réalisés dans ce domaine sur différentes plateformes quantiques, notamment les atomes ultrafroids, l'optique quantique et les champs quantiques. Pour commencer, examinons les concepts fondamentaux d'identité et d'indiscernabilité.

Identité vs indiscernabilité

Dans notre vie quotidienne, nous rencontrons de nombreux objets que nous percevons comme des individus distincts, chacun possédant des propriétés uniques qui les distinguent. Selon le réductionnisme

leibnizien, ce sont ces propriétés spécifiques qui rendent les objets matériels véritablement individuels, représentant essentiellement une collection ou un "ensemble" de propriétés. Même des objets qui semblent remarquablement similaires, comme des jumeaux identiques, ont des différences subtiles dans leurs propriétés qui nous permettent de les différencier. La mécanique classique renforce cette idée, en indiquant que les particules se repoussent les unes les autres lorsqu'elles se rapprochent, les empêchant d'occuper la même position spatiale. En conséquence, les particules classiques sont toujours discernables en fonction de leurs positions spatiales distinctes, garantissant leur individualité.

Cependant, la perspective classique est remise en question en ce qui concerne la mécanique quantique. Dans le domaine quantique, les particules élémentaires comme les électrons présentent une propriété appelée l'indiscernabilité. Ces particules possèdent des propriétés intrinsèques identiques, telles que la masse au repos, la charge et le spin, quelle que soit leur position dans l'univers. Par conséquent, chaque électron partage la même masse, la même charge et d'autres caractéristiques intrinsèques que n'importe quel autre électron. Cette indiscernabilité des particules quantiques contredit la compréhension traditionnelle de l'individualité et exige un cadre conceptuel différent pour comprendre leur comportement.

En plus des propriétés intrinsèques, la mécanique quantique introduit des propriétés dépendant de l'état pour décrire les systèmes quantiques élémentaires. Cela signifie que les particules peuvent être différenciées en utilisant des mesures dépendantes de leurs états. Par exemple, un polariseur peut distinguer entre des photons polarisés verticalement et horizontalement. Cette approche alternative pour distinguer des objets identiques ouvre une perspective de théorie des champs, représentant les particules comme des champs dichotomiques "Oui/Non". Dans ce cadre, l'amplitude du champ se voit attribuer une valeur de "Oui" si la particule est présente à un endroit particulier et "Non" si elle ne l'est pas. En conclusion, les particules classiques sont discernables en raison de leurs ensembles uniques de propriétés, tandis que les particules quantiques remettent en question cette notion en exhibant une indiscernabilité basée sur leurs propriétés intrinsèques identiques. L'incorporation de propriétés dépendant de l'état en mécanique quantique permet de différencier entre des particules identiques grâce à des mesures spécifiques. Ce changement de perspective éclaire la disparité entre les statistiques classiques et quantiques et soulève des questions intrigantes sur l'individualité dans les systèmes quantiques.

Non-individualité quantique

J'aimerais commencer par un modèle simplifié impliquant deux particules indiscernables réparties sur deux côtés d'une boîte ou dans deux états généraux, comme illustré dans la Figure 1.1. La tâche de l'observateur est de compter les particules dans chaque région, ce qui donne trois cas possibles : avoir les deux particules du même côté (cas Fig.1.1(b) et Fig.1.1(c)), ou une particule de chaque côté (cas Fig.1.1(a)). Selon la physique classique, le cas Fig.1.1(a) a un poids deux fois supérieur aux autres cas, car il existe deux façons d'obtenir cet agencement en permutant les particules. Par exemple, en supposant des probabilités égales pour les quatre combinaisons, la probabilité de trouver une particule de chaque côté est de $1/2$, suivant les statistiques bien connues de Maxwell-Boltzmann.

En revanche, la mécanique statistique quantique introduit deux formes courantes : les statistiques de Bose-Einstein et les statistiques de Fermi-Dirac. Les statistiques de Bose-Einstein considèrent les trois agencements possibles : les deux particules du même côté (cas Fig.1.1(b) et Fig.1.1(c)), et une particule de chaque côté (cas Fig.1.1(a)). En supposant des probabilités égales pour les trois cas, chacun a une probabilité de $1/3$. Les statistiques de Fermi-Dirac, quant à elles, prennent en compte le résultat observable consistant à trouver les deux particules de chaque côté, entraînant une dégénérescence d'échange et des états antisymétriques.

Pour comprendre l'origine des états symétriques et antisymétriques, l'auteur introduit une représentation formelle utilisant des états élémentaires pour chaque particule. Par exemple, une particule dans l'état mono-particule α, associé aux valeurs propres d'un groupe d'observables qui commutent, est étiquetée comme "1", tandis qu'une autre particule dans l'état β est étiquetée comme "2". Cependant, en raison de l'incertitude de l'identité des particules, le système ne peut pas être décrit de manière unique comme $|\Psi\rangle = |\alpha\rangle_1 \otimes |\beta\rangle_2$ ou $|\Psi\rangle = |\alpha\rangle_2 \otimes |\beta\rangle_1$, mais plutôt comme une combinaison linéaire des deux,

$|\Psi\rangle = a\,|\alpha\rangle_1 \otimes |\beta\rangle_2 + b\,|\alpha\rangle_2 \otimes |\beta\rangle_1$, où l'état est normalisé, c'est-à-dire que $|a|^2 + |b|^2 = 1$. Cette dégénérescence d'échange, résultat des statistiques quantiques, découle de quantités qui ne peuvent pas être physiquement observées, rendant différentes possibilités mathématiques également valides.

Pour résoudre ce problème, le postulat de symétrisation est introduit. Les particules ayant un état symétrique sont appelées bosons, tandis que celles ayant un état antisymétrique sont des fermions. Pour l'exemple précédent des deux particules, l'état $|\Psi\rangle$ est représenté de manière unique comme $\frac{1}{\sqrt{2}}\big(\,|\alpha\rangle_1 \otimes |\beta\rangle_2 + |\alpha\rangle_2 \otimes |\beta\rangle_1\,\big)$ pour les bosons et $\frac{1}{\sqrt{2}}\left(|\alpha\rangle_1 \otimes |\beta\rangle_2 - |\alpha\rangle_2 \otimes |\beta\rangle_1\right)$ pour les fermions. Le postulat de symétrisation garantit que les particules dans le même état physique présentent des propriétés de symétrie différentes dans leurs descriptions mathématiques, entraînant un comportement distinct sous les permutations de particules pour les bosons et les fermions. Les états bosoniques restent inchangés tandis que les états fermioniques changent de signe avec un changement de phase de π. De plus, le principe d'exclusion de Pauli, conséquence du postulat de symétrisation, interdit à deux fermions ou plus d'occuper simultanément le même état quantique.

Cette classification des bosons et des fermions a des implications profondes dans divers domaines de la physique. Cependant, elle soulève également la question intrigante de savoir si l'entrelacement observé dans la description mathématique des particules identiques, selon le postulat de symétrisation, est physiquement observable. Pour explorer cela davantage, l'auteur prévoit de donner un aperçu des mesures d'entrelacement pour les particules identiques dans les sections suivantes.

Entrelacement des particules identiques

Cette section explore les complexités de la caractérisation de l'entrelacement entre particules identiques en utilisant des étiquettes fictives. Ces défis découlent de la (anti)symétrisation des états et de l'étiquetage des particules, ce qui entraîne des difficultés sur le plan méthodologique et pratique. De plus, les méthodes et critères conventionnels utilisés pour étudier l'entrelacement entre particules non identiques ne s'appliquent pas directement aux particules identiques [1]. La section commencera par un aperçu de la description standard de l'entrelacement, qui utilise des étiquettes fictives pour quantifier et caractériser les états intriqués.

Approche de première quantification (approche standard)

Cette partie se penche sur les complexités de la caractérisation de l'entrelacement entre particules identiques en utilisant des étiquettes fictives. Considérez un système noté comme S, composé de deux particules non identiques étiquetées comme 1 et 2, décrites par un état pur $|\Psi\rangle$ dans les deux espaces de Hilbert monoparticules $\mathcal{H}_1$ et $\mathcal{H}_2$, qui ensemble forment l'espace de Hilbert du système à deux particules, $\mathcal{H}_S$. Dans le cas où $|\Psi\rangle = |\phi\rangle_1 \otimes |\chi\rangle_2$, l'état est séparable, reflétant la structure de produit tensoriel de l'espace de Hilbert total, et les états intriqués ne sont pas présents dans la structure du produit tensoriel.

Le degré d'entrelacement est généralement mesuré à l'aide de la décomposition de Schmidt, où l'état est exprimé comme $|\Psi\rangle = \sum_{i=1}^{r} \sqrt{\lambda_i}\,|\phi_i\rangle_1 \otimes |\chi_i\rangle_2$, avec λ_i comme coefficient de Schmidt et $|\phi_i\rangle_1$ et $|\chi_i\rangle_2$ comme vecteurs de base dans $\mathcal{H}_1$ et $\mathcal{H}_2$, respectivement. L'entropie de von Neumann est une mesure couramment utilisée pour quantifier l'entrelacement entre deux particules.

Cependant, pour les particules indiscernables, étiquetées comme $\pm$, l'état à deux particules est représenté par $|\Psi\rangle_\pm = \dfrac{1}{\sqrt{2}}(|\phi\rangle_1 \otimes |\chi\rangle_2 \pm |\phi\rangle_2 \otimes |\chi\rangle_1)$ pour les bosons $(+)$ et les fermions $(-)$. En raison de la présence d'étiquettes et du postulat de symétrisation, les particules identiques sont toujours intriquées, même si elles sont éloignées et préparées indépendamment. L'entropie de von Neumann, lorsqu'on trace une des particules, reflète un entrelacement non physique résultant des étiquettes fictives utilisées pour décrire l'état.

De plus, dans certains scénarios tels que les systèmes de points quantiques, des particules identiques peuvent occuper le même emplacement, rendant leur statistique cruciale pour déterminer la dynamique et les corrélations. Dans de telles situations, distinguer l'entrelacement physique réel des corrélations

formelles dues aux étiquettes fictives devient une tâche difficile. Cette section met en évidence les complexités de la quantification de l'entrelacement impliquant des particules identiques et la nécessité de prendre en compte leur indiscernabilité et leurs statistiques dans des contextes spécifiques.

Approche "sans étiquette" pour les particules identiques

L'approche "sans étiquette" pour les particules identiques propose une méthode alternative pour détecter et quantifier l'entrelacement, en abordant les défis auxquels fait face l'approche de première quantification [2, 3]. Dans cette approche, deux particules identiques dans des régions spatiales séparées, désignées par L et R, sont considérées. Les états de ces particules sont représentés par $|\phi\rangle$ et $|\chi\rangle$, respectivement. Importamment, les mesures de particules individuelles à l'aide de dispositifs localisés dans les régions L et R n'affectent pas les prédictions physiques, rendant l'effet de symétrisation non pertinent dans ce contexte [4, 5, 6, 7]. Par conséquent, la matrice de densité d'une particule est calculée sans appliquer de symétrisation, et l'état initial est représenté comme un état factorisé $|\Psi\rangle = |\phi\rangle_{\mathrm{L}} \otimes |\chi\rangle_{\mathrm{R}}$, applicable à la fois aux bosons et aux fermions.

Dans l'approche "sans étiquette", un état d'une particule est défini à l'aide d'un ensemble complet d'observables commutantes, représentées comme une liste d'états de particules individuelles : $|\phi_1\rangle$ et $|\phi_2\rangle$. La représentation de l'état ne peut pas être exprimée comme un produit tensoriel d'états de vecteurs de particules individuelles. Donc, il est entièrement caractérisé en listant les états comme $|\phi_1, \phi_2\rangle / \sqrt{\mathcal{N}}$, avec $\mathcal{N}$ comme facteur de normalisation.

Les opérateurs d'une particule, notés $A^{(1)}$, dans l'approche "sans étiquette" agissent sur un état à deux particules une à la fois, entraînant une combinaison linéaire d'états à deux particules, comme défini par la définition standard [6]. L'action d'un opérateur d'une particule est exprimée comme $A^{(1)} = \sum_{i,j} a_{ij} |\psi_i\rangle \langle\psi_j|$ en utilisant un produit intérieur symétrique entre des espaces d'états de dimensions différentes. Le produit intérieur prend en compte l'effet d'indiscernabilité; c.-à-d. l'endroit où l'amplitude de la probabilité de trouver une particule dans l'état ϕ_1' (ϕ_2') provient de la possibilité d'avoir une particule dans l'un ou l'autre état ϕ_1 ou ϕ_2.

L'approche "sans étiquette" permet la quantification de l'entrelacement entre deux particules identiques en utilisant l'entropie de von Neumann de la matrice de densité réduite d'une particule obtenue à partir d'une trace partielle localisée. Le degré d'entrelacement est donné par la formule de l'entropie de von Neumann (1.2). Par exemple, dans un scénario de deux particules identiques dans des régions spatiales différentes, la trace partielle sur une région donne un état séparable. En revanche, lorsque les deux particules sont amenées au même endroit, la trace partielle donne un état de particule unique différent, qui peut également être considéré comme séparable.

En résumé, l'approche "sans étiquette" fournit un cadre pour étudier l'entrelacement dans des systèmes de particules identiques, en évitant l'utilisation d'étiquettes non observables. Elle permet l'analyse de l'entrelacement en utilisant des concepts usuels de la théorie de l'entrelacement pour les particules discernables, tels que l'entropie de von Neumann par le biais de la trace partielle. La quantification de l'entrelacement dans cette approche est basée sur des mesures locales et s'avère être dépendante du contexte. Cette approche offre des aperçus précieux sur le comportement des particules identiques et leurs propriétés d'entrelacement, qui sont importantes pour diverses applications dans le traitement de l'information quantique et les technologies quantiques.

Approche de la quantification du champ (deuxième quantification)

Les critères de séparabilité et d'entrelacement dans les systèmes quantiques dépendent du choix des observables qui commutes et qui ne sont pas des concepts absolus [8, 9, 10]. L'approche de la quantification du champ en mécanique statistique quantique offre un cadre cohérent pour analyser la séparabilité et l'entrelacement dans les systèmes quantiques [11]. Cette approche introduit des opérateurs de création et d'annihilation qui agissent sur les états vectoriels de particules individuelles, représentant les modes dans un espace de Hilbert pour une seule particule, noté $\mathcal{H}$. Dans le cadre de la quantification du champ, un état est considéré comme séparable par rapport à un ensemble donné de modes orthogonaux s'il peut être

exprimé comme un produit de polynômes en opérateurs de création correspondant à ces modes [10]. Les états qui ne peuvent pas être exprimés sous cette forme sont considérés comme entrelacés. Le concept de séparabilité et d'entrelacement pour les particules identiques dépend du contexte, en fonction du choix des observables. Par exemple, des états qui sont entrelacés par rapport à un ensemble d'observables peuvent être séparables en considérant un autre ensemble d'observables [7, 12, 13]. L'approche de la quantification du champ permet l'analyse de l'entrelacement dans des systèmes à plusieurs corps composés de bosons et de fermions [8]. Une opération linéaire qui transfère des particules entre les modes montre que la structure d'entrelacement peut changer sous de telles transformations [2]. L'entrelacement de particules identiques peut être transféré à un état entrelacé de modes indépendants, montrant que le critère de séparabilité n'est pas une propriété absolue [14]. Dans le contexte des particules identiques, l'entrelacement induit par la mesure joue un rôle important [6, 13]. Des mesures ambiguës, où l'appareil ne peut pas déterminer quelle particule correspond au résultat détecté par chaque détecteur, peuvent conduire à la génération intrinsèque d'entrelacement induit par la mesure de manière probabiliste, même dans des cas où l'entrelacement initial était absent [6, 13]. En conclusion, l'approche de la quantification du champ offre un cadre complet pour comprendre la nature contextuelle de la séparabilité et de l'entrelacement dans les systèmes quantiques. Les particules identiques présentent des comportements uniques, et leurs propriétés d'entrelacement dépendent du choix des observables et des procédures de mesure. Cela a des implications pour diverses applications dans le traitement de l'information quantique et les technologies quantiques, où l'entrelacement joue un rôle crucial dans l'obtention d'avantages quantiques. Comprendre la dépendance du contexte de l'entrelacement dans les systèmes de particules identiques est essentiel pour la caractérisation et l'utilisation appropriées des corrélations quantiques dans des applications pratiques.

Traitement de l'information quantique avec des particules identiques

Cette section aborde les implications de l'indiscernabilité des particules identiques dans le traitement de l'information quantique. Le principal défi est que les particules identiques ne sont pas facilement adressables individuellement, ce qui limite leur utilisation dans les tâches d'information quantique. L'approche courante consiste à utiliser la deuxième quantification dans le cadre des opérations locales et de la communication classique (OLCC), où les modes orthogonaux sont manipulés et adressés individuellement, car ils peuvent toujours être distingués dans des configurations expérimentales.

Cependant, lorsque les particules identiques se chevauchent spatialement, les opérations locales sur des modes spécifiques deviennent inaccessibles. Pour résoudre ce problème, le cadre des opérations localisées spatialement et de la communication classique (sOLCC) a été introduit. Ce cadre, basé sur une approche sans étiquette basée sur les particules, permet d'adresser et de manipuler des particules identiques se chevauchant spatialement. Cette section procurera, avant de se plonger dans le rôle de l'indiscernabilité dans le traitement de l'information quantique, un bref rappel du cadre sOLCC[15, 16].

Opérations localisées spatialement et communication classique (sOLCC)

Dans le cadre du sOLCC (opérations localisées spatialement et communication classique) est introduit pour deux particules identiques préparées indépendamment dans un état conjoint $|\Psi\rangle = |\psi \uparrow, \psi' \downarrow\rangle$ avec des fonctions d'onde spatiales ψ et ψ' représentant les degrés de liberté externes et les états de pseudospin $\uparrow$ et $\downarrow$ représentant les états internes. En effectuant des mesures locales sur les états de pseudospin d'une seule particule dans des régions spatiales localisées séparées désignées par L et R, l'entrelacement dans le système peut être accédé. L'opérateur de mesure du sOLCC projette l'état sur les états de base et produit un état biparticulaire non normalisé. La probabilité de succès de sOLCC dépend de la probabilité de trouver les particules dans chaque région. L'entrelacement opérationnel est quantifié en utilisant l'entropie de von Neumann. Lorsque les particules sont séparées spatialement dans deux régions, l'état est séparable et a un entrelacement nul. Cependant, s'il y a une probabilité non nulle de chevauchement spatial entre les particules, l'état devient entrelacé. Pour un chevauchement spatial complet, où les deux particules sont également réparties dans les deux régions, l'état devient entrelacé de manière max-

imale. Le cadre théorique du sOLCC est étendu à des scénarios avec de multiples particules identiques réparties entre de multiples régions, permettant d'étudier l'entrelacement dans des systèmes de particules indiscernables. La mesure de l'entrelacement est également étendue pour englober n'importe quel état mixte arbitraire de deux particules identiques se chevauchant spatialement, offrant un cadre complet pour quantifier et caractériser l'entrelacement dans de tels systèmes. Le cadre du sOLCC, basé sur l'approche sans étiquette et sur les opérations localisées spatialement et la communication classique, permet de manipuler et d'exploiter directement les états de ressource associés aux particules identiques. Cela a des implications significatives pour le traitement de l'information quantique, car l'indiscernabilité des particules identiques peut être utilisée efficacement comme une ressource quantique précieuse. Le cadre permet diverses applications et avantages dans les tâches de traitement de l'information quantique. Les sections suivantes donneront un aperçu de certaines de ces applications et des avantages de l'utilisation de particules indiscernables pour le traitement de l'information quantique [16, 17].

Interférence quantique à deux particules et statistiques des particules

L'indiscernabilité des particules identiques a historiquement conduit à des conséquences significatives, en particulier dans le contexte de l'interférence quantique à deux photons. Les chercheurs ont généré des superpositions de l'origine d'une paire de photons, créant des phénomènes d'interférence. Historiquement, l'action d'un diviseur de faisceau a été formulée en utilisant la deuxième quantification, où les opérateurs de création de photons $\hat{a}^\dagger$ et $\hat{b}^\dagger$ représentent les deux ports d'entrée du diviseur de faisceau, et $\hat{c}^\dagger$ et $\hat{d}^\dagger$ représentent les deux ports de sortie. Pour les photons, le diviseur de faisceau induit une interférence à deux photons, connue sous le nom d'effet Hong, Ou et Mandel (HOM), qui se traduit par un "creux" caractéristique dans la détection en coïncidence à la sortie. Lorsque les photons se chevauchent spatialement au niveau du diviseur de faisceau, ils deviennent indiscernables, conduisant à une interférence. Dans l'effet HOM, la détection simultanée aux deux ports de sortie se comporte comme l'état singulet pour deux photons polarisés de manière orthogonale. La contrepartie fermionique, impliquant des fermions qui obéissent au principe d'exclusion de Pauli, présente un anti-regroupement , et l'information concernant l'origine des fermions reste insaisissable.

La formalisme de l'action du diviseur de faisceau peut être traduit dans l'approche sans étiquette, où les particules ne dépendent pas des étiquettes, et la forme élémentaire de l'état à deux particules est prise en compte. Pour les bosons dans le cas 50:50, l'effet de regroupement est retrouvé, similaire à l'effet HOM, tandis que pour les fermions, le seul état accessible est $|\mathrm{L}\,\sigma, \mathrm{R}\,\sigma\rangle$, l'effet d'anti-regroupement.

L'interférence à deux particules a été observée non seulement avec des particules élémentaires telles que des électrons et des atomes, mais également avec des systèmes quantiques plus massifs et complexes, tels que les plasmons. Ce phénomène se produit à différentes échelles et complexités, en faisant un aspect fondamental de la physique quantique avec de larges applications dans le traitement de l'information quantique et les technologies quantiques

Génération d'entrelacement

Dans la manipulation d'états quantiques, un émetteur fiable capable de produire des particules élémentaires identiques est essentiel. L'optique quantique utilise la conversion descendante paramétrique spontanée (SPDC), un processus non linéaire qui génère des paires de photons (passif et signal) avec une polarisation orthogonale, résultant en des états d'entrelacement de polarisation véritable [18, 19]. De telles sources sont largement utilisées pour créer des états d'entrelacement photoniques complexes, y compris la création de systèmes d'entrelacement de 12 photons [20]. Après la génération des particules, des opérations locales telles que des diviseurs de faisceau et des polariseurs sont utilisées pour l'ingénierie d'états quantiques et les tâches de traitement de l'information quantique telles que la téléportation quantique et le transfert d'information quantique entre une source et un destinataire en utilisant des états d'entrelacement [15, 21, 22]. Cependant, le chevauchement spatial dans une région spécifique n'est pas nécessaire pour l'ingénierie d'états quantiques, car l'entrelacement des particules indiscernables est directement déterminé par leur chevauchement spatial [16]. Une proposition expérimentale

importante a réalisé la première porte d'entrelacement à distance exploitant des particules indiscernables [23]. D'autres travaux ont également mis en œuvre des portes d'entrelacement basées sur sOLCC en utilisant le chevauchement spatial entre des particules identiques, démontrant sa valeur dans l'ingénierie d'états quantiques [24, 25].

Téléportation quantique et entrelacement swapping

Une façon de tester l'entrelacement consiste à démontrer que l'état de sortie peut accomplir des tâches d'information quantique qui sont classiquement impossibles. La téléportation quantique en est un exemple typique, où l'entrelacement sous forme d'un état de Bell est utilisé pour transmettre un état quantique arbitraire entre deux observateurs distants, Alice et Bob. Cette technique permet le transfert d'information quantique d'une source à une destination en utilisant des états d'entrelacement et joue un rôle crucial dans le réseau quantique [15]. L'entrelacement swapping est une autre application importante dans la communication quantique, permettant l'entrelacement de deux particules qui ne partagent pas un passé commun. Récemment, un protocole d'entrelacement basé sur l'indiscernabilité a été mis en œuvre expérimentalement en utilisant l'indiscernabilité spatiale contrôlée de quatre photons indépendants répartis parmi trois nœuds d'un réseau, démontrant des perspectives prometteuses pour une communication quantique réalisable dans des réseaux quantiques photoniques à plusieurs nœuds [26]. L'indiscernabilité inhérente des particules identiques offre une ressource précieuse pour diverses tâches de communication quantique [27, 15].

Métrologie quantique avec des particules indiscernables

L'effet Hong-Ou-Mandel (HOM) démontre que, en raison de la nature indiscernable et bosonique de deux photons, ils peuvent être entièrement dans l'un ou l'autre de deux modes (A ou B) sans que leur identité soit connue. Cette observation est étendue à N photons dans le mode A, donnant lieu à l'état N00N, qui est défini comme $|\psi_{N00N}\rangle = \frac{1}{\sqrt{2}}\left(|N,0\rangle + |0,N\rangle\right)$. Les états N00N permettent une résolution spatiale et de phase améliorée, atteignant la limite de Heisenberg pour la sensibilité de phase avec un facteur d'échelle de $1/N$. Des schémas expérimentaux de générations des états N00N avec un grand nombre de photons ont été proposés et démontrés. Le comportement collectif de N particules identiques interagissant avec un déphaseur donne lieu à un déphasage proportionnel à N, contrairement aux états cohérents classiques. Le caractère adressable est cruciale pour les opérations quantiques, mais pour les particules identiques, sOLCC peut être utilisé pour surmonter les limitations et réaliser des opérations telles que la porte CNOT. Le chevauchement spatial des fonctions d'onde est la raison de la cohérence, et dans la métrologie quantique, la cohérence quantique activée par l'indiscernabilité est considérée comme une ressource précieuse pour les tâches de discrimination de phase, surpassant les approches de particules discernables [28, 29, 30, 31].

Protection, récupération et distillation de l'entrelacement assistées par l'indiscernabilité

Dans les sections précédentes, j'ai donné un bref aperçu de la façon dont le chevauchement spatial ou l'indiscernabilité permet la cohérence quantique. En outre, dans une étude précédente [32] a démontré expérimentalement que le maintien du chevauchement spatial et de l'indiscernabilité entre deux photons permet de préserver la cohérence quantique. Dans ce mécanisme, deux particules indiscernables et sans interaction se propagent ensemble à travers des réseaux quantiques affectés par un bruit non dissipatif, conduisant à un état stable où la cohérence, qui tient compte de l'indiscernabilité des particules, persiste indéfiniment.

Dans le cadre de ma thèse de doctorat, j'ai démontré l'utilisation de l'indiscernabilité des particules identiques pour préserver l'entrelacement à différentes étapes. Dans ce qui suit, je résume brièvement les résultats de quatre articles, comme discuté dans quatre chapitres.

Préparation robuste de l'entrelacement contre le bruit en contrôlant l'indiscernabilité spatiale

Dans le **Chapitre II** de ma thèse de doctorat, nous étudions et caractérisons le rôle de l'indiscernabilité dans le maintien de l'entrelacement quantique malgré le bruit environnemental. Notre étude se concentre sur l'utilisation des ressources quantiques, en particulier l'entrelacement, en mécanique quantique et en traitement de l'information quantique. L'entrelacement joue un rôle crucial dans diverses applications quantiques telles que la métrologie quantique, la distribution de clés quantiques, la téléportation et la détection quantique. Cependant, l'entrelacement est sensible au bruit environnemental, ce qui entraîne l'incohérence et la perte de ses propriétés quantiques. Préserver l'entrelacement en présence de bruit est un objectif principal pour la technologie quantique améliorée.

Notre étude utilise des sous-systèmes quantiques identiques, tels que les qubits, comme blocs de construction pour les réseaux quantiques à plusieurs corps. Nous explorons l'indiscernabilité des particules et ses implications dans les systèmes quantiques composites. Plus spécifiquement, nous étudions le contrôle continu des configurations spatiales des fonctions d'onde des particules individuelles et l'influence la préparation des états entrelacés en présence de bruit. Nous introduisons le concept de degré d'indiscernabilité comme une mesure entropique de l'information, donnée par l'équation (2.10), qui peut être ajustée en modulant les fonctions d'onde spatiales. En utilisant le cadre expérimentalement réalisable des opérations spatialement localisées et de la communication classique (sLOCC), nous définissons l'entrelacement de formation pour un état arbitraire de deux qubits indiscernables (bosons ou fermions), donné par l'équation (4.13). Ce quantificateur nous permet d'évaluer l'entrelacement dans différentes configurations de chevauchement spatial. Nos résultats montrent que l'indiscernabilité spatiale peut être adaptée pour protéger la génération d'entrelacement contre le bruit, le rendant ainsi plus résistant dans les applications quantiques pratiques.

Le graphique dans la figure 2.2 démontre que la préparation de l'entrelacement, modélisée par l'état de Werner, peut être efficacement protégée contre le bruit pour un chevauchement spatial non nul entre les deux particules. Une information cruciale dans ce scénario est le degré minimum de $\mathcal{I}_{\mathrm{LR}}$ qui garantit un entrelacement non local dans $\mathcal{L}$ et $\mathcal{R}$, en violant une inégalité de Bell CHSH [33], indépendamment de la probabilité de bruit p. Dans l'ensemble, notre étude met en lumière les caractéristiques fondamentales des systèmes quantiques composites et contribue à l'avancement des technologies améliorées par la quantique.

Entrelacement quantique expérimental et téléportation en ajustant l'indiscernabilité spatiale à distance de photons indépendants

Dans le **Chapitre III** de ma thèse de doctorat, nous explorons les caractéristiques fondamentales des constituants quantiques et leur rôle dans le contrôle des systèmes quantiques composites, qui sont essentiels pour avancer dans notre compréhension du monde naturel et développer des technologies améliorées par la quantique. Les réseaux quantiques à plusieurs corps sont souvent constitués de blocs de construction identiques, tels que les qubits, les photons, les atomes ou les électrons. L'indiscernabilité de ces sous-systèmes identiques émerge comme une caractéristique quantique fondamentale qui peut influencer les tâches de traitement de l'information quantique. Pour les systèmes à plusieurs corps avec des qubits non identiques, ces tâches sont réalisées par des opérations locales et une communication classique (LOCC), où l'adressage individuel des qubits est possible. Cependant, pour les qubits identiques, l'adressage individuel n'est pas toujours réalisable en raison du manque de discernabilité des particules.

Dans cette étude, nous proposons une proposition théorique pour mettre en œuvre expérimentalement une porte d'interaction à distance. Il a été démontré dans Ref. [16] que la superposition spatiale de deux particules identiques, même celles qui ne partagent aucun historique, peut générer un entrelacement. Nous mettons en œuvre un cadre opérationnel basé sur les opérations spatialement localisées et la communication classique (sLOCC), qui repose sur le concept de localité spatiale des mesures plutôt que de la localité des particules. En utilisant cette configuration illustrée dans la figure 3.5, nous contrôlons la distribution des paquets d'ondes de deux photons identiques indépendants et initialement non corrélés vers

des régions opérationnelles séparées, ce qui nous permet d'ajuster en continu le degré d'indiscernabilité spatiale à distance. Nous quantifions cette indiscernabilité à l'aide d'une mesure entropique et informationnelle appropriée [17].

En effectuant des mesures localisées de photons uniques, nous démontrons que les deux photons initialement non corrélés deviennent entrelacés, et la quantité d'entrelacement est directement liée au degré d'indiscernabilité spatiale, comme le montre le graphique dans la figure 3.3. Cet entrelacement non local viole l'inégalité de Bell, comme illustré dans la figure 3.3 et permet la téléportation conditionnelle de l'état d'un photon supplémentaire avec des fidélités supérieures aux seuils classiques [17]. Cette preuve expérimentale met en évidence l'importance de l'indiscernabilité spatiale en tant que ressource directe pour les protocoles quantiques et souligne son impact potentiel dans le traitement de l'information quantique.

Dynamique des particules indiscernables spatialement et protections de l'entrelacement quantique

Dans le **Chapitre IV** de ma thèse de doctorat, nous abordons le défi de traiter les particules identiques dans les réseaux quantiques et la difficulté de caractériser leurs corrélations quantiques. Les particules identiques, étant de la même espèce et ayant les mêmes propriétés intrinsèques, posent des défis uniques en mécanique quantique. Contrairement, les particules non identiques, ou discernables, peuvent être adressées individuellement et leur traitement dynamique est bien compris. Cependant, en ce qui concerne les particules indiscernables, le manque de discernabilité complique la compréhension de leur évolution dynamique de l'état du système.

Grâce au cadre sLOCC dans l'approche sans étiquette, il a été démontré que l'indiscernabilité spatiale est quantifiable par une mesure d'entropie informationnelle [17], qui est directement liée à la quantité d'entrelacement généré [23]. Une question ouverte reste de savoir comment les particules indiscernables, dans des conditions générales de chevauchement spatial, interagissent avec des environnements locaux et, par conséquent, comment leur état de système évolue dynamiquement. L'approche sans étiquette plus le cadre sLOCC semblent être des outils idéaux pour combler cette lacune dans le contexte des systèmes quantiques ouverts.

Nous étudions l'interaction des particules indiscernables avec des environnements locaux, ce qui entraîne une décohérence et la perte de ressources quantiques telles que la cohérence et l'entrelacement. Nous constatons que l'indiscernabilité spatiale peut jouer un rôle crucial dans la protection de l'entrelacement quantique contre le bruit préjudiciable dans des environnements non markoviens. En étudiant la dynamique de l'entrelacement de deux qubits identiques, nous montrons que l'indiscernabilité spatiale préserve l'entrelacement contre le bruit environnemental. Elle est ensuite appliquée pour étudier la dynamique de deux qubits identiques sous des bruits markoviens paradigmatiques, tels que l'amortissement de phase, la désexcitation et l'amortissement d'amplitude. Dans les figures 4.2, 4.3 et 4.4, nous montrons que l'indiscernabilité spatiale des qubits identiques est une propriété inhérente contrôlable du système qui protège l'entrelacement quantique exploitable contre le bruit préjudiciable. La combinaison de l'approche sans étiquette et du cadre sLOCC offre un ensemble d'outils puissants pour étudier les particules identiques dans les systèmes quantiques ouverts, ouvrant la voie à de futures avancées dans les technologies améliorées par la quantique et le traitement de l'information quantique.

Distillations de l'entrelacement assistées par l'indiscernabilité de deux qubits

Dans le **Chapitre IV**, nous nous concentrons sur la compréhension du rôle de l'indiscernabilité dans les systèmes composés d'entités quantiques identiques. Le chevauchement spatial de ces particules conduit au phénomène d'indiscernabilité, qui affecte profondément la formation des états quantiques composites [1, 13, 2]. Au-delà de son importance fondamentale, le chevauchement spatial permet de générer un entrelacement contrôlable et joue un rôle essentiel dans les tâches d'information quantique telles que la téléportation, l'estimation quantique et la distribution de l'entrelacement dans les réseaux quantiques [34, 16, 23, 24, 25, 35]. L'indiscernabilité des bosons a également été démontrée pour améliorer la

conversion d'information et de travail [36, 37, 38], conduisant à une efficacité à puissance maximale supérieure à la limite classique de Curzon-Ahlborn [39].

Cependant, l'entrelacement et la cohérence quantique, qui sont des ressources essentielles pour les technologies améliorées par la quantique, sont sensibles au bruit et aux interactions environnementales, ce qui entraîne l'incohérence et une dégradation [40, 41]. La préservation des ressources quantiques en présence de bruit devient un défi critique pour l'information et le calcul quantiques. Diverses méthodes de protection ont été proposées, notamment la préservation à l'aide de protocoles de distillation, qui convertissent des états mixtes en états entrelacés en utilisant des opérations locales et une communication classique (LOCC) [42, 43].

Dans ce contexte, nous introduisons une procédure de distillation probabiliste de l'entrelacement basée sur le chevauchement spatial entre particules identiques dans le cadre sLOCC. Nous établissons les conditions pour un taux de succès non nul de distillation d'entrelacement parfait. De plus, nous optimisons la probabilité de succès au détriment d'un degré d'entrelacement inférieur. Notre protocole repose uniquement sur les propriétés inhérentes des particules identiques, ce qui le rend particulièrement adapté aux scénarios de communication quantique, où il permet de convertir des états bruités apparemment inutiles en états opérationnels pour le transfert d'information. Pour démontrer l'applicabilité de notre procédure, nous examinons les exigences de distillation d'entrelacement à partir d'états thermiques dans la figure 5.2 et d'états de Werner dans la figure 5.5. En exploitant le chevauchement spatial et les opérations sLOCC, notre approche offre un moyen pratique et efficace de distiller l'entrelacement à partir d'états bruités, renforçant ainsi le potentiel de communication quantique et de traitement de l'information quantique.

Partie II : Traitement de l'information quantique basé sur des marches quantiques photoniques

Dans la partie II de ma thèse de doctorat, j'explore l'application des marches quantiques dans le traitement de l'information quantique. Cette partie comprend des chapitres basés sur des articles précédemment publiés dans des revues scientifiques réputées. Avant de plonger dans les résultats, je fournis une brève introduction au contexte.

Le concept de marches aléatoires quantiques sert de contrepartie quantique aux marches aléatoires classiques et a été initialement introduit par Aharonov et al. en 1993 [44]. Les marches quantiques modélisent l'évolution cohérente de particules quantiques, et leur caractéristique la plus remarquable est la capacité du marcheur à exister dans des états de superposition pendant la propagation. Cette propriété entraîne l'émergence d'effets d'interférence, qui différencient considérablement les marches quantiques de leurs contreparties classiques. Les marches quantiques ont démontré une accélération computationnelle dans divers algorithmes, tels que la recherche spatiale [45]. Au cours de la dernière décennie, elles sont devenues un modèle computationnel universel et ont été utilisées dans la conception d'ordinateurs quantiques [46, 47].

Rôle du désordre dans les marches quantiques en temps discret en tant que dispositif de mesure Le désordre dans les marches quantiques en temps discret se réfère à l'introduction de hasard ou d'irrégularité dans l'évolution du marcheur. Dans une marche quantique standard, l'évolution est déterminée par un ensemble fixe d'opérateurs unitaires, à savoir l'opérateur de pièce et l'opérateur de décalage. Pour une marche quantique ordonnée, nous disons que le comportement de diffusion est balistique, car la mesure de la variance de la position est proportionnelle à un nombre quadratique d'étapes $\sigma^2(\hat{X}) \propto t^2$ par rapport au cas classique, qui est linéaire. Cela signifie que le marcheur quantique se propage de manière quadratique plus rapidement dans l'espace des positions. Cependant, lorsque le désordre est introduit, ces règles montrent des variations. Le rôle du désordre dans les marches quantiques en temps discret peut avoir plusieurs effets sur le comportement du système. Par exemple, le désordre peut conduire à un phénomène appelé la localisation d'Anderson [48], où le marcheur devient localisé ou confiné dans une région particulière du réseau. Cela contraste avec le comportement de diffusion observé dans une marche quantique ordonnée. Cet effet s'applique aux marches quantiques et a été étudié en utilisant des

plates-formes physiques de marche quantique telles que l'optique photonique [49, 50, 51, 52]. De plus, on peut simuler l'incohérence en utilisant le désordre aléatoire, qui est un phénomène physique qui apparaît généralement de l'interaction entre les systèmes quantiques et leur environnement. Le désordre peut également conduire à différents schémas de propagation, tels que la super-diffusion (la propagation du marcheur est plus rapide que celle observée dans les marches aléatoires classiques), le modèle classique, et la sous-diffusion (la propagation du marcheur est plus lente que celle observée dans les marches aléatoires classiques). Cela se produit lorsque les fluctuations aléatoires introduites par le désordre affectent l'exploration du réseau par le marcheur. De plus, les désordres dans les marches quantiques peuvent interagir avec la topologie sous-jacente du réseau. Selon le type spécifique de désordre et la structure du réseau, l'interaction entre le désordre et la topologie peut donner lieu à des phénomènes intéressants, tels que les isolants d'Anderson topologiques ou l'apparition d'états de bord localisés [53, 54].

En outre, le désordre peut entraîner la génération d'entrelacement entre les états de la pièce et de la position du marcheur, ainsi que des corrélations entre différentes parties du système [55]. Comme discuté dans le chapitre VIII, nous démontrons l'optimisation du contrôle du désordre pour améliorer la corrélation quantique entre deux photons indiscernables dans des modes distincts d'un réseau de marches quantiques [56].

Marches quantiques en temps discret en tant que dispositif de mesure

En plus de leur rôle dans les algorithmes et les simulations quantiques, les marches quantiques en temps discret peuvent également être considérées comme des dispositifs de mesure généralisés [57]. En mécanique quantique, une mesure consiste généralement à obtenir des informations sur un système quantique en le projetant sur un état avec une base précise. De même, dans une marche quantique en temps discret, la position du marcheur peut être interprétée comme un résultat de mesure. Dans le chapitre X de ma thèse, nous démontrons comment le modèle de marche quantique en temps discret peut être utilisé de manière efficace pour effectuer une interférence quantique biphoton à haute dimension et extraire la visibilité dans un système de boucle de fibres couplées.

Réalisation physique de la marche quantique en temps discret

De nombreuses propositions et réalisations expérimentales ont été faites pour réaliser physiquement différents types de marches quantiques en utilisant différentes techniques optiques et à semi-conducteurs. L'implémentation de la marche quantique en temps discret se distingue par la manière dont elle code la pièce et la position des marcheurs quantiques. Différentes plates-formes physiques ont été explorées, notamment les systèmes de pièges à ions [58], les systèmes de cavités en électrodynamique quantique [59], les qubits supraconducteurs [60] et les atomes ultra-froids [61, 62]. De plus, les marches quantiques peuvent également être mises en œuvre en utilisant des photons uniques et des éléments optiques linéaires [63, 64]. De manière surprenante, il a été découvert que la nature quantique de la lumière n'est pas essentielle pour le développement des marches quantiques. L'optique classique peut simuler les marches quantiques en utilisant une analogie interférométrique [65]. Dans l'approche classique dans les systèmes optiques, les chemins optiques sont couramment utilisés pour coder la position tandis que la polarisation est utilisée pour coder l'état de la pièce , "quantum walker's coin state", du marcheur quantique [63, 64]. Cette approche implique l'utilisation d'un maillage optique constitué d'éléments optiques spatialement séparés, de déphaseurs, de diviseurs de faisceau et d'autres composants pour construire un processeur quantique [66, 67, 67, 68]. De plus, le moment angulaire orbital (OAM) peut servir d'attribut de position et fonctionner comme une dimension synthétique pour simuler le modèle [69, 70]. Une autre approche consiste à utiliser une configuration en boucle de fibre optique qui imite le comportement d'un réseau photonique synthétique pour simuler la marche quantique de temps discret [71, 72]. Dans le cadre de ma recherche de doctorat, je résume brièvement les résultats de trois articles, comme discuté dans trois chapitres.

Lecture de la propagation de l'information quantique en utilisant des marches quantiques désordonnées

Dans le **Chapitre VII**, nous présentons un protocole de sonde quantique utilisant des marches quantiques pour étudier le modèle de propagation de l'information quantique. Nous utilisons « l'Information Quantique de Fisher » comme mesure pour quantifier les informations extraites sur un paramètre inconnu encodé dans l'évolution des marches quantiques. Bien que l'approche soit universelle, nous nous concentrons sur le désordre statique et dynamique cohérent pour étudier le transport anormal et classique, ainsi que la localisation d'Anderson.

Dans la Fig. 7.3, nous montrons comment nous pouvons détecter la transition quantique-classique en utilisant « l'Information Quantique de Fisher » lorsque le désordre dynamique est appliqué. De même, nous illustrons comment le modèle de propagation ralentit jusqu'à la sous-diffusion dans la Fig. 7.3, conduisant éventuellement à la localisation d'Anderson dans la Fig. 7.4. Pour enrichir la physique du phénomène, nous considérons deux marcheurs quantiques d'entrée, soit discernables, soit indiscernables. En général, l'état de deux particules indiscernables présente une valeur plus élevée que « l'Information Quantique de Fisher » l'état discernable. Cette propriété s'explique par le fait que l'indiscernabilité des particules est une ressource enrichissante pour la distribution de l'information quantique dans un système composite de particules identiques [16, 17, 23].

Fait intéressant, nous remarquons également que les deux états d'entrée suivent le même modèle de propagation. Nous proposons une stratégie expérimentale réalisable pour mettre en œuvre, en principe, le protocole de sonde quantique basé sur « l'Information Quantique de Fisher » en utilisant une configuration interférométrique similaire à celle de Mach-Zehnder. Nos résultats montrent qu'une marche quantique peut servir de dispositif de lecture d'informations sur les défauts et les perturbations se produisant dans des réseaux complexes, à la fois classiques et quantiques.

Amélioration des corrélations bosoniques non classiques dans un réseau de marches quantiques grâce au contrôle expérimental du désordre

Dans le **Chapitre VIII**, nous étudions théoriquement et expérimentalement le rôle du désordre et des inhomogénéités dans les réseaux quantiques. Il est important de comprendre comment les caractéristiques quantiques basées sur l'indiscernabilité se comportent dans un cadre dynamique. Pour de nombreux systèmes, le désordre joue un rôle néfaste, car il entraîne une incohérence du système [73]. Cependant, pour certains systèmes, le désordre peut améliorer les propriétés physiques telles que le transport cohérent [74], l'accélération des algorithmes quantiques [75], et les corrélations quantiques [76, 77, 78, 55]. Ces effets apparaissent généralement en raison de l'interaction avec un environnement externe, bien que ne présentant pas toujours un mécanisme de rétroaction [79, 80].

Contrairement aux études précédentes [55], les stratégies pour enrichir les corrélations à deux particules dans des modes séparés d'un réseau de marches quantiques grâce au contrôle du désordre restent à être trouvé. Ici, nous comblons cette lacune en injectant deux photons indiscernables (biphoton) dans une marche quantique discrète unidimensionnelle inhomogène et en ajustant expérimentalement des configurations de désordre spécifiques tout en maintenant le système isolé. Comme observé expérimentalement dans la Fig. 8.7, il est possible d'ajuster l'amélioration à deux modes et totale de la non-classique en position et en intensité. Cela correspond à un réseau adaptatif où l'évaluation des paramètres détermine la focalisation des ressources non classiques dans des modes sélectionnés. Ces résultats permettent d'enrichir la corrélation quantique grâce au contrôle de l'évolution unitaire (ingénierie d'Hamiltonien efficace) du biphoton. De plus, nous montrons numériquement dans la Fig. 8.4 que la moyenne sur des configurations de désordre aléatoires conduit à une diminution des corrélations quantiques initiales du biphoton. Nos résultats prouvent de manière incontestable que la présence de désordre favorise l'amélioration dynamique des corrélations quantiques du biphoton de manière contrôlable, ouvrant la voie à son utilisation potentielle dans des scénarios d'information quantique.

Génération et vérification d'états intriqués de grande dimension via des réseaux photoniques temporels

Dans le **Chapitre X**, nous présentons un processeur de marche quantique potentiellement évolutif en exploitant des réseaux photoniques temporels basés sur un système de boucles de fibres couplées. Nous utilisons un tel système pour démontrer des opérations critiques, telles que la génération de paires de photons intriqués à deux et quatre niveaux discrets dans le temps, la manipulation d'états quantiques et la vérification de l'intrication. Les modes discrets dans le temps (également appelés intervalles de temps) ont montré de nombreux avantages parmi les degrés de liberté des photons, notamment la résistance au bruit et la facilité de manipulation avec des composants standard compatibles avec les télécommunications [81, 82, 83, 84]. À cet égard, les réseaux photoniques temporels (RPT), dans lesquels les intervalles de temps sont réalisés via des retards temporels entre les impulsions optiques, offrent des plates-formes idéales pour créer des dimensions synthétiques évolutives. Les RPT peuvent être facilement mis en œuvre à l'aide de technologies de fibres accessibles et offrent d'excellents bancs d'essai pour simuler des effets intrigants tels que la symétrie temps-parité [85, 86], la superfluidité de la lumière [87], et les questions topologiques [88]. Cependant, malgré les multiples propositions d'utiliser les RPT pour le traitement quantique [89, 90, 91, 92], les mises en œuvre expérimentales sont freinées par l'inefficacité des dispositifs actuels, tels que la faible tolérance aux erreurs et les inefficacités des portes.

Nous présentons une nouvelle approche pour l'utilisation de RPT pour le traitement pratique et évolutif de l'information quantique sur des états de photons intriqués dans le temps discrets. Nous réalisons expérimentalement le réseau photonique temporel sur un système de boucles couplées entièrement intégré dans la fibre et l'utilisons pour la préparation, la manipulation et la vérification de l'état biphoton basé sur la marche quantique en temps discret [44, 92]. La polyvalence de notre réalisation nous permet de contrôler la marche d'un état biphoton de sorte qu'elle résulte en une mesure d'interférence quantique sans post-sélection pour deux niveaux. Cela permet également l'optimisation de l'évolution de la marche quantique pour une plus grande efficacité de détection et un plus grand nombre de coïncidences potentiellement pour n'importe quel nombre de niveaux. De plus, notre stratégie de mesure peut être théoriquement généralisée pour effectuer une interférence quantique pour des niveaux d'ordre d. Ainsi, la route proposée peut inspirer de nouvelles conceptions pour l'ingénierie de RPT capables de générer et de traiter des modes intriqués supérieurs à quatre et d'effectuer l'interférence quantique biphoton avec des efficacités maximales. Les marches quantiques contrôlées le long des RPT offrent une route rentable et pratique vers des opérations d'état complexes avec des instabilités considérablement réduites et des limitations de performance des nombreux éléments optiques requis pour effectuer des opérations comparables dans des dispositifs photoniques basés sur les modes de trajet et le MAO [66, 68, 93, 57]. Nous avons montré qu'une boucle de fibre dynamiquement couplée peut remplacer une cascade d'interféromètres optiques de Mach-Zehnder non équilibrés sans aucun réglage fin des retards successifs. De plus, notre mise en œuvre entièrement intégrée dans la fibre est compatible avec les infrastructures de télécommunications, étant ainsi rentable et applicable en pratique.

Remarques conclusives

En résumé, cette thèse est divisée en deux parties principales, chacune englobant des domaines distincts de recherche. Dans la première partie, quatre chapitres ont exploré différents aspects du traitement de l'information quantique en utilisant l'indistinguabilité de particules identiques. Le **Chapitre II** a introduit une nouvelle mesure d'entrelacement pour deux qubits identiques, mettant en évidence la protection de l'entrelacement non local contre le bruit de préparation grâce à l'indistinguabilité spatiale. Dans le **Chapitre III**, j'ai discuté d'une structure expérimentale pour des portes de création d'entrelacement à distance et réalisé la téléportation quantique avec des fidélités dépassant les seuils classiques. Le **Chapitre IV** a étudié la préservation de l'entrelacement pendant les dynamiques de système ouvert sous l'indistinguabilité spatiale. Dans le **Chapitre V**, une méthode de distillation de l'entrelacement a été présentée, maximisant l'entrelacement à partir d'états mixtes par chevauchement spatial et ex-

aminant l'influence des paramètres de bruit et des températures. Ces chapitres ont contribué à notre compréhension du traitement de l'information quantique en utilisant l'indistinguabilité, offrant des perspectives précieuses pour des applications pratiques. Ces dernières années, l'intérêt de la recherche pour le concept de superposition spatiale de particules identiques dans différentes régions a augmenté pour exploiter l'effet de l'indistinguabilité dans le traitement de l'information quantique. Des études antérieures ont démontré que l'indistinguabilité peut être utilisée pour effectuer diverses tâches de traitement de l'information quantique telles que la téléportation [16, 23], l'estimation quantique [94, 31], et la distribution d'entrelacement entre les nœuds d'un réseau quantique [28, 26].

De nombreuses conceptions théoriques et expérimentales ont été proposées pour exploiter l'indistinguabilité pour générer de l'entrelacement. Ces conceptions vont de l'extension de la génération de ressources bipartites de plusieurs particules [25, 95], à l'utilisation d'approches basées sur la théorie des graphes pour générer des états multipartites complexes à l'aide de réseaux quantiques linéaires [96]. En nous appuyant sur ces études, nous avons développé un schéma général et contrôlable pour générer une classe complète d'états intriqués multipartites, notamment les états W, Dicke, GHZ et de regroupement (ce travail est en cours de préparation pour soumission prochaine). Notre schéma repose sur des opérations spatialement localisées et une communication classique. De plus, la concurrence d'entrelacement basée sur sLOCC, comme introduite dans la référence [17], a permis aux chercheurs d'étudier la monogamie d'entrelacement [97], d'étudier l'entrelacement dans les systèmes anioniques [98, 99], et bien plus encore. De plus, nous avons proposé un protocole de récupération de l'entrelacement dû à l'effet d'indistinguabilité [100, 101]. Des développements récents ont également motivé l'ingénierie robuste d'états intriqués de manière maximale [35, 102]. Cependant, la vérification expérimentale de la préservation de l'entrelacement reste un domaine prospectif majeur pour nos schémas proposés. Dans le domaine de la thermodynamique quantique, il a été démontré que l'indistinguabilité peut jouer un rôle en tant que carburant dans les moteurs quantiques pour améliorer la conversion d'information en travail [36, 37, 38] ce qui conduit à une efficacité plus élevée à puissance maximale dépassant la limite classique de Curzon-Ahlborn [39]. Dans un travail en préparation, nous proposons une machine de refroidissement quantique cyclique basée sur l'indistinguabilité qui peut refroidir les particules du système à une très basse température. Néanmoins, l'indistinguabilité spatiale ou le chevauchement spatial, comme discuté dans le **Chapitre VI**, est prévu d'être observé. Nous pouvons évaluer l'indistinguabilité spatiale en mesurant la probabilité de trouver des particules dans chaque région. Par exemple, si la probabilité de trouver une particule dans chaque région est égale à un, alors les deux particules sont spatialement distinguables. Quantifier une telle mesure est une perspective immédiate.

Dans la partie II de ma thèse, trois articles de recherche ont été présentés, correspondant chacun à un chapitre séparé et publié ou soumis dans des revues à comité de lecture. Le **Chapitre VII** introduit un protocole de sonde basé sur les marches quantiques discrètes, permettant la détection des désordres cohérents statiques et dynamiques, ainsi que l'étude des phénomènes de transport et de localisation d'Anderson. Ce protocole offre une stratégie expérimentale réalisable pour la sonde quantique en utilisant l'information quantique de Fisher. Le **Chapitre VIII** explore le rôle du désordre contrôlé dans l'amélioration de la corrélation quantique entre deux photons identiques. Les résultats indiquent que des configurations de désordre soigneusement imposées peuvent améliorer les corrélations quantiques, dépassant celles observées dans les marches quantiques ordonnées. Enfin, le **Chapitre IX** présente un processeur de marches quantiques discrètes évolutif utilisant des réseaux photoniques temporels. Ce processeur permet de générer, de manipuler et de tester l'entrelacement de modes de temps de haute dimension. La démonstration expérimentale met en évidence le contrôle de l'interférence quantique biphoton de haute dimension et met en évidence le potentiel des réseaux photoniques temporels en tant que circuits photoniques quantiques reconfigurables. En perspective, nos recherches ouvrent plusieurs voies d'exploration. Premièrement, il est possible d'étudier différents types de désordres, y compris les désordres spatiotemporellement corrélés, pour mieux comprendre leurs effets sur les systèmes quantiques. En outre, l'étude du rôle du désordre dans les marches quantiques avec des fermions pourrait fournir des perspectives précieuses. De plus, il reste à voir si le désordre peut améliorer les corréla-

tions quantiques entre plus de deux particules, ce qui pourrait avoir des implications importantes dans les théories des ressources quantiques. Une autre perspective passionnante est la possibilité de concevoir des réseaux photoniques synthétiques capables de générer et de traiter des modes intriqués avec des dimensions supérieures à quatre. Cela permettrait de manipuler efficacement l'interférence quantique biphoton et conduirait à des avancées en tomographie quantique, en discrimination de phase et en détection. Globalement, nos recherches ouvrent la voie à la mise au point de concept et de protocoles innovants dans le domaine du traitement de l'information quantique. En conclusion, cette thèse met en évidence l'importance de l'indistinguabilité en tant que ressource précieuse pour les tâches de traitement de l'information quantique. Elle met également en évidence les perspectives prometteuses pour de nouvelles avancées dans ce domaine. De plus, la thèse démontre la polyvalence du modèle de marche quantique et son applicabilité dans les plates-formes optiques quantiques avec différents degrés de liberté. Tout au long de la thèse, nous avons approfondi et analysé divers sujets d'intérêt pour la communauté scientifique travaillant dans les sciences et technologies quantiques. L'impact substantiel de notre travail peut être observé à travers les publications référencées dans ce texte. Cependant, la véritable valeur de cette thèse réside non seulement dans les connaissances acquises en explorant divers sujets liés à l'information quantique, mais aussi dans l'expérience pratique acquise en travaillant avec différents cadres théoriques et en collaborant avec de nombreux chercheurs différents.

Contents

List of publications

Here, I provide my entire publication list, including thirteen published papers, one under review, and one under submission. I have collaborated with various colleagues during my Ph.D. research. This is why I explicitly describe my contribution to each paper in the list.

1. **Farzam Nosrati**, Alessia Castellini, Giuseppe Compagno, and Rosario Lo Franco. Robust entanglement preparation against noise by controlling spatial indistinguishability. *npj Quant. Inf.*, 6(1):1–7, 2020.

   The author is the main contributor to this project. In particular, he performed the main calculations and numerical simulation, contributed to proposing ideas, and prepared the paper.

2. Kai Sun, Yan Wang, Zheng-Hao Liu, Xiao-Ye Xu, Jin-Shi Xu, Chuan-Feng Li, Guang-Can Guo, Alessia Castellini, **Farzam Nosrati**, Giuseppe Compagno, and Rosario Lo Franco. Experimental quantum entanglement and teleportation by tuning remote spatial indistinguishability of independent photons. *Opt. Lett.*, 45(23):6410–6413, 2020.

   The author provided feedback on the performed experiment, proposing ideas and contributing to preparation of the paper.

3. **Farzam Nosrati**, Alessia Castellini, Giuseppe Compagno, and Rosario Lo Franco. Dynamics of spatially indistinguishable particles and quantum entanglement protection. *Phys. Rev. A*, 102(6):062429, 2020.

   The author is the main contributor to this project. In particular, he performed the main calculations and numerical simulation, contributed to proposing ideas, and prepared the paper.

4. **Farzam Nosrati**, Bruno Bellomo, Gabriele De Chiara, Giuseppe Compagno, Roberto Morandotti, and Rosario Lo Franco. Indistinguishability-assisted two-qubit entanglement distillation. *arXiv preprint*, arXiv:2305.11964, 2023.

   The author is the main contributor to this project. In particular, he performed the main calculations and numerical simulation, contributed to proposing ideas, and prepared the paper.

5. **Farzam Nosrati**, Alessandro Laneve, Mahshid Khazaei Shadfar, Andrea Geraldi, Kobra Mahdavipour, Federico Pegoraro, Paolo Mataloni, and Rosario Lo Franco. Readout of quantum information spreading using a disordered quantum walk. J. Opt. Soc. Am. B, 38(9):2570–2578, Sep 2021.

   The author is the main contributor to this project. In particular, he performed the main calculations and numerical simulation, contributed to proposing ideas, and prepared the paper.

6. Alessandro Laneve, **Farzam Nosrati**, Andrea Geraldi, Kobra Mahdavipour, Federico Pegoraro, Mahshid Khazaei Shadfar, Rosario Lo Franco, and Paolo Mataloni. Enhancing nonclassical bosonic correlations in a quantum walk network through experimental control of disorder. Phys. Rev. Research., 3:033235, 2021.

   The author is the main contributor to this project. In particular, he performed the main calculations and numerical simulation, contributed to proposing ideas about the performed experiment, and prepared the paper.

7. Monika Monika[†], **Farzam Nosrati**[†], Agnes George, André Luiz Marques Muniz, Arstan Bisianov, Stefania Sciara, Mario Chemnitz, Rosario Lo Franco, Ulf Peschel, and Roberto Morandotti. Generation and bi-photon quantum interference of high-dimensional entangled states via temporal photonic lattices. *To be submitted*.

   The author is the main contributor to this project. In particular, he performed the main calculations and numerical simulation, contributed to proposing ideas about the performed experiment, and prepared the paper.

The following publications are not included in this thesis

8. Alireza Dehghani, Bashir Mojaveri, Rasoul Jafarzadeh Bahrbeig, **Farzam Nosrati**, and Rosario Lo Franco. Entanglement transfer in a noisy cavity network with parity-deformed fields. *J. Opt. Soc. Am. B*, 36(7):1858–1866, 2019.

   The author provided feedback on the performed calculations, ideas and contributed to the preparation of the paper.

9. Hossein Gholipour, Ali Mortezapour, **Farzam Nosrati**, and Rosario Lo Franco. Quantum- ness and memory of one qubit in a dissipative cavity under classical control. *Ann. Phys.*, 414:168073, 2020.

   The author proposed ideas, performed calculations for a specific part, and contributed to the preparation of the paper.

10. **Farzam Nosrati**, Ali Mortezapour, and Rosario Lo Franco. Validating and controlling quan- tum enhancement against noise by the motion of a qubit. *Phys. Rev. A*, 101:012331, 2020.

    The author is the main contributor to this project. In particular, he performed the main calculations a specific part, contributed to proposing ideas, and prepared the paper.

11. Matteo Piccolini, **Farzam Nosrati**, Giuseppe Compagno, Patrizia Livreri, Roberto Moran- dotti, and Rosario Lo Franco. Entanglement robustness via spatial deformation of identical particle wave functions. *Entropy*, 23:708, 2021.

    The author is one of the main contributors to this project. In particular, he contributed to performing the main calculations, proposed ideas, and prepared the paper.

12. Matteo Piccolini, **Farzam Nosrati**, Roberto Morandotti, and Rosario Lo Franco. Indistinguishability enhanced entanglement recovery by spatially localized operations and classical communication. *Open Syst. Inf. Dyn.*, 28(04):2150020, 2021.

    The author provided feedback on the performed calculations, ideas, and contributed to the preparation of the paper.

13. Negar Nikdel Yousefi, Ali Mortezapour, Ghasem Naeimi, **Farzam Nosrati**, Aref Pariz, and Rosario Lo Franco. Quantum enhancement of qutrit dynamics through driving field and photonic-band-gap crystal. *Phys. Rev. A*, 105:042212, 2022

The author proposed ideas, performed calculations for a specific part, and contributed to the preparation of the paper.

14. Amin Rajabalinia, Mahshid Khazaei Shadfar, **Farzam Nosrati**, Ali Mortezapour, Roberto Morandotti, and Rosario Lo Franco. Quantumness and speedup limit of a qubit under transition-frequency modulation. *Phys. Rev. A*, 106:062431, 2022.

    The author provided ideas, performed calculations for a specific part, and contributed to the preparation of the paper.

15. Matteo Piccolini, **Farzam Nosrati**, Gerardo Adesso, Roberto Morandotti, and Rosario Lo Franco. Generating indistinguishability within identical particle systems: spatial deformations as quantum resource activators. Phil. Trans. R. Soc. A, in press. *arXiv preprint*, arXiv:2205.12136, 2022.

    The author provided feedback on the performed calculations, ideas, and contributed to the preparation of the paper.

List of Figures

List of Tables

General introductory remarks

This ongoing doctoral dissertation introduces novel research that focuses on the characterization and preservation of quantum resources in composite quantum systems. Part I of the study primarily explores the concept of indistinguishability among identical particles, which is a pivotal resource for quantum information processing. Moving to Part II, the thesis delves deeply into the controllable dynamics of indistinguishable particles, specifically emphasizing photons, as they propagate through diverse quantum photonic configurations. These setups have the potential to serve as promising photonic-based processors for advancing quantum technologies. The driving force behind the investigation stems from the fact that identical particles, such as photons and electrons, serve as the foundational building blocks of our quantum-enhanced technologies. Therefore, it is crucial to establish a robust operational framework for handling these particles, especially when they spatially overlap, resulting in their indistinguishability and individual unaddressability. This becomes even more vital when the aim is to dynamically control the evolution of these identical quantum entities, as observed in the propagation of a few identical photons in quantum optics platforms. These composite systems have the potential to offer non-classical advantages, which can be harnessed for a multitude of quantum information tasks, surpassing classical alternatives.

As I delve into further detail in the introductory remarks, it is important to note that the terms "identical particles" and "indistinguishable particles" are often used interchangeably in much of the literature. However, "identical particles" specifically refer to elementary quantum particles that typically share the same intrinsic properties, such as mass and spin. On the other hand, "indistinguishable" arises from the type of measurement that an observable may choose to take. For instance, when two photons are in the same optical path with different polarizations, they are indistinguishable to an observer measuring their locations, but distinguishable when their polarizations can be measured.

Nevertheless, when these identical entities become indistinguishable, they exhibit collective behaviors that differ from those of classical particles. Indistinguishability, being a genuinely quantum property, gives rise to two fundamental traits inherent in these building blocks of the Universe: the symmetrization postulate and the spin-statistics theorem [6, 103]. The symmetrization postulate asserts that when the state of any two particles is exchanged, the global state or wavefunction of a system of identical particles can exhibit either symmetry, remaining unchanged, or antisymmetry, leading to a change in sign. This leads to classifying identical particles into two types based on this collective behavior: bosons, which adhere to Bose-Einstein statistics and can occupy the same single-particle state, and fermions, which follow Fermi-Dirac statistics and are prohibited from occupying identical quantum states due to the Pauli exclusion principle. The exchange symmetry associated with the symmetrization postulate governs how identical particles combine to form complex structures of light and matter in nature. In fact, this phenomenon is the reason behind electron orbital occupation and photon bunching. For instance, particle statistics, whether bosonic, fermionic, or even anyonic, fundamentally influence the dynamics of two identical entities as they navigate various networks, ultimately resulting in different probability distributions at the output. In fact, when multiple identical particles co-propagate in the same medium, quantum correlations present in the initial state, or induced by the quantum statistics of the involved particles, influence the overall wavefunction evolution.

Apart from these foundational aspects, systems consisting of indistinguishable particles also carry

significant technological implications. Indeed, indistinguishable particles serve as the essential constituents of complex quantum networks designed for tasks related to quantum information and computation. As I elaborate further in the introductory remarks, the true physical essence of entanglement among identical particles has been a topic of discussion, mainly due to the conventional portrayal of (anti)symmetric states of the entire system through non-observable labels assigned to the particles. In the words of Asher Peres [1], "Two particles of the same kind are always entangled, even if they are independently prepared far apart in different laboratories..." It's important to reassure ourselves that this entanglement is not a cause for concern.

Among several frameworks, the concept of spatially local operation and classical communication (sLOCC) [16] within the no-labeling formalism [2, 3] has been introduced to quantify and harness the entanglement of spatially identical particles. During my Ph.D., I extend the previous approach [16] to encompass arbitrary mixed states by introducing a novel entanglement measure for two identical qubits [17] (see Chapter II). Bringing two independent identical photons together and rendering them spatially indistinguishable enables entangling gates [16] that have been experimentally realized through various setups [23, 24] (see Chapter III). This concept is generalized to multi-partite entangled state generation schemes, where indistinguishability serves as a direct resource [25, 95]. Furthermore, indistinguishability is an exploitable resource in quantum information processing, such as quantum [16, 23], quantum estimation [94, 31], and entanglement distribution of identical particles between nodes of a quantum network [28, 26].

Realistic quantum systems are inevitably influenced by their surrounding environment, much like the propagation of photons in media with random disorder. This is why crucial quantum resources, such as coherence and entanglement, tend to degrade within the system. Even a minor perturbation can lead the entire system towards the phenomenon of decoherence [40]. The challenge of preserving these quantum resources is a significant one in the field of quantum information and computation. To address this challenge, various protection schemes have been devised, including error correction, utilizing structured environments [104, 105, 106], decoherence-free subspaces [107, 108], dynamical decoupling and control techniques [109, 110, 111],

quantum error corrections [112, 113, 114] and topological properties [115, 116], and others. Throughout my Ph.D., as presented in chapters II, IV, and V, I demonstrate that maintaining the indistinguishability of two identical particles can uphold the quantum correlation between them [17, 117, 118]. These findings contribute to our comprehension of how indistinguishability provides valuable protection mechanisms for entanglement among identical particles, with the potential for practical applications.

In the subsequent phase of my Ph.D., I venture into an exploration of how identical particles propagate through disordered networks and the role that indistinguishability plays in this context. Quantum walks [44], which extend the classical notion of random walks, were selected as the framework to model the propagation of one and two identical particles in optical networks with and without disorders. Quantum walks, characterized by their interference and superposition properties leading to nonclassical dynamic evolution, serve as a valuable model to describe transport phenomena across various networks. They also serve as a valuable computational model for quantum information computation. Furthermore, a quantum walk involving two or more indistinguishable particles can yield additional computational power, scaling exponentially with the resources used [119] (see chapter VI for more details on quantum walk).

To explore the effects of disorder on the evolution of identical particles, I first delve deeply into the quantum walk model in which disorder results in different propagation behaviors, namely normal, anomalous, and Anderson localization. Consequently, in chapter VII, I propose interferometric detection schemes based on the quantum Fisher information figure of merit to observe these distinct propagation behaviors in various randomized networks involving one or a few identical particles [120]. Subsequently, in chapter VIII, I conduct analyses to explore what happens when indistinguishable photons propagate in ordered networks. This investigation revealed that the non-classical correlation resulting from indistinguishability tends to fade away after a few steps. To address this, I introduced a controllable walk designed to maintain the indistinguishability and non-classical correlation between the two photons [56].

This evidence empirically underscores that the controllable propagation of indistinguishable photons depends significantly on maintaining correlations within the quantum network. Lastly, in chapter chapter IX, I introduce a dynamically controllable quantum system capable of measuring biphoton quantum interference across various dimensions. This dynamic reconfigurability, facilitated by a coupled fiber-loop system circuitry, is crucial in controlling the walk and realizing its full operational potential. The outcomes of this research offer practical approaches to harnessing synthetic dimensions for the efficient execution of quantum algorithms, including tasks such as quantum phase estimation or boson sampling.

Part I

Indistinguishability of identical particles as genuine quantum resource for quantum information processing

Chapter 1

Introductory remarks I

In **Part I** of my PhD thesis, I investigate the indistinguishability of identical particles as a genuine quantum resource for quantum information processing. It consists of chapters based on previously published papers in reputable scientific journals. Before presenting the results, I briefly introduce the topic by addressing the following questions:

1. What is the physical concept behind identity and non-individuality of quantum entities?
2. Do states of two identical particles in the form $|\phi_1\rangle \otimes |\phi_2\rangle \pm |\phi_2\rangle \otimes |\phi_1\rangle$ exhibit true entanglement, as their form would suggest? Establishing a concept of entanglement that is both physically meaningful and practically applicable is of utmost importance.
3. What are the underlying frameworks for quantifying and characterizing entanglement between identical particles?
4. Can the indistinguishability of identical particles serve as a non-classical resource for performing quantum information processing tasks?

These questions form the basis for further exploration and understanding of systems made of identical particles (e.g., qubits, two-level atoms, photons, electrons, quasiparticles), which constitute the elementary building blocks (particles) of quantum networks. This task becomes particularly significant in integrated architectures with inherently significant quantum operations. Encouraging progress has been made in this area across various quantum platforms, including ultracold atoms, quantum optics, and quantum fields. As a starting point, let us begin with the fundamental concepts of identity and indistinguishability.

1.1 Identity vs indistinguishability

In our daily lives, we come across numerous objects that we perceive as individuals. The notion of individuality arises from the fact that each object possesses unique properties that allow an observer to set them apart. According to Leibnizian reductionism [121], precisely these distinct properties render material objects individual. In other words, an object can be understood as nothing more than a collection or "bundle" of properties. Even objects that appear remarkably similar, such as identical twins, possess slight differences in their properties that allow us to distinguish between them. For instance, classical mechanics imply that repulsive forces between particles become stronger as the particles get close, preventing the particles from occupying the exact spatial location. Consequently, any two particles can be distinguished by their distinct spatial locations. This implies that no two objects can possess precisely the same set of properties, ensuring their true individuality. This is why classical particles are considered distinguishable, as distinct bundles can describe their properties.

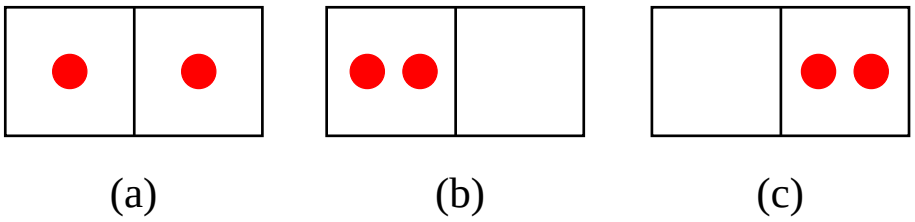

Figure 1.1: Schematic illustration depicting two identical particles within a box, where an observer may attempt to locate them on both sides.

However, this classical approach has faced criticism based on the principles of quantum mechanics [121]. Quantum mechanics has demonstrated that elementary quantum particles, such as electrons, can exhibit a property known as indistinguishability. Consequently, these particles possess identical intrinsic properties, including rest mass, charge, and spin. In fact, regardless of their spatial locations within the universe, every electron will consistently exhibit the same mass, charge, and other intrinsic characteristics as any other electron. Hence, two electrons can possess an exact identical set of property bundles, distinct from classical particles that are always distinguishable. The indistinguishability of quantum particles challenges the conventional understanding of individuality and necessitates a different conceptual framework to comprehend their behavior.

In addition to state-independent or intrinsic properties, quantum mechanics incorporates state-dependent properties to describe elementary quantum systems [122]. Consequently, it becomes possible to differentiate between particles by employing a set of measurements that rely on state-dependent properties. For instance, a polarizer can discern vertically polarized photons from horizontally polarized ones. As a result, an alternative approach to distinguishing identical objects is to adopt a field-theoretic perspective in which particles are represented as dichotomic "Yes/No" fields. In this framework, the field amplitude is assigned a value of "Yes" at a particular location if the particle is present and "No" if it is not [123].

In conclusion, while identity mainly refers to the intrinsic properties of identical things, indistinguishability is a consequence of measurement outcomes. Objects can still be distinguished and regarded as identical if they share common state-independent properties. On the other hand, if the particles are taken to possess both their intrinsic and state-dependent properties in common, they cannot be distinguished from one another. The fact that identical particles cannot be distinguished has a necessary consequence. It allows us to view collections of classical and quantum particles, providing a different perspective on how they behave. This immediately raises the difference between classical and different quantum statistics. This argument is not solely related to the lack of individuality of the particles but rather in terms of which states are accessible to them [122]. With this, I will begin the following discussion on the state of quantum non-individuality.

1.2 Quantum non-individuality

I would like to begin the discussion in this section with a toy model. Let us consider the distribution of two indistinguishable particles across two sides of a box or two general states, as illustrated in Fig. 1.1. An observer attempts to count the particles in both regions, which could result in two particles on each side of the box or one particle on the left and one on the right.

According to classical physics, case Fig. 1.1 (a) has twice the weight of case Fig. 1.1 (b) or case Fig. 1.1 (c). This is because there are two ways to achieve case (a) by permuting the particles. For instance, if we assume that the four combinations are equally probable, the probability of finding one particle on each side is $1/2$. This example demonstrates the well-known Maxwell-Boltzmann statistics.

In quantum statistical mechanics, there are two common forms. The first form has three possible arrangements in the given situation: finding both particles on the same side of the box (cases Fig. 1.1 (b) and Fig. 1.1 (c)), and finding one particle on each side of the box (case Fig. 1.1 (a)), which corresponds

to Bose-Einstein statistics. Again, assuming equal probabilities for all three cases, each case has a probability of $1/3$, known as Bose-Einstein statistics. However, fermions obey Fermi-Dirac statistics, which underpins the Pauli Exclusion Principle, resulting in the observable outcome of finding both particles on each side of the box. It is important to note that rearranging particles through permutation in quantum statistics is not considered as creating a new arrangement, despite the differences between the two types of quantum statistics. This result lies at the very heart of quantum physics, known as the *indistinguishability postulate*: If a particle permutation is applied to any state function for an assembly of particles, then there is no way to distinguish the resulting permuted state function from the original unpermuted one through any observation at any time. In this sense, Bose-Einstein statistics correspond to a symmetric state function for the assembly of particles, while Fermi-Dirac statistics correspond to an anti-symmetric state function.

To understand the emergence of symmetric and anti-symmetric states, I will assign elementary states to each particle in a formal manner. Let us assume there is a particle in the $\{\alpha\}$ single-particle state, where $\{\alpha\}$ is associated with the eigenvalues of a group of commuting observables. Similarly, another particle is in the $\{\beta\}$ state. I will label one of the particles as "1" and the other as "2." However, due to uncertainty about the identity of the particles, we cannot determine whether our system is in the state $|\Psi\rangle = |\{\alpha\}\rangle_1 \otimes |\{\beta\}\rangle_2$ or $|\Psi\rangle = |\{\alpha\}\rangle_2 \otimes |\{\beta\}\rangle_1$, or even a linear combination of the two, given as $|\Psi\rangle = a\,|\{\alpha\}\rangle_1 \otimes |\{\beta\}\rangle_2 + b\,|\{\alpha\}\rangle_2 \otimes |\{\beta\}\rangle_1$, where the state is normalized as $|a|^2 + |b|^2 = 1$. This is known as exchange degeneracy [6].

Even though the particles exist in the same physical state, they have different mathematical descriptions due to the inclusion of labels 1 and 2. These labels are known as quantum numbers and make the particles non-identical, even though they are fictitious and impossible to observe. Essentially, no measurement performed on each particle can provide complete knowledge of the exact form of the state $|\Psi\rangle$. This is because different mathematical possibilities arise from quantities that cannot be physically observed.

One way to address this issue is by considering exchange degeneracy or the symmetrization postulate [6]. According to this postulate, particles characterized by a symmetric state are referred to as bosons, while those described by an anti-symmetric state are known as fermions. In the previously considered two-particle example, the state $|\Psi\rangle$ is uniquely represented by setting $a = b = \dfrac{1}{\sqrt{2}}$ for bosons and $a = -b = \dfrac{1}{\sqrt{2}}$ for fermions. Therefore, the symmetric and anti-symmetric states are written as follows:

$$\begin{aligned} |\Psi_{\text{sym}}\rangle =& \frac{1}{\sqrt{2}} \left(|\{\alpha\}\rangle_1 \otimes |\{\beta\}\rangle_2 + |\{\alpha\}\rangle_2 \otimes |\{\beta\}\rangle_1 \right), \\ |\Psi_{\text{asym}}\rangle =& \frac{1}{\sqrt{2}} \left(|\{\alpha\}\rangle_1 \otimes |\{\beta\}\rangle_2 - |\{\alpha\}\rangle_2 \otimes |\{\beta\}\rangle_1 \right). \end{aligned} \tag{1.1}$$

The symmetrization postulate ensures that particles in the same physical state exhibit different symmetry properties in their mathematical descriptions, leading to distinct behavior under particle permutations for bosons and fermions. Bosonic states remain unchanged when particles are exchanged, while fermionic states switch signs with a π phase change. Also, Pauli's exclusion principle, a direct consequence of the symmetrization postulate, prohibits two or more fermions from simultaneously occupying the same quantum state. This classification has profound implications in quantum field theory, condensed matter physics, and particle physics. However, the mathematical description represented by Eq. 1.1, which embodies the symmetrization postulate, suggests that two identical particles, whether fermions or bosons are always entangled [1]. This raises the question of whether this entanglement is physically observable or simply a consequence of the mathematical descriptions of the symmetrization postulate. To address this question, I will provide a brief overview of the entanglement measures for identical particles in the following sections.

1.3 Entanglement of identical particles

This section explores the challenges of characterizing entanglement between identical particles using mocking labels. These challenges are rooted in the need for (anti)symmetrization of states and labeling of particles, which create difficulties in both methodology and practicality. Additionally, traditional methods and criteria for studying entanglement between non-identical particles are not directly applicable to identical particles [1]. Firstly, I will briefly review the standard description of entanglement that uses mocking labels to quantify and characterize labels.

1.3.1 First quantization approach (standard approach)

Consider a system denoted as S, consisting of two non-identical particles labeled as 1 and 2. Suppose that the entire system is described by a pure state, denoted as $|\Psi\rangle$, which lives in the two single-particle Hilbert spaces, $\mathcal{H}_1$ and $\mathcal{H}_2$, that together make up the Hilbert space of the two-particle system, denoted as $\mathcal{H}_S$. In the case where the state $|\Psi\rangle = |\phi\rangle_1 \otimes |\chi\rangle_2$, where $|\phi\rangle_1 \in \mathcal{H}_1$ and $|\chi\rangle_2 \in \mathcal{H}_2$, is separable, it reflects the tensor product structure of the total Hilbert space. In other words, the state can be expressed as a product of the individual states associated with each particle. However, such a particular case is itself a subset of the total set, implying that we cannot find entangled states in the tensor product structure.

The degree of entanglement is commonly measured using the Schmidt decomposition of the state [15]. We define the bipartite state as $|\Psi\rangle = \sum_{i=1}^{r} \sqrt{\lambda_i} |\phi_i\rangle_1 \otimes |\chi_i\rangle_2$, based on two basis vectors $|\phi_i\rangle_1$ and $|\chi_i\rangle_2$ in the orthonormal single-particle Hilbert spaces $\mathcal{H}_1$ and $\mathcal{H}_2$, where λ_i are non-negative real numbers known as Schmidt coefficients that satisfy $\sum_i \lambda_i = 1$. These basis vectors are the eigenstates of the single-particle reduced density matrices $\hat{\rho}_1 = \mathrm{Tr}_2[|\Psi\rangle \langle\Psi|]$ and $\hat{\rho}_2 = \mathrm{Tr}_1[|\Psi\rangle \langle\Psi|]$, obtained by tracing out the degrees of freedom of the other particle. Then, the von Neumann entropy is a commonly used measure for quantifying entanglement between two particles, given by

$$S(\hat{\rho}_1) = S(\hat{\rho}_2) = -\sum_i \lambda_i \log_2 \lambda_i. \tag{1.2}$$

Here, This measure reflects our lack of knowledge about the states of the individual subsystems. A pure state of a bipartite system is separable if and only if its Schmidt coefficient is equal to 1.

On the contrary, let us examine the scenario where the two particles are indistinguishable, and assume that one occupies the single-particle state $|\phi\rangle$ and the other occupies the state $|\chi\rangle$. For non-identical particles, the labels 1 and 2 are physical properties that differentiate them, but for identical particles, they are not physically observable. In the case of indistinguishable particles, the two-particle state $|\Psi\rangle$ in the first quantization approach is given by

$$|\Psi\rangle_{\pm} = \frac{1}{\sqrt{2}}(|\phi\rangle_1 \otimes |\chi\rangle_2 \pm |\phi\rangle_2 \otimes |\chi\rangle_1), \tag{1.3}$$

where $+$ is for bosons and $-$ is for fermions. Due to the presence of labels 1 and 2 and the symmetrization postulate, two identical particles are always entangled, even if they were prepared independently in different laboratories and were far away from each other, as can be shown by Von Neumann's entropy. In fact, when one trace out either particle 1 or 2 to obtain the single-particle reduced density matrix, denoted as $\hat{\rho}^{(1 \text{ or } 2)} = \mathrm{Tr}_2[|\Psi\rangle \langle\Psi|] = \mathrm{Tr}_1[|\Psi\rangle \langle\Psi|]$, this operation is physically meaningless. The lack of knowledge about the state is not due to any real physical correlation between the particles but rather a consequence of the mathematical labels used to describe the state. This operation serves as a measure of the unphysical entanglement resulting from these fictitious labels [1].

Furthermore, in the scenario described above, particles are treated as distinguishable, and their statistics are considered irrelevant to their dynamics or correlations. However, in certain situations, like in quantum dot systems, two identical particles may occupy the same spot. In such cases, the statistics of the particles must be considered and play a crucial role in determining their dynamics and correlations [124, 125, 126]. In such situations, it becomes vague how to measure the physical entanglement of states

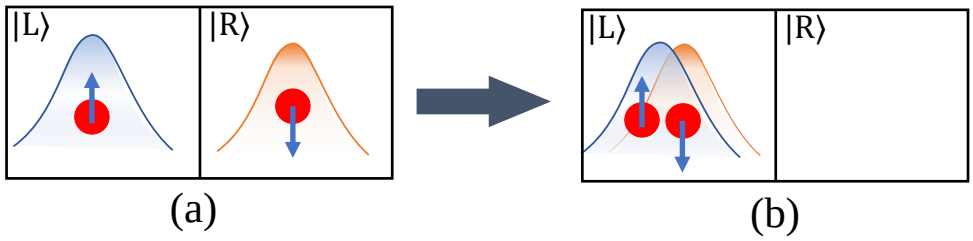

Figure 1.2: Schematic illustration depicting two identical particles within a box with two distinct regions: (a) Both particles are in different regions, and (b) Both particles are in the same region.

that involve identical particles occupying the same spatial regions with opposite pseudospins. Differentiating between formal correlations caused by fictitious labels and genuine physical entanglement poses a challenge.

1.3.2 No-label approach to identical particles

In the previous subsection, I have discussed the challenges faced in detecting and quantifying entanglement between identical particles using the first quantization approach. In order to tackle this issue, an alternative approach known as the "no-label" approach to identical particles has been proposed [2, 3]. This approach avoids using non-observable properties for identical particles and instead relies on observables to define states.

As a brief recap of the no-label approach, let us consider two identical particles in separate spatial regions labeled as L and R. Let $|\phi\rangle$ and $|\chi\rangle$ represent the states of these particles, respectively. It is worth noting that performing single-particle measurements using devices localized in regions L and R does not affect the physical predictions. Therefore, the effect of symmetrization, solely due to the particles being identical, is irrelevant in this context [4, 5, 6, 7]. Consequently, the single-particle density matrix is calculated by treating the labels L (R) without applying symmetrization. Therefore, the initial state is a factorized state $|\Psi\rangle = |\phi\rangle_{\mathrm{L}} \otimes |\chi\rangle_{\mathrm{R}}$, which applies to both bosons and fermions.

Also, a one-particle state is defined by a complete set of commuting observables in the no-label approach. Thus, the state is represented as a list of one-particle states: $|\phi_1\rangle$ and $|\phi_2\rangle$. Since this representation cannot be expressed as a tensor product of one-particle vector states, we fully characterize the state by listing the states as $|\phi_1, \phi_2\rangle / \sqrt{\mathcal{N}}$, where $\mathcal{N}$ is a normalization factor.

In the operational context, a one-particle operator $A^{(1)}$ acts on a two-particle state one at a time, resulting in $A^{(1)} |\Psi\rangle := |A^{(1)}\phi_1, \phi_2\rangle + |\phi_1, A^{(1)}\phi_2\rangle$, according to the standard definition [6]. The action of a one-particle operator is given by $A^{(1)} = \sum_{i,j} a_{ij} |\psi_i\rangle \langle\psi_j|$ in a general form, obtained by a symmetric inner product between state spaces of different dimensions. The inner product can be expressed as [2]:

$$\langle\psi_k |\phi_1, \phi_2\rangle := \langle\psi_k |\phi_1\rangle |\phi_2\rangle + \eta \langle\psi_k |\phi_2\rangle |\phi_1\rangle , \tag{1.4}$$

where $\eta = 1$ (-1) represents bosonic or fermionic statistics. The Eq. (1.4) above represents the unnormalized reduced one-particle pure state obtained after projecting a two-particle state onto $|\psi_k\rangle$ (one-particle projective measurement). Similarly, the symmetric inner product between state spaces of two-particle vector state is given by

$$\langle\phi_1', \phi_2' |\phi_1, \phi_2\rangle := \langle\phi_1' |\phi_1\rangle \langle\phi_2' |\phi_2\rangle + \eta \langle\phi_1' |\phi_2\rangle \langle\phi_2' |\phi_1\rangle . \tag{1.5}$$

The expression arises from the indistinguishability effect, where the probability amplitude of finding one particle in state ϕ_1' (ϕ_2') arises from the possibility of having one particle in either state ϕ_1 or ϕ_2.

The no-label approach [2] provides fundamental preliminary results that allow us to quantify the entanglement of two identical particles. This quantification can be achieved by evaluating the von Neumann entropy of the one-particle reduced density matrix obtained from a localized partial trace. The

reduced density matrix, denoted as $\hat{\rho}^{(1)} = \mathrm{Tr}^{(1)}\left[|\Psi\rangle\langle\Psi|\right]/\mathcal{M}$, where $\mathcal{M}$ is a normalization constant such that $\mathrm{Tr}^{(1)}\left(\hat{\rho}^{(1)}\right) = 1$, and the partial trace is given by $\mathrm{Tr}^{(1)}\left(|\Psi\rangle\langle\Psi|\right) = \sum_k \langle\psi_k|\phi_1,\phi_2\rangle$. Thus, the degree of entanglement is given by (1.2). To illustrate this point, let us consider the scenario of two identical particles in different sites, as shown in Fig. 1.2(a). One particle is in the state $|\phi\rangle = |\mathrm{L}\downarrow\rangle$, where L represents the spatial mode and $\downarrow$ represents the pseudospin. The other particle is in the state $|\chi\rangle = |\mathrm{R}\uparrow\rangle$. Thus, the global quantum state is $|\Psi\rangle = |\mathrm{L}\uparrow,\mathrm{R}\downarrow\rangle$. Performing the partial trace on region L, given as $\hat{\rho}^{(1)}_{\mathrm{R}} = \mathrm{Tr}_{\mathrm{L}}\left[|\Psi\rangle\langle\Psi|\right]$ result in a separable state as

$$\hat{\rho}^{(1)}_{\mathrm{R}} = |\mathrm{R}\downarrow\rangle\langle\mathrm{R}\downarrow|. \tag{1.6}$$

Now, let us assume we perform an operation that brings both particles into the same site, resulting in the states $|\Psi'\rangle = |\mathrm{L}\uparrow,\mathrm{L}\downarrow\rangle$. By performing the partial trace on the region L and re-normalizing the state, we obtain the single-particle state as

$$\hat{\rho}^{(1)}_{\mathrm{L}} = \frac{1}{2}|\mathrm{L}\downarrow\rangle\langle\mathrm{L}\downarrow| + \frac{1}{2}|\mathrm{L}\uparrow\rangle\langle\mathrm{L}\uparrow|. \tag{1.7}$$

In conclusion, the no-label approach describes identical particles that are not dependent on particle labels. This approach enables the analysis of their entanglement using the same concepts commonly employed in entanglement theory for distinguishable particles, such as the von Neumann entropy obtained through the partial trace. Particularly within this framework, the amount of entanglement exhibited by identical particles depends on local measurements [2, 3].

1.3.3 Second quantization approach

The criteria for separability in quantum systems arise from the absence of quantum correlations among commuting observables. In this respect, the second quantization approach to quantum statistical mechanics provides a consistent framework for analyzing this aspect [8, 9, 10]. Consequently, these examinations reveal that the notions of separability and entanglement are not absolute or fixed concepts. Instead, their classification depends on the choice of commuting observables. These observables form sets that possess the mathematical structure of a C^*-algebra [11]. In simpler terms, the same quantum state can be regarded as separable when considering one specific set of commuting observables, while being classified as entangled when examining a different set of commuting observables. This realization highlights the contextual nature of separability and entanglement, as their characterization depends on the specific context defined by the chosen observables.

The framework of second quantization is built upon a single-particle Hilbert space $\mathcal{H}$ and introduces creation and annihilation operators, denoted as $\hat{a}^\dagger(f)$ and $\hat{a}(g)$, respectively. These operators act on single-particle vector states g and f belonging to $\mathcal{H}$, which are commonly referred to as modes. When the creation operator $\hat{a}^\dagger(f)$ acts on the vacuum state $|0\rangle$, it produces the single-particle vector state in mode f, expressed as $|f\rangle = \hat{a}^\dagger(f)|0\rangle$. The commutation or anticommutation relations satisfied by these operators are known as the canonical commutation or anticommutation relations:

$$[\hat{a}^\dagger(f),\hat{a}(g)] = \langle f|g\rangle, \qquad \{\hat{a}^\dagger(f),\hat{a}(g)\} = \langle f|g\rangle. \tag{1.8}$$

Polynomials in these creation and annihilation operators form the algebra $\mathcal{A}$ of operators used to describe many-body systems consisting of bosons and fermions. For instance, in second quantization, the state $|\Psi\rangle = |\mathrm{L}\uparrow,\mathrm{R}\downarrow\rangle$ is given by $|\Psi\rangle = \hat{a}^\dagger_{\mathrm{L}\uparrow}\hat{a}^\dagger_{\mathrm{R}\downarrow}|0\rangle$. This representation captures the concept of locality, similar to its application to non-identical particles, at the level of observables. Furthermore, any two orthogonal modes can be addressed by a set of observables. However, when considering entities such as atoms that are not truly elementary identical particles and cannot be regarded as excitations of a field, second quantization becomes purely mathematical in nature.

In this context, a state $\hat{\rho}$ is considered separable with respect to the bipartition $\hat{\mathcal{A}}_1 = \hat{a}_j, \hat{a}^\dagger_j$ for $j = 1,\ldots,m$ and $\mathcal{A}_2 = \hat{a}_j, \hat{a}^\dagger_j$ for $j = m+1,\ldots,N$ of a given set of orthogonal modes if and only if it

can be expressed in the form [10]:

$$P\left(\hat{a}_1^\dagger, \ldots, \hat{a}_m^\dagger\right) Q\left(\hat{a}_{m+1}^\dagger, \ldots, \hat{a}_N^\dagger\right) |0\rangle\,, \tag{1.9}$$

where P and Q are general polynomials of the creation operators in the N modes. Separable mixed states can be expressed as convex combinations of separable pure states, while all other states are considered entangled. For example, the state $|\Psi\rangle = \hat{a}_{\mathrm{L}\uparrow}^\dagger \hat{a}_{\mathrm{R}\downarrow}^\dagger |0\rangle$ is considered separable. However, in contrast to the no-label approach described in Eq. (1.7), the state $|\Psi'\rangle = \hat{a}_{\mathrm{L}\uparrow}^\dagger \hat{a}_{\mathrm{L}\downarrow}^\dagger |0\rangle$ can also be considered separable by applying the criteria mentioned above for both bosons and fermions [7, 12, 13]. This clearly demonstrates that the entanglement of identical particles is not an absolute property but depends on the choice of observables.

To further illustrate the comparison between the two approaches, let us consider a linear operation that transfers a particle from the localized mode C to two distinct modes C and D. This operation can be described by the creation operator $\hat{a}_{\mathrm{L}\,\sigma}^\dagger = r\hat{a}_{\mathrm{C}\,\sigma}^\dagger + t\hat{a}_{\mathrm{D}\,\sigma}^\dagger$, where $\sigma = \uparrow, \downarrow$, and r and t are amplitudes satisfying the condition $|t|^2 + |r|^2 = 1$. These transformations, familiar from optics, are passive linear optical networks with no polarization dependence and are equivalent to a tunneling operation for Bose-Einstein condensates, where particles can leak from one mode to another. The output state is given by [2]:

$$|\Psi_{\text{out}}\rangle = r^2 |\Phi_{\mathrm{C}}\rangle + t^2 |\Phi_{\mathrm{D}}\rangle + \sqrt{2}st\, |\Phi_{\mathrm{CD}}\rangle\,, \tag{1.10}$$

where $|\Phi_{\mathrm{C}}\rangle = |\mathrm{C}\uparrow, \mathrm{C}\downarrow\rangle$, $|\Phi_{\mathrm{D}}\rangle = |\mathrm{D}\uparrow, \mathrm{D}\downarrow\rangle$, and $|\Phi_{\mathrm{CD}}\rangle = \frac{1}{\sqrt{2}}\left(|\mathrm{C}\uparrow, \mathrm{C}\downarrow\rangle + |\mathrm{C}\downarrow, \mathrm{C}\uparrow\rangle\right)$. This mapping has significant implications for the analysis of entanglement. The states $|\Phi_{\mathrm{C}}\rangle$ and $|\Phi_{\mathrm{D}}\rangle$ retain the same form as the input state, while the state $|\Phi_{\mathrm{CD}}\rangle$ represents a maximal linear combination of two identical particles in two distinct orthogonal modes, similar to a Bell state. This means that the initial state and the latter do not possess the same entanglement structure based on the criteria in Eq. (1.9). This allows us to conclude that any entanglement that formally arises among identical particles, including entanglement purely due to symmetrization, can be transferred to an entangled state of independent modes, which can then be utilized for any desired task. In fact, the entanglement of the mode system corresponds one-to-one with the entanglement between the inaccessible identical particles [14]. Furthermore, this shows that the separability (entanglement) criterion in Eq. (1.9) is not an absolute property but depends on the choice of orthogonal modes: mode transformations are mode non-local and thus do not preserve entanglement.

This observation is also in line with the concept of measurement-induced entanglement. When particles are non-identical, it is stated that «only interaction between particles can lead to an entangled state» [13]. However, in the case of identical particles, measurements play a significant role in the emergence of entanglement. Particularly, the utilization of ambiguous measurements, where the apparatus is unable to determine which particle corresponds to the result detected by each detector (similar to the Hong-Ou-Mandel experiment), allows for the intrinsic generation of probabilistic measurement-induced entanglement, even in situations where the initial entanglement before the measurement was absent [6, 13].

1.4 Quantum information processing with identical particles

In this section, I explore various research directions and discuss the implications of the indistinguishability of identical particles in quantum information processing. The ability to perform quantum information tasks relies on the capability to address identical particles. However, a significant challenge arises from the fact that identical particles are not generally individually addressable. In this sense, the most common approach is to utilize second quantization within the framework of local operations and classical operations (LOCC) [15], which is based on addressing and performing local operations on orthogonal modes. The rationale behind this approach is that orthogonal modes, unlike identical particles, can always be manipulated and addressed individually in experimental settings.

However, when particles spatially overlap, such local operations on specific modes may not be accessible. To address the issue of operational accessibility for spatially overlapping identical particles,

the spatially localized operations and classical communication (sLOCC) framework has been introduced [16]. Based on a particle-based no-label approach, this framework provides a means to address and manipulate spatially overlapping identical particles. Before diving into the discussion of the role of indistinguishability in quantum information processing, I briefly recall the sLOCC framework.

1.4.1 Spatially localized operations and classical communication (sLOCC)

To introduce the sLOCC framework, let us take a system of two independently prepared identical particles in the state

$$|\Psi\rangle = |\psi\uparrow, \psi'\downarrow\rangle\,, \tag{1.11}$$

where ψ and ψ' are spatial wave functions representing external degrees of freedom, and $\uparrow$ and $\downarrow$ denote pseudospin states representing internal states. In order to activate and access the entanglement present in this system, local measurements of the single-particle pseudospin states are performed in separate localized spatial regions, labeled as L and R, as illustrated in fig. 1.3. The local particle counting process is given by the measurement operator:

$$\hat{\Pi}^{(2)} = \sum_{\sigma,\tau=\uparrow,\downarrow} |\mathrm{L}\,\sigma, \mathrm{R}\,\tau\rangle\langle \mathrm{L}\,\sigma, \mathrm{R}\,\tau|\,, \tag{1.12}$$

which projects the state $|\Psi\rangle$ onto the basis states $\mathcal{B}_{\mathrm{LR}} = \{|\mathrm{L}\uparrow, \mathrm{R}\uparrow\rangle, |\mathrm{L}\uparrow, \mathrm{R}\downarrow\rangle, |\mathrm{L}\downarrow, \mathrm{R}\uparrow\rangle, |\mathrm{L}\downarrow, \mathrm{R}\downarrow\rangle\}$. Therefore, the action of the measurement operator on the state $\hat{\Pi}^{(2)}|\Psi\rangle$ results in a two-particle state given by the inner product of two-particle states, as described by Eq. (1.5). The resulting non-normalized two-particle state is given by

$$|\psi_{\mathrm{LR}}\rangle = lr'|\mathrm{L}\uparrow, \mathrm{R}\downarrow\rangle + \eta l' r|\mathrm{L}\downarrow, \mathrm{R}\uparrow\rangle\,, \tag{1.13}$$

$l = \langle \mathrm{L}|\psi\rangle$, $r' = \langle \mathrm{R}|\psi'\rangle$, $l' = \langle \mathrm{L}|\psi'\rangle$, and $r = \langle \mathrm{R}|\psi\rangle$ are the probability amplitudes of finding a particle in the sites in L and R. The operation resource state provided in the equation above is inherently post-selective since there exists a non-zero probability of both particles being found in the same regions. The probability of successful sLOCC, denoted as P_{LR}, is given by

$$P_{\mathrm{LR}} = P_{\mathrm{L}}P'_{\mathrm{R}} + P'_{\mathrm{L}}P_{\mathrm{R}}, \tag{1.14}$$

where $P_{\mathrm{L}} = |l|^2$, $P_{\mathrm{R}} = |r|^2$, $P'_{\mathrm{L}} = |l'|^2$, and $P'_{\mathrm{R}} = |r'|^2$ are the probabilities of finding a particle in region L and R, respectively, based on the wave functions ψ and ψ'.

Subsequently, a partial trace can be performed on one region, such as L, followed by a projection onto the site R, resulting in the reduced density matrix

$$\hat{\rho}^{(1)}_R = \frac{1}{P_{\mathrm{L}}P'_{\mathrm{R}} + P'_{\mathrm{L}}P_{\mathrm{R}}}\left(P'_{\mathrm{L}}P_{\mathrm{R}}|\mathrm{R}\uparrow\rangle\langle \mathrm{R}\uparrow| + P_{\mathrm{L}}P'_{\mathrm{R}}|\mathrm{R}\downarrow\rangle\langle \mathrm{R}\downarrow|\right). \tag{1.15}$$

Here, $|\mathrm{R}\uparrow\rangle$ and $|\mathrm{R}\downarrow\rangle$ represent the states of the particle in region R with the corresponding pseudospin states. The normalization factor in the denominator ensures that the reduced density matrix is properly normalized. Therefore, the von Neumann entropy gives the operational entanglement as

$$E(|\psi_{\mathrm{LR}}\rangle) = -\frac{P_{\mathrm{L}}P'_{\mathrm{R}}}{P_{\mathrm{L}}P'_{\mathrm{R}} + P'_{\mathrm{L}}P_{\mathrm{R}}}\log_2\frac{P_{\mathrm{L}}P'_{\mathrm{R}}}{P_{\mathrm{L}}P'_{\mathrm{R}} + P'_{\mathrm{L}}P_{\mathrm{R}}} - \frac{P'_{\mathrm{L}}P_{\mathrm{R}}}{P_{\mathrm{L}}P'_{\mathrm{R}} + P'_{\mathrm{L}}P_{\mathrm{R}}}\log_2\frac{P'_{\mathrm{L}}P_{\mathrm{R}}}{P_{\mathrm{L}}P'_{\mathrm{R}} + P'_{\mathrm{L}}P_{\mathrm{R}}} \tag{1.16}$$

which characterizes the quantum correlations between the pseudospins of the particles as observed through local measurements. The extent of this entanglement is influenced by the probabilities of finding the particles in the two localized sites, L and R.

As observed, the concept of spatial overlap between the two particles becomes relevant in this context. When each particle is exclusively found in one region, denoted by $P_{\mathrm{R}} = 1$ and $P'_{\mathrm{L}} = 1$ (or $P'_{\mathrm{R}} = 1$ and $P_{\mathrm{L}} = 1$), the particles are spatially separated into two regions. In such cases, the state

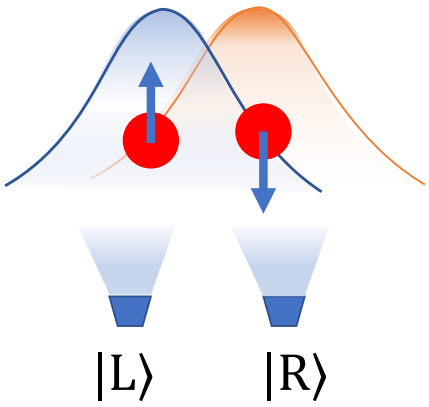

Figure 1.3: Schematic illustration of two identical particles with opposite pseudospins (internal states) have spatial wave functions ψ, ψ' with a given degree of overlap. The entanglement between pseudospins is operationally defined by local measurements in two separated localized spatial regions L and R.

$|\psi_{\mathrm{LR}}\rangle = |\mathrm{L}\uparrow, \mathrm{R}\downarrow\rangle$ is separable with zero entanglement, i.e., $E(|\psi_{\mathrm{LR}}\rangle) = 0$. However, if there exists a non-zero probability of spatial overlap between the particles, then the state becomes entangled. Specifically, when the particles are equally distributed in both regions, complete spatial overlap occurs. This happens when the region where a particle can be found with non-zero probability is the same for both particles, for example, $P_{\mathrm{R}} = P_{\mathrm{L}} = P'_{\mathrm{L}} = P'_{\mathrm{R}} = 1/2$. In this scenario, the operational state becomes maximally entangled, given by $|\psi_{\mathrm{LR}}\rangle = (|\mathrm{L}\uparrow, \mathrm{R}\downarrow\rangle + \eta\,|\mathrm{L}\downarrow, \mathrm{R}\uparrow\rangle)/\sqrt{2}$, with a success probability of sLOCC (P_{LR}) equal to $1/2$.

Based on the aforementioned discovery presented in Ref. [16], the sLOCC formalism is expanded to encompass scenarios involving N particles distributed among N regions [17], as discussed in Section I, which is a main result of my PhD thesis. This extension allows for the investigation of entanglement in systems with multiple identical particles. Furthermore, the entanglement measure is extended to encompass any arbitrary mixed state of two spatially overlapping identical particles, also discussed in Section I. This development provides a comprehensive framework for quantifying and characterizing the entanglement present in systems of indistinguishable particles.

The sLOCC framework, based on the no-label approach and the operational techniques of spatially localized operations and classical communication, enables the direct manipulation and exploitation of the resource states associated with identical particles. This has significant implications for quantum information processing tasks, as the indistinguishability of identical particles can be effectively harnessed as a valuable quantum resource. In the following sections, I will provide a brief overview of some of the applications and benefits of utilizing indistinguishable particles in quantum information processing

1.4.2 Two-particle quantum interference and particle statistics

One of the significant historical consequences of indistinguishability is bi-photon quantum interference (see the review [127]). In this scenario, an event can occur in multiple alternative ways, and it becomes impossible to distinguish between these alternatives, leading to interference phenomena. Instead of creating superpositions of single (or multiple) photons, researchers have generated superpositions of the origin of a photon pair itself. These consequences stem from the theoretical understanding of the beam splitter's action within the framework of quantum mechanics.

Historically speaking, Prasad, Scully, and Martienssen [128] derived a unitary transformation that connects the input mode set to the outgoing transmitted and reflected mode set. This observation was then formulated through second quantization [129], considering the contributions of input and output modes. In this formalism, $\hat{a}^\dagger$ and $\hat{b}^\dagger$ represent photon creation operators at the two input ports of the beam splitter, while $\hat{c}^\dagger$ and $\hat{d}^\dagger$ represent photon creation operators at the two output ports of the beam splitter. In general, it is worth mentioning that the creation and annihilation operators for the input and

output ports satisfy the commutation relations $[\hat{a}^\dagger, \hat{b}^\dagger] = 0$ and $[\hat{c}^\dagger, \hat{d}^\dagger] = 0$ for bosons, and the anti-commutation relations $\hat{a}^\dagger, \hat{b}^\dagger = 0$ and $\hat{c}^\dagger, \hat{d}^\dagger = 0$ for fermions. The action of the beam splitter on two photons can be described as follows:

$$\hat{a}^\dagger = l\hat{c}^\dagger + r\hat{d}^\dagger, \;\; \hat{b}^\dagger = r\hat{c}^\dagger - l\hat{d}^\dagger. \tag{1.17}$$

Here, r and l represent the reflectance and transmittance of the lossless beam splitter, respectively. Therefore, the action of beam splitter on two photons is given by

$$\begin{aligned} &\hat{a}^\dagger\hat{b}^\dagger \left|0\right\rangle \rightarrow \left(l\hat{c}^\dagger + r\hat{d}^\dagger\right)\left(r\hat{c}^\dagger - l\hat{d}^\dagger\right)\left|0\right\rangle, \\ &\hat{a}^\dagger\hat{b}^\dagger \left|0\right\rangle \rightarrow \left(lr\left((\hat{c}^\dagger)^2 - (\hat{d}^\dagger)^2\right) + l^2\hat{d}^\dagger\hat{c}^\dagger - r^2\hat{c}^\dagger\hat{d}^\dagger\right)\left|0\right\rangle. \end{aligned} \tag{1.18}$$

It is important to note that in the context of quantum optics, we assume that the two photons mentioned above are indistinguishable in all degrees of freedom, including polarization, time, frequency, position, and momentum, as they are in the same mode of the electromagnetic field. Thus, due to the bosonic commutation relation $[\hat{d}^\dagger, \hat{c}^\dagger] = 0$ and using a lossless beam splitter with a 50:50 reflectance/transmittance, two-photon interference, known as the bunching effect, occurs. This leads to the output state given by

$$\hat{a}^\dagger\hat{b}^\dagger \left|0\right\rangle \xrightarrow{50:50} \frac{1}{2}\left((\hat{c}^\dagger)^2 - (\hat{d}^\dagger)^2\right)\left|0\right\rangle. \tag{1.19}$$

This effect, famously known as the Hong, Ou, and Mandel (HOM) effect [130], demonstrates that for a balanced beam splitter, simultaneous detection at the two output ports behaves like the singlet state for two orthogonally polarized photons, i.e., $\frac{1}{\sqrt{2}}\left(\left|\uparrow,\downarrow\right\rangle - \left|\downarrow,\uparrow\right\rangle\right)$. In their seminal experimental work, Hong, Ou, and Mandel showed that this interference of two identical photons at a beam splitter, represented by the characteristic "dip" in the coincidence detection at the output, can be utilized to measure very short time intervals. Essentially, when photons overlap spatially at the beam splitter, they become indistinguishable from the beam splitter's perspective.

On the other hand, when considering fermions, the action of a beam splitter on fermions is given by

$$\begin{aligned} &\hat{a}^\dagger\hat{b}^\dagger \left|0\right\rangle \rightarrow \left(rl\left(\cancelto{0}{(\hat{c}^\dagger)^2} - \cancelto{0}{(\hat{d}^\dagger)^2}\right) + l^2\hat{d}^\dagger\hat{c}^\dagger - r^2\hat{c}^\dagger\hat{d}^\dagger\right)\left|0\right\rangle, \\ &\hat{a}^\dagger\hat{b}^\dagger \left|0\right\rangle \xrightarrow{r^2+l^2=1} \hat{c}^\dagger\hat{d}^\dagger \left|0\right\rangle. \end{aligned} \tag{1.20}$$

Here, the only accessible state is one fermion per mode, in accordance with the Pauli exclusion principle. The fermionic creation operators $\hat{d}^\dagger$ and $\hat{c}^\dagger$ obey the anti-commutation relation $\hat{d}^\dagger, \hat{c}^\dagger = 0$. This is why we say fermions will anti-bunch. However, the information regarding the fermions' origin remains elusive.

Furthermore, the above formalism can be easily translated into the no-label approach [2, 3]. Let us assume that we have one particle localized in each region with the same pseudospin, and the elementary form of the two-particle state is given as $\left|\mathrm{L}\,\sigma, \mathrm{R}\,\sigma\right\rangle$. Then, a unitary transformation (a beam splitter) is applied: $\left|\mathrm{L}\,\sigma\right\rangle \rightarrow l\left|\mathrm{L}\,\sigma\right\rangle + r\left|\mathrm{R}\,\sigma\right\rangle$ and $\left|\mathrm{R}\,\sigma\right\rangle \rightarrow r\left|\mathrm{L}\,\sigma\right\rangle - l\left|\mathrm{R}\,\sigma\right\rangle$. The transformed state is then given by

$$\left|\mathrm{L}\,\sigma, \mathrm{R}\,\sigma\right\rangle \rightarrow lr\left(\left|\mathrm{L}\,\sigma, \mathrm{L}\,\sigma\right\rangle - \left|\mathrm{R}\,\sigma, \mathrm{R}\,\sigma\right\rangle\right) + l^2\left|\mathrm{L}\,\sigma, \mathrm{R}\,\sigma\right\rangle - r^2\left|\mathrm{R}\,\sigma, \mathrm{L}\,\sigma\right\rangle. \tag{1.21}$$

Additionally, the two-particle state follows the standard phase change associated with particle exchange, $\left|\mathrm{L}\,\sigma, \mathrm{R}\,\tau\right\rangle = \eta\left|\mathrm{R}\,\tau, \mathrm{L}\,\sigma\right\rangle$, where $\eta = 1$ (-1) for bosons (fermions). For bosons in the 50:50 case, the bunching effect is retrieved, similar to Eq. (1.19): $\left|\mathrm{L}\,\sigma, \mathrm{R}\,\sigma\right\rangle \xrightarrow[\eta=1]{50:50} \frac{1}{\sqrt{2}}\left(\left|\mathrm{L}\,\sigma, \mathrm{L}\,\sigma\right\rangle - \left|\mathrm{R}\,\sigma, \mathrm{R}\,\sigma\right\rangle\right)$. Again, due to the Pauli exclusion principle for fermions, the only accessible state in this case is $\left|\mathrm{L}\,\sigma, \mathrm{R}\,\sigma\right\rangle$.

It is crucial to highlight an essential aspect that emerges from the symmetrization postulate: when exchanging a pair of identical particles, the overall state acquires a global phase [131]. This phase can

be represented as $|\mathrm{L}\,\sigma, \mathrm{R}\,\tau\rangle = e^{i\phi}\,|\mathrm{R}\,\sigma, \mathrm{L}\,\sigma\rangle$, where ϕ denotes the relative phase associated with the particle exchange, with $\phi = 0$ for bosons and $\phi = \pi$ for fermions [132]. The measurement of this phase resulting directly from particle exchange has been successfully demonstrated through the implementation of a state transport protocol . Additionally, a recent study utilized the sLOCC protocol to directly measure the exchange described in Eq. (1.12) [133].

Such findings have profound implications for simulating intricate physical systems and enhancing the accuracy of precise measurements. This transition from classical to quantum physics has spurred physicists to investigate the phenomenon of two-particle interference in both fermionic and bosonic quantum entities. Notably, two-particle interference has been observed not only with elementary particles like electrons and atoms but also with more massive and intricate quantum systems such as plasmons [134], showcasing the widespread occurrence of this phenomenon across various scales and complexities.

1.4.3 Entanglement generation

Undoubtedly, the first and crucial step towards quantum state manipulation is to have an emitter or source that can produce a few identical elementary particles. In the field of quantum optics, this is often accomplished through a nonlinear process called Spontaneous Parametric Down-Conversion (SPDC), where a single pumped photon is converted into a pair of photons known as the idler and signal photons. When these photons are generated with orthogonal polarization, the resulting state is genuinely polarization-entangled [18, 19]. The design of such sources continues to be widely used today, particularly in the generation of highly complex photonic entanglement states. Notable examples include the creation of a 12-photon entangled system [20]

Nevertheless, once the particles are generated, passive or active local operations, such as beam splitters and polarizers in optics, and projective measurements are employed to engineer the quantum state for quantum information processing. For instance, as discussed in the previous section, one can determine the fermionic and bosonic nature of two identical particles by sending both particles to the inputs of a single beamsplitter. Furthermore, local manipulation plays a crucial role in performing various tasks, including entanglement swapping [21], quantum teleportation [22], and more, which will be discussed in the forthcoming sections. Additionally, the output state resulting from the Hong-Ou-Mandel (HOM) effect, as shown in Eq. (1.19)), takes the form of an N00N state [135]. This state is a valuable quantum resource for precision measurement in quantum (photonic) metrology, where the N00N state is utilized to achieve higher measurement precision for physical properties. I will discuss this point in more detail later.

Although having a single particle source (such as a single-photon source) is crucial, it is not necessary to achieve spatial overlap of particles within a specific region, such as making two photons interfere in a single beam splitter for quantum state engineering or performing a quantum protocol, as demonstrated in most of the previous works. In fact, the entanglement of indistinguishable particles is directly determined by their spatial overlap [16]. Consequently, an experimental proposal was developed in collaboration with the University of Science and Technology of China (USTC), resulting in the creation of the first remote entangling gate that exploits the indistinguishability of identical particles [23]. This significant achievement is discussed in Chapter II of my thesis. It is also worth mentioning that the sLOCC-based entangling gate, which utilizes spatial overlap between identical particles, was also implemented in an independent work [24]. Two years later, they extended this approach to the generation of three-partite entangled states [25]. Such findings show how spatial overlap in separated regions can serve as fundamental tools for quantum state engineering.

1.4.4 Quantum teleportation and entanglement swapping

One indirect but reliable way to test entanglement is to demonstrate that the output state can perform quantum information tasks that are classically impossible. In this context, if we rely solely on separable states without any other quantum resources, the use of local operators on separable states should not enhance the performance of informational tasks compared to classical counterparts. A prime example

of such a task is quantum teleportation, which cannot be achieved using classical or separable states alone. Quantum teleportation [15] is a technique used to transfer quantum information from a source to a destination by utilizing entangled states, and it plays a crucial role in quantum networking.

In quantum teleportation [27, 15], entanglement in the form of a Bell state is employed to transmit an arbitrary quantum state $|\psi\rangle$ between two distant observers, commonly referred to as Alice and Bob. Let us briefly recap the underlying algorithm of quantum state teleportation. The quantum teleportation system utilizes three qubits, where the first two qubits are in the Bell state

$$|\Phi_0\rangle_{\mathrm{AB}} = \frac{1}{\sqrt{2}} \left(|\uparrow\rangle_{\mathrm{A}} |\uparrow\rangle_{\mathrm{B}} + |\downarrow\rangle_{\mathrm{A}} |\downarrow\rangle_{\mathrm{B}} \right), \tag{1.22}$$

and the third qubit is an arbitrary state $|\Psi\rangle_{\mathrm{C}} = c_1 |\uparrow\rangle_{\mathrm{C}} + c_2 |\downarrow\rangle_{\mathrm{C}}$ that needs to be teleported. The state of the full system consisting of three particles is therefore given by $|\Psi\rangle_{\mathrm{ABC}} = |\Psi\rangle_{\mathrm{AB}} \otimes |\Psi\rangle_{\mathrm{C}}$, which represents a product state between the entangled pair AB and the non-entangled state C. Alice performs a measurement on the Bell state of particles A and C, entangling A and C while disentangling B. The measurement of the Bell state projects a non-entangled state into an entangled state, resulting in the following expression:

$$|\Psi\rangle = \frac{1}{2} \sum_{i=0,x,y,z} |\Phi_i\rangle_{\mathrm{AC}} \otimes \sigma_i^{(\mathrm{B})} |\Psi\rangle_{\mathrm{B}} . \tag{1.23}$$

Here, $\sigma_0 = \mathbf{I}$ represents the identity matrix for the qubit, and the rest are the Pauli matrices. The states $|\Phi_i\rangle$ correspond to the four Bell diagonal states:

$$\begin{aligned}
|\Phi_0\rangle_{\mathrm{AC}} &= \left(\mathbf{I}^{(\mathrm{A})} \otimes \sigma_0^{(\mathrm{C})} \right) |\Phi_0\rangle_{\mathrm{AC}} = \frac{1}{\sqrt{2}} \left(|\uparrow\rangle_{\mathrm{A}} |\uparrow\rangle_{\mathrm{C}} + |\downarrow\rangle_{\mathrm{A}} |\downarrow\rangle_{\mathrm{C}} \right), \\
|\Phi_1\rangle_{\mathrm{AC}} &= \left(\mathbf{I}^{(\mathrm{A})} \otimes \sigma_x^{(\mathrm{C})} \right) |\Phi_0\rangle_{\mathrm{AC}} = \frac{1}{\sqrt{2}} \left(|\uparrow\rangle_{\mathrm{A}} |\downarrow\rangle_{\mathrm{C}} + |\downarrow\rangle_{\mathrm{A}} |\uparrow\rangle_{\mathrm{C}} \right), \\
|\Phi_2\rangle_{\mathrm{AC}} &= \left(\mathbf{I}^{(\mathrm{A})} \otimes \sigma_y^{(\mathrm{C})} \right) |\Phi_0\rangle_{\mathrm{AC}} = \frac{1}{\sqrt{2}} \left(|\uparrow\rangle_{\mathrm{A}} |\downarrow\rangle_{\mathrm{C}} - |\downarrow\rangle_{\mathrm{A}} |\uparrow\rangle_{\mathrm{C}} \right), \\
|\Phi_3\rangle_{\mathrm{AC}} &= \left(\mathbf{I}^{(\mathrm{A})} \otimes \sigma_z^{(\mathrm{C})} \right) |\Phi_0\rangle_{\mathrm{AC}} = \frac{1}{\sqrt{2}} \left(|\uparrow\rangle_{\mathrm{A}} |\uparrow\rangle_{\mathrm{C}} - |\downarrow\rangle_{\mathrm{A}} |\downarrow\rangle_{\mathrm{C}} \right).
\end{aligned} \tag{1.24}$$

When Alice measures the Bell state of particles A and C, she will obtain one of the four Bell states, each with a probability of $\frac{1}{4}$. Depending on which $|\Phi_i\rangle_{\mathrm{AC}}$ state she measures, the state of particle B after the measurement will be $\sigma_i^{(\mathrm{B})} |\Psi\rangle_{\mathrm{B}}$. To transmit the state of particle C to Bob, Alice doesn't need to send him the potentially infinite amount of information represented by the coefficients c_1 and c_2, which can be real numbers with arbitrary precision. Instead, she only needs to send the integer i that corresponds to the Bell state she measured for particles A and C, which requires a maximum of two bits of information. Alice can use any classical method to communicate this information to Bob.

Bob receives the integer i from Alice, which identifies the Bell state that she measured. After Alice's measurement, the overall state of the system becomes $|\Phi_i\rangle_{\mathrm{AC}} \otimes \sigma_i^{(B)} |\Psi\rangle_{\mathrm{B}}$. Bob then applies the corresponding σ_i operation on his end, resulting in the overall state $|\Phi_i\rangle_{\mathrm{AC}} \otimes |\Psi\rangle_{\mathrm{B}}$. Thus, Bob has successfully transformed the spin state of particle B to $|\Psi\rangle_{\mathrm{B}} = c_1 |\uparrow\rangle_{\mathrm{B}} + c_2 |\downarrow\rangle_{\mathrm{B}}$, which is identical to the original state of particle C that Alice intended to send. The information initially encoded in state C has been "teleported" to Bob's state, and the final spin state of particle B now matches the original state of particle C. It is important to note that the particles involved in the process never change between observers: Alice always has particles A and C, and Bob always has particle B.

As shown above, the necessary condition is that all particles are addressable for any operation using A, B, and C labels. For identical particles, typically, each particle is assigned to a different orthogonal and distinguishable mode, such as an optical path in quantum optics. In the case of a no-label approach, the exact condition must be met to accomplish the task. As shown in ref. [16], the elementary form of the state $|\psi\uparrow, \psi'\downarrow\rangle$ does not allow for individual local operations on identical particles. Therefore, an sLOCC operation (equation (1.12)) is performed to separate one particle per region, allowing each

particle to be addressed according to its spatial region. In fact, as shown in Ref. [16], the elementary form of the state $|\psi\uparrow, \psi'\downarrow\rangle$ is potentially entangled, which suggests the possibility of performing quantum teleportation. The experimental implementation and underlying protocol are the subject of my thesis in Chapter II.

Another important application in quantum communication is entanglement swapping. Entanglement swapping plays a crucial role in the large-scale distribution of quantum information [136, 137, 138, 139], as it enables the creation of quantum relays and quantum repeaters [140, 141]. Entanglement swapping is a fundamental quantum phenomenon that allows the entanglement of two particles that do not share a common past, with each particle located outside the light cone of the other. In all the implemented systems thus far, the key components have been the preparation of entangled pairs and Bell measurements (see Eq. (1.24)). In the standard entanglement swapping process [142], two pairs of entangled particles are initially prepared (the particles in each pair are not independently prepared), and a Bell measurement is successively performed on two particles from different pairs. As a result, the other two particles become entangled even though they have never directly interacted [143, 144]. Entanglement swapping has been experimentally realized using identical but distinguishable particles (photons) by applying the usual operational framework for non-identical particles, which is based on particle addressability and involves local operations and classical communication (LOCC) [145].

In the sLOCC-based protocol, the goal is to spatially overlap identical particles in different operational regions. Similar to the previous section, two pairs of identical particles with opposite pseudospin are independently prepared. First, one particle from each pair is distributed in two spatially separated nodes, allowing both particles to overlap spatially. Then, it is possible to obtain entanglement in the pseudospin degrees of freedom associated with the spatial overlap of particles in each pair, achieved through sLOCC [16]. As a result, each node contains one particle As a result, each node contains one particle and the state becomes

$$|\Psi^{(4)}_{\mathrm{PS}}\rangle = |1^{\eta}_{\mathrm{AC}}, 1^{\eta}_{\mathrm{DB}}\rangle\,, \tag{1.25}$$

where $|1^{\eta}_{\mathrm{AC}}\rangle$ and $|1^{\eta}_{\mathrm{DB}}\rangle$ are the two-particle Bell states

$$|1^{\eta}_{\mathrm{AC}}\rangle = \frac{1}{\sqrt{2}}(|\mathrm{A}\downarrow, \mathrm{C}\uparrow\rangle + \eta|\mathrm{A}\uparrow, \mathrm{C}\downarrow\rangle),\ |1^{\eta}_{\mathrm{DB}}\rangle = \frac{1}{\sqrt{2}}(|\mathrm{D}\downarrow, \mathrm{B}\uparrow\rangle + \eta|\mathrm{D}\uparrow, \mathrm{B}\downarrow\rangle).$$

Even though the particles have been independently prepared, the sLOCC procedure leads to the state $|\Psi^{(4)}_{\mathrm{PS}}\rangle$, which demonstrates that the pair of particles in nodes A and C is maximally entangled in the pseudospin degrees of freedom, similar to the DB-pair. The probability of obtaining this state is $P(4) = |\langle\Psi^{(4)}_{\mathrm{PS}}|\Psi^{(4)}\rangle|^2 = 1/4$. The procedure is valid only for identical particles and does not require two entangled pairs at the preparation stage. Very recently, an indistinguishability-based entanglement swapping protocol has been experimentally implemented using controlled spatial indistinguishability of four independent photons in three separated nodes of a network [26]. The success of this experiment demonstrates that the inherent indistinguishability of identical particles provides promising prospects for feasible quantum communication in multinode photonic quantum networks.

1.4.5 Quantum metrology with indistinguishable particles

Returning to the HOM effect in Eq. (1.19), we observe that two photons can be entirely in either the upper mode A or the lower mode B. However, due to their indistinguishable and bosonic nature, we cannot determine which photon is in which mode. This observation allows us to extend the concept to cases where the total number of N photons is in mode A, which is typically associated with the optical path or spatial mode. This generalization gives rise to the N00N state, defined as:

$$|\psi_{N00N}\rangle = \frac{1}{\sqrt{2}}\left(|N, 0\rangle + |0, N\rangle\right), \tag{1.26}$$

where $|N\rangle$ represents the state with N photons in the Fock basis. The N00N state allows for improved spatial and phase resolution by a factor of N, scaling as $1/N$. To achieve the fundamental quantum limit,

known as the Heisenberg limit, for phase sensitivity, it is necessary to consider N00N states with a high number of photons. Several experimental schemes have been proposed to generate N00N states with a large photon number [146, 135], and some of these schemes have been demonstrated experimentally [147, 148]. This enhancement arises from the behavior of a coherent state passing through a phase shifter. When a coherent state interacts with a phase shifter, it acquires a phase shift of ϕ. This property is intrinsic to classical monochromatic light beams and is also inherited by coherent states in a quantum mechanical context. However, when N indistinguishable particles in a single mode are employed, the phase shift experienced is directly proportional to the number of photons, N. In fact, the evolution of any photon state passing through a phase shifter is governed by the operator $U_\phi = e^{\hat{a}^\dagger \hat{a}\phi}$, and its effect on the state $|N\rangle$ is given by $U_\phi |N\rangle = e^{N\phi} |N\rangle$. This behavior arises from the collective behavior of N identical particles.

Such observation arises from the fact that orthogonal modes can be collectively manipulated, unlike identical particles, using local operations that address their specific properties, such as their path or other degrees of freedom. This addressability is crucial for performing various quantum operations, including computation as described in the Knill, Laflamme, and Milburn (KLM) protocol [149]. The significance of addressability becomes apparent when considering the elementary state $|\psi \uparrow, \psi' \downarrow\rangle$, which, in its current form, does not allow for individual local operations on identical particles. One way to overcome this limitation, as briefly discussed previously, is to utilize the sLOCC formalism, which enables the addressing of identical particles based on their spatial regions. For example, the CNOT gate can be realized for identical particles by identifying the measurement regions L and R as the control and target regions, respectively.

It is worth noting, as demonstrated in Ref. [28], that the spatial overlap of wave functions is the sole reason for coherence. The coherence measure explicitly depends on the overlap between particles in the two operational regions. In the context of quantum metrology, the quantum coherence of states composed of non-identical particles is known to serve as a resource for phase discrimination tasks [29, 30]. Therefore, indistinguishability-enabled quantum coherence [94] can be regarded as a resource for quantum metrology. This operational advantage of using indistinguishable particles over distinguishable ones has been explicitly highlighted in [31], where it has been demonstrated and experimentally shown to be employed in a phase discrimination protocol.

1.4.6 Indistinguishability-assisted entanglement protection, recovery and distillation

A realistic quantum system inevitably interacts with its surrounding environment, resulting in the loss of coherence within the system, a phenomenon known as decoherence [40]. Therefore, it is important to manipulate and control decoherence to preserve and utilize the quantum resources of the system. Various protection strategies have been proposed to tackle this issue, including the quantum Zeno effect [150], the utilization of structured environments [151, 106, 152], distillation protocols [153], the implementation of decoherence-free subspaces [107, 108], and the application of dynamical decoupling and control techniques [109, 110, 111, 154, 155, 156, 157]. Additionally, researchers have explored quantum error correction methods [112, 113, 114] and the study of topological properties [115, 116]. However, many of these techniques require the manipulation of numerous system parameters, and the complexity increases with the number of particles involved. Furthermore, they often demand near-perfect suppression of experimental imperfections [158]. Therefore, there is a strong desire to discover inherent properties of the system that naturally protect entanglement from noise during its dynamics.

In the previous sections, I provided a brief discussion on how spatial overlap or indistinguishability enables quantum coherence. Furthermore, a previous study [32] experimentally demonstrated that maintaining spatial overlap and indistinguishability between two photons enables the protection of quantum coherence. In this mechanism, two indistinguishable non-interacting particles propagate together through quantum networks affected by non-dissipative noise, resulting in a steady state where coherence, which accounts for particle indistinguishability, persists indefinitely.

As a contribution to my Ph.D. research, I have demonstrated the use of the indistinguishability of identical particles to preserve entanglement at various stages, as summarized in the previous sections.

In **Chapter II**, I discuss the role of spatial indistinguishability, even in partial form, as a property that safeguards non-local entanglement from preparation noise, regardless of the specific shape of spatial wave functions. These findings establish quantum indistinguishability as an inherent control mechanism for generating entanglement free from noise [17]. In **Chapter III**, I employ a dynamical approach, utilizing open quantum system theory, to demonstrate how the spatial indistinguishability of identical qubits can be a controllable intrinsic property of the system. This property effectively protects exploitable quantum entanglement against detrimental noise [117].

In **Chapter V**, I introduce a distillation protocol that operates within the sLOCC. This protocol takes advantage of the effect of indistinguishability to maximize the distillation of entanglement from mixed states of two identical qubits under general conditions. This result provides a comprehensive explanation of the entanglement distillation process and its success probability. I consider standard noisy states, such as thermal Gibbs states and Werner states, to analyze the protocol's performance.

It is worth mentioning that throughout my PhD research, I contributed to using the indistinguishability of identical particles within the sLOCC formalism for an entanglement recovery protocol [100, 101, 159]. The entanglement recovery protocol is based on the sudden bringing together of two initially spatially separated identical particles prepared in a Bell state and independently interacting with different environments [100]. By utilizing the operation of spatial overlap, we restore quantum correlations lost due to the interaction between the particles and their respective environments. In a more generalized approach presented in Ref. [101], we extended the procedure to consider a realistic scenario where noise was present throughout the entire process while still exploiting the spatial indistinguishability of identical particles. Furthermore, in Ref. [159], we provided a coherent formalization of the deformation concept as the operation that enables spatial overlap among N particles. There, we also discussed the inherent role of spatial deformations as activators of entanglement within the framework of spatially localized operations and classical communication.

Chapter 2

Robust entanglement preparation against noise by controlling spatial indistinguishability

Abstract

Initialization of composite quantum systems into highly entangled states is usually a must to enable their use for quantum technologies. However, unavoidable noise in the preparation stage makes the system state mixed, hindering this goal. Here we address this problem in the context of identical particle systems within the operational framework of spatially localized operations and classical communication (sLOCC). We define the entanglement of formation for an arbitrary state of two identical qubits. We then introduce an entropic measure of spatial indistinguishability as an information resource. Thanks to these tools we find that spatial indistinguishability, even partial, can be a property shielding nonlocal entanglement from preparation noise, independently of the exact shape of spatial wave functions. These results prove quantum indistinguishability is an inherent control for noise-free entanglement generation. This Chapter is related to Publication 1 in the List of Publications.

2.1 Introduction

The discovery and utilization of purely quantum resources is an ongoing issue for basic research in quantum mechanics and quantum information processing [160, 161]. Processes of quantum metrology [162], quantum key distribution [163], teleportation [164] or quantum sensing [165] essentially rely on the entanglement feature [166, 33]. Unfortunately, entanglement is fragile due to the inevitable interaction between system and surrounding environment already in the initial stage of pure state preparation, making the state mixed [15, 104]. As a result, protecting entanglement from unavoidable noises remains a main objective for quantum-enhanced technology [167].

Many-body quantum networks usually employ identical quantum subsystems (e.g., qubits) as building blocks [168, 169, 170, 171, 172, 173, 174, 175]. Characterizing peculiar features linked to particle indistinguishability in composite systems assumes importance from both the fundamental and technological points of view. Discriminating between indistinguishable and distinguishable particles has always been a big challenge for which different theoretical [176, 177, 178, 179] and experimental [180, 181, 182, 183, 184] techniques have been suggested. Recently, particle identity and statistics have been shown to be a resource [185, 186, 187, 188, 189, 16] and experiments which witness its presence have been performed [190]. One aspect that remains unexplored is how the continuous control of the spatial configurations of one-particle wave functions, ruling the degree of indistinguishability of the particles, influences noisy entangled state preparation. Moreover, a measure of the degree of indistin-

guishability lacks.

Pursuing this study requires an entanglement quantifier for an arbitrary (mixed) state of the system with tunable spatial indistinguishability. It is desirable that this quantifier is defined within a suitable operational framework reproducible in the laboratory. The natural approach to this aim is the recent experimentally-friendly framework based on spatially localized operations and classical communication (sLOCC), which encompasses entanglement under generic spatial overlap configurations [16]. This approach has been shown to also enable remote entanglement [28, 34] and quantum coherence [94].

Here we adopt the sLOCC framework to unveil further fundamental traits of composite quantum systems. We first define the entanglement of formation for an arbitrary state of two indistinguishable qubits (bosons or fermions). We then introduce the degree of indistinguishability as an entropic measure of information, tunable by the shapes of spatial wave functions. We finally apply these tools to a situation of experimental interest, that is noisy entangled state preparation. We find spatial indistinguishability can act as a tailored property protecting entanglement generation against noise.

2.2 Results

sLOCC-based entanglement of formation of an arbitrary state of two identical qubits. We first focus on the quantification of entanglement for an arbitrary state (pure or mixed) of identical particles. For identical particles we in general mean identical constituents of a composite system. In quantum mechanics identical particles are not individually addressable, as are instead non-identical (distinguishable) particles, so that specific approaches are needed to treat their collective properties [13, 191, 192, 14, 193, 2, 3, 194]. Our goal is accomplished by straightforwardly redefining the entanglement of formation known for distinguishable particles [195] to the case of indistinguishable particles, thanks to the sLOCC framework [16].

The separability criterion in the standard theory of entanglement for distinguishable particles [33, 195] maintains its validity also for a state of indistinguishable particles once it has been projected by sLOCC onto a subspace of two separated locations $\mathcal{L}$ and $\mathcal{R}$. In fact, after the measurement, the particles are individually addressable into these regions and the criteria known for distinguishable particles can be adopted [16, 94].

Consider two identical qubits, with spatial wave functions ψ_1 and ψ_2, for which one desires to characterize the entanglement between the pseudospins between the separated operational regions. States of the system can be expressed by the elementary-state basis $\{|\psi_1\sigma_1, \psi_2\sigma_2\rangle\,,\ \sigma_1, \sigma_2 = \uparrow, \downarrow\}$, expressed in the no-label particle-based approach [2, 3] where fermions and bosons are treated on the same footing. The density matrix of an arbitrary state of the two identical qubits can be written as

$$\rho = \sum_{\sigma_1,\sigma_2,\sigma_1',\sigma_2'=\downarrow,\uparrow} p_{\sigma_1\sigma_2}^{\sigma_1',\sigma_2'} \left|\psi_1\sigma_1, \psi_2\sigma_2\right\rangle \left\langle\psi_1\sigma_1', \psi_2\sigma_2'\right| / \mathcal{N}, \tag{2.1}$$

where $\mathcal{N}$ is a normalization constant. Projecting ρ onto the (operational) subspace spanned by the computational basis $\mathcal{B}_{\rm LR} = \{|{\rm L}\uparrow, {\rm R}\uparrow\rangle\,, |{\rm L}\uparrow, {\rm R}\downarrow\rangle\,, |{\rm L}\downarrow, {\rm R}\uparrow\rangle\,, |{\rm L}\downarrow, {\rm R}\downarrow\rangle\}$ by the projector

$$\Pi_{\rm LR}^{(2)} = \sum_{\tau_1,\tau_2=\uparrow,\downarrow} |{\rm L}\tau_1, {\rm R}\tau_2\rangle \langle {\rm L}\tau_1, {\rm R}\tau_2|\,, \tag{2.2}$$

one gets the distributed resource state

$$\rho_{\rm LR} = \Pi_{\rm LR}^{(2)} \rho \Pi_{\rm LR}^{(2)} / {\rm Tr}(\Pi_{\rm LR}^{(2)}\rho), \tag{2.3}$$

with probability $P_{\rm LR} = {\rm Tr}(\Pi_{\rm LR}^{(2)}\rho)$. We call $P_{\rm LR}$ sLOCC probability since it is related to the post-selection procedure to find one particle in $\mathcal{L}$ and one particle in $\mathcal{R}$. The state $\rho_{\rm LR}$ is then exploitable for quantum information tasks by addressing the individual pseudospins in the separated regions $\mathcal{L}$ and $\mathcal{R}$, which represent the nodes of a quantum network. The state $\rho_{\rm LR}$ can be in fact remotely entangled in the

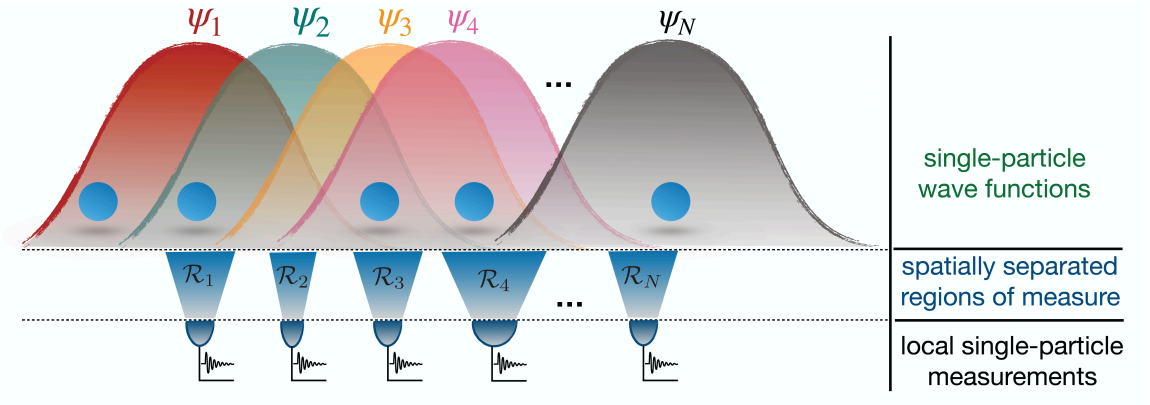

Figure 2.1: **Projective measurements based on sLOCC.** Illustration of different single-particle spatial wave functions ψ_i $(i = 1, \ldots, N)$ associated to N identical particles in a generic spatial configuration. The amount of spatial indistinguishability of the particles can be defined by using spatially localized single-particle measurements in N separated regions $\mathcal{R}_i$.

pseudospins and constitute the distributed resource state. The trace operation is clearly performed in the LR-subspace (see Supplementary Notes 1 and 3 for details). The state $\rho_{\rm LR}$, containing one particle in $\mathcal{L}$ and one particle in $\mathcal{R}$, can be diagonalized as $\rho_{\rm LR} = \sum_i p_i \left|\Psi_i^{\rm LR}\right\rangle \left\langle\Psi_i^{\rm LR}\right|$, where p_i is the weight of each pure state $\left|\Psi_i^{\rm LR}\right\rangle$ which is in general non-separable. Entanglement of formation of $\rho_{\rm LR}$ is as usual [42] $E_f(\rho_{\rm LR}) = \min \sum_i p_i E(|\Psi_i^{\rm LR}\rangle)$, where minimization occurs over all the decompositions of $\rho_{\rm LR}$ and $E(\Psi_i^{\rm LR})$ is the entanglement of the pure state $\left|\Psi_i^{\rm LR}\right\rangle$. We thus define the operational entanglement $E_{\rm LR}(\rho)$ of the original state ρ obtained by sLOCC as the entanglement of formation of $\rho_{\rm LR}$, that is

$$E_{\rm LR}(\rho) := E_f(\rho_{\rm LR}). \tag{2.4}$$

We can conveniently quantify the entanglement of formation $E_f(\rho_{\rm LR})$ by the concurrence $C(\rho_{\rm LR})$, according to the well-known relation $E_f = h[(1+\sqrt{1-C^2})/2]$ [196, 195], where $h(x) = -x\log_2 x - (1-x)\log_2(1-x)$. The concurrence $C_{\rm LR}(\rho)$ in the sLOCC framework can be easily introduced by

$$C_{\rm LR}(\rho) := C(\rho_{\rm LR}) = \max\{0, \sqrt{\lambda_4} - \sqrt{\lambda_3} - \sqrt{\lambda_2} - \sqrt{\lambda_1}\}, \tag{2.5}$$

where λ_i are the eigenvalues, in decreasing order, of the non-Hermitian matrix $R = \rho_{\rm LR}\,\rho_{\rm LR}$, being $\rho_{\rm LR} = \sigma_y^{\rm L} \otimes \sigma_y^{\rm R} \rho_{\rm LR}^* \sigma_y^{\rm L} \otimes \sigma_y^{\rm R}$ with localized Pauli matrices $\sigma_y^{\rm L} = \left|{\rm L}\right\rangle \left\langle{\rm L}\right| \otimes \sigma_y$, $\sigma_y^{\rm R} = \left|{\rm R}\right\rangle \left\langle{\rm R}\right| \otimes \sigma_y$. The entanglement quantifier of ρ so obtained contains all the information about spatial indistinguishability and statistics (bosons or fermions) of the particles.

sLOCC-based entropic measure of indistinguishability. In quantum mechanics, identical particles can be given the property of indistinguishability associated to a specific set of quantum measurements, being different from identity that is an intrinsic property of the system. With respect to the set of measurements, it seems natural to define a continuous degree of indistinguishability, which quantifies how much the measurement process can distinguish the particles. In this section, we deal with this aspect within sLOCC. For simplicity, the treatment is first presented for a two-particle pure state and then generalized to N-particle pure states. It is worth to mention that the framework is universal and also valid for mixed states.

Let us consider an elementary pure state of two identical particles $|\Psi^{(2)}\rangle = |\chi_1, \chi_2\rangle$, where $|\chi_i\rangle$ is a generic one-particle state containing a set of commuting observables such as spatial wave function $|\psi_i\rangle$ and an internal degree of freedom $|\sigma_i\rangle$ (e.g., pseudospin with basis $\{\uparrow, \downarrow\}$). The 2-particle state $|\Psi^{(2)}\rangle$ is thus

$$|\Psi^{(2)}\rangle = |\chi_1, \chi_2\rangle = |\psi_1\sigma_1, \psi_2\sigma_2\rangle\,. \tag{2.6}$$

In general, the degree of indistinguishability depends on both the quantum state and the measurement performed on the system. This means a given set of operations allows one to distinguish the particles while another set of operations does not. Let us narrow the analysis down to spatial indistinguishability within the sLOCC framework, linked to the incapability of distinguish which one of the two particles is found in each of the separated operational region. This framework thus leads to the concept of remote spatial indistinguishability of identical particles. The suitable class of measurements to this aim is represented by local counting of particles, leaving the pseudospins untouched. Inside this class, the joint projective measurement $\Pi_{\rm LR}^{(2)}$ defined in Eq. (3.4) represents the detection of one particle in $\mathcal{L}$ and of one particle in $\mathcal{R}$. We indicate with $P_{{\rm X}\psi_{\rm i}} = |\langle {\rm X}|\psi_i\rangle|^2$ (${\rm X} = {\rm L}, {\rm R}$ and $i = 1, 2$) the probability of finding one particle in the region $\mathcal{X}$ ($\mathcal{X} = \mathcal{L}, \mathcal{R}$) coming from $|\psi_i\rangle$. We then define the joint probabilities of the two possible events when one particle is detected in each region: (i) $\mathcal{P}_{12} = P_{{\rm L}\psi_1} P_{{\rm R}\psi_2}$ related to the event of finding a particle in $\mathcal{L}$ emerging from $|\psi_1\rangle$ and a particle in $\mathcal{R}$ emerging from $|\psi_2\rangle$, (ii) $\mathcal{P}_{21} = P_{{\rm L}\psi_2} P_{{\rm R}\psi_1}$ related to the vice versa. The amount of the no-which way information emerging from the outcomes of the joint sLOCC measurement $\Pi_{\rm LR}^{(2)}$ is a measure of the spatial indistinguishability of the particles in the state $|\Psi^{(2)}\rangle$. We thus use $\mathcal{Z}^{(2)} := {\rm Tr}(\Pi_{\rm LR}^{(2)} |\Psi^{(2)}\rangle \langle\Psi^{(2)}|) = \mathcal{P}_{12} + \mathcal{P}_{21}$, that encloses the essence of this lack of information, to introduce the entropic measure of the degree of remote spatial indistinguishability

$$\mathcal{I}_{\rm LR} := -\frac{\mathcal{P}_{12}}{\mathcal{Z}} \log_2 \frac{\mathcal{P}_{12}}{\mathcal{Z}} - \frac{\mathcal{P}_{21}}{\mathcal{Z}} \log_2 \frac{\mathcal{P}_{21}}{\mathcal{Z}}. \tag{2.7}$$

The entropic expression above naturally arises from the requirement of quantifying the *no which-way information* associated to the uncertainty about the origin (spatial wave function) of the particle found in each of the operational regions. If particles do not spatially overlap in both remote regions, we have maximum information ($\mathcal{P}_{12} = 1$, $\mathcal{P}_{21} = 0$ or vice versa) and $\mathcal{I}_{\rm LR} = 0$ (the particles can be distinguished by their spatial location). On the other hand, $\mathcal{I}_{\rm LR} = 1$ when there is no information at all about each particle origin ($\mathcal{P}_{12} = \mathcal{P}_{21}$) and the particles are maximally overlapping in both regions. Notice that a given value of $\mathcal{I}_{\rm LR}$ corresponds to a class of different shapes of the single-particle spatial wave functions $|\psi_i\rangle$. Moreover, in an experiment which reconstructs the identical particle state by standard quantum tomography, the corresponding value of $\mathcal{I}_{\rm LR}$ can be indirectly obtained.

The above definition of the degree of spatial indistinguishability for two identical particles allows us to defining a more general degree of indistinguishability for N identical particles. In general, N different operational regions $\mathcal{R}_i$ ($i = 1, \ldots, N$) are needed to quantify the indistinguishability of N identical particles (see Fig. 2.1). Let us consider a N-identical particle elementary pure state $|\Psi^{(N)}\rangle = |\chi_1, \chi_2, ..., \chi_N\rangle$, where $|\chi_i\rangle$ is the i-th single-particle state. Each $|\chi_i\rangle$ is characterized by the set of values $\chi_i = \chi_i^a, \chi_i^b, \ldots, \chi_i^n$ corresponding to a complete set of commuting observables $\hat{a}, \hat{b}, \ldots, \hat{n}$. For example, if $\hat{a}$ describes the spatial distribution of the single-particle states, χ_i^a is a spatial wavefunction ψ_i. To define a suitable class of measurements, we take the N-particle state

$$|\alpha\beta\rangle_N := |\alpha_1\beta_1, \alpha_2\beta_2, \ldots, \alpha_N\beta_N\rangle\,, \tag{2.8}$$

where the i-th single-particle state $|\alpha_i\beta_i\rangle$ is characterized by a subset $\hat{a}, \hat{b}, \ldots, \hat{j}$ of the $\hat{a}, \hat{b}, \ldots, \hat{n}$ commuting observables with eigenvalues $\alpha_i = \alpha_i^a, \alpha_i^b, \ldots, \alpha_i^j$, and by the remaining observables $\hat{k}, \ldots, \hat{n}$ with eigenvalues $\beta_i = \beta_i^k, \ldots, \beta_i^n$. In the first member of Eq. (2.8) we have set $\alpha := \{\alpha_1, ..., \alpha_N\}$ and $\beta := \{\beta_1, ..., \beta_N\}$. The N-particle projector on outcomes (α, β) of the complete set of observables is $\Pi_{\alpha\beta}^{(N)} = |\alpha\beta\rangle_N \langle\alpha\beta|$, while the projector on outcomes α of the partial set of observables is

$$\Pi_{\alpha}^{(N)} = \sum_{\beta} \Pi_{\alpha\beta}^{(N)}. \tag{2.9}$$

Within the sLOCC framework, we can quantify to which extent particles in the state $|\Psi^{(N)}\rangle$ can be distinguished by knowing the results α of the local measurements described by $\Pi_{\alpha}^{(N)}$ of Eq. (2.9), considering that single-particle spatial wave functions $\{\psi_i\}$ can overlap (see Figure 2.1). The (sLOCC) measurements have to satisfy the following properties: 1) the N single-particle states $\{|\alpha_i\beta_i\rangle\}$ are peaked

in separated spatial regions $\{\mathcal{R}_i\}$ (see Figure 2.1); 2) $\langle\Psi^{(N)}|\Pi_\alpha^{(N)}|\Psi^{(N)}\rangle \neq 0$, i.e. the probability of obtaining the projected state must be different from zero (see Methods and Supplementary Note 1 for the general formulas).

We indicate with $P_{\alpha_i\chi_j}$ the single-particle probability that the result α_i comes from the state $|\chi_j\rangle$. We then define the joint probability $P_{\alpha\mathcal{P}} := P_{\alpha_1\chi_{p_1}} P_{\alpha_2\chi_{p_2}} \cdots P_{\alpha_N\chi_{p_N}}$, where $\mathcal{P} = \{p_1, p_2, ..., p_N\}$ is one of the $N!$ permutations of the N single-particle states $\{|\chi_i\rangle\}$. Notice that $P_{\alpha\mathcal{P}}$ can be nonzero for each of the $N!$ permutations, since in general the outcome α_i can come from any of the single-particle state $|\chi_j\rangle$. The quantity $\mathcal{Z} = \sum_{\mathcal{P}} P_{\alpha\mathcal{P}}$ thus accounts for this no which-way effect concerning the probabilities. The degree of indistinguishability is finally given by

$$\mathcal{I}_\alpha := -\sum_{\mathcal{P}} \frac{P_{\alpha\mathcal{P}}}{\mathcal{Z}^{(N)}} \log_2 \frac{P_{\alpha\mathcal{P}}}{\mathcal{Z}^{(N)}}. \tag{2.10}$$

This quantity depends on measurements performed on the state. If the particles are initially all spatially separated, each in a different measurement region, only one permutation remains and $\mathcal{I}_\alpha = 0$: we have complete knowledge on the single-particle state $|\chi_j\rangle$ which gives the outcome α_i, meaning that the particles are distinguishable with respect to the measurement $\Pi_\alpha^{(N)}$. On the other hand, if for any possible permutation $\mathcal{P}' \neq \mathcal{P}$ one has $P_{\alpha\mathcal{P}'} = P_{\alpha\mathcal{P}}$, indistinguishability is maximum and reaches the value $\mathcal{I}_\alpha = \log_2 N!$. As a specific example, when $\chi_i^a = \psi_i$ (spatial wave functions) and $\chi_i^b = \sigma_i$ (pseudospins), $\mathcal{I}_\alpha$ of Eq. (2.10) is the direct generalization of $\mathcal{I}_{\rm LR}$ of Eq. (4.14) and provides the degree of spatial indistinguishability under sLOCC for N identical particles.

Application: Noisy preparation of pure entangled state. We now apply the tools above to a situation of experimental interest, namely noisy entanglement generation with identical particles.

Werner state [197] $W_{\rm AB}^{\pm}$ for two nonidentical qubits A and B is considered as the paradigmatic example of realistic noisy preparation of a pure entangled state subject to the action of white noise. In the usual formulation, it is defined as a mixture of a pure maximally entangled (Bell) state and of the maximally mixed state (white noise). Its explicit expression, assuming to be interested in generating the Bell state $|\Psi_\pm^{\rm AB}\rangle = (|\uparrow_{\rm A},\downarrow_{\rm B}\rangle \pm |\downarrow_{\rm A},\uparrow_{\rm B}\rangle)/\sqrt{2}$, is $W_{\rm AB}^{\pm} = (1-p)\,|\Psi_\pm^{\rm AB}\rangle\langle\Psi_\pm^{\rm AB}| + p\mathbb{I}_4/4$, where $\mathbb{I}_4$ is the 4×4 identity matrix and p is the noise probability which accounts for the amount of white noise in the system during the pure state preparation stage. The Werner state $W_{\rm AB}^{\pm}$ is also the product of a single-particle depolarizing channel induced by the environment applied to an initial Bell state [166, 33]. It is known that the concurrence for such state is $C(W_{\rm AB}^{\pm}) = 1 - 3p/2$ when $0 \leq p < 2/3$, being zero otherwise [33] (see black dot-dashed line of Fig. 2.3**a**).

In perfect analogy, the Werner state for two identical qubits with spatial wave functions ψ_1, ψ_2 can be defined by

$$\mathcal{W}^{\pm} = (1-p)\,|1_\pm\rangle\langle 1_\pm| + p\mathcal{I}_4/4, \tag{2.11}$$

where $\mathcal{I}_4 = \sum_{i=1,2;s=\pm} |i_s\rangle\langle i_s|$, having used the orthogonal Bell-state basis $\mathcal{B}_{\{1_\pm,2_\pm\}} = \{|1_+\rangle, |1_-\rangle, |2_+\rangle, |2_-\rangle\}$ with

$$\begin{aligned} |1_\pm\rangle &:= (|\psi_1\uparrow, \psi_2\downarrow\rangle \pm |\psi_1\downarrow, \psi_2\uparrow\rangle)/\sqrt{2}, \\ |2_\pm\rangle &:= (|\psi_1\uparrow, \psi_2\uparrow\rangle) \pm |\psi_1\downarrow, \psi_2\downarrow\rangle)/\sqrt{2}. \end{aligned} \tag{2.12}$$

The Werner state of Eq. (2.11) is justified as a model of noisy state. In fact, it is straightforward to see that $\mathcal{W}^{\pm}$ is produced by a localized depolarizing channel acting on one of two initially separated identical qubits, followed by a quick single-particle spatial deformation procedure which makes the two identical qubits spatially overlap (see Supplementary Note 2). Hence, in Eq. (2.11), $|1_\pm\rangle$ is the target pure state to be prepared and $\mathcal{I}_4/4$ is the noise as a mixture of the four Bell states.

Given the configuration of the spatial wave functions and using the sLOCC framework, the amount of operational entanglement contained in $\mathcal{W}^{\pm}$ can be obtained by the concurrence $C_{\rm LR}(\mathcal{W}^{\pm}) = C(\mathcal{W}_{\rm LR}^{\pm})$ of Eq. (4.13). Notice that the state of Eq. (2.11) is in general not normalized, depending on the specific spatial degrees of freedom [3]. This is irrelevant at this stage, since the entanglement of $\mathcal{W}^{\pm}$ is calculated

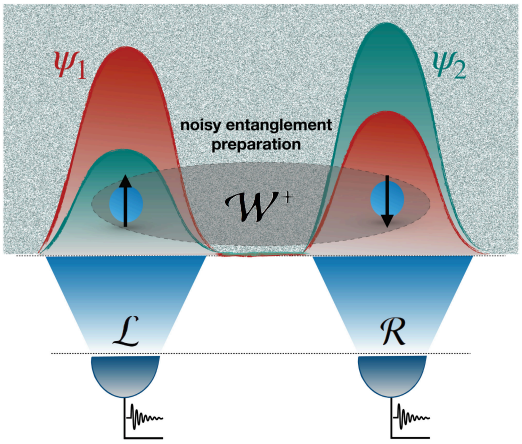

Figure 2.2: **Noisy entanglement preparation with tailored spatial indistinguishability.** Illustration of two controllable spatially overlapping wave functions ψ_1, ψ_2 peaked in the two localized regions of measurement $\mathcal{L}$ and $\mathcal{R}$. The two identical qubits are prepared in an entangled state under noisy conditions, giving $\mathcal{W}^{\pm}$. The degree of spatial indistinguishability can be tuned, being $0 \leq \mathcal{I}_{\rm LR} \leq 1$.

on the final distributed state $\mathcal{W}^{\pm}_{\rm LR}$, which is obtained from $\mathcal{W}^{\pm}$ after sLOCC and is normalized (see Eq. (4.12)). Focusing on the observation of entanglement, a well-suited configuration for the spatial wave functions is $|\psi_1\rangle = l\,|{\rm L}\rangle + r\,|{\rm R}\rangle$ and $|\psi_2\rangle = l'\,|{\rm L}\rangle + r' e^{i\theta}\,|{\rm R}\rangle$, where l, r, l', r' are non-negative real numbers ($l^2{+}r^2 = l'^2{+}r'^2 = 1$) and θ is a phase. The wave functions are thus peaked in the two localized measurement regions $\mathcal{L}$ and $\mathcal{R}$, as depicted in Figure 2.2. The degree of spatial indistinguishability $\mathcal{I}_{\rm LR}$ of Eq. (4.14) is tailored by adjusting the shapes of $|\psi_1\rangle$, $|\psi_2\rangle$, with $P_{{\rm L}\psi_1} = l^2$, $P_{{\rm L}\psi_2} = l'^2$ (implying $P_{{\rm R}\psi_1} = r^2$, $P_{{\rm R}\psi_2} = r'^2$). The interplay between $C_{\rm LR}(\mathcal{W}^{\pm})$ and $\mathcal{I}_{\rm LR}$ versus noise probability p can be then investigated (see Supplementary Note 3 for some explicit expressions of $C_{\rm LR}(\mathcal{W}^{\pm})$).

Generally, the entanglement amount is conditional since the state is obtained by postselection. As a result, the entangled state ρ_{LR} is detectable if the sLOCC probability $P_{\rm LR}$ is high enough to be of experimental relevance. Let us see what happens for $\mathcal{I}_{\rm LR} = 1$ ($l = l'$). When the target pure state in Eq. (2.11) is $|1_-\rangle$, using in Eq. (4.20) the explicit expressions of $|\psi_1\rangle$, $|\psi_2\rangle$ with $\theta = 0$ ($\theta = \pi$) for fermions (bosons), from $\mathcal{W}^-$ we obtain by sLOCC the distributed Bell state $\mathcal{W}^-_{\rm LR} = |1^{\rm LR}_-\rangle\langle 1^{\rm LR}_-|$, with $|1^{\rm LR}_-\rangle = (|{\rm L}\uparrow,{\rm R}\downarrow\rangle - |{\rm L}\downarrow,{\rm R}\uparrow\rangle)/\sqrt{2}$, therefore (see blue solid line of Fig. 2.3**a**)

$$C_{\rm LR}(\mathcal{W}^-) = C(\mathcal{W}^-_{\rm LR}) = 1, \textit{ for any noise probability } p \tag{2.13}$$

for which the probabilities of detecting this state for fermions and bosons are, respectively,

$$P^{\rm (f)}_{\rm LR} = 2l^2(1-l^2), \quad P^{\rm (b)}_{\rm LR} = \frac{2l^2\left(1-l^2\right)(4-3p)}{2-\left(1-2l^2\right)^2(2-3p)}. \tag{2.14}$$

Notice that the sLOCC probability for fermions, $P^{\rm (f)}_{\rm LR}$, is in this case independent of the noise probability. Fixing $l^2 = 1/2$ we maximize the sLOCC probability, which is $1/2$ for fermions and $1/4$ for bosons in the worst scenario of maximum noise probability $p = 1$. Differently, targeting the pure state $|1_+\rangle$ in Eq. (2.11), for fermions (bosons) with $\theta = \pi$ ($\theta = 0$), one gets a p-dependent $\mathcal{W}^+_{\rm LR}$ by sLOCC with $C_{\rm LR}(\mathcal{W}^+) = C(\mathcal{W}^+_{\rm LR}) = (4-5p)/(4-p)$ when $0 \leq p < 4/5$, being zero elsewhere. The entanglement now decreases with increasing noise, remaining however larger than that for nonidentical qubits (see red dashed line of Fig. 2.3**a**). The choice of the state to generate makes a difference concerning noise protection by indistinguishability. However, we remark that identical qubits in the distributed resource state after sLOCC, $\mathcal{W}^{\pm}_{\rm LR}$, are individually addressable. Local unitary operations (rotations) in $\mathcal{L}$ and $\mathcal{R}$ can be applied to each qubit to transform the noise-free prepared $|1^{\rm LR}_-\rangle$ into any other Bell state [33]. Another relevant aspect is that the phase θ in $|\psi_2\rangle$ acts as a switch between fermionic and bosonic

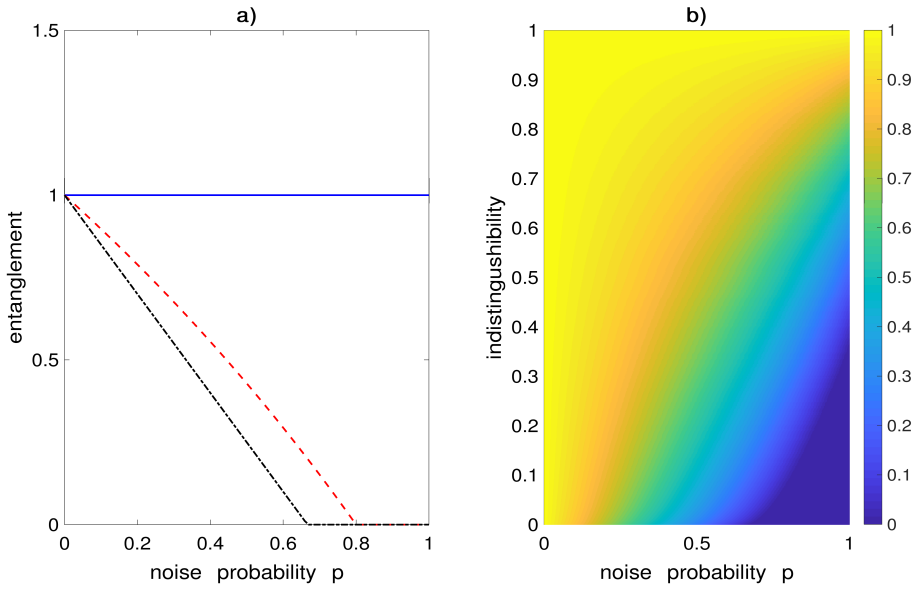

Figure 2.3: **Prepared entanglement and indistinguishability. a.** Entanglement $C_{\rm LR}(\mathcal{W}^{\pm})$ as a function of noise probability p for different degrees of spatial indistinguishability $\mathcal{I}_{\rm LR}$ and system parameters: blue solid line is for target state $|1_{-}\rangle$, $\mathcal{I}_{\rm LR}=1$ ($l=l'$), fermions (with $\theta=0$) or bosons (with $\theta=\pi$); red dashed line is for target state $|1_{+}\rangle$, $\mathcal{I}_{\rm LR}=1$ ($l=l'$), fermions (with $\theta=\pi$) or bosons (with $\theta=0$); black dot-dashed line is for distinguishable qubits ($\mathcal{I}_{\rm LR}=0$, $l=1$ and $l'=0$ or vice versa). **b.** Contour plot of entanglement $C_{\rm LR}(\mathcal{W}^{-})$ versus noise probability p and spatial indistinguishability $\mathcal{I}_{\rm LR}$ for target state $|1_{-}\rangle$, fermions (with $\theta=0$) or bosons (with $\theta=\pi$), fixing $l=r'$.

behavior of entanglement (see Supplementary Note 3 for details on more general instances). The result for nonidentical particles is retrieved when the qubits become distinguishable ($\mathcal{I}_{\rm LR}=0$, $l=r'=1$ or $l=r'=0$).

Since the preparation of $|1_{-}\rangle$, as represented by Eq. (2.11), results to be noise-free for both fermions and bosons when $\mathcal{I}_{\rm LR}=1$, it is important to know what occurs for a realistic imperfect degree of spatial indistinguishability. In Fig.2.3**b** we display entanglement as a function of both p and $\mathcal{I}_{\rm LR}$. The plot reveals that entanglement preparation can be efficiently protected against noise also for $\mathcal{I}_{\rm LR}<1$. A crucial information in this scenario is the minimum degree of $\mathcal{I}_{\rm LR}$ that guarantees nonlocal entanglement in $\mathcal{L}$ and $\mathcal{R}$, by violating a CHSH-Bell inequality [33], whatever the noise probability p. We remark that a Bell inequality violation based on sLOCC provides a faithful test of local realism [198]. Using the Horodecki criterion [199], we find that the Bell inequality is violated for any p whenever $0.76<\mathcal{I}_{\rm LR}\leq 1$, implying $0.56<C_{\rm LR}(\mathcal{W}^{-})\leq 1$ (see Supplementary Note 4 for details). This is basically different from the case of distinguishable qubits where, as known [33], $W^{\pm}_{\rm AB}$ violates Bell inequality only for small white noise probabilities $0\leq p<0.292$ (giving $0.68<C(W^{\pm}_{\rm AB})\leq 1$). These results show robust quantum entanglement preparation against noise through spatial indistinguishability, even partial. In fact, rather than addressing individual qubits, here one controls the shapes of their spatial wave functions $|\psi_1\rangle$, $|\psi_2\rangle$. Significant changes in these shapes can occur that anyway maintain $\mathcal{I}_{\rm LR}$ of Eq. (4.14) beyond the threshold (≈ 0.76) assuring noise-free generation of nonlocal entanglement. Indistinguishability here emerges as a property of composite quantum systems inherently robust to surrounding-induced disorder, protecting exploitable quantum correlations.

2.3 Discussion

In this work, we have studied the effect of spatial indistinguishability on entanglement preparation under noise, within the sLOCC framework. Firstly, thanks to the analogy with known methods for distin-

guishable particles, the entanglement of formation, and the related concurrence, has been defined for an arbitrary pure or mixed state of two identical qubits. Secondly, we have introduced the degree of spatial indistinguishability of identical particles by an entropic measure of information. This achievement entails a continuous quantitative identification of indistinguishability as an informational resource. Hence, one can evaluate the amount of entanglement exploitable by sLOCC into two separated operational sites under general conditions of spatial indistinguishability and state mixedness.

The Werner state $\mathcal{W}^{\pm}$ has been then chosen as a typical instance of noisy mixed state of two identical qubits, with tunable spatial overlap of their wave functions on the two remote operational regions. The tunable spatial overlap rules the indistinguishability degree. We have found that, under conditions of complete spatial indistinguishability, maximally entangled pure states between internal (spin-like) degrees of freedom can be prepared unaffected by noise. Even in the more realistic scenario of experimental errors in controlling particle spatial overlap, we have supplied a lower bound for the degree of spatial indistinguishability beyond which the generated entangled state violates the CHSH-Bell inequality independently of the amount of noise. These findings are independent of particle statistics, holding for both bosons and fermions. One reasonably may expect that also coherence can be protected by spatial indistinguishability, based on a previous work showing that the latter enables quantum coherence [94]. This supports the observed effects in an experiment of coherence endurance due to particle indistinguishability [32].

The degree of spatial indistinguishability exhibits robustness to variations in the configuration of spatial wave functions, being then capable of shielding nonlocal entangled states against preparation noise. Therefore, indistinguishability represents a resource of quantum networks made of identical qubits enabling noise-free entanglement generation by its physical nature. Such a finding, which is promising to fault-tolerant quantum information tasks under environmental noise, adds to other known protection techniques of quantum states based on, for example, topological properties [115, 200, 201, 202, 203, 204, 205, 53], dynamical decoupling or decoherence-free subspace [206, 207, 208, 108, 111]. As an outlook, the effects of spatial indistinguishability on quantumness protection for different types of environmental noises will be addressed elsewhere.

Various experimental contexts can be thought for implementing the above theoretical scenario. For example, in quantum optics, spatially localized detectors can perform the required measurements while beam splitters can serve as controller of spatial wave functions of independent traveling photons (bosons) with given polarization pseudospin. In a more sophisticated example with circular polarizations, one may employ orbital angular momentum of photons as spatial wave function and spin angular momentum as spin-like degree of freedom [209, 210, 211]. Setups using integrated quantum optics can also simulate fermionic statistics using photons [212]. Other suitable platforms for fermionic subsystems can be supplied either by superconducting quantum circuits with Ramsey interferometry [213], or by quantum electronics with quantum point contacts as electronic beam splitters [214, 215, 216]. The results of this work are expected to stimulate further theoretical and experimental studies concerning the multiple facets of indistinguishability as a controllable fundamental quantum trait and its exploitation for quantum technologies.

2.4 Methods

Amplitudes and probabilities in the no-label approach. For calculating all the necessary probabilities and traces to obtain the results of the work, under different spatial configurations of the wave functions, we need to compute scalar products (amplitudes) between states of N identical particles.

The N-particle probability amplitude has been defined in the literature by means of the no-label particle-based approach, here adopted, to deal with systems of identical particles [3]. Indicating with χ_i, χ'_i $(i = 1, \ldots, N)$ single-particle states containing all the degrees of freedom of the particle, the general

expression of the N-particle probability amplitude is

$$\begin{aligned}&\langle\chi_1',\chi_2',\ldots,\chi_n'|\chi_1,\chi_2,\ldots,\chi_n\rangle\\ &:=\textstyle\sum_P \eta^P\langle\chi_1'|\chi_{P_1}\rangle\langle\chi_2'|\chi_{P_2}\rangle\ldots\langle\chi_n'|\chi_{P_n}\rangle,\end{aligned}\tag{2.15}$$

where $P=\{P_1,P_2,...,P_n\}$ in the sum runs over all the one-particle state permutations, $\eta=\pm1$ for bosons and fermions, respectively, and η^P is 1 for bosons and 1 (-1) for even (odd) permutations for fermions. Notice that the explicit dependence on the particle statistics appears, as expected.

Along our manuscript, we especially need two-particle probabilities and trace operations. For $N=2$, the general expression above reduces to the following two-particle probability amplitude

$$\langle\chi_1',\chi_2'|\chi_1,\chi_2\rangle=\langle\chi_1'|\chi_1\rangle\langle\chi_2'|\chi_2\rangle+\eta\langle\chi_1'|\chi_2\rangle\langle\chi_2'|\chi_1\rangle.\tag{2.16}$$

Supplementary Material

A. Amplitudes and probabilities in the no-label approach

For calculating all the necessary probabilities and traces to obtain the results of the work, under different spatial configurations of the wave functions, we need to compute scalar products (amplitudes) between states of N identical particles.

The N-particle probability amplitude has been defined in the literature by means of the no-label particle-based approach, here adopted, to deal with systems of identical particles [3]. Indicating with χ_i, χ_i' $(i=1,\ldots,N)$ single-particle states containing all the degrees of freedom of the particle, the general expression of the N-particle probability amplitude is

$$\begin{aligned}&\langle\chi_1',\chi_2',\ldots,\chi_n'|\chi_1,\chi_2,\ldots,\chi_n\rangle\\ &:=\textstyle\sum_P \eta^P\langle\chi_1'|\chi_{P_1}\rangle\langle\chi_2'|\chi_{P_2}\rangle\ldots\langle\chi_n'|\chi_{P_n}\rangle,\end{aligned}\tag{2.17}$$

where $P=\{P_1,P_2,...,P_n\}$ in the sum runs over all the one-particle state permutations, $\eta=\pm1$ for bosons and fermions, respectively, and η^P is 1 for bosons and 1 (-1) for even (odd) permutations for fermions. Notice that the explicit dependence on the particle statistics appears, as expected.

Along our manuscript and in the rest of the Supplementary Information, we especially need two-particle probabilities and trace. For $N=2$, the general expression above reduces to the following two-particle probability amplitude

$$\langle\chi_1',\chi_2'|\chi_1,\chi_2\rangle=\langle\chi_1'|\chi_1\rangle\langle\chi_2'|\chi_2\rangle+\eta\langle\chi_1'|\chi_2\rangle\langle\chi_2'|\chi_1\rangle.\tag{2.18}$$

B. Werner state $\mathcal{W}^{\pm}$ of two indistinguishable qubits

In the following, we describe two different ways which produce the Werner state $\mathcal{W}^{\pm}$ of two indistinguishable particles, given in the main text.

Analogy with distinguishable particles. Let us consider the orthogonal Bell states of two indistinguishable qubits, with spatial wave functions ψ_1 and ψ_2, which are defined as

$$\begin{aligned}|1_\pm\rangle &= (|\psi_1\uparrow,\psi_2\downarrow\rangle\pm|\psi_1\downarrow,\psi_2\uparrow\rangle)/\sqrt{2},\\ |2_\pm\rangle &= (|\psi_1\uparrow,\psi_2\uparrow\rangle)\pm|\psi_1\downarrow,\psi_2\downarrow\rangle)/\sqrt{2}.\end{aligned}\tag{2.19}$$

Each of these Bell states is not normalized in general. Their normalized expressions are

$$\begin{aligned}|\bar{1}_\pm\rangle &= \frac{1}{\sqrt{2\mathcal{N}_{1_\pm}}}(|\psi_1\uparrow,\psi_2\downarrow\rangle\pm|\psi_1\downarrow,\psi_2\uparrow\rangle),\\ |\bar{2}_\pm\rangle &= \frac{1}{\sqrt{2\mathcal{N}_{2_\pm}}}(|\psi_1\uparrow,\psi_2\uparrow\rangle)\pm|\psi_1\downarrow,\psi_2\downarrow\rangle),\end{aligned}\tag{2.20}$$

where $\mathcal{N}_{1_-} = (1 - \eta|\langle\psi_1|\psi_2\rangle|^2)$ and $\mathcal{N}_{1_+} = \mathcal{N}_{2_\pm} = (1 + \eta|\langle\psi_1|\psi_2\rangle|^2)$.

For two distinguishable (or nonidentical) qubits A and B, a Werner state $W^{\pm}_{\rm AB}$ is a mixture of a pure maximally entangled (Bell) state and of the maximally mixed state [197]. Its explicit expression, assuming to be interested in preparing the Bell state $|\Psi^{\rm AB}_{\pm}\rangle = (|\uparrow_{\rm A},\downarrow_{\rm B}\rangle \pm |\downarrow_{\rm A},\uparrow_{\rm B}\rangle)/\sqrt{2}$, is

$$W^{\pm}_{\rm AB} = (1-p)\,|\Psi^{\rm AB}_{\pm}\rangle\,\langle\Psi^{\rm AB}_{\pm}| + p\mathbb{I}_4/4, \tag{2.21}$$

where $\mathbb{I}_4$ is the 4×4 identity matrix and p is the noise probability accounting for the amount of white noise in the system [33]. Notice that $\mathbb{I}_4$ can be written either in the computation basis or in the basis of the four Bell states. The Werner state is of wide interest since it can be meant as a state representing a (realistic) noisy preparation of pure two-qubit entangled states [166, 33].

In strict analogy with $W^{\pm}_{\rm AB}$, the Werner state of a pair of identical qubits with spatial wave functions ψ_1 and ψ_2 can be expressed in the orthogonal Bell-state basis $\mathcal{B}_{\{1_\pm,2_\pm\}} = \{|1_+\rangle, |1_-\rangle, |2_+\rangle, |2_-\rangle\}$ by

$$\mathcal{W}^{\pm} = (1-p)\,|1_{\pm}\rangle\,\langle 1_{\pm}| + p\mathcal{I}_4/4, \tag{2.22}$$

where $\mathcal{I}_4 = \sum_{i=1,2;s=\pm} |i_s\rangle\,\langle i_s|$. The state $\mathcal{W}$ is in general unnormalized. Its normalized expression $\bar{\mathcal{W}} = \mathcal{W}/\mathcal{N}_{\pm}$ requires a global normalization constant

$$\mathcal{N}_{\pm} = 1 + \eta|\langle\psi_1|\psi_2\rangle|^2[p/2 \pm (1-p)]. \tag{2.23}$$

Using normalized Bell states of Eq. (4.20), this state can be equivalently expressed by

$$\bar{\mathcal{W}^{\pm}} = \frac{1}{\mathcal{N}_{\pm}}\left((1-p)\mathcal{N}_{1_\pm}\,|\bar{1}_{\pm}\rangle\,\langle\bar{1}_{\pm}| + \frac{p}{4}\sum_{i=1,2;s=\pm}\mathcal{N}_{i_s}\,|\bar{i}_s\rangle\,\langle\bar{i}_s|\right). \tag{2.24}$$

Notice that the state $\mathcal{W}^{\pm}$ reduces to the usual Werner state of two distinguishable qubits $W^{\pm}_{\rm AB}$ of Eq. (2.21) when there is no spatial overlap between the qubits, so that the latter can be individually addressed in their separated locations.

$\mathcal{W}^{\pm}$ as a model of noisy state. The Werner state of Eq. (2.22) is justified as a model of noisy state, being produced by a localized single-particle depolarizing channel acting on one of two initially separated identical qubits, followed by a quick single-particle spatial deformation procedure which makes the two identical qubits spatially overlap. In the following we show this in detail.

It is known that the Werner state $W^{\pm}_{AB} = (1-p)\,|\Psi^{AB}_{\pm}\rangle\,\langle\Psi^{AB}_{\pm}| + p\mathbb{I}_4/4$ for two distinguishable (nonidentical) qubits A and B is the output of the single-qubit depolarizing channel action on one of the two qubits of an initial Bell state [166]. The process is such that the initial (maximally entangled) pure state tends to remain in the initial state with probability $1-p$ and changes to the maximally mixed state $\mathbb{I}_4/4$ with probability p. The Kraus (operator-sum) representation of the single-qubit depolarizing channel acting on an elementary pure state like $\rho_{AB} = |\phi_A,\phi_B\rangle\,\langle\phi_A,\phi_B|$ is given by [15, 166]

$$\rho(t) = \sum_{i=0}^{4} |K^A_i\phi_A\rangle \otimes |\mathbb{I}^B_2\phi_B\rangle\,\langle K^A_i\phi_A| \otimes \langle\mathbb{I}^B_2\phi_B|\,, \tag{2.25}$$

where the Kraus operators are $K_0 = \sqrt{1-3p/4}\;\mathbb{I}_2$ and $K_i = \sqrt{p/4}\sigma_i$ $(i=1,2,3)$, with $\mathbb{I}_2$ being the single-particle (2×2) identity operator and σ_i the usual Pauli matrices. Notice that here the channel individually acts on the internal degrees of freedom (pseudospins) of qubit A and $\langle K^A_i\phi_A| = \langle\phi_A|\,K^{A\dagger}_i$. Using the action on the elementary state of Eq. (2.25), it is then straightforward to see that $W^{\pm}_{AB}$ is obtained by the single-qubit depolarizing channel starting from a Bell state $|\Psi^{AB}_{\pm}\rangle = (|\uparrow_{\rm A},\downarrow_{\rm B}\rangle \pm |\downarrow_{\rm A},\uparrow_{\rm B}\rangle)/\sqrt{2}$ [166].

Now, let us consider a pair of two identical qubits which are initially separated, for example one in a location $\rm L_1$ and one a in location $\rm L_2$. If these qubits are initially in a Bell state $|\Psi^{\rm L_1L_2}_{\pm}\rangle = (|{\rm L_1}\uparrow,{\rm L_2}\downarrow\rangle \pm |{\rm L_1}\downarrow,{\rm L_2}\uparrow\rangle)/\sqrt{2}$ and the localized single-particle depolarizing channel of Eq. (2.25) acts on $\rm L_1$ ($A \leftrightarrow$

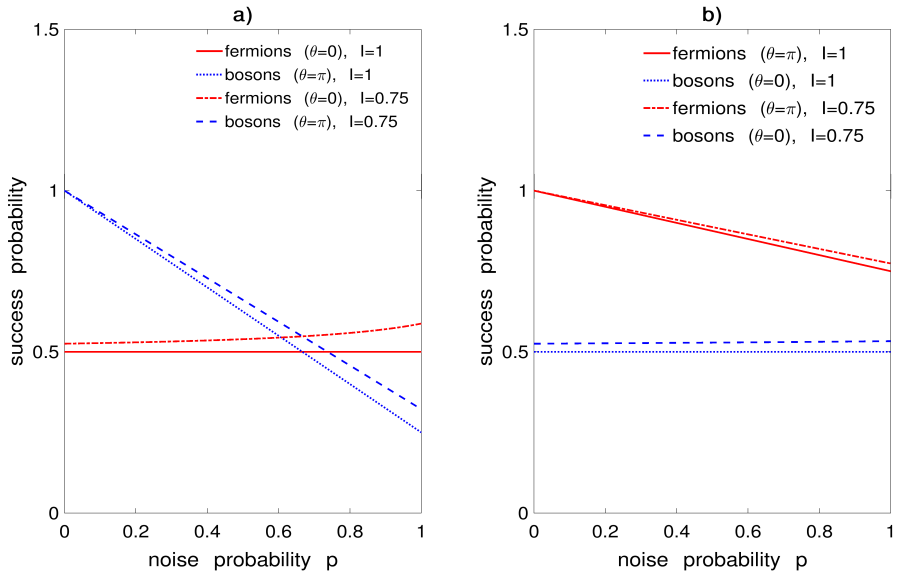

Figure 2.4: sLOCC probability $P_{\rm LR}$ (success probability) as a function of noise probability p for some degrees of spatial indistinguishability $\mathcal{I}_{\rm LR}$ and particle statistics, fixing $l = r'$ in the wave functions of Eq. (4.15). **a.** Target pure state $|1_-\rangle$ in Eq. (2.22). **b.** Target pure state $|1_+\rangle$ in Eq. (2.22).

L_1, $B \leftrightarrow \mathrm{L}_2$), for instance, the qubits behave as distinguishable particles labeled, respectively, by L_1 and L_2. Therefore, the resulting state at this stage is $W^{\pm}_{\mathrm{L}_1\mathrm{L}_2} = (1-p)\,|\Psi^{\mathrm{L}_1\mathrm{L}_2}_{\pm}\rangle\langle\Psi^{\mathrm{L}_1\mathrm{L}_2}_{\pm}| + p\mathbb{I}_4/4$, where $\mathbb{I}_4 = \sum_{k=\pm}(|\Psi^{\mathrm{L}_1\mathrm{L}_2}_k\rangle\langle\Psi^{\mathrm{L}_1\mathrm{L}_2}_k| + |\Phi^{\mathrm{L}_1\mathrm{L}_2}_k\rangle\langle\Phi^{\mathrm{L}_1\mathrm{L}_2}_k|)$, with $|\Phi^{\mathrm{L}_1\mathrm{L}_2}_k\rangle = (|\mathrm{L}_1\uparrow,\mathrm{L}_2\uparrow\rangle \pm |\mathrm{L}_1\downarrow,\mathrm{L}_2\downarrow\rangle)/\sqrt{2}$ being the other couple of Bell states. After the action of this localized depolarizing channel, one can apply a quick spatial deformation procedure on each qubit making the following transformation on the spatial degree of freedom: $|\mathrm{L}_1\rangle \to |\psi_1\rangle$, $|\mathrm{L}_2\rangle \to |\psi_2\rangle$. The two final spatial wave functions $|\psi_1\rangle$, $|\psi_2\rangle$ are in general spatially overlapping and the final output state of the entire procedure (localized depolarizing channel plus spatial deformation) immediately results to be

$$\mathcal{W}^{\pm} = (1-p)\,|1_{\pm}\rangle\langle 1_{\pm}| + p\mathcal{I}_4/4, \tag{2.26}$$

which is just the Werner state defined in Eq. (2.22). This result justifies the introduced Werner state for indistinguishable particles, $\mathcal{W}^{\pm}$, as a proper noisy state. We stress that a general analysis of different environmental noises and more general derivations of noise models for systems of indistinguishable particles is beyond the aim of the present paper and will be provided elsewhere.

C. Concurrence of $\mathcal{W}^{\pm}$ state

Given the state $\mathcal{W}^{\pm}$ of Eq. (2.22) and the structure of the spatial wave functions, the amount of operational entanglement contained in $\mathcal{W}^{\pm}$ can be obtained by sLOCC. Aiming at observing entanglement in separated regions, also in view of CHSH-Bell inequality violations [33], a suitable form for the spatial wave functions appearing in Eq. (2.22) is

$$|\psi_1\rangle = l\,|\mathrm{L}\rangle + r\,|\mathrm{R}\rangle\,, \quad |\psi_2\rangle = l'\,|\mathrm{L}\rangle + r'e^{i\theta}\,|\mathrm{R}\rangle\,, \tag{2.27}$$

where l, r, l' and r' are non-negative real numbers (with $l^2 + r^2 = l'^2 + r'^2 = 1$) and θ is a phase.

Projecting $\mathcal{W}$ onto the (operational) subspace spanned by the computational basis $\mathcal{B}_{\rm LR} = \{|\mathrm{L}\uparrow \mathrm{R}\uparrow\rangle, |\mathrm{L}\uparrow,\mathrm{R}\downarrow\rangle, |\mathrm{L}\downarrow,\mathrm{R}\uparrow\rangle, |\mathrm{L}\downarrow,\mathrm{R}\downarrow\rangle\}$ by means of the projector

$$\Pi^{(2)}_{\rm LR} = \sum_{\tau_1,\tau_2=\uparrow,\downarrow} |\mathrm{L}\tau_1,\mathrm{R}\tau_2\rangle\langle\mathrm{L}\tau_1,\mathrm{R}\tau_2|\,, \tag{2.28}$$

and using the scalar product of Eq. (2.18), we obtain the distributed resource state

$$\mathcal{W}_{\rm LR}^{\pm} = \Pi_{\rm LR}^{(2)} \mathcal{W}^{\pm} \Pi_{\rm LR}^{(2)} / {\rm Tr}(\Pi_{\rm LR}^{(2)} \mathcal{W}^{\pm}), \tag{2.29}$$

with probability $P_{\rm LR} = {\rm Tr}(\Pi_{\rm LR}^{(2)} \bar{\mathcal{W}}^{\pm})$. The trace operation is performed in the LR-subspace. The (normalized) state $\mathcal{W}_{\rm LR}^{\pm}$ can be then treated as the state of two distinguishable qubits in separated bound states $|{\rm L}\rangle$, localized in the region $\mathcal{L}$, and $|{\rm R}\rangle$, localized in the region $\mathcal{R}$ [16]. Therefore, the sLOCC-based concurrence $C_{\rm LR}(\mathcal{W}^{\pm}) := C(\mathcal{W}_{\rm LR}^{\pm})$ can be calculated by the usual criterion for distinguishable qubits [196, 195], that is by

$$C(\mathcal{W}_{\rm LR}^{\pm}) = \max\{0, \sqrt{\lambda_4} - \sqrt{\lambda_3} - \sqrt{\lambda_2} - \sqrt{\lambda_1}\}, \tag{2.30}$$

where the λ_i's are the eigenvalues, in decreasing order, of the non-Hermitian matrix $R = \rho_{\rm LR}\, \rho_{\rm LR}$, being

$$\rho_{\rm LR} = \sigma_y^{\rm L} \otimes \sigma_y^{\rm R} \rho_{\rm LR}^{*} \sigma_y^{\rm L} \otimes \sigma_y^{\rm R}, \tag{2.31}$$

with localized Pauli matrices defined as $\sigma_y^{\rm L} \equiv |{\rm L}\rangle\langle{\rm L}| \otimes \sigma_y$ and $\sigma_y^{\rm R} \equiv |{\rm R}\rangle\langle{\rm R}| \otimes \sigma_y$.

Thanks to the explicit expressions of the spatial wave functions of Eq. (4.15) above, the degree of spatial indistinguishability under sLOCC $\mathcal{I}_{\rm LR}$, defined in Eq. (9) of the main text, can be then explicitly calculated by substituting $P_{{\rm L}\psi_1} = l^2$, $P_{{\rm L}\psi_2} = l'^2$, $P_{{\rm R}\psi_1} = r^2$ and $P_{{\rm R}\psi_2} = r'^2$.

We can now report the explicit expressions of $C_{\rm LR}(\mathcal{W}^{\pm}) := C(\mathcal{W}_{\rm LR}^{\pm})$ for some cases of particular interest. As a remarkable aspect, our calculations show that the phase θ of $|\psi_2\rangle$, when assuming binary values $0, \pi$, acts as a switch between fermionic and bosonic entanglement behavior. This is why in the main text and in the following expressions, only these values of θ are chosen.

When the pure state $|1_-\rangle$ is considered in the $\mathcal{W}^-$ state of Eq. (2.22), for fermions (bosons) with $\theta = 0$ ($\theta = \pi$) we find

$$C(\mathcal{W}_{\rm LR}^{-}) = \max\left\{0, \frac{(4-3p)(lr'+l'r)^2 - 3p(lr'-l'r)^2}{4\left(l^2r'^2 + l'^2r^2 + lr'rl'(2-3p)\right)}\right\}, \tag{2.32}$$

with probability

$$P_{\rm LR} = \frac{2\left(l^2r'^2 + l'^2r^2 + lr'rl'(2-3p)\right)}{2 - \eta(2-3p)(ll' - \eta rr')^2}, \tag{2.33}$$

where $\eta = +1$ for bosons and $\eta = -1$ for fermions, as said before. The plot of this concurrence as a function of $\mathcal{I}_{LR}$ and p, fixing $l = r'$, is reported in Figure 3b of the main text. As can be seen from Eq. (4.31), by setting $l = l'$ (implying $r = r'$) so to have maximum indistinguishability $\mathcal{I}_{\rm LR} = 1$, one gets $C(\mathcal{W}_{\rm LR}^{-}) = 1$ independently of p. The sLOCC probability is maximized when $l = l' = 1/\sqrt{2}$, taking the values $P_{\rm LR} = 1/2$ for fermions and $P_{\rm LR} = 1 - 3p/4$ for bosons. The sLOCC probability $P_{\rm LR}$ of Eq. (2.33) is plotted in Fig. 2.4(a) as a function of noise probability p for some degrees of spatial indistinguishability $\mathcal{I}_{\rm LR}$.

Differently, when the pure state $|1_+\rangle$ is chosen in the $\mathcal{W}^+$ state of Eq. (2.22), for fermions (bosons) with $\theta = \pi$ ($\theta = 0$) we obtain

$$C(\mathcal{W}_{\rm LR}^{+}) = \max\left\{0, \frac{(4-5p)(lr'+l'r)^2 - p(lr'-l'r)^2}{4\left(l^2r'^2 + l'^2r^2 + lr'rl'(2-p)\right)}\right\}, \tag{2.34}$$

with probability

$$P_{\rm LR} = \frac{2\left(l^2r'^2 + l'^2r^2 + lr'rl'(2-p)\right)}{2 + \eta(2-p)(ll' + \eta rr')^2}. \tag{2.35}$$

The concurrence of Eq. (2.34) is plotted in Fig. 2.5 in terms of both indistinguishability degree $\mathcal{I}_{\rm LR}$ and noise probability p, fixing $l = r'$. By choosing maximal indistinguishability $\mathcal{I}_{\rm LR} = 1$ ($l = l'$), one has $C(\mathcal{W}_{\rm LR}^{+}) = (4-5p)/(4-p)$ when $0 \leq p < 4/5$, being zero elsewhere. The sLOCC probability is maximized when $l = l' = 1/\sqrt{2}$, taking the expression $P_{\rm LR} = 1 - p/4$ for fermions and $P_{\rm LR} = 1/2$ for bosons. The probability $P_{\rm LR}$ of Eq. (2.35) is plotted in Fig. 2.4(b) as a function of noise probability p for some degrees of spatial indistinguishability $\mathcal{I}_{\rm LR}$.

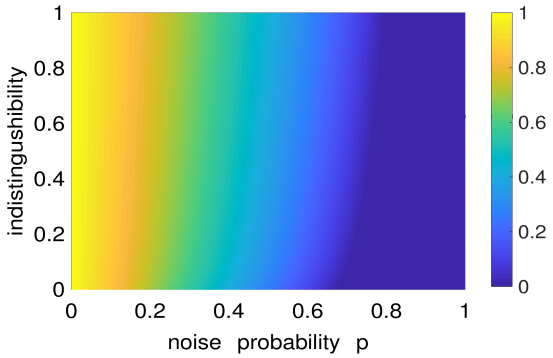

Figure 2.5: Contour plot of entanglement versus noise probability p and spatial indistinguishability $\mathcal{I}_{\rm LR}$ when the pure state $|1_+\rangle$ is chosen in Eq. (2.22), for fermions (with $\theta = \pi$) or bosons (with $\theta = 0$), fixing $l = r'$ in the spatial wave functions of Eq. (4.15).

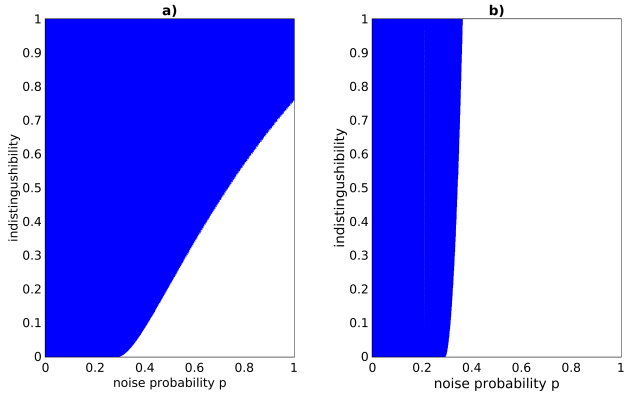

Figure 2.6: Regions of Bell inequality violation $B(\mathcal{W}^{\pm}_{\rm LR}) > 2$ in terms of noise probability p and degree of spatial indistinguishability $\mathcal{I}_{\rm LR}$. To vary $\mathcal{I}_{\rm LR}$ we fix $l = r'$ in Eq. (4.15). **a.** Target pure state $|1_-\rangle$ in Eq. (2.22) for both fermions (with $\theta = 0$) and bosons (with $\theta = \pi$). **b.** Target pure state $|1_+\rangle$ in Eq. (2.22) for both fermions (with $\theta = \pi$) and bosons (with $\theta = 0$).

Finally, the amount of entanglement for a Werner state of distinguishable qubits $W^{\pm}_{\rm AB}$ can be retrieved by both Eqs. (4.31) and (2.34) of $C(\mathcal{W}^{\pm}_{\rm LR})$ for spatially separated wave functions ($\mathcal{I}_{\rm LR} = 0$). This is reached when $l = r' = 1$ or $l = r' = 0$ in Eq. (4.15). In this case, in fact, one can associate $\mathrm{A} \equiv \mathrm{L}$ and $\mathrm{B} \equiv \mathrm{R}$. We thus obtain the known result [33] about the concurrence, that is $C(W^{\pm}_{\rm AB}) = 1 - 3p/2$ for $0 < p \leq 2/3$, being zero elsewhere.

D. CHSH-Bell inequality violation for the $\mathcal{W}^{\pm}$ state

It is known that for mixed states of distinguishable particles, which are the ones encountered in practice, a given value of entanglement by itself does not guarantee that the correlations cannot be reproduced by a classical local hidden variable model [197, 33]. Criteria based on Bell inequality violations are therefore those utilized to show that a given amount of entanglement of mixed states assures nonlocal quantum correlations, which are not classically reproducible [33]. For two distinguishable qubits in an arbitrary state ρ, the experimentally-friendly CHSH-Bell inequality can be written as $B(\rho) \leq 2$ [33], where 2 represents the classical threshold. Whenever a quantum state produces $B(\rho) > 2$, its corresponding entanglement is inherently nonlocal.

Thanks to the sLOCC framework, we can straightforwardly translate these arguments to the case of arbitrary mixed states of indistinguishable particles. In fact, after sLOCC the identical qubits can be individually addressed and a Bell test can be performed on their global state by spin-like measurements

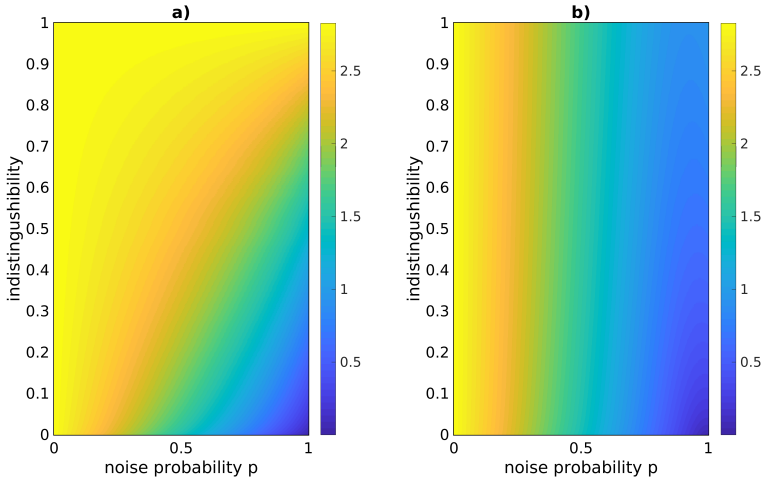

Figure 2.7: Contour plot of Bell function $B(\mathcal{W}_{\rm LR}^{\pm})$ versus noise probability p and degree of spatial indistinguishability. To vary $\mathcal{I}_{\rm LR}$ we fix $l = r'$ in Eq. (4.15). **a.** Target pure state $|1_-\rangle$ in Eq. (2.22) for both fermions (with $\theta = 0$) and bosons (with $\theta = \pi$). **b.** Target pure state $|1_+\rangle$ in Eq. (2.22) for both fermions (with $\theta = \pi$) and bosons (with $\theta = 0$).

onto the separated bound states $|{\rm L}\rangle$, localized in the region $\mathcal{L}$, and $|{\rm R}\rangle$, localized in the region $\mathcal{R}$ [16].

It is simple to see that the distributed resource state $\mathcal{W}_{\rm LR}^{\pm}$, stemming from $\mathcal{W}^{\pm}$ of Eq. (2.22) after sLOCC, has an X structure in the computational basis $\mathcal{B}_{\rm LR} = \{|{\rm L}\uparrow, {\rm R}\rangle, |{\rm L}\uparrow, {\rm R}\downarrow\rangle, |{\rm L}\downarrow, {\rm R}\uparrow\rangle, |{\rm L}\downarrow, {\rm R}\downarrow\rangle\}$. That is, only the diagonal and off-diagonal elements are in general nonzero. According to the Horodecki criterion for the CHSH-Bell inequality violation of a two-qubit density matrix [199], the expression of the optimized Bell function for an X-shape density matrix ρ_X can be written as [217]

$$B(\rho_X) = 2\sqrt{\mathcal{P}^2 + \mathcal{Q}^2}, \tag{2.36}$$

with

$$\mathcal{P} = \rho_{11} + \rho_{44} - \rho_{22} - \rho_{33}, \quad \mathcal{Q} = 2(|\rho_{14}| + |\rho_{23}|), \tag{2.37}$$

where ρ_{ij} are the density matrix elements in the computational basis. For the state of our interest, $\mathcal{W}_{\rm LR}^{\pm}$, these elements are functions of both the degree of spatial indistinguishability $\mathcal{I}_{\rm LR}$, through the wave function parameters l and l', and the noise probability p. It is thus possible to look for Bell inequality violations, that is $B_{\rm LR}(\mathcal{W}^{\pm}) := B(\mathcal{W}_{\rm LR}^{\pm}) > 2$, for different values of $\mathcal{I}_{\rm LR}$ and p. To continuously vary the degree of indistinguishability and forbid that the sLOCC probability $P_{\rm LR}$ to get $\mathcal{W}_{\rm LR}^{\pm}$ is zero, we fix $l = r'$ in the wave functions $|\psi_1\rangle$ and $|\psi_2\rangle$ of Eq. (4.15). It is worth to recall that a Bell inequality violation based on sLOCC, that is based on local postselection with $P_{\rm LR} > 0$, provides a faithful test of local realism [198].

When the target pure state in Eq. (2.22) is $|1_-\rangle$, for both fermions (with $\theta = 0$) and bosons (with $\theta = \pi$), the behavior of the Bell function $B(\mathcal{W}_{\rm LR}^{-})$ is displayed in Fig. 2.6**a**, where only the regions of violation are evidenced, while in Fig. 2.7**a** all the possible values of $B(\mathcal{W}_{\rm LR}^{-})$ are shown. From Fig. 2.6**a**, it is clear that when $0.76 < \mathcal{I}_{\rm LR} \leq 1$, that is $0.56 < C(\mathcal{W}_{\rm LR}^{-}) \leq 1$, the Bell inequality is violated independently of noise probability p. The fact that this result is independent of p implies that, under the conditions above, the nonlocal entanglement preparation is always noise free. Moreover, notice that the degree of $\mathcal{I}_{\rm LR}$ beyond the (nonlocality) threshold (≈ 0.76) is reached for many different shapes of the spatial wave functions of Eq. (4.15). Disturbance in the control of the exact shape of spatial wave functions does not significantly affect the degree of spatial indistinguishability of the identical qubits.

On the other hand, when the target pure state in Eq. (2.22) is $|1_+\rangle$, for both fermions (with $\theta = \pi$) and bosons (with $\theta = 0$), the behavior of $B_{\max}(\mathcal{W}_{\rm LR}^{+})$ is reported in Fig. 2.6**b**, where only the regions of

violation are evidenced, while in Fig. 2.7**b** all the possible values of the Bell function are plotted. In this case, Fig. 2.6**b** evidences that the Bell inequality, also for a high degree of indistinguishability, can be violated for a finite range of p. For instance, when $\mathcal{I}_{\rm LR} = 1$, one has $B(\mathcal{W}^{+}_{\rm LR}) > 2$ for $0 \leq p < 0.363$, which means $0.6 < C(\mathcal{W}^{+}_{\rm LR}) \leq 1$.

Finally, from both panels of Fig. 2.6 one can also retrieve the range of values of p for which the Bell inequality is violated in the case of distinguishable qubits A, B. In fact, when $\mathcal{I}_{\rm LR} = 0$, one gets $B(W^{\pm}_{\rm AB}) > 2$ for noise probability $0 \leq p < 0.29$, which means an entanglement amount $0.68 < C(W^{\pm}_{\rm AB}) \leq 1$ [33]. Nonlocal entanglement of distinguishable particles is unavoidably affected by the amount of noise present in the state and is violated only for a small amount of white noise.

The main message of this analysis is the following: spatial indistinguishability, even partial, can guarantee a noise-free preparation of highly entangled states of identical particles, capable to violate the Bell inequality. Moreover, this result is robust to changes in the configurations of the spatial wave functions $|\psi_1\rangle$, $|\psi_2\rangle$, which highlights the behavior of quantum indistinguishability as a protection of quantum states against external noise.

Chapter 3

Experimental quantum entanglement and teleportation by tuning remote spatial indistinguishability of independent photons

Abstract

Quantitative control of spatial indistinguishability of identical subsystems as a direct quantum resource at distant sites has not been yet experimentally proven. We design a setup capable to tune remote spatial indistinguishability of two independent photons by individually adjusting their spatial distribution in two distant regions, leading to polarization entanglement from uncorrelated photons. This is achieved by spatially localized operations and classical communication (sLOCC) on photons which only meet at the detectors. The amount of entanglement uniquely depends on the degree of spatial indistinguishability, quantified by an entropic measure $\mathcal{I}$, which enables teleportation with fidelities above the classical threshold. The results open the way to viable indistinguishability-enhanced quantum information processing. This Chapter is related to Publication 2 in the List of Publications.

3.1 Introduction

Discovering how fundamental traits of quantum constituents can facilitate preparation and control of composite systems is strategic for the scientific progress. In fact, this achievement impacts both on the advance of our knowledge of the basic features of the natural world and on the development of quantum-enhanced technologies. Many-body quantum networks are usually made of identical building blocks, such as atoms, electrons, photons or generic qubits [161, 218, 219, 220, 175]. Indistinguishability of identical subsystems thus emerges as inherent quantum feature that may play a role in quantum information processing.

The usual request to implement quantum tasks in many-body systems is that qubits are individually addressed, which have been experimentally realized with various apparatuses [33]. For nonidentical qubits, this requirement is fulfilled by local operations and classical communication (LOCC), where the term "local" refers to particle-locality independently of their spatial configuration [33]. Differently, identical qubits are not in general individually addressable [13], spatial distribution of their wave functions becoming crucial. Despite the long debate about formal aspects on entanglement of identical particles [13, 12, 221, 222, 223, 192, 224, 225, 191, 14, 2, 226, 3, 227] and some proposals using particle identity for quantum protocols [175, 187, 188, 28, 16, 94], experimental evidence of spatial indistinguishability as a direct resource has remained elusive, because of the lack of its proper informational measure and a suitable control technique.

Here we experimentally implement the operational framework based on spatially localized opera-

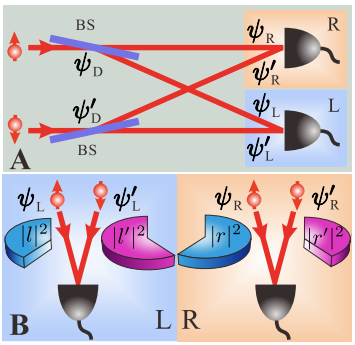

Figure 3.1: (A) Theoretical setup. (B) Generic spatial distribution of particles in the state $|\Psi\rangle = |\psi_{\rm D}\uparrow, \psi'_{\rm D}\downarrow\rangle$, with $|\psi_{\rm D}\rangle = l\,|\psi_{\rm L}\rangle + r\,|\psi_{\rm R}\rangle$ and $|\psi'_{\rm D}\rangle = l'\,|\psi'_{\rm L}\rangle + r'\,|\psi'_{\rm R}\rangle$ ($0 < \mathcal{I} < 1$).

tions and classical communication (sLOCC) which, at variance with the idea of particle locality, relies on the concept of spacial locality of measurement as in quantum field theory [16]. The setup is capable to control the distribution of the wave packets of two independent initially-uncorrelated identical photons towards two separated (remote) operational regions where the photons are collected. This allows for continuously adjusting the degree of their remote spatial indistinguishability, quantified via a suitable entropic-informational measure [17]. The two photon paths remain separated along the setup and only meet in the operational regions. By single-photon localized measurements, we prove that the two uncorrelated photons with opposite polarizations get entangled, the amount of entanglement being only related to the degree of spatial indistinguishability. We show that the nonlocal entanglement so generated violates the Bell inequality and activates conditional teleportation of the state of an additional photon with fidelities higher than the classical threshold.

3.2 Theory

We start describing the basic theoretical setup, depicted in Fig. 3.1A. Two identical particles, coming from independent sources, are in the initial uncorrelated state $|\psi\uparrow, \psi'\downarrow\rangle$, written in the no-label formalism [2] (see section A in Supplementary Material (SM)). Each particle wave packet is then distributed in a controllable manner towards two remote operational regions L and R by a beam splitter (BS), $|\psi\rangle \xrightarrow{\rm BS} |\psi_{\rm D}\rangle$ and $|\psi'\rangle \xrightarrow{\rm BS} |\psi'_{\rm D}\rangle$. The sLOCC measurements, represented by the two detectors in Fig. 3.1A, are realized by localized single-particle counting in each region (sLO) and coincidence measures (CC). Taking photons as identical particles, this scheme can be seen as a modified Hanbury Brown and Twiss experiment [228, 229], the modification consisting in initially polarizing the photons and in controlling their spatial distribution. Before sLOCC, the two-particle state is $|\Psi\rangle = |\psi_{\rm D}\uparrow, \psi'_{\rm D}\downarrow\rangle$, where $|\psi_{\rm D}\rangle = l\,|\psi_{\rm L}\rangle + r\,|\psi_{\rm R}\rangle$ ($|l|^2 + |r|^2 = 1$) and $|\psi'_{\rm D}\rangle = l'\,|\psi'_{\rm L}\rangle + r'\,|\psi'_{\rm R}\rangle$ ($|l'|^2 + |r'|^2 = 1$), with $|\psi_{\rm X}\rangle$, $|\psi'_{\rm X}\rangle$ (X = L, R) indicating the two wave packets located in the operational region X. Particle paths do not share any common past and meet only at the detection level, so that to the eyes of the localized measurement devices the particles are indistinguishable and individually unaddressable. The question arises whether $|\Psi\rangle$ contains useful pseudospin entanglement in L and R, a longly debated conceptual issue [16]. Particle spatial overlap occurs at distant sites, defining a remote spatial indistinguishability quantified by the entropic measure [17]

$$\mathcal{I} = -\sum_{i=1}^{2} p_{\rm LR}^{(i)} \log_2 p_{\rm LR}^{(i)}, \tag{3.1}$$

where $p_{\rm LR}^{(1)} = |lr'|^2/(|lr'|^2 + |l'r|^2)$ and $p_{\rm LR}^{(2)} = 1 - p_{\rm LR}^{(1)}$ (see section A in SM for details). Here $|lr'|^2$ is the joint probability of finding a particle in L coming from $|\psi_{\rm D}\rangle$ and a particle in R coming from $|\psi'_{\rm D}\rangle$, whilst $|l'r|^2$ is clearly the vice versa (see Fig. 3.1B). This measure ranges from $\mathcal{I} = 0$ for separated wave

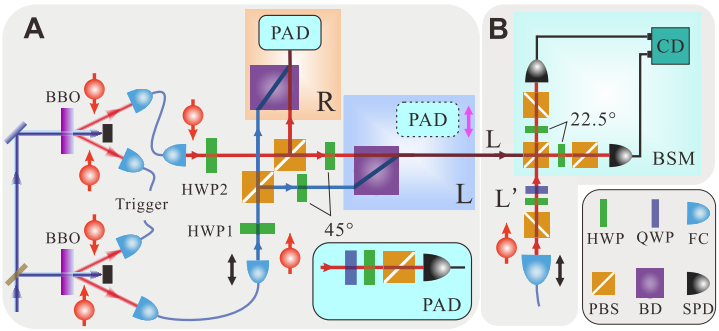

Figure 3.2: **Experimental setup.** (A) Using fiber couplers (FCs), half-wave plates (HWPs) and polarized beam splitters (PBSs), two oppositely-polarized independent photons generated from two BBO crystals go to the separated regions L and R, where a beam displacer (BD) makes the photon paths meet at detectors. The inset displays the unit of polarization analysis detection (PAD), including a quarter-wave plate (QWP) and a single-photon detector (SPD). (B) Teleportation part. PAD is removed and the photons in L proceed to the Bell state measurement (BSM) with coincidence device (CD). The photon state to be teleported is generated in L′.

packets ($|l|^2 = |r'|^2 = 1$ or $|l|^2 = |r'|^2 = 0$) to $\mathcal{I} = 1$ for equally distributed wave packets ($|l|^2 = |l'|^2$) (see section B in SM). Any other particle degree of freedom, apart spatial location, has no effect on $\mathcal{I}$. Applying the projector $\hat{\Pi}_{\rm LR} = \sum_{\sigma,\tau=\uparrow,\downarrow} |{\rm L}\sigma, {\rm R}\tau\rangle \langle {\rm L}\sigma, {\rm R}\tau|$, which defines localized single-particle counting in L and R, on $|\Psi\rangle$ gives [16]

$$|\Psi_{\rm LR}\rangle = (lr'|{\rm L}\uparrow, {\rm R}\downarrow\rangle + \eta rl'|{\rm L}\downarrow, {\rm R}\uparrow\rangle)/(\sqrt{|lr'|^2 + |rl'|^2}), \tag{3.2}$$

with probability $P_{\rm LR} = |lr'|^2 + |rl'|^2$, where $\eta = \pm 1$ for bosons and fermions, respectively.

3.3 Experiment

The experimental setup realizing this theoretical scheme is displayed in Fig. 3.5A. Two (uncorrelated) heralded single photons are emitted independently via spontaneous parametric down conversion (SPDC) from two BBO crystals, designed to satisfy beamlike type-II SPDC [230] and pumped by pulsed ultraviolet light at 400 nm. The two photons (of wavelength 800 nm) are initially polarized in $|H\rangle$ (horizontal, $H \equiv\uparrow$) and $|V\rangle$ (vertical, $V \equiv\downarrow$) polarization, respectively, and then collected separately by two single-mode fibers via fiber couplers (FCs). At this stage, the photons are completely uncorrelated in the state $|H\rangle \otimes |V\rangle$, as verified with high fidelity $(95.2 \pm 0.7)\%$ (see section C in SM). Before the main experiment, we perform usual two-photon interference to reveal the identity of the employed operational photons characterized by visibility of Hong-Ou-Mandel (HOM) dip [130], giving a value of $\approx 83.8\%$ (see section C in SM). The BSs of Fig. 3.1A are actually substituted by the sequence of a half-wave plate (HWPi, $i = 1, 2$), a polarizing beam-splitter (PBS) and two final HWPs at 45° before the location L. By rotating HWP1 and HWP2 at angles $(\pi/2 - \alpha)/2$ and $-\beta/2$, respectively, we can conveniently adjust the weights of the linear spatial distribution of the photons on the two measurement sites, while the PBSs separate the different polarizations. The final HWPs at 45° are needed to maintain the initial polarization of each photon unvaried. In each region L and R a beam displacer (BD) makes the paths of the two photons meet at the detection level. It is straightforward to see that this setup prepares the desired state $|\Psi_{\rm prep}\rangle = |\psi_{\rm D} H, \psi'_{\rm D} V\rangle$ with $|\psi_{\rm D}\rangle = \cos\alpha\, |\psi_{\rm L}\rangle + \sin\alpha\, |\psi_{\rm R}\rangle$ and $|\psi'_{\rm D}\rangle = \sin\beta\, |\psi'_{\rm L}\rangle + \cos\beta\, |\psi'_{\rm R}\rangle$. By setting α and β, we can prepare a series of $|\Psi_{\rm prep}\rangle$ for different spatial distributions and thus for various values of $\mathcal{I}$. All the optical elements of the setup independently act on each photon, so the photon states $|\psi_{\rm D} H\rangle$, $|\psi'_{\rm D} V\rangle$ are independently prepared regardless of the specific photon spatial mode (e.g., transversal electric magnetic mode like Hermite-Gaussian mode or Laguerre-Gaussian mode). The sLOCC measurements are implemented by single-photon detectors (SPDs) placed on L and R for single-particle counting (sLO) and by a coincidence device (CD), which deals with the electrical signals of

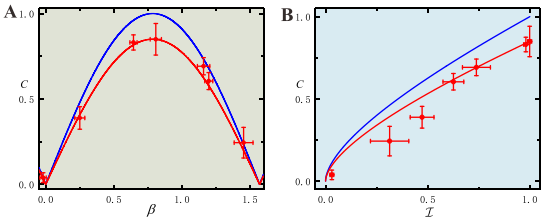

Figure 3.3: Concurrence C for $\alpha = \pi/4$, versus β (A) and $\mathcal{I}$ (B). Blue (upper) curves are ideal theoretical predictions, red curves are the performance of the setup considering reduced visibility. Red dots (with error bars) are experimental results.

SPDs and the trigger signals outputting coincidence counting on L and R, for classical communication (CC). An interference filter, whose full width at half maximum is 1 nm, and a single mode fiber (both not shown here) are placed before each SPD. A unit of polarization analysis detection (PAD), made of a quarter-wave plate (QWP), a HWP and a PBS (see inset of Fig. 3.5A), is locally employed to verify the predicted polarization entanglement by tomographic measurements and Bell test.

The setup generates from $|\Psi_{\rm prep}\rangle$ by sLOCC the distributed resource state $|\Psi_{\rm LR}\rangle$ of Eq. (3.2), with $\eta = 1$ (bosons), $l = \cos\alpha$, $r = \sin\alpha$, $l' = \sin\beta$ and $r' = \cos\beta$. This polarization entanglement is revealed in coincidence post-selection as in a common type of polarization-entangled photon source [231]. However, its origin is fundamentally different, arising from independently-prepared photons which do not share any common past but only need to meet at detectors. This entanglement is zero when the two spatial distributions remain separated each in a local region, being $\mathcal{I} = 0$ since the photons are distinguished by their locations (see section D in SM). We verify the entanglement versus $\mathcal{I}$ by adjusting different spatial distributions $|\psi_{\rm D}\rangle$, $|\psi'_{\rm D}\rangle$. To this aim we fix $\alpha = \pi/4$, implying $|\psi_{\rm D}\rangle = (|\psi_{\rm L}\rangle + |\psi_{\rm R}\rangle)/\sqrt{2}$ and

$$|\Psi_{\rm LR}\rangle = \cos\beta\ |{\rm L}H, {\rm R}V\rangle + \sin\beta\ |{\rm L}V, {\rm R}H\rangle\,, \tag{3.3}$$

whose concurrence quantifying entanglement [33] is $C(\Psi_{\rm LR}) = \sin 2\beta$, while $\mathcal{I} = -\cos^2\beta\ \log_2(\cos^2\beta) - \sin^2\beta\ \log_2(\sin^2\beta)$, as obtained from Eq. (3.1), coincides with the entanglement of formation $E_f(\Psi_{\rm LR})$ of $|\Psi_{\rm LR}\rangle$ [16]. Thus, a monotonic relation $C = f(\mathcal{I})$ exists between concurrence and spatial indistinguishability. The experimental results of C, obtained after state reconstruction, versus both β and $\mathcal{I}$ are shown in Fig. 3.3A and B where the experimental points are lower than the ideal theoretical prediction due to the reduction of visibility while fit with the performance of this setup (see section C in SM). For $\beta = \pi/4$ ($\mathcal{I} = 1$), $|\Psi_{\rm LR}\rangle$ in Eq. 3.3 becomes the Bell state $|\Psi^+_{\rm LR}\rangle$. The generated state, in correspondence of $\beta = 0.808 \pm 0.041$, whose reconstructed density matrix is shown in Fig. 3.14A, has fidelity $(88.3 \pm 2.5)\%$ compared to $|\Psi^+_{\rm LR}\rangle$. We also perform the Bell inequality violation test ($S > 2$) [33] on this distributed resource state to directly prove the presence of nonlocal entanglement [198]. We experimentally achieve $S = 2.32 \pm 0.12$, violating the Bell inequality by about 2.7 standard deviations. Moreover, when $\beta = 3\pi/4$, that is when $|\psi'_{\rm D}\rangle = (|\psi'_{\rm L}\rangle - |\psi'_{\rm R}\rangle)/\sqrt{2}$ and $|\psi_{\rm D}\rangle$ are orthogonal yet completely spatially indistinguishable ($\mathcal{I} = 1$), the Bell state $|\Psi^-_{\rm LR}\rangle$ is expected. In the experiment, this state is created with fidelity $(88.3 \pm 2.4)\%$ for $\beta = 2.406 \pm 0.040$ (see Fig. 3.14B) and Bell inequality violation $S = 2.33 \pm 0.16$. These results prove that nonlocal entanglement is activated only by the remote spatial indistinguishability of independent photons.

Due to reduced visibility of the two heralded single photons, the experimental results that fit well with the performance of the employed setup are obviously lower than the theoretical prediction. Redoing the experiment with two photons from one BBO crystal, instead of two independent sources, allows us to obtain data closer to theory (see section E in SM).

Teleportation. We now show the indistinguishability-enabled entanglement is large enough to realize quantum teleportation. We can follow the standard protocol [33, 22] once the cases when both photons are either in L or in R are discarded. Following the above setup preparing the entangled state, the setup implementing teleportation is displayed in Fig. 3.5B. One of the two photons used as the trigger signals in Fig. 3.5A is sent to the side of L$'$ as the target to be teleported. The combination of a HWP

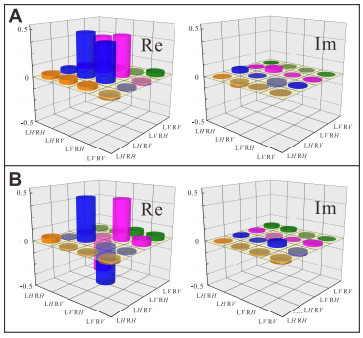

Figure 3.4: Real and imaginary part of the reconstructed density matrix for $\alpha = \pi/4$ and: (A) $\beta = 0.808 \pm 0.041$ (expected state $|\Psi^+_{\rm LR}\rangle$); (B) $\beta = 2.406 \pm 0.040$ (expected state $|\Psi^-_{\rm LR}\rangle$).

cccc

state	$\|H\rangle$	$\|V\rangle$	$\|+\rangle$
$F_{\rm exp}$ (%)	90.4 ± 4.4	84.6 ± 5.9	78.7 ± 5.0
state	$\|-\rangle$	$\|\phi_-\rangle$	$\|\phi_+\rangle$
$F_{\rm exp}$ (%)	79.3 ± 4.9	93.2 ± 5.7	88.2 ± 5.4

Table 3.1: Fidelities of the six states $\rho_{\rm exp}$ with respect to the ideal state in the quantum teleportation process.

and a QWP prepares the photon in a state $|\phi\rangle = a\,|H\rangle + b\,|V\rangle$ ($|a|^2 + |b|^2 = 1$). For teleporting the state $|\phi\rangle$ to the photon in R, we perform a Bell-state measurement (BSM) between L and L$'$, where the Bell state $|\Phi_{\rm LL'}\rangle = (|{\rm L}H, {\rm L}'H\rangle + |{\rm L}V, {\rm L}'V\rangle)/\sqrt{2}$ is measured by using a PBS and two HWPs at 22.5° [232, 233]. Correspondingly, the operation in R rotating its photon state to the desired one is $\sigma_x = |H\rangle\langle V| + |V\rangle\langle H|$, implemented by a 45° HWP. The signals from two SPDs are processed by a CD to coincide with the signals from R and triggers. Teleportation is achieved exploiting the distributed Bell state $|\Psi^+_{\rm LR}\rangle$, generated by $\mathcal{I} = 1$ of the original photons. We set $\alpha = \beta = \pi/4$ to maximize the generation probability ($P_{\rm LR} = 50\%$). The six eigenvectors of σ_i ($i = x, y, z$) are the photon states in L$'$ to be teleported: $|\phi_{\rm ideal}\rangle \in \{|H\rangle, |V\rangle, |\pm\rangle = \frac{1}{\sqrt{2}}(|H\rangle \pm |V\rangle), |\phi_\pm\rangle = \frac{1}{\sqrt{2}}(|H\rangle \pm i|V\rangle)\}$. Performing quantum tomography of single-qubit state in R, the experimental teleported states $\rho_{\rm exp}$ are reconstructed based on four-photon coincidence. Fidelity $F_{\rm exp} = \langle\phi_{\rm ideal}|\rho_{\rm exp}|\phi_{\rm ideal}\rangle$ compared to the ideal state $\rho_{\rm ideal}$ is the figure of merit of teleportation efficiency. The measured fidelities, without background subtraction, are reported in Table 3.2, being higher than the classical fidelity limit of $2/3$ [234]. The quantum process matrix χ of teleportation is reconstructed by comparing $\rho_{\rm ideal}$ and $\rho_{\rm exp}$ (see section D in SM), giving fidelity $F_\chi = (73.6 \pm 7.7)\%$. All error bars are estimated as standard deviation from the statistical variation of the photon counts, assumed to follow a Poisson distribution.

3.4 Discussion

We have designed a neat all-optical experiment generating nonlocal polarization entanglement by only adjusting the degree of remote spatial indistinguishability $\mathcal{I}$ of two initially-uncorrelated independent photons in two separated regions of measurement. This is basically different from swapping or heralded sources strategies, requiring initially entangled pairs. The value of $\mathcal{I}$ is tuned by controlling the spatial distribution of each photon wave packet towards the two operational regions. The photon paths only meet at the detection level. The setup implements the sLOCC [16] necessary to directly assess the relation between $\mathcal{I}$ and the amount of produced entanglement, verified by both state tomography and CHSH-Bell test. We remark that the sLOCC framework cannot produce any entanglement if the photons remain separated in the two regions, differently from optical interferometry with spread detection [235]. Notice

that if the setup was run by two initially uncorrelated nonidentical particles, no entanglement would be obtained by measurements distinguishing particles from one another (LOCC). We have performed teleportation between the two operational regions, with fidelities (78-93%) above the classical threshold, by just tuning spatial indistinguishability of photons, with the advantage of not requiring inefficient or demanding entanglement source devices.

Our experiment fulfills an elementary entangling gate by bringing (uncorrelated independent) photons with opposite polarizations to the same local regions (nodes) and accessing the (nonlocal) entanglement by sLOCC measurements (see also a recent independent experiment [24]). So, entanglement activated by spatial indistinguishability is the product of both state structure and local measurements. Multiphoton entanglement can be produced by scalability of this elementary gate. The results open the way to viable indistinguishability-enhanced quantum information processing and quantum networking.

Supplementary Material

A. Degree of remote spatial indistinguishability

In this section we summarize the theory which brings to the definition of the entropic measure of spatial indistinguishability of particles by sLOCC in two separated operational regions [17], given in Eq. (1) of the main text.

Consider the state of two identical two-level subsystems (particles) $|\Psi^{(2)}\rangle = |\chi_1, \chi_2\rangle = |\psi_1\sigma_1, \psi_2\sigma_2\rangle$, where ψ_i ($i = 1, 2$) is the spatial degree of freedom and σ_i is the pseudospin with basis $\{\uparrow, \downarrow\}$). In general, $|\psi_1\rangle$ and $|\psi_2\rangle$ can be defined in the same space regions so that they spatially overlap. We are interested in defining the degree of remote spatial indistinguishability $\mathcal{I}$ of two identical particles between the local operational regions L and R, where both particles have nonzero probability to be found. Such a definition has to quantify how much the measurement process of finding one particle in each location can distinguish the particles from one another. Spatially localized operations (sLO) are thus made by single-particle local counting ignoring the pseudospins, represented by the projector

$$\Pi^{(2)}_{\mathrm{LR}} = \sum_{\tau_1,\tau_2=\uparrow,\downarrow} |\mathrm{L}\tau_1, \mathrm{R}\tau_2\rangle \langle \mathrm{L}\tau_1, \mathrm{R}\tau_2| \,, \tag{3.4}$$

which projects the original state onto the operational subspace spanned by the computational basis $\mathcal{B}_{\mathrm{LR}} = \{|\mathrm{L}\uparrow, \mathrm{R}\uparrow\rangle, |\mathrm{L}\uparrow, \mathrm{R}\downarrow\rangle, |\mathrm{L}\downarrow, \mathrm{R}\uparrow\rangle, |\mathrm{L}\downarrow, \mathrm{R}\downarrow\rangle\}$. We point out that $|\mathrm{L}\rangle$ and $|\mathrm{R}\rangle$ represent, respectively, one particle in L and one particle in R. Also, classical communication (CC) is required to the detection level to know that each of the two separated regions counted one particle. Indicating with $P_{\mathrm{X}\psi_{\mathrm{i}}} = |\langle \mathrm{X}|\psi_i\rangle|^2$ ($\mathrm{X} = \mathrm{L}, \mathrm{R}$ and $i = 1, 2$) the probability of counting in $|X\rangle$ the particle coming from $|\psi_i\rangle$, the degree of the (remote) spatial indistinguishability of qubits is [17]

$$\mathcal{I} = -\frac{P_{\mathrm{L}\psi_1} P_{\mathrm{R}\psi_2}}{\mathcal{Z}} \log_2 \frac{P_{\mathrm{L}\psi_1} P_{\mathrm{R}\psi_2}}{\mathcal{Z}} - \frac{P_{\mathrm{L}\psi_2} P_{\mathrm{R}\psi_1}}{\mathcal{Z}} \log_2 \frac{P_{\mathrm{L}\psi_2} P_{\mathrm{R}\psi_1}}{\mathcal{Z}}, \tag{3.5}$$

where $\mathcal{Z} = P_{\mathrm{L}\psi_1} P_{\mathrm{R}\psi_2} + P_{\mathrm{L}\psi_2} P_{\mathrm{R}\psi_1}$ represent the probability that the two possible events (joint probabilities) occur. In general, $0 \leq \mathcal{I} \leq 1$. If the spatial distributions $|\psi_1\rangle$, $|\psi_2\rangle$ of the particles are separated, we have maximal information for distinguishing the particles and $\mathcal{I} = 0$. Instead, $\mathcal{I} = 1$ when $P_{\mathrm{L}\psi_1} = P_{\mathrm{L}\psi_2}$ and $P_{\mathrm{R}\psi_2} = P_{\mathrm{R}\psi_1}$: in this case the two spatial distributions have the same probability amplitudes (in modulus), meaning that there is no information about the origin (which way) of the two particles found one in L and one in R.

For our theoretical and experimental setup, where $|\psi_1\rangle \equiv |\psi_{\mathrm{D}}\rangle = l\,|\psi_{\mathrm{L}}\rangle + r\,|\psi_{\mathrm{R}}\rangle$ and $|\psi_2\rangle \equiv |\psi'_{\mathrm{D}}\rangle = l'\,|\psi'_{\mathrm{L}}\rangle + r'\,|\psi'_{\mathrm{R}}\rangle$, we have $P_{\mathrm{L}\psi_1} \equiv P_{\mathrm{L}\psi_{\mathrm{D}}} = |l|^2$, $P_{\mathrm{R}\psi_1} \equiv P_{\mathrm{R}\psi_{\mathrm{D}}} = |r|^2$, $P_{\mathrm{L}\psi_2} \equiv P_{\mathrm{L}\psi'_{\mathrm{D}}} = |l'|^2$, $P_{\mathrm{R}\psi_2} \equiv P_{\mathrm{R}\psi'_{\mathrm{D}}} = |r'|^2$. Therefore, the expression of Eq. (4.14) above for $\mathcal{I}$ becomes that of Eq. (1) in the main text. Notice that this entropic measure of spatial indistinguishability at a distance is completely independent of any other degree of freedom of the particles apart their spatial location.

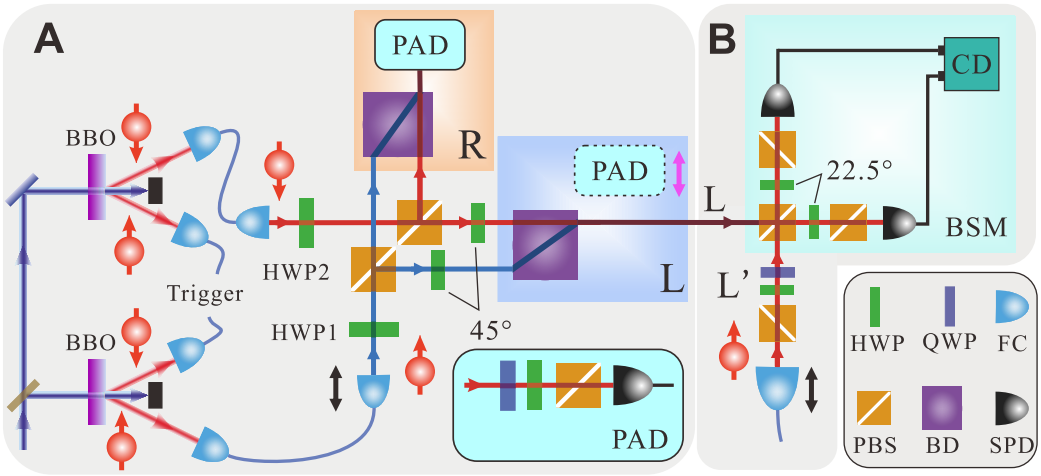

Figure 3.5: **Sketch of the experimental setup.** (A) Two heralded single photons independently generated from two BBO crystals with polarization $|H\rangle$ ($\uparrow$) and $|V\rangle$ ($\downarrow$), respectively, are collected separately by two single-mode fibers via fiber couplers (FCs). The control of the spatial wave function of each photon is realized by the sequence of a half-wave plate (HWP1, HWP2), a polarization beam splitter (PBS) and a final HWP at 45° placed before L, which leaves the initial polarization of each photon unchanged. Wave packet distributions $\psi_{\rm D}$ and $\psi'_{\rm D}$, in which the photons share the same wavelength, are marked as the blue and red colors, respectively, to differentiate. In each region L and R one beam displacer (BD), made by a calcite crystal which separates the input beam into two with orthogonal polarization, is here used to make the photon paths meet at the detection level. The inset displays the unit of polarization analysis detection (PAD) at the final detection placed in L and R, consisting of a quarter-wave plate (QWP), a HWP and a PBS before the single-photon detector (SPD). A coincidence device (CD) (not shown in (A)) deals with the electrical signals of the two SPDs and the trigger signals, and outputs the coincidence counting. (B) Experimental illustration of quantum teleportation. The photons in L are sent to perform the Bell state measurement (BSM) and meanwhile the PAD here which is marked by the dashed frame is removed. One of the two photons treated as the trigger signals in (B) is prepared as the state to be teleported. BSM is implemented with a PBS followed by two HWPs at 22.5° and PBSs. The signals from two SPDs are processed by a CD to coincide with the signals from R and trigger.

B. Spatial distribution of particle wave packets

Consider the prepared state $|\Psi\rangle = |\psi_{\rm D}\uparrow, \psi'_{\rm D}\downarrow\rangle$, with

$$|\psi_{\rm D}\rangle = l\,|\psi_{\rm L}\rangle + r\,|\psi_{\rm R}\rangle\,, \quad |\psi'_{\rm D}\rangle = l'\,|\psi'_{\rm L}\rangle + r'\,|\psi'_{\rm R}\rangle \tag{3.6}$$

where $|l|^2 + |r|^2 = 1$, $|l'|^2 + |r'|^2 = 1$, and $|\psi_{\rm X}\rangle$, $|\psi'_{\rm X}\rangle$ (X = L, R) are the two particle wave packets located in the operational region X. With the self-evident assumption that $|\psi_{\rm D}\rangle$ and $|\psi'_{\rm D}\rangle$ cannot locate in only one measurement region simultaneously, that is $l = l' = 1$ or $l = l' = 0$ do not occur, we have:

- Zero spatial indistinguishability. This case occurs when the two wave packet distributions remain spatially separated, that is when $l = r' = 1$ (0), giving $|\psi_{\rm D}\rangle = |\psi_{\rm L}\rangle$ ($|\psi_{\rm R}\rangle$) and $|\psi'_{\rm D}\rangle = |\psi'_{\rm R}\rangle$ ($|\psi'_{\rm L}\rangle$). Here the degree of remote spatial indistinguishability of Eq. (4.14) is clearly zero, $\mathcal{I} = 0$, and the distributed state after sLOCC, coming from Eq. (2) of the main text, is the product state $|\Psi_{\rm LR}\rangle = |{\rm L}\uparrow, {\rm R}\downarrow\rangle$ ($|{\rm L}\downarrow, {\rm R}\uparrow\rangle$).
- Partial spatial indistinguishability. For $0 < l, l' < 1$, the spatial distributions $|\psi_{\rm D}\rangle$ and $|\psi'_{\rm D}\rangle$ are linear combinations of the particle wave packets being simultaneously in L and R with different weights. This leads to an intermediate value of the degree of spatial indistinguishability, $0 < \mathcal{I} < 1$, as depicted in Figure 1B of the main text. The distributed state $|\Psi_{\rm LR}\rangle$ obtained by sLOCC is that of Eq. (2) of the main text.

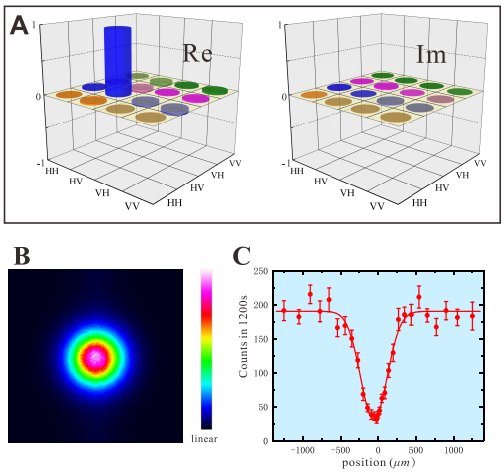

Figure 3.6: (A) Experimental tomography of the initial state $|\psi H, \psi' V\rangle \equiv |\psi H\rangle \otimes |\psi' V\rangle$ of the two photons from two BBO crystals with a high fidelity $(95.2 \pm 0.7)\%$. Two subgraphs show the real and imaginary parts of the density matrix, respectively. (B) The intensity distribution of photon with TEM (transversal electric magnetic) 00 mode generated from the single-mode fiber. (C) The HOM dip of the two-photon interference. The counts are obtained in 1200 seconds with the pumping power 200 mW. The red dots are the experimental results. And the red curve presents the fitting Gaussian function G_x.

- Maximum spatial indistinguishability. This case occurs when the two particle wave packets $|\psi_{\rm D}\rangle$ and $|\psi'_{\rm D}\rangle$ are equally distributed in the two operational regions, that is with equal moduli of the probability amplitudes to be located in the same regions. This means that $|l| = |l'|$ (and thus $|r| = |r'|$). In this case the degree of remote spatial indistinguishability is maximum, $\mathcal{I} = 1$ and the distributed state of Eq. (2) of the main text is the maximally entangled state $|\Psi^{\pm}_{\rm LR}\rangle = (|{\rm L}\uparrow, {\rm R}\downarrow\rangle \pm |{\rm L}\uparrow, {\rm R}\downarrow\rangle)/\sqrt{2}$. A special case is retrieved when $|l = |l'| = |r| = |r'| = 1/\sqrt{2}$, for which this state $|\Psi^{\pm}_{\rm LR}\rangle$ is generated with maximum probability ($P_{\rm LR} = 50\%$) from $|\Psi_{\rm prep}\rangle$.

Summarizing, by controlling the spatial distribution of the wave packets $|\psi_{\rm D}\rangle$ and $|\psi'_{\rm D}\rangle$, we can design different configurations with various degrees of remote spatial indistinguishability, continuously ranging from $\mathcal{I} = 0$ to $\mathcal{I} = 1$.

C. Experimental preparation

For the sake of convenience, we report here again in Fig. 3.5 the sketch of the experimental setup together with its detailed description in the caption.

Two heralded single photons with the wavelength 800nm from pumping two BBO crystals are emitted independently in the product state $|\Psi\rangle = |\psi H, \psi' V\rangle \equiv |\psi H\rangle \otimes |\psi' V\rangle$, where $H \equiv\uparrow$ and $V \equiv\downarrow$. The corresponding experimental reconstructed matrices of this initial state are presented in Fig. 3.6A with a very high fidelity $(95.2 \pm 0.7)\%$. It is then verified that the two photons are initially completely uncorrelated in polarization. Each photon is then collected in a single-mode fiber via fiber couplers. In this experiment, the single-mode fiber generates an intensity shape (spatial mode) of each photon with TEM (transversal electric magnetic) 00 mode, as shown in Fig 3.6B.

Before carrying on the main experiment for the continuous tuning of the degree of remote spatial indistinguishability of the two photons, we perform the usual two-photon interference and employ the visibility of Hong-Ou-Mandel (HOM) dip [130] to character the identity of the photons. Fig. 3.7 shows the setup for the HOM measurement. Fitting HOM dip data with a Gaussian function $G(x) = a\,(1 - d\,e^{-b\,(x-c)^2})$, the parameters a, b, c, d are determined. The visibility of HOM dip is defined as $\mathcal{V} = (G_{\rm max} - G_{\rm min})/G_{\rm max} = d$ and obtained with a value of about 83.8%, which reveals the identity of the employed operational photons. Due to the reduced visibility of the setup, a model dealing with this

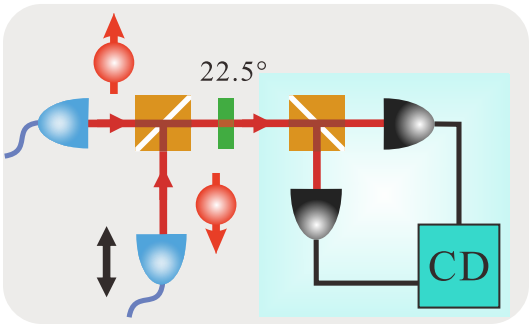

Figure 3.7: Experimental illustration of HOM measurement. The first polarization beam splitter (PBS) combines two photons which are in the polarization $|H\rangle$ (spin up) and $|V\rangle$ (spin down), respectively. One photon is placed on a movable stage to scan the position. The photons are detected by two single photon detectors (SPD) after a half-wave plate (HWP) at 22.5° and a second PBS. The coincidence device (CD) analyzes the signals from two SPDs and outputs the coincidence counting.

reduction is introduced to characterise the performance of the setup. Here, we can write the prepared state as $\rho = x\rho_{\rm LR} + (1-x)\rho_{\rm noise}$, where $\rho_{\rm LR} = |\Psi_{\rm LR}\rangle\langle\Psi_{\rm LR}|$ (i.e., Eq. (3)), $\rho_{\rm noise} = (|HV\rangle\langle HV| + |VH\rangle\langle VH|)/2$. In this sense, we can estimate the prediction of experimental setup.

A series of target states $|\Psi_{\rm prep}\rangle = |\psi_{\rm D}H, \psi'_{\rm D}V\rangle$ are then prepared by controlling the spatial distribution $|\psi_{\rm D}\rangle$ and $|\psi'_{\rm D}\rangle$ of each photon wave packet towards the two separated operational regions L and R (see Fig. 3.5A). These distributions are determined by adjusting the angles of HWP1 and HWP2. Notice that the operation of a HWP on the photon polarization with an angle θ with respect to the optical axis can be written as $\left(\begin{smallmatrix}\cos 2\theta & \sin 2\theta \\ \sin 2\theta & -\cos 2\theta\end{smallmatrix}\right)$. As shown in Fig. 3.5A, by setting HWP1 at $(\pi/2-\alpha)/2$, the photon in $|\psi\rangle$ with polarization $|H\rangle$ changes to $\sin\alpha\,|H\rangle + \cos\alpha\,|V\rangle$. Since the PBS transmits $|H\rangle$ polarization and reflects $|V\rangle$ polarization, we have $|V\rangle$ before L which should be instead $|H\rangle$ (the photon polarization has to remain invariant along the setup). Thus, before the detection device in L, a HWP at 45° is used to flip $|V\rangle$ to $|H\rangle$. As a result, the initial single-photon state $|\psi H\rangle$ is spatially distributed in a controlled manner by the linear combination $|\psi_{\rm D}H\rangle = \cos\alpha|\psi_{\rm L}H\rangle + \sin\alpha|\psi_{\rm R}H\rangle$. Following the same method with HWP2 at $-\beta/2$, it is immediate to see that the other initial single-photon state $|\psi' V\rangle$ is spatially distributed by the linear superposition $|\psi'_{\rm D}V\rangle = \sin\beta|\psi'_{\rm L}V\rangle + \cos\beta|\psi'_{\rm R}V\rangle$. Since the spatial and polarization degrees of freedom are independent, the setup eventually distributes each photon wave packet towards the two operational regions

$$\begin{aligned} |\psi\rangle &\rightarrow |\psi_{\rm D}\rangle = \cos\alpha|\psi_{\rm L}\rangle + \sin\alpha|\psi_{\rm R}\rangle, \\ |\psi'\rangle &\rightarrow |\psi'_{\rm D}\rangle = \sin\beta|\psi'_{\rm L}\rangle + \cos\beta|\psi'_{\rm R}\rangle. \end{aligned} \tag{3.7}$$

These spatial states for the photons are the same of those of Eq (3.6), predicted by the theoretical scheme, with the associations $l = \cos\alpha$, $r = \sin\alpha$, $l' = \sin\beta$ and $r' = \cos\beta$.

D. More experimental results

As mentioned in the main text and in the section above, via changing the values of α and β of HWP1 and HWP2, respectively, a series of $|\Psi_{\rm prep}\rangle$ with different spatial distributions of the wave packets, and thus of the degree of (remote) spatial indistinguishability $\mathcal{I}$, are prepared by the setup. The angles α and β are both fixed at the beginning of each experiment and the corresponding values are obtained from the rotated devices in which the HWPs are mounted. To describe the experimental results more accurately, the angles' values are adjusted to increase the fidelity of the experimental state compared with the desired state. In fact, as $|\Psi_{\rm prep}\rangle$ owns two unknown parameters, namely α and β, there will be several groups of solutions of α and β. Thus, it is necessary to fix one angle first. Here, α is directly read from the mounted device and the value is fixed at $\alpha = \pi/4$ in the experiment. While the other angle β is modulated in

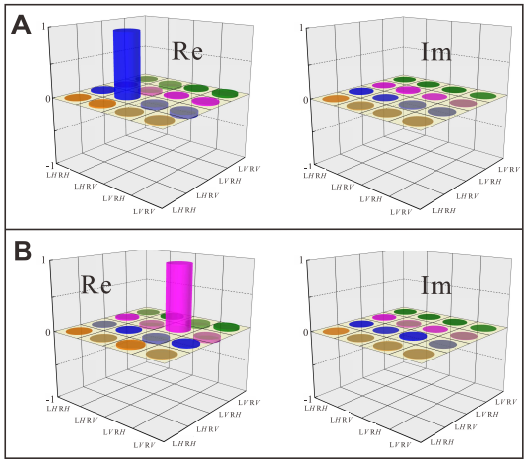

Figure 3.8: Results for spatially separated wave packet distributions. (A) The two panels correspond to the real and imaginary part of $|\Psi_{\mathrm{LR}}\rangle$, respectively, for $\alpha = \beta = 0$. The fidelity is $(95.2 \pm 0.7)\%$. (B) The two panels correspond to the real and imaginary part of $|\Psi_{\mathrm{LR}}\rangle$, respectively, for $\alpha = \beta = \pi/2$. The fidelity is $(95.1 \pm 0.5)\%$.

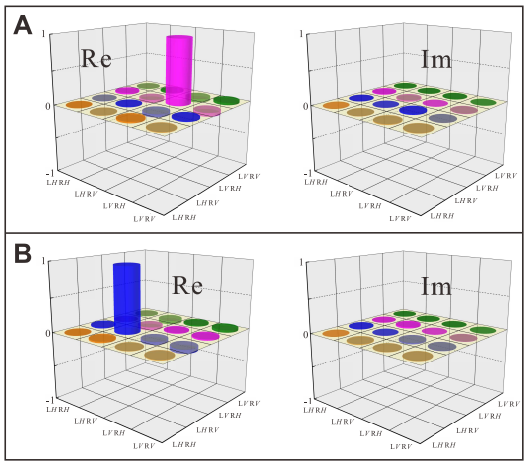

Figure 3.9: Results for wave packet distributions sharing only one operational region. (A) Real and imaginary part of $|\Psi_{\mathrm{LR}}\rangle$ with $\alpha = \pi/4$ and $\beta = \pi/2$, with the fidelity $(95.2 \pm 0.9)\%$. (B) Real and imaginary part of $|\Psi_{\mathrm{LR}}\rangle$ with $\alpha = \pi/4$ and $\beta = 0$ with a fidelity $(95.1 \pm 0.8)\%$.

order to increase the fidelity and the corresponding value is estimated around the display of its mounted device.

When $\alpha = \beta = 0$ $(\pi/2)$, the two spatial distributions $|\psi_{\mathrm{D}}\rangle$ and $|\psi'_{\mathrm{D}}\rangle$ of Eq. (3.7) are separated, each one going to only one operational region. The two photons can be thus distinguished by their spatial locations, $\mathcal{I} = 0$ and the distributed state $|\Psi_{\mathrm{LR}}\rangle$ obtained by sLOCC is uncorrelated in theory (see Sec. B. above). The experimental results are presented in Fig. 3.8 and strongly confirm the theoretical prediction.

The condition of zero entanglement is also retrieved when the two spatial distributions of the wave packets share only one of the two operational regions. In this case, one of α, β is 0 $(\pi/2)$. Assuming the parameter α takes one of these values, one has $\sin\alpha\cos\alpha = 0$ and thus $\sin\beta\cos\beta \neq 0$. Fixing $\alpha = \pi/4$, this configuration is retrieved when β is set at 0 or $\pi/2$. The corresponding results are shown in Fig. 3.9 and confirm the theoretical predictions.

In the teleportation protocol, we first perform the tomography of the effectively prepared ρ_{prep} in L$'$. Compared to $|\phi_{\mathrm{ideal}}\rangle$, the fidelity $F = \langle\phi_{\mathrm{ideal}}|\rho_{\mathrm{prep}}|\phi_{\mathrm{ideal}}\rangle$ of ρ_{prep} in our experiment is $\approx 99.8\%$. To

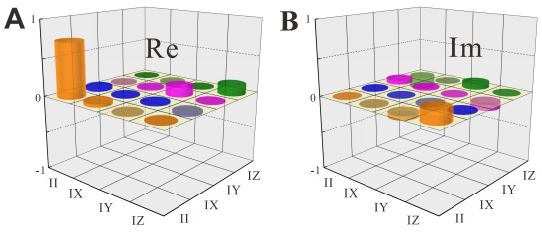

Figure 3.10: The quantum process matrix of quantum teleportation. Experimental reconstruction of quantum process matrix χ for the teleportation protocol. (A, B) show the real and imaginary parts of χ, respectively. Here, I is identity matrix σ_1 and X, Y, Z correspond to σ_x, σ_y, σ_z, respectively.

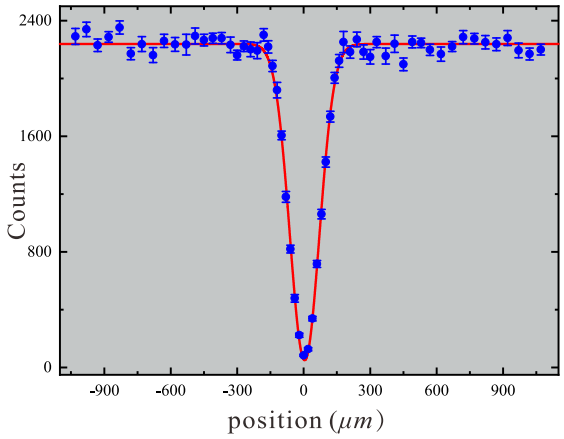

Figure 3.11: The HOM dip of the two-photon interference. The counts are obtained in 5 seconds with the pumping power 30 mW. The blue dots are the experimental results. And the red curve presents the fitting Gaussian function G_x.

characterize quantum teleportation of the photon state from L' to R, we make the tomographic analysis of the process and reconstruct its matrix χ [236], which is shown in Fig. 3.10. Here, χ is defined by $\rho_{\text{exp}} = \Sigma_{i,\,j=1}^{4}\, \chi_{ij}\ \sigma_i \cdot \rho_{\text{ideal}} \cdot \sigma_j$ where $\sigma_1 = I$ and $\sigma_{2,3,4} = \sigma_{x,y,z}$, which in the ideal case gives $\chi_{11} = 1$ with all the other elements equal to 0 [15]. By assuming χ with several unknown parameters and comparing the experimental results of ρ_{prep} and ρ_{exp}, we can calculate the elements of χ. The experimental results are obtained with a fidelity $F_\chi = (73.6 \pm 7.7)\%$.

D..1 Results using two photons from one BBO crystal

To obtain the experimental results close to theory, we use two photons from one BBO crystal instead of two independent sources to redo the experiment. The corresponding results are followed.

First, we re-investigate the identity of these two photons. The visibility of HOM dip (shown in Fig. 3.11) is obtained with a value of about 97.7%. Experimental tomography of the initial state $|\psi H, \psi' V\rangle \equiv |\psi H\rangle \otimes |\psi' V\rangle$ of the two photons from BBO crystal with a high fidelity $(99.9 \pm 0.1)\%$.

Fixing $\alpha = \pi/4$, we study the distribution of $|\psi'_{\text{D}}\rangle$ in the operational regions L and R. Here, we choose the probability that the wave packet $|\psi'_{\text{D}}\rangle$ is located in L to character the distribution, the theoretical prediction being $\sin^2\beta$. The corresponding results are shown in Fig. 3.12 and significantly confirm the theoretical curve.

We redo the experiment quantifying entanglement of state $|\Psi_{\text{LR}}\rangle$ in the main text, i.e., the concurrence C. The Bell function S is employed for the Clauser-Horne-Shimony-Holt (CHSH) test that for the state is $S = 2\sqrt{1+C^2} = 2\sqrt{1+\sin^2 2\beta}$. The experimental results of C, obtained after state reconstruction, and S versus both β and $\mathcal{I}$ are shown in Fig. 3.13(A)-(D). Most of the generated states exhibit

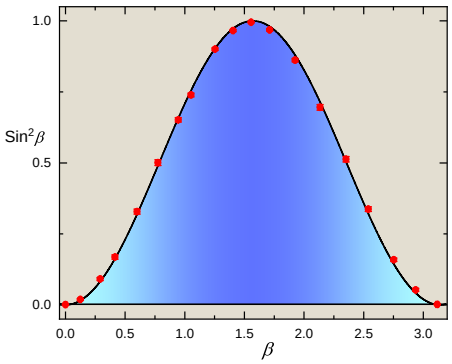

Figure 3.12: Experimental results of probability of $|\psi'_{\rm D}\rangle$ in L. The black line represents theoretical prediction while the red points are the experimental results.

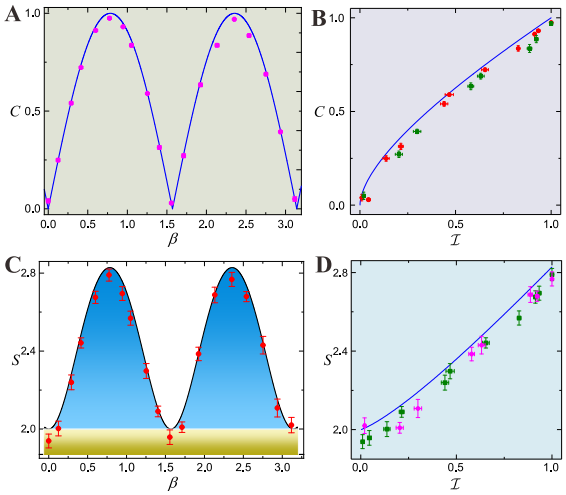

Figure 3.13: Concurrence C (A, B) and Bell function S in the CHSH test (C, D), for $\alpha = \pi/4$ (parameter fixing $|\psi_{\rm D}\rangle$), versus β (parameter adjusting $|\psi'_{\rm D}\rangle$) and $\mathcal{I}$ (remote spatial indistinguishability of Eq.(1)). Blue lines in (A), (B), (D) and black curve in (C) are theoretical predictions. Pink dots in (A) and red points in (C) (with error bars) are experimental results. Red and green dots in (B) (pink and green dots in (D)) denote experimental data for, respectively, $\beta \in [0, \pi/2]$ and $\beta \in (\pi/2, \pi]$.

$S > 2$, demonstrating nonlocal entanglement. For $\beta = \pi/4$ ($\mathcal{I} = 1$), $|\Psi_{\rm LR}\rangle$ in Eq.(3) becomes the Bell state $|\Psi^+_{\rm LR}\rangle$. In the experiment, in correspondence of $\beta = 0.776 \pm 0.006$ we achieve $S = 2.79 \pm 0.03$, violating the Bell inequality by 26 standard deviations. The generated state, whose reconstructed density matrix is shown in Fig. 3.14(A), holds a fidelity of $(98.6 \pm 0.2)\%$ compared to $|\Psi^+_{\rm LR}\rangle$. Moreover, when $\beta = 3\pi/4$, that is when $|\psi'_{\rm D}\rangle = (|\psi'_{\rm L}\rangle - |\psi'_{\rm R}\rangle)/\sqrt{2}$ and $|\psi_{\rm D}\rangle$ are orthogonal yet completely spatially indistinguishable ($\mathcal{I} = 1$), the Bell state $|\Psi^-_{\rm LR}\rangle$ is expected. In the experiment, this state is created with fidelity $(98.0 \pm 0.8)\%$ for $\beta = 2.352 \pm 0.004$ (see Fig. 3.14(B)).

Furthermore, the teleportation is also redone. The second BBO crystal is used to generate a heralded single photon. One photon is used as the trigger signal while the other photon is sent to the side of L′ as the target to be teleported. The eigenvectors of σ_i ($i = x, y, z$) are chosen as the photon states $|\phi\rangle$ in L′ to be teleported, namely $|\phi_{\rm ideal}\rangle \in \{|H\rangle, |V\rangle, |\pm\rangle = (|H\rangle \pm |V\rangle)/\sqrt{2}, |\phi_\pm\rangle = (|H\rangle \pm i|V\rangle)/\sqrt{2}\}$. First, we perform the tomography of the effectively prepared $\rho_{\rm prep}$ in L′. Compared to $|\phi_{\rm ideal}\rangle$, the fidelity $F = \langle\phi_{\rm ideal}|\rho_{\rm prep}|\phi_{\rm ideal}\rangle$ of $\rho_{\rm prep}$ in our experiment is about 99.8%. With tomographic measurements performed in R, the experimental teleported states $\rho_{\rm exp}$ can be reconstructed based on the four-photon

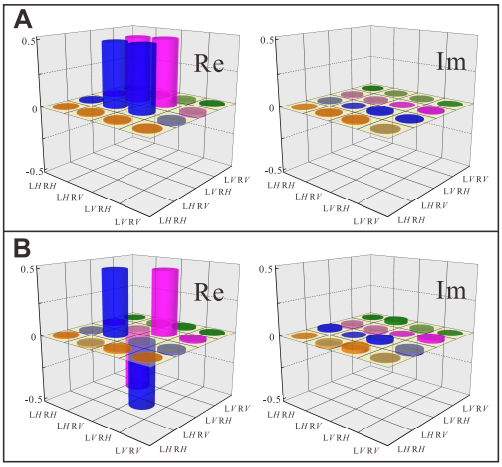

Figure 3.14: Real and imaginary part of the reconstructed density matrix for $\alpha = \pi/4$ and: (A) $\beta = 0.776 \pm 0.006$ (expected state $|\Psi^+_{\rm LR}\rangle$); (B) $\beta = 2.352 \pm 0.004$ (expected state $|\Psi^-_{\rm LR}\rangle$).

cccc

state	$\|H\rangle$	$\|V\rangle$	$\|+\rangle$
$F_{\rm exp}$ (%)	90.0 ± 2.0	84.7 ± 1.9	83.1 ± 2.0
state	$\|-\rangle$	$\|\phi_-\rangle$	$\|\phi_+\rangle$
$F_{\rm exp}$ (%)	82.2 ± 1.9	84.3 ± 1.7	86.3 ± 2.2

Table 3.2: Fidelities of the six states $\rho_{\rm exp}$ with respect to the initially prepared state in the quantum teleportation process.

coincidence. The fidelity $F_{\rm exp}$ compared to the initially prepared state $\rho_{\rm prep}$ is then introduced as figure of merit of teleportation efficiency. For the six initial states above, without background subtraction, the measured fidelities are reported in Table 3.2 which are clearly higher than the classical fidelity limit of $2/3$.

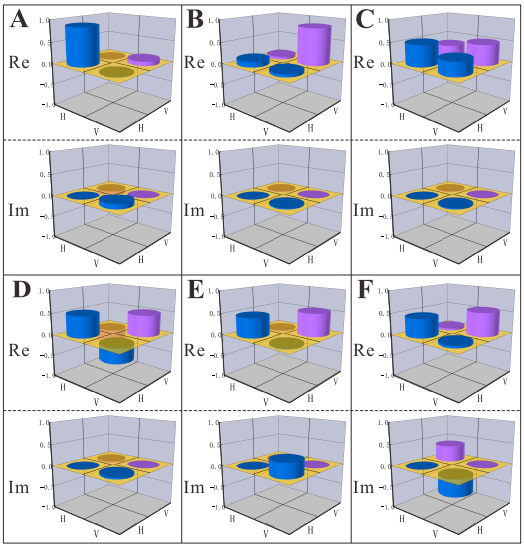

Figure 3.15: Experimental reconstruction of the teleported states $|\phi_{\rm exp}\rangle$. (A), (B), (C), (D), (E) and (F) correspond to the density matrices of $|H\rangle$, $|V\rangle$, $|+\rangle$, $|-\rangle$, $|\phi_-\rangle$, $|\phi_+\rangle$, respectively. In each panel, the upper (lower) subgraph represents the real (imaginary) part of the density matrix.

For the six prepared states of the additional qubit to be teleported, namely $|H\rangle, |V\rangle, |\pm\rangle, |\phi_{\pm}\rangle$ (see main text for their expressions), the corresponding teleported state ρ_{exp} is reconstructed via performing tomographic measurements. The results are shown in Fig. 3.15. Characterizing teleportation by the usual process matrix χ, the experimental results are obtained with a fidelity $F_{\chi} = (79.4 \pm 1.6)\%$.

Chapter 4

Dynamics of spatially indistinguishable particles and quantum entanglement protections

Abstract

A complete treatment of open quantum systems made of identical particles has remained elusive due to the intrinsic problem of these particles being individually unaddressable. Filling this gap is essential for the full characterization of quantum networks which are typically built by identical subsystems. We provide a general framework which allows one to obtain the dynamics of N noninteracting spatially indistinguishable particles locally coupled to separated environments. This framework is universal, being valid for both bosons and fermions and for any type of system-environment interaction. It is then applied to study the dynamics of two identical qubits under paradigmatic Markovian noises, such as phase damping, depolarizing and amplitude damping. We find that spatial indistinguishability of identical qubits is a controllable inherent property of the system which protects exploitable quantum entanglement against detrimental noise. This Chapter is related to Publication 3 in the List of Publications.

4.1 Introduction

Dealing with identical particles, as building blocks of quantum networks, has been subject of debate because of the difficulty in characterizing their physical quantum correlations [237, 238, 239, 240, 5, 223, 241, 13, 191, 224, 242, 192, 14, 221, 193, 2, 3, 194, 243, 244, 10]. In quantum mechanics, particle identity refers to particles of the same species having the same intrinsic properties (such as mass, charge, spin) [6], while indistinguishability can be given a continuous degree related to a given set of quantum measurements [17]. In contrast, nonidentical (distinguishable) particles are individually addressable bodies of a composite system, where individual operations on a given particle can be performed by means of local operations and classical communication [33, 145]. As a direct consequence of the addressability notion (particle-locality), the dynamical treatment of a composite quantum system of distinguishable particles is well understood [15, 40, 104]. This is not the case when the system is made of indistinguishable particles, for which the concept of addressability is lost.

A particle-based no-label approach has been introduced to characterize states composed of identical particles, where the many-body system state is considered as a whole state vector of single-particle states [2, 3]. Employing this approach together with the operational framework of spatially localized operations and classical communication (sLOCC) [16], one can directly access exploitable entanglement between internal degrees of freedom of indistinguishable particles having arbitrary spatial configurations of wave functions. Experimental evidence of spatial indistinguishability as a direct resource for remote entangle-

ment has been recently reported [23, 24]. The no-label approach has been compared with other methods in both first and second quantization [245, 194, 227] and has been applied to analyze the Hanbury Brown-Twiss effect with wave packets [229] and the quantum entanglement in one-dimensional systems of anyons [98]. Indistinguishable particles have revealed to be useful as a resource for entanglement activation and quantum-enhanced information processing [23, 24, 246, 188, 94, 189, 34, 247, 248, 249]. Thanks to the sLOCC framework within the no-label approach, spatial indistinguishability has been proven to be quantifiable by an entropic-informational measure [17] which is directly connected to the amount of generated entanglement [23]. A remaining open question is how indistinguishable particles, under general conditions of spatial overlap, interact with local environments and, as a result, how their system state dynamically evolves. In fact, some reported studies about the effect of environmental noise on identical particles have been so far limited to particles occupying specific modes of a system [250, 251, 252], due to the lack of a method to treat a continuous degree of spatial indistinguishability. The no-label approach plus sLOCC framework appear to be the ideal tools to fill this gap in the context of open quantum systems.

Any realistic quantum system inevitably interacts with the surrounding environment, leading to the decoherence process [40, 253]. Quantum resources, like coherence and entanglement, are more fragile than the classical ones since even a small perturbation would drive the whole system towards decoherence phenomena [254, 255]. Also, the decay rate increases as the number of degrees of freedom of the quantum system increases. As a consequence of local Markovian environments, for example, the entanglement between two separated (distinguishable) qubits completely disappears at a finite time [256, 257, 258, 259]. This is why the preservation of quantum resources is an important challenge in quantum information and computation science. It is known that quantum entanglement can revive as a result of local non-Markovian (quantum or classical) environments [104, 105, 106, 167, 260, 261, 154, 79, 80, 262, 263, 264]. However, the degree of entanglement decreases and eventually vanishes after a certain critical time. Other possible protection strategies have been purposed, such as quantum Zeno effect [150], structured environments [151, 106, 152], distillation protocols [153], decoherence-free subspaces [107, 108], dynamical decoupling and control techniques [109, 110, 111, 154, 155, 156, 157], quantum error corrections [112, 113, 114] and topological properties [115, 116]. Some of these techniques rely on harnessing many system parameters, whose number increases as the number of particles increases. Also, they require near-perfect suppression of experimental imperfections [158]. Finding intrinsic properties of the system which can naturally shield entanglement from noise during the dynamics is highly desirable.

In the present study, we accomplish a twofold purpose: quantum dynamics of indistinguishable subsystems (particles) and quantumness protection. Identical particles are here meant as quantum subsystems of the same type (e.g., artificial atoms or qubits) of a larger composite system. We extend previous results [17] to the general case when spatial indistinguishability of particles is present during the open system dynamics. In fact, we first provide a dynamical framework for noninteracting identical particles with an arbitrary amount of spatial overlap which are locally coupled to separated environmental noise sources. Our derivation, valid for both bosons and fermions, sheds light on the microscopic processes of N spatially indistinguishable particles that interact with M independent environments. Afterward, we apply the procedure to study the entanglement dynamics of two identical (bosonic and fermionic) qubits under general conditions of spatial overlap in Markovian environments at zero temperature under the effect of the phase damping process, depolarizing process and amplitude damping process. We show that spatial indistinguishability plays an important role in preserving entanglement against detrimental noise.

The paper is organized as follows. In Sec. 4.2, we supply the general procedure to deal with the dynamics of noninteracting spatially overlapping identical particles coupled to separated environments. The entanglement dynamics is reported in Sec. 4.3 for the case of phase damping, in Sec. 4.4 for the depolarizing noise, in Sec. 4.5 for the amplitude damping process. Finally, in Sec. 4.6 we summarize our results.

4.2 General framework

In this section, we introduce the general framework to treat the dynamics of identical particles under arbitrary conditions of spatial overlap in the case of localized separated environments. We recall that this is a typical situation in composite physical systems where the noise sources are localized in space. While nonidentical (distinguishable) particles individually interact with their own environment [167, 256], when particles are identical and spatially overlapping, they can no longer be individually addressed by the local environment, so a dedicated treatment is needed.

In the following we provide this treatment by adopting the no-label approach to identical particles [2, 3] together with the sLOCC measurements [16], which are performed to access the indistinguishability-enabled quantumness contained in the evolved distributed resource state of the system.

4.2.1 System-environment Hamiltonian

A global state composed of N identical particles, taken as the set of one-particle states $|\Psi\rangle := |\phi_1, \phi_2, \ldots, \phi_N\rangle$ [2], must be considered as an holistic indivisible entity. In this notation, as usual, each ϕ_i contains all the degrees of freedom characterizing the particle. According to the standard definition [6], a single-particle operation $\hat{A}$ linearly acts on a N-particle state one at a time, namely: $\hat{A}\,|\Psi\rangle := \sum_i |\phi_1, \ldots, \hat{A}\phi_i, \ldots, \phi_N\rangle$. On the other hand, a single-particle quantum operation can be physically restricted to act locally on a given region of space where the identical particles of the composite system can be found with a given probability. Therefore, a suitable definition of a localized single-particle operation acting on a global state of identical particles with arbitrary spatial wave functions is needed to encompass the locality of the quantum operator.

Definition. *A spatially localized single-particle operator $\hat{S}_X$, performed on a region of space X, acts on a N-particle state of identical particles $|\Psi\rangle = |\phi_1, \phi_2, \ldots, \phi_N\rangle$ as follows*

$$\hat{S}_X\,|\Psi\rangle := \sum_i |\,\langle X|\,\phi_i\rangle\,|\,|\phi_1, \ldots, \hat{S}\phi_i, \ldots, \phi_N\rangle\,, \tag{4.1}$$

where $|\,\langle X|\,\phi_k\rangle\,|$ is the absolute value of the probability amplitude of finding a particle in the region X, which weights the strength of the operation as physically desired.

The operator $\hat{S}$ is any operator on internal degrees of freedom of single particle. Notice that, if the region X represents all the space where the particles of the system can be found, the operator $\hat{S}_X$ reduces to the usual single-particle operator $\hat{A}$ above, as expected. Also, the above operator $\hat{S}_X$ is similar to the so-called *weighted spin operator* [265] which accounts for the different probing strengths of the particles of a spin system. The definition of Eq. (4.1) shall be a central ingredient to describe the time evolution of spatially overlapping identical particles that interact with localized environments.

For the sake of simplicity and without loss of generality, we limit our analysis to two identical two-level (spin $\frac{1}{2}$-like) particles (qubits) coupled to two separated bosonic environments E_L and E_R, as depicted in Fig. 4.1, localized in separated sites L and R, respectively. The elementary two-particle system state $|\Psi\rangle_S = |\phi_1, \phi_2\rangle$ is characterized by the set of single-particle states $\{|\phi_i\rangle = |\psi_i s_i\rangle\,,\ i = 1, 2\}$, where ψ_i is the spatial wave function with associated pseudospin state s_i of basis $\{\uparrow, \downarrow\}$. Since the system-environment interaction occurs locally in two distant space regions, any environmental action on the internal degrees of freedom of the particles has to take into account the locality of the interaction. So, indicating with g_{kL} and g_{kR} the coupling constants between the system and the environmental mode k in regions L and R, respectively, the general system-environment interaction Hamiltonian can be written as

$$H_I := \sum_k \left(g_{kL}\hat{E}_{kL}\hat{\sigma}_L + g_{kR}\hat{E}_{kR}\hat{\sigma}_R \right) + h.c., \tag{4.2}$$

where $\hat{E}_{kX}$ ($X = \{L, R\}$) is some environmental operator in terms of annihilation or creation operators of local mode k, $\hat{\sigma}_X$ is a generic localized pseudospin single-particle operator and *h.c.* indicates Hermitian conjugation. The explicit form of $\hat{\sigma}_X$ clearly depends on the type of local system-environment

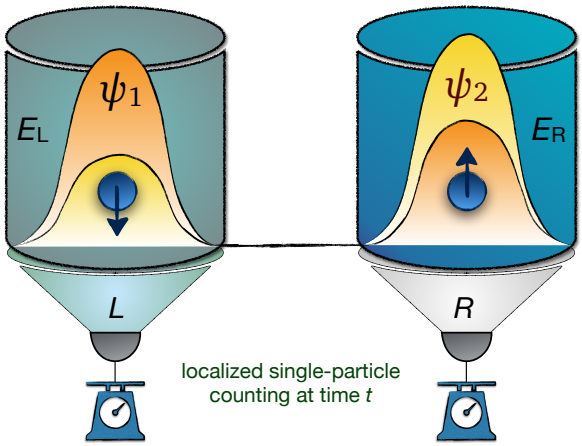

Figure 4.1: **Sketch of the open quantum system.** Two noninteracting identical spin $\frac{1}{2}$-like subsystems (qubits), with spatial wave functions ψ_1 and ψ_2, locally interact with separated environments E_L and E_R placed in the spatial regions L and R, respectively. At time t, single-particle local counting is performed (sLOCC measurement).

interaction and its action on the system state follows the definition of Eq. (4.1). The explicit types of environmental and pseudospin operators are assigned by the given physical process, as we shall see in the applications of the following sections. To achieve a general treatment of the system dynamics, it is useful to see how the interaction Hamiltonian above acts on a global system-environment elementary state vector $|\Psi\rangle_{SE} = |\phi_1, \phi_2\rangle \otimes |\xi_L, \xi_R\rangle$, where $|\xi_X\rangle$ represents a global pure state of the modes of the local environment E_X. By using Eqs. (4.1) and (4.2), we have

$$\begin{aligned} H_I |\Psi\rangle_{SE} = &\sum_k g_{kL} |\hat{E}_{kL}\xi_L, \xi_R\rangle \otimes |\langle L|\psi_1\rangle| \, |\psi_1\hat{\sigma}_L s_1, \psi_2 s_2\rangle \\ &+ \sum_k g_{kL} |\hat{E}_{kL}\xi_L, \xi_R\rangle \otimes |\langle L|\psi_2\rangle| \, |\psi_1 s_1, \psi_2\hat{\sigma}_L s_2\rangle \\ &+ \sum_k g_{kR} |\xi_L, \hat{E}_{kR}\xi_R\rangle \otimes |\langle R|\psi_1\rangle| \, |\psi_1\hat{\sigma}_R s_1, \psi_2 s_2\rangle \\ &+ \sum_k g_{kR} |\xi_L, \hat{E}_{kR}\xi_R\rangle \otimes |\langle R|\psi_2\rangle| \, |\psi_1 s_1, \psi_2\hat{\sigma}_R s_2\rangle \\ &+ h.c. \end{aligned} \tag{4.3}$$

From this equation, it is immediate to see that the interaction Hamiltonian of Eq. (4.2) can be recast as a sum of two terms

$$H_I = H_I^{(1)} + H_I^{(2)}, \tag{4.4}$$

with

$$H_I^{(j)} = \sum_k \sum_{X=L,R} g_{kX}^{(j)} \hat{E}_{kX} \hat{\sigma}_X^{(j)} + h.c., \quad (j = 1, 2) \tag{4.5}$$

where $\hat{\sigma}^{(j)}$, and thus $H_I^{(j)}$, is defined as applied only on the particle pseudospin at the j-th slot of the system state vector and $g_{kX}^{(j)} = g_{kX} |\langle X|\psi_j\rangle|$ $(X = L, R)$ is the effective coupling constant between the particle with spatial wave function ψ_j and the mode k of the environment E_X. The latter shows that the localized single-particle operator defined in Eq. (4.1) naturally leads to effective coupling constants $g_{kX}^{(j)}$ directly dependent on the probability amplitude of finding the particle in the regions L and R where the environment (noise source) is placed, as physically expected. Hereafter, the notation $\hat{O}^{(j)}$ shall indicate a single-particle operator which only acts on the particle state at the j-th position of the system state vector.

Having the above Hamiltonian model of the system-environment interaction, the global (unitary) time evolution operator is

$$\hat{U} = e^{-\frac{i}{\hbar}\left(H_I^{(1)}+H_I^{(2)}\right)t}. \tag{4.6}$$

Looking at Eq. (4.4), one can see an analogy with the usual total interaction Hamiltonian $H_{\rm tot} = H_A + H_B$ of two nonidentical (distinguishable) particles A and B. However, while H_A and H_B always commute due to the individual addressability of the particles (particle-locality), this is not in general the case for $H_I^{(1)}$ and $H_I^{(2)}$. Indeed, two important aspects need to be pointed out when one deals with an open quantum system of identical particles and separated environments:

- A unitary time evolution cannot generally be factorized, that is $\hat{U} \neq e^{-\frac{i}{\hbar}H_I^{(1)}t}e^{-\frac{i}{\hbar}H_I^{(2)}t}$ because of the nonzero commutative property of interaction Hamiltonians, $[H_I^{(i)}, H_I^{(j)}] \neq 0$ for $i \neq j$. This property describes the process that particles can interact with the same environment and, as a result, collective effects of the environment show up. Hamiltonians $H_I^{(1)}$ and $H_I^{(2)}$ commute only when the spatial wave functions of the identical particles are spatially separated in correspondence of each local environment, e.g. $|\psi_1\rangle = |L\rangle$, $|\psi_2\rangle = |R\rangle$ (or vice versa), as easily seen from Eq. (4.5). In this case, in fact, the identical particles are distinguishable by their position and individually interact with their own environment.

- On the other hand, one can write the interaction Hamiltonian of Eq. (4.4) as a sum of two terms corresponding to the two interaction spatial regions $H_I = H_{IL} + H_{IR}$, where each $H_{IX} = H_{IX}^{(1)} + H_{IX}^{(2)}$ (see Eqs. (4.3) and (4.4)). Since each environmental operator $\hat{E}_X$ is localized and independent, one has $[H_{IL}, H_{IR}] = 0$ and the global time evolution of Eq. (4.6) can be written as product of two (localized) operations $\hat{U} = e^{-\frac{i}{\hbar}H_{IL}t}e^{-\frac{i}{\hbar}H_{IR}t} = \hat{U}_L \otimes \hat{U}_R$. However, each operator H_{IX} (and thus $\hat{U}_X$) does not address in general an individual particle of the system state vector due to the spatial overlap (indistinguishability) of the identical particles. Again, this happens only if the identical particles are separated and placed each in a given local environment.

In the following, on the basis of the above points, we shall give the techniques to determine the dynamics of the reduced density matrix of the two-particle system. These techniques are easily extendable to many-particle system and multiple environments, as we shall discuss later (see subsection 4.2.5).

4.2.2 Kraus representation for the reduced density matrix

Assuming that system and environment are initially uncorrelated $\rho(0) = \rho_S(0) \otimes \rho_E(0)$, a typical condition fulfilled within the Born approximation [15, 40], the evolved reduced density matrix of the system can be obtained by

$$\rho_S(t) = \mathrm{Tr}_E\left[\hat{U}_L \otimes \hat{U}_R \left(\rho_S(0) \otimes \rho_E(0)\right) \hat{U}_L^\dagger \otimes \hat{U}_R^\dagger\right], \tag{4.7}$$

where the trace is taken, as usual, over the environmental degrees of freedom [40]. From this equation, one formally obtains the following operator-sum representation (or Kraus representation) for the reduced density matrix

$$\rho_S(t) = \sum_{\alpha,\beta} \mathcal{K}_{\alpha L} \cdot \mathcal{K}_{\beta R}\, \rho_S(0)\, \mathcal{K}_{\alpha L}^\dagger \cdot \mathcal{K}_{\beta R}^\dagger, \tag{4.8}$$

where $\mathcal{K}_{\alpha X} = \langle e_\alpha | \hat{U}_X | e_0 \rangle$ ($X = L, R$) are Kraus operators defined by means of a complete set of orthonormal states $\{e_\alpha\}$ of the local environment E_X [266] and $\mathcal{K}_{\alpha L} \cdot \mathcal{K}_{\beta R}$ indicates the product of the operators.

We notice that the assumption of independent (separated) environments implies that the dynamical map of Eq. (4.8) is given by means of a factorization of operators related to each local environment. However, as expected in this case due to the general particle indistinguishability, each (local) Kraus operator is a two-particle operator which cannot be written in a tensor product form of single-particle operators, that is $\mathcal{K}_{\alpha X} \neq \mathcal{K}_\alpha^{(1)} \otimes \mathcal{K}_\alpha^{(2)}$. On the other hand, when the particles are separated,

one in E_L and one in E_R and so spatially distinguishable, the local Kraus operators assume the tensor product form $\mathcal{K}_{\alpha L} = \mathcal{K}_{\alpha}^{(1)} \otimes_2^{(2)}$ and $\mathcal{K}_{\beta R} =_2^{(1)} \otimes \mathcal{K}_{\beta}^{(2)}$, where $_2$ is the 2×2 identity matrix: this means that each environmental operator only acts on an individual particle of the state vector. As can be immediately seen, when the Kraus operators take this tensor product form, the dynamical map of Eq. (4.8) reduces to the well-known operator-sum representation for nonidentical (distinguishable) particles $\rho_S(t) = \sum_{\alpha,\beta} \mathcal{K}_{\alpha}^{(1)} \otimes \mathcal{K}_{\beta}^{(2)} \, \rho_S(0) \, \mathcal{K}_{\alpha}^{(1)\dagger} \otimes \mathcal{K}_{\beta}^{(2)\dagger}$ [40, 15].

The Kraus representation of Eq. (4.8) for indistinguishable particles remains a formal solution for the system dynamics, which can be of difficult practical utility. Finding explicit expressions for the Kraus operators under general conditions is in fact a challenging task. The next step is therefore to look for a convenient solution by means of a master equation.

4.2.3 Master equation for the reduced density matrix

The most general dynamics of an open quantum system, under Born-Markov approximation, can be described by the Gorini-Kossakowski-Sudarshan-Lindblad equation [267, 268, 40]. We are interested in deriving this master equation for our system of two indistinguishable qubits, considering local memoryless bosonic environments at zero temperature. Each local noise channel, at the site X, is thus assumed to phenomenologically induce a typical single-particle decay rate γ_{0X}. Following the standard procedure, i.e. performing the Born-Markov approximation (weak coupling) $\rho_{SE} = \rho_S \otimes \rho_E$ and tracing out the environment degrees of freedom, we obtain the general structure of the master equation for the reduced density matrix of the two-qubit system in the interaction picture as follows

$$\dot{\rho}_S = \sum_{X=L,R} \sum_{i,j=1,2} \gamma_X^{(i,j)} \left(\hat{\sigma}_X^{(i)} \rho_S \hat{\sigma}_X^{(j)\dagger} - \frac{1}{2} \{ \hat{\sigma}_X^{(i)\dagger} \hat{\sigma}_X^{(j)}, \rho_S \} \right), \tag{4.9}$$

where $\hat{\sigma}^{(i)}$, $\hat{\sigma}^{(j)}$ are pseudospin single-particle jump operators, whose explicit form depends on the system-environment interaction, and

$$\gamma_X^{(i,j)} = \gamma_{0X} | \langle X | \psi_i \rangle \langle \psi_j | X \rangle |, \quad (i,j = 1,2) \tag{4.10}$$

are effective decay rates associated to the noise action. We remark that these effective decay rates $\gamma_X^{(i,j)}$ are independent of particle statistics and crucially depend on particle spatial overlap, so manifesting the effects of spatial indistinguishability (even partial) of the identical qubits on the system evolution.

When the qubits are spatially separated, Eq. (4.9) reduces to the well-known master equation of two distinguishable particles each one embedded in its own local environment, as expected. In fact, in this case the qubits are distinguishable by their location, e.g., $|\psi_1\rangle = |L\rangle$ and $|\psi_2\rangle = |R\rangle$, so that the only nonzero effective decay rates are $\gamma_L^{(11)} = \gamma_{0L}$ and $\gamma_R^{(22)} = \gamma_{0R}$.

One can also immediately see the effect of maximal spatial indistinguishability for the two qubits. This is the situation when particles are present in the same region X with same probability P_X ($| \langle X | \psi_i \rangle | = | \langle X | \psi_j \rangle | = \sqrt{P_X}$), so they are completely indistinguishable to the eyes of the local environments [23, 16]. In this case, the effective decay rates of Eq. (4.10) are equal for a given location X, that is $\gamma_X^{(i,j)} = \gamma_{0X} P_X$ and the master equation of Eq. (4.9) becomes

$$\dot{\rho}_S = \sum_{X=L,R} \gamma_{0X} P_X \left(\hat{\sigma}'_X \rho_S \hat{\sigma}'^{\dagger}_X - \frac{1}{2} \{ \hat{\sigma}'^{\dagger}_X \hat{\sigma}'_X, \rho_S \} \right) \tag{4.11}$$

where $\hat{\sigma}'_X = \hat{\sigma}_X^{(1)} + \hat{\sigma}_X^{(2)}$ is a collective single-particle pseudospin operator related to the noise action at location X. Notice that the above master equation is similar to the situation of noninteracting nonidentical (distinguishable) particles coupled to a common environment, which is known to give rise to collective effects [269, 270]. However, we remark that here the collective interaction is only due to the spatial indistinguishability of the identical particles, which continuously rules the interplay between collective and individual effects of the localized environments.

The master equation of Eq. (4.9) represents the main tool to solve the dynamics of two identical qubits, with an arbitrary spatial overlap configuration, coupled to two local environments. The two-particle basis in which the master equation is solved will be conveniently chosen according to the specific system-environment interaction. To complete the analysis, one just needs to recall the operational framework of sLOCC [16], which is required to study the dynamics of quantum properties exploitable at separated sites, and a suitable degree of spatial indistinguishability [17]. This shall be done in the following section for convenience.

4.2.4 sLOCC operational framework and degree of spatial indistinguishability

We briefly recall the sLOCC formalism [16] and the spatial indistinguishability measure [17] needed to exploit, at time t, a state of two spatially overlapping identical particles distributed in two remote regions L and R.

The state $\rho_S(t)$, determined by solving Eq. (4.9), is finally projected by the operator $\Pi^{(2)}_{LR} = \sum_{s_1,s_2=\uparrow,\downarrow} |Ls_1, Rs_2\rangle \langle L$
onto the operational subspace, spanned by the basis $\mathcal{B}_{\rm LR} = \{|\mathrm{L}\uparrow, \mathrm{R}\uparrow\rangle, |\mathrm{L}\uparrow, \mathrm{R}\downarrow\rangle, |\mathrm{L}\downarrow, \mathrm{R}\uparrow\rangle, |\mathrm{L}\downarrow, \mathrm{R}\downarrow\rangle\}$,
to get the distributed state [17]

$$\rho_{LR}(t) = \Pi^{(2)}_{LR}\rho_S(t)\Pi^{(2)}_{LR}/\mathrm{Tr}(\Pi^{(2)}_{LR}\rho_S(t)), \tag{4.12}$$

with sLOCC probability $P_{LR}(t) = \mathrm{Tr}(\Pi^{(2)}_{LR}\rho_S(t))$ (we provide in Appendix A. detailed information about the sLOCC probability for the physical examples we shall treat in the following sections). Now the final state $\rho_{LR}(t)$ is activated to be used for any quantum information tasks. The action of the projection operator $\Pi^{(2)}_{LR}$ on the two-particle state is obtained by using the probability amplitude $\langle\phi_1', \phi_2'|\phi_1, \phi_2\rangle = \langle\phi_1'|\phi_1\rangle\langle\phi_2'|\phi_2\rangle + \eta\langle\phi_1'|\phi_2\rangle\langle\phi_2'|\phi_1\rangle$ [2, 3], where $\eta = \pm 1$ with the upper or lower sign for bosons or fermions. Particle statistics is thus expected to play a role in the dynamics, especially in the behavior of the sLOCC probability. Once the state $\rho_{LR}(t)$ is obtained, with one particle in L and another one R, the amount of useful entanglement of $\rho(t)$ within the sLOCC framework can be calculated by the concurrence [17]

$$C_{LR}(\rho_S) := C(\rho_{LR}) = \max\{0, \sqrt{\lambda_4} - \sqrt{\lambda_3} - \sqrt{\lambda_2} - \sqrt{\lambda_1}\}, \tag{4.13}$$

where λ_i are the eigenvalues, in decreasing order, of the matrix $R = \rho_{LR}\,\rho_{LR}$, being $\rho_{LR} = \sigma_y^L \otimes \sigma_y^R \rho^*_{LR} \sigma_y^L \otimes \sigma_y^R$ with localized Pauli matrices $\sigma_y^L = |L\rangle\langle L| \otimes \sigma_y$, $\sigma_y^{\rm R} = |R\rangle\langle R| \otimes \sigma_y$.

The degree of spatial indistinguishability of the two identical qubits, emerging from the outcomes of the joint sLOCC measurement $\Pi^{(2)}_{LR}$, is given by [17]

$$\begin{aligned}\mathcal{I} = &- \frac{P_{L\psi_1}P_{R\psi_2}}{\mathcal{Z}} \log_2 \frac{P_{L\psi_1}P_{R\psi_2}}{\mathcal{Z}} \\ &- \frac{P_{L\psi_2}P_{R\psi_1}}{\mathcal{Z}} \log_2 \frac{P_{L\psi_2}P_{R\psi_1}}{\mathcal{Z}},\end{aligned} \tag{4.14}$$

where $\mathcal{Z} = P_{L\psi_1}P_{R\psi_2} + P_{L\psi_2}P_{R\psi_1}$ and $P_{X\psi_i} = |\langle X|\psi_i\rangle|^2$ ($X = L, R$ and $i = 1, 2$) is the probability of finding in $|X\rangle$ the particle coming from $|\psi_i\rangle$. One has $\mathcal{I} \in [0, 1]$, being equal to 0 for separated (spatially distinguishable) particles (e.g., $P_{L\psi_1} = P_{R\psi_2} = 1$) and equal to 1 for maximally indistinguishable particles ($P_{X\psi_1} = P_{X\psi_2}$).

Hereafter, we assume that the spatial wave functions have the form

$$|\psi_1\rangle = l\,|\mathrm{L}\rangle + r\,|\mathrm{R}\rangle, \quad |\psi_2\rangle = l'\,|\mathrm{L}\rangle + r'e^{i\theta}\,|\mathrm{R}\rangle, \tag{4.15}$$

where l, r, l', r' are non-negative real numbers ($l^2 + r^2 = l'^2 + r'^2 = 1$) and θ is a phase. Such a situation, illustrated in Fig. 4.1, is particularly convenient for studying the role of spatial indistinguishability when one is interested in exploiting the state at the two distant operational locations L and R, which can be two nodes of a quantum network. For this choice, we have $\mathcal{I} = 0$ when ($l = r' = 1$ or $l = r' = 0$) and

$\mathcal{I} = 1$ (when $l = l'$). It is known that, switching the value of θ, bosonic and fermionic behaviors can be interchanged for some initial state configurations [17]. Of course, one has to pay attention to the specific values of the parameters defining the spatial wave functions of Eq. (4.15), in order that the system state at time t obeys selection rules due to the particle statistics and the sLOCC probability remains nonzero.

We now have all the elements to study the dynamics of entanglement of two spatially indistinguishable qubits. Before showing the study for three typical noise channels, we briefly discuss the generalization of the above formalism.

4.2.5 Generalization to N particles and M separated environments

We notice that the dynamical formalism introduced above naturally leads to define the local coupling of N noninteracting identical qubits to M independent environments E_{L_m} placed in separated locations L_m ($m = 1, \ldots, M$). In fact, one can easily extend Eqs. (4.4) and (4.5) to this more general case as

$$H_I := \sum_{j=1}^{N} \sum_{k} \sum_{m=1}^{M} g_{kL_m}^{(j)} \hat{E}_{kL_m} \hat{\sigma}_{L_m}^{(j)} + h.c., \tag{4.16}$$

where $g_{kL_m}^{(j)} = g_{kL_m} \langle L_m | \psi_j \rangle$ ($j = 1, 2, \ldots, N$) is the effective coupling constant between the particle with spatial wave function ψ_j and the mode k of the environment E_{L_m}. The operators $\hat{E}_{kL_m}$ are some environmental operators as a function of annihilation or creation operators of local field mode k, while $\hat{\sigma}_{L_m}^{(j)}$ are single-particle pseudospin operators acting on the particle state at the j-th position in the global state vector. From Eq. (4.16), one immediately has

$$H_I = \sum_{j=1}^{N} H_I^{(j)} = \sum_{m}^{M} H_{IL_m}, \tag{4.17}$$

so that the evolved reduced density matrix $\rho_S(t)$ of the system of N indistinguishable qubits can be formally derived by straightforward generalization of the master equation provided in Eq. (4.9).

We highlight that the evolution for a system made of d-level identical particles (qudits) can be easily derived by the above formalism, by simply changing the pseudospin operators $\hat{\sigma}$ appearing in the Hamiltonian of Eq. (4.16) with suitable d-level single-particle operators. Analogously, different types of local environments can be considered (such as spin-like or fermionic environments) by adopting the suitable environment operators in place of $\hat{E}_{kL_m}$. Finally, it is clear how the dynamical framework above is flexible and generalizable to specific system-environment interactions, provided that the identical subsystems are noninteracting and the environments are localized and separated.

4.3 Phase damping noise

Phase damping as a noise process describes the loss of quantum coherence without loss of energy (nondissipative channel). For example, it is the result of random telegraph noise or phase noisy lasers [271, 272, 273, 274, 275, 276] and characterizes typical nanodevices and superconducting qubits under low-frequency noise [277, 278, 279, 280, 281, 282].

We study the dynamics of two identical qubits interacting with two spatially separated phase damping environments. The environments are assumed to be Markovian and identical, so that $\gamma_{0X} = \gamma_0$ ($X = L, R$). From the general expressions of Eqs. (4.4) and (4.5), the total interaction Hamiltonian is $H_I = H_I^{(1)} + H_I^{(2)}$ with

$$H_I^{(j)} = \sum_{X=L,R} \sum_{k} g_{kX}^{(j)} \hat{a}_{kX} \hat{\sigma}_z^{(j)} + h.c., \tag{4.18}$$

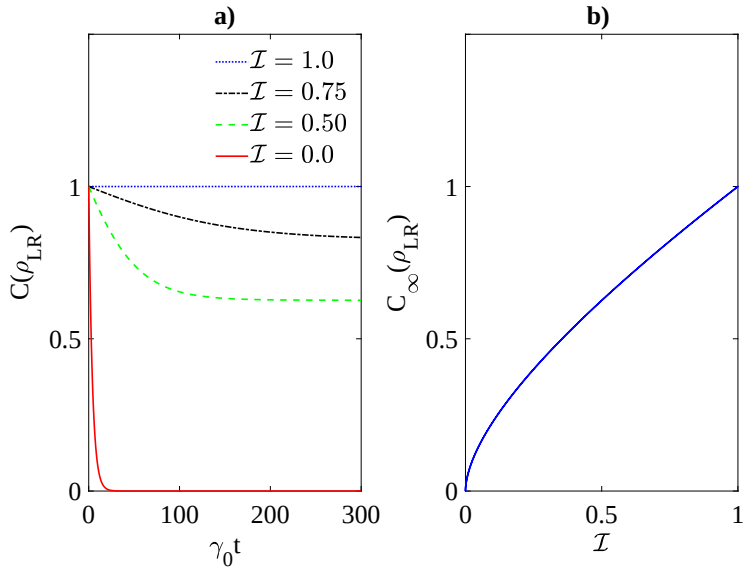

Figure 4.2: **Entanglement evolution under localized phase damping environments. a.** Concurrence dynamics $C(\rho_{LR}(t))$ as a function of dimensionless time $\gamma_0 t$ starting from the initial state $|1_-\rangle$ for different degrees of spatial indistinguishability $\mathcal{I}$, fixing $l = r'$: blue dotted line $\mathcal{I} = 1$ ($l = l'$), black dot-dashed line $\mathcal{I} = 0.75$, green dashed line $\mathcal{I} = 0.5$ and red solid line $\mathcal{I} = 0$. **b.** Stationary entanglement $C_\infty(\rho_{LR})$ as a function of $\mathcal{I}$. All the plots are valid for both fermions (with $\theta = 0$) and bosons (with $\theta = \pi$).

where $\hat{\sigma}_z^{(j)}$ is the usual Pauli pseudospin operator representing the pure dephasing interaction. Substituting $\hat{\sigma}_X = \hat{\sigma}_z$ in Eq. (4.9), the master equation for the phase damping process is

$$\dot{\rho}_S = \sum_{X=L,R} \sum_{i,j=1,2} \gamma_X^{(i,j)} \left(\sigma_z^{(i)} \rho_S \sigma_z^{(j)} - \frac{1}{2} \{ \sigma_z^{(i)} \sigma_z^{(j)}, \rho_S \} \right), \tag{4.19}$$

where $\gamma_X^{(i,j)} = \gamma_0 |\langle X | \psi_i \rangle \langle \psi_j | X \rangle|$ are the effective decay rates.

For the case of two distinguishable qubits undergoing nondissipative channels (such as pure dephasing and depolarizing processes), a Bell-diagonal state structure is maintained during the evolution, the preferred basis being that of the four usual Bell states [283, 284]. We find here an analogous behavior. So, we study the dynamics in the basis of the four orthonormal Bell states $\mathcal{B} = \{|1_\pm\rangle, |2_\pm\rangle\}$ for spatially indistinguishable qubits, defined as [17]

$$\begin{aligned} |1_\pm\rangle &= \frac{1}{\sqrt{2\mathcal{N}_{1_\pm}}} (|\psi_1 \uparrow, \psi_2 \downarrow\rangle \pm |\psi_1 \downarrow, \psi_2 \uparrow\rangle), \\ |2_\pm\rangle &= \frac{1}{\sqrt{2\mathcal{N}_{2_\pm}}} (|\psi_1 \uparrow, \psi_2 \uparrow\rangle) \pm |\psi_1 \downarrow, \psi_2 \downarrow\rangle), \end{aligned} \tag{4.20}$$

where $\mathcal{N}_{1_-} = (1 - \eta |\langle \psi_1 | \psi_2 \rangle|^2)$, $\mathcal{N}_{1_+} = \mathcal{N}_{2_\pm} = (1 + \eta |\langle \psi_1 | \psi_2 \rangle|^2)$. As a consequence, the evolved two-particle density matrix can be written in Bell-diagonal form as

$$\rho_S(t) = \sum_{u=\{1_\pm, 2_\pm\}} p_u(t) \, |u\rangle \langle u| \tag{4.21}$$

where $p_u(t)$ is the probability that the system occupies the Bell state $|u\rangle$ at time t, with $\sum_i p_u(t) = 1$. One expects that the time-dependent population coefficients $p_u(t)$ will be affected by the degree of spatial indistinguishability. Moreover, effects of the specific spatial wave functions reflect on the initial

population coefficients $p_u(0)$, establishing selection rules allowing or forbidding some initial states due to the particle statistics.

Using the master equation of Eq. (4.19) and for any ψ_1, ψ_2, we obtain the time-dependent populations $p_u(t)$ of the four Bell states

$$\begin{aligned} p_{1\pm}(t) =& \frac{1}{2}\left(1+e^{-\gamma_- t/2}\right)p_{1\pm}(0) + \frac{1}{2}\left(1-e^{-\gamma_- t/2}\right)p_{1\mp}(0), \\ p_{2\pm}(t) =& \frac{1}{2}\left(1+e^{-\gamma_+ t/2}\right)p_{2\pm}(0) + \frac{1}{2}\left(1-e^{-\gamma_+ t/2}\right)p_{2\mp}(0), \end{aligned} \tag{4.22}$$

where the decay rates $\gamma_\pm$ are

$$\gamma_\pm = \sum_{X=L,R}\sum_{i,j=1,2}(\pm 1)^{i+j}\gamma_0 |\langle X|\psi_i\rangle\langle\psi_j|X\rangle|. \tag{4.23}$$

Notice that, as expected, one-excitation states ($|1_\pm\rangle$) and two-excitation states ($|2_\pm\rangle$) remain in their own subspace during the dynamics. The expressions above make it evident how specific choices of the spatial wave functions $|\psi_1\rangle$, $|\psi_2\rangle$ determine the two-particle state evolution under localized Markovian pure dephasing. This is a direct consequence of spatially indistinguishable particles. From Eq. (4.22) one can easily see that the system eventually tends to a steady state.

We first analyze the dynamics of the two extreme cases: spatially distinguishable qubits ($\mathcal{I}=0$) and maximally indistinguishable qubits ($\mathcal{I}=1$). For spatially distinguishable qubits, when one qubit interacts with the environment E_L and the other qubit with E_R (e.g., $l=r'=1$), the decay rates of Eq. (4.23) are $\gamma_+=\gamma_-=2\gamma_0$ and the well-known dynamical behavior due to independent Markovian dephasing noises is retrieved. When particles are perfectly spatially indistinguishable ($l=l'$), the dynamics drastically change. The decay rates from Eq. (4.23) become $\gamma_+=4\gamma_0$ and $\gamma_-=0$, so that the evolved Bell-state populations of Eq. (4.22) are

$$\begin{aligned} p_{1\pm}(t) =& p_{1\pm}(0), \\ p_{2\pm}(t) =& \frac{1}{2}\left(1+e^{-2\gamma_0 t}\right)p_{2\pm}(0) + \frac{1}{2}\left(1-e^{-2\gamma_0 t}\right)p_{2\mp}(0). \end{aligned} \tag{4.24}$$

The above equations clearly show an interesting consequence of maximum spatial indistinguishability, which decouple the states $|1_\pm\rangle$ from the phase damping process as noise-free subspaces, provided that the initial states are allowed by the particle statistics. Quantum properties contained in the states $|1_\pm\rangle$ are thus frozen and exploitable by sLOCC at any time.

Starting from the initial state $|1_-\rangle$, for fermions (bosons) with $\theta=0$ ($\theta=\pi$), and obtaining $\rho_{LR}(t)$ after sLOCC on $\rho_S(t)$, we calculate the entanglement amount $C_{LR}(\rho_S(t)) = C(\rho_{LR}(t))$, which is plotted versus the dimensionless time $\gamma_0 t$ in Fig. 4.2**a** for different values of $\mathcal{I}$, fixing $l=r'$. The sLOCC probability is $P_{LR}(t)\geq 0.5$ for any time (see Appendix A.; the choice $l=r'$ is just made to maximize the sLOCC probability in the case of maximal indistinguishability). As can be seen in Fig. 4.2**a**, entanglement sudden death (occurring for $\mathcal{I}=0$) is forbidden thanks to the spatial overlap of the identical qubits and the entanglement evolution achieves a stationary value which increases as spatial indistinguishability increases. The reason for this entangled steady state is that the randomization process of the relative phase between the states $|L\uparrow, R\downarrow\rangle$ and $|L\downarrow, R\uparrow\rangle$, due to the dephasing process, is mitigated or even prevented for $\mathcal{I}\neq 0$. The characteristic time of the evolution is $\tau_- = 1/\gamma_-$ and spatial indistinguishability has the effect of inhibiting the decay rate γ_-. The asymptotic amount of entanglement can be analytically found as

$$C_\infty(\rho_{LR}) = \frac{2(ll')^2}{l^4+l'^4}, \tag{4.25}$$

with associated sLOCC probability depending on the degree of spatial indistinguishability, namely: $P_{LR}=l^4+l'^4$ when $\mathcal{I}<1$, $P_{\rm LR}=1/2$ for fermions and $P_{\rm LR}=1$ for bosons when $\mathcal{I}=1$ (see Appendix A. for details). The stationary entanglement $C_\infty(\rho_{LR})$ is plotted as a function of $\mathcal{I}$ in Fig. 4.2**b**.

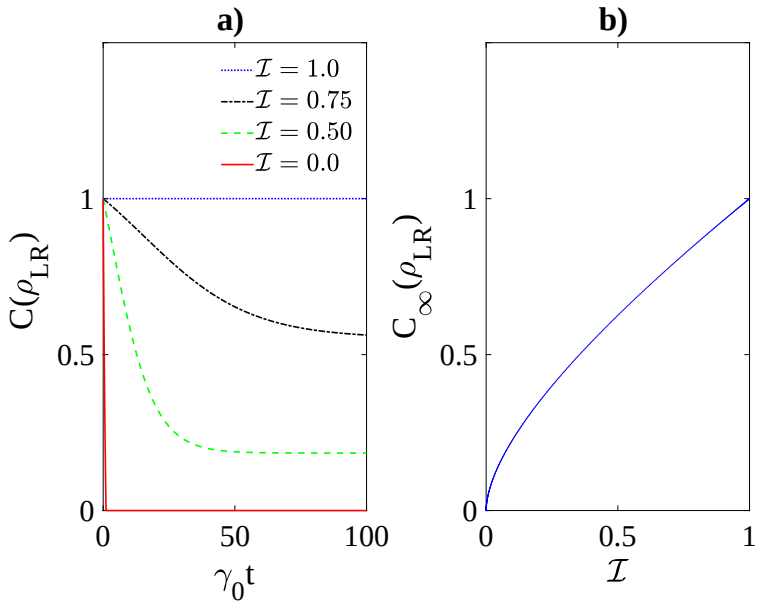

Figure 4.3: **Entanglement evolution under a localized depolarizing environment. a.** Entanglement dynamics $C(\rho_{LR}(t))$ as a function of dimensionless time $\gamma_0 t$ starting from the initial state $|1_-\rangle$ for different degrees of spatial indistinguishability $\mathcal{I}$, fixing $l = r'$: blue dotted line $\mathcal{I} = 1$ ($l = l'$), black dot-dashed line $\mathcal{I} = 0.75$, green dashed line $\mathcal{I} = 0.5$ and red solid line $\mathcal{I} = 0$. **b.** Stationary entanglement $C_\infty(\rho_{LR})$ as a function of $\mathcal{I}$. All plots are valid for both fermions (with $\theta = 0$) and bosons (with $\theta = \pi$).

It is remarkable that the amount of preserved quantum correlations directly depends on how much the two identical qubits are spatially indistinguishable in the two separated environmental sites. In particular, maximum entanglement is frozen ($C_\infty(\rho_{LR}) = 1$) for $\mathcal{I} = 1$ ($l = l'$). Adjusting the value of $\mathcal{I}$ in the initial preparation stage allows one to exploit the remote entanglement at any time during the evolution, despite the action of the pure dephasing. Spatial indistinguishability is a shield for quantum correlations against local dephasing.

4.4 Depolarizing noise

Depolarizing noise is an isotropic (symmetric) decoherence process of a qubit, such that the qubit state remains untouched with a given probability p while an error (white noise) occurs with probability $1 - p$ [15, 285, 286]. This kind of noise can be the result of an isotropic interaction of a spin-$1/2$-like particle (qubit) with a bosonic or spin-like environment [287, 288, 289, 290]. Experimentally, the depolarization process can be found in nuclear magnetic resonance setups [291, 292] and Bose-Einstein condensates [293, 294], where decoherence process is often caused by a residual fluctuating magnetic field. Depolarization processes for photons can also occur, caused by optical scattering when photons become randomly polarized [295, 296, 297].

We consider two identical qubits isotropically interacting with a single Markovian bosonic reservoir localized in region L, characterized by the decay rate $\gamma_{0L} = \gamma_0$ (there is no noise channel assumed at location R). From Eqs. (4.4) and (4.5), being $g_{kR} = 0$, the total interaction Hamiltonian is $H_I = H_I^{(1)} + H_I^{(2)}$ with

$$H_I^{(j)} = \sum_{n=1}^{3} \sum_k g_{kL}^{(j)} \hat{\sigma}_n^{(j)} (\hat{a}_{kL} + \hat{a}_{kL}^\dagger), \tag{4.26}$$

where $\hat{\sigma}_n^{(j)}$ ($n = 1, 2, 3$) are the Pauli pseudospin operators. Substituting $\hat{\sigma}_X = \sum_{n=1}^{3} \hat{\sigma}_n$ in Eq. (4.9),

the Markovian master equation corresponding to the depolarizing process is

$$\dot{\rho}_S = \sum_{n=1}^{3} \sum_{i,j} \gamma_L^{(i,j)} \left(\sigma_n^{(i)} \rho_S \sigma_n^{(j)} - \frac{1}{2} \{ \sigma_n^{(i)} \sigma_n^{(j)}, \rho_S \} \right), \tag{4.27}$$

where the effective decay rate $\gamma_L^{(i,j)}$ is defined in Eq. (4.10) with $X = L$. The depolarizing noise is also nondissipative, like the phase damping noise, so the convenient basis for the dynamical description is the Bell-state basis of Eq. (4.20). The solution of the master equation of Eq. (4.27) gives an evolved density matrix of the form of Eq. (4.21), with time-dependent population coefficients

$$\begin{aligned} p_{1_-}(t) &= p_{1_-}(0) e^{-\gamma_- t} + \frac{1}{4} \left(1 - e^{-\gamma_- t} \right), \\ p_{u'}(t) &= p_{u'}(0) e^{-(3\gamma_+ + \gamma_-)t/4} + \frac{1}{4} (1 - e^{-(3\gamma_+ + \gamma_-)t/4}) \\ &\quad + \frac{1 - 4p_{1_-}(0)}{12} (e^{-\gamma_- t} - e^{-(3\gamma_+ + \gamma_-)t/4}), \end{aligned} \tag{4.28}$$

where $u' = \{ |1_+\rangle, |2_\pm\rangle \}$ and $\gamma_\pm$ are given in Eq. (4.23) with $X = L$ only, that is $\gamma_\pm = \sum_{i,j=1,2} (\pm 1)^{i+j} \gamma_L^{(i,j)}$.

In the case of distinguishable (separated) qubits ($\mathcal{I} = 0$), the decay rates are $\gamma_+ = \gamma_- = \gamma_0$, so that the state at time t is determined by the population coefficients

$$p_u(t) = p_u(0) e^{-\gamma_0 t} + \frac{1}{4} \left(1 - e^{-\gamma_0 t} \right), \tag{4.29}$$

which, from Eq. 4.21), gives the well-known Werner state $\rho_W = p\rho_0 + (1-p)_4/4$ [33, 197], with $p = e^{-\gamma_0 t}$, as expected. In fact, the Werner state describes the action of a depolarizing channel on an individual qubit of the pair, with the system which remains in its initial state ρ_0 with probability p and degrades to the maximally mixed state ${}_4/4$ with probability $1 - p$. In contrast, for maximally spatially indistinguishable qubits ($\mathcal{I} = 1$, $l = l'$), the decay rates become $\gamma_+ = 4l^2\gamma_0$ and $\gamma_- = 0$. The most interesting consequence is that, from Eq. (4.28), one has

$$p_{1_-}(t) = p_{1_-}(0), \tag{4.30}$$

so that the initial state $|1_-\rangle$ ($p_{1_-}(0) = 1$) is a noise-free state. Quantum features of this state can be utilized by sLOCC at any time.

For the intermediate cases, we plot the entanglement dynamics individuated by $C(\rho_{\rm LR}(t))$ in Fig. 4.3**a** for different values of $\mathcal{I}$, fixing $l = r'$, starting from the initial state $|1_-\rangle$ for fermions (bosons) with $\theta = 0$ ($\theta = \pi$). Analogously to the findings for the dephasing noise, the two-qubit entanglement is protected against the depolarizing noise thanks to nonzero spatial indistinguishability. Early-stage disentanglement, occurring for distinguishable qubits ($\mathcal{I} = 0$) is prevented when $\mathcal{I} > 0$, for which a stationary entangled state is achieved. The characteristic decay time of the evolution is $\tau_- = 1/\gamma_-$, which increases as $\mathcal{I}$ increases. Eventually, the concurrence $C(\rho_{\rm LR}(t))$ converges to the asymptotic value

$$C_\infty(\rho_{\rm LR}) = \max \left\{ 0, \frac{3l^2 l'^2}{2\left(l^4 + l'^4 - l^2 l'^2\right)} - \frac{1}{2} \right\}, \tag{4.31}$$

which is plotted in Fig. 4.3**b** as a function of $\mathcal{I}$. For $\mathcal{I} = 1$, one has $C_\infty(\rho_{\rm LR}) = 1$ with probability $P_{LR} = 1/2$ for fermions and $P_{LR} = 1$ for bosons (see Appendix A. for details on the sLOCC probabilities). In contrast with what happens for distinguishable qubits, for which the steady-state $\rho(\infty)_{LR} =_4 /4$ is always a maximally mixed state, the spatial indistinguishability modifies the time-dependent population of each Bell state during the evolution so that the steady state can be entangled. The frozen entanglement is exclusively due to nonzero spatial indistinguishability, which tends to suppress the decay rate γ_- and protects entanglement from depolarizing noise.

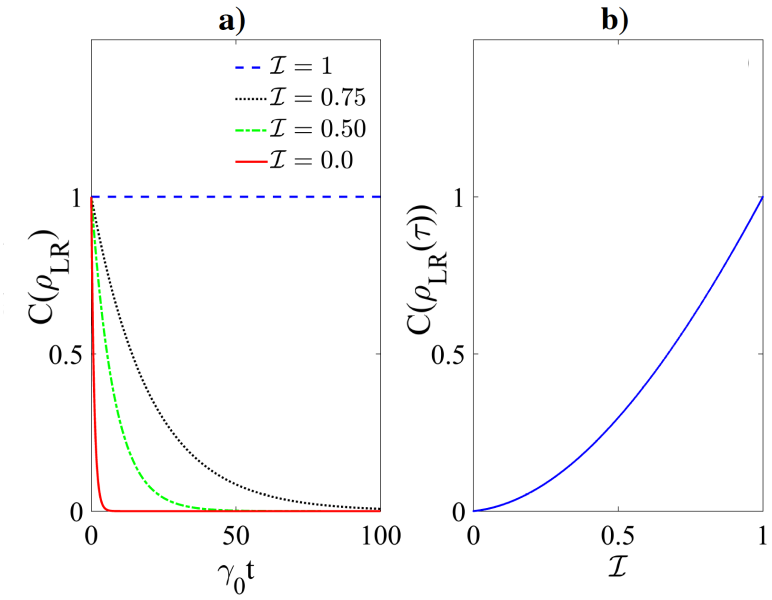

Figure 4.4: **Entanglement evolution under localized amplitude damping environments a.** Entanglement dynamics $C(\rho_{LR}(t))$ as a function of dimensionless time $\gamma_0 t$ starting from the initial state $|1_-\rangle$ for different degrees of spatial indistinguishability $\mathcal{I}$, fixing $l = r'$: blue dashed line $\mathcal{I} = 1$ ($l = l'$), black dotted line $\mathcal{I} = 0.75$, green dot-dashed line $\mathcal{I} = 0.5$ and red solid line $\mathcal{I} = 0$. **b.** Entanglement $C(\rho_{LR}(\tau))$ at the critical time τ versus $\mathcal{I}$. All plots are valid for both fermions and bosons with $\theta = \pi/2$.

4.5 Amplitude damping noise

The amplitude damping process is a well-known model for energy dissipation in open quantum systems. It describes a two-level system (a qubit) of transition frequency ω_0 that interacts with a reservoir by excitation exchange due to spontaneous emission [15]. This kind of dissipative channel is found in different contexts, such as atoms in cavities [298, 299, 300], superconducting qubits in circuit QED [301, 302], spin chains with ferromagnetic Heisenberg interactions [303] or photon scattering from a single-mode optical fiber [304], and is also well simulated by linear-optics devices [305, 306].

We take here two identical qubits, with a given degree of spatial indistinguishability, interacting with two localized amplitude damping environments in L and R sites, respectively. The environments are assumed to be Markovian and identical, so that the (local) characteristic decay rates are $\gamma_{0X} = \gamma_0$ ($X = L, R$). From Eqs. (4.4) and (4.5), the total interaction Hamiltonian is $H_I = H_I^{(1)} + H_I^{(2)}$ with

$$H_I^{(j)} = \sum_{X=L,R} \sum_k g_{kX}^{(j)} \hat{a}_{kX}^\dagger \hat{\sigma}_-^{(j)} + h.c., \tag{4.32}$$

where $\hat{\sigma}_\pm^{(j)}$ are single-particle pseudospin creation and annihilation operators. Substituting $\hat{\sigma}_X = \hat{\sigma}_-^{(j)}$ in Eq. (4.9) we have the master equation for localized amplitude damping noises

$$\dot{\rho} = \sum_{X=L,R} \sum_{i,j} \gamma_X^{(i,j)} \left(\sigma_-^{(i)} \rho \sigma_+^{(j)} - \frac{1}{2} \{ \sigma_+^{(i)} \sigma_-^{(j)}, \rho \} \right). \tag{4.33}$$

Considering the dissipative effects of this type of evolution, the general dynamics can be easily solved in the basis $\mathcal{B}_1 = \{|1_\pm\rangle, |2\rangle, |0\rangle\}$, where $|1_\pm\rangle$ are the two Bell states defined in Eq. (4.20) and

$$|2\rangle = \frac{1}{\sqrt{\mathcal{N}_1}} |\psi_1 \uparrow, \psi_2 \uparrow\rangle, \quad |0\rangle = \frac{1}{\sqrt{\mathcal{N}_0}} |\psi_1 \downarrow, \psi_2 \downarrow\rangle, \tag{4.34}$$

with $\mathcal{N}_0 = \mathcal{N}_1 = (1 + \eta |\langle \psi_1 | \psi_2 \rangle|^2)$. Starting from a state which is a mixture of the four basis states above, the structure is maintained during the evolution: $\rho_S(t) = \sum_{u'} p_{u'}(t) |u'\rangle \langle u'|$, where $|u'\rangle \in \mathcal{B}_1$.

This choice leads to the following differential equations for the basis state populations

$$\begin{aligned} \dot{p}_{1_-} &= (1-\xi)\gamma_0 \left(p_2 - p_{1_-}\right), \\ \dot{p}_{1_+} &= (1+\xi)\gamma_0 \left(p_2 - p_{1_+}\right), \\ \dot{p}_2 &= -2\gamma_0 p_2, \end{aligned} \tag{4.35}$$

with $p_0(t) = 1 - (p_{1_+}(t) + p_{1_-}(t) + p_2(t))$ and where $\xi = ll' + rr'$ is a spatial overlap parameter (see Appendix B. for details on the general solutions).

For spatially separated qubits ($\mathcal{I} = \xi = 0$), one retrieves the known dissipative two-qubit dynamics, eventually decaying to the ground state $|0\rangle$. On the other hand, for maximally indistinguishable qubits ($\mathcal{I} = \xi = 1$), from Eq. (4.35) we obtain

$$p_{1_-}(t) = p_{1_-}(0), \tag{4.36}$$

which clearly shows that state $|1_-\rangle$ is unaffected from the detrimental environment. Perfect spatial indistinguishability prevents the decay to the ground state of the two-qubit system and maintains the Bell state $|1_-\rangle$ frozen (noise-free).

The evolution of two-qubit entanglement, identified by $C(\rho_{\rm LR}(t))$, is displayed in Fig. 4.4**a** for different values of $\mathcal{I}$, starting from the initial state $|1_-\rangle$ for fermions and bosons with $\theta = \pi/2$. As can be seen, spatial indistinguishability significantly extends the timescale of entanglement decay in the system compared to the one for distinguishable particles (red solid line, entanglement asymptotically goes to zero [167, 257]). In Fig. 4.4**b** we plot the concurrence $C(\rho_{LR}(\tau))$, calculated at a fixed critical time τ when the distinguishable-qubit entanglement is very small ($\sim 10^{-5}$), as a function of $\mathcal{I}$, which highlights the direct relationship between preserved entanglement and spatial indistinguishability. When $\mathcal{I} < 1$ the system eventually decays to the unentangled ground state $|0\rangle_{LR} = |L\downarrow, R\downarrow\rangle$ after sLOCC. We remark that the probability to obtain the frozen exploitable maximum entanglement $C(\rho_{\rm LR}(t) = 1$, contained in the state $|1_-\rangle$ when $\mathcal{I} = 1$, is $P_{LR} = 1/3$ for fermions and $P_{LR} = 1$ for bosons (see Appendix A. for details on the sLOCC probabilities). Collective effects enabled by spatial indistinguishability can thus very efficiently preserve two-qubit entanglement from decoherence also under dissipative noise.

4.6 Conclusions

In conclusion, we have introduced a formalism that allows us in principle to obtain the dynamics of a system of noninteracting identical particles, with an arbitrary degree of spatial indistinguishability $\mathcal{I}$, coupled to separated localized environments. The value of $\mathcal{I}$ is related to the amount of spatial overlap of the particle wave functions in the operational sites where the noises operate. The distributed resource state of the system at a given time is then activated by spatially localized operations and classical communications (sLOCC). The procedure is valid for any form of system-environment interaction and for any particle statistics (fermions and bosons). As a general aspect, we have found that environmental collective effects on the many-particle system are inevitable as long as particles are spatially indistinguishable. In fact, the dynamics of identical particles is not only determined by the localized interaction between system and environment but also directly by the value of $\mathcal{I}$. Spatial indistinguishability is the property of the system acting as a continuous knob which governs the interplay between collective and individual effects of the localized environments.

The introduced dynamical framework has been then applied to the typical case of two identical qubits interacting with local Markovian (memoryless) environments. In particular, we have considered paradigmatic quantum noises such as phase damping, depolarizing and amplitude damping. As a result valid for all the noise channels, we have found that spatial indistinguishability plays a sort of dynamical decoupling role of some states of the system from the environment, in that it inhibits the effective decay rate: the larger $\mathcal{I}$, the smaller the decay rate. For maximal spatial indistinguishability ($\mathcal{I} = 1$), a maximally entangled state can be perfectly preserved against noise, leading to frozen entanglement. Ultimately, spatial indistinguishability is a property capable to efficiently shield exploitable entangled states at distant sites against noise.

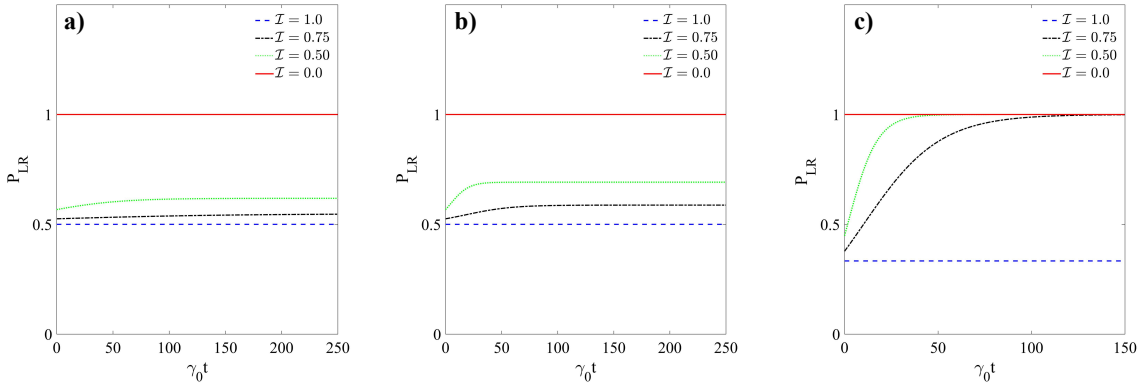

Figure 4.5: **sLOCC probability for fermions.** P_{LR} as a function of dimensionless time $\gamma_0 t$, starting from the initial state $|1_-\rangle$, fixing $l = r'$, under localized: **a)** phase damping noise, **b)** depolarizing noise, **c)** amplitude damping noise. The plots are given for different degrees of spatial indistinguishability: $\mathcal{I} = 1$ (blue dashed line), $\mathcal{I} = 0.75$ (black dot-dashed line), $\mathcal{I} = 0.5$ (green dotted line) and $\mathcal{I} = 0$ (red solid line).

Generalizing previous results [17], these findings are very promising to fault-tolerant quantum information tasks, since controllable indistinguishability is an intrinsic resource of a composite quantum network made of identical subsystems. Experimental verification of our predictions is thus one of the main outlook of this work. Various experimental platforms can be indeed brought up for implementing protection by spatial indistinguishability, such as quantum optics [23], integrated photonics [172], superconducting circuit QED [213], Bose-Einstein condensates [307] and quantum electronics [215].

The setups are to be engineered in such a way that the identical quantum building blocks remain spatially indistinguishable from the local observer viewpoint, so they can globally interact remotely and simultaneously with separated environments. Spatial wave functions of the subsystems have to be controlled (e.g., by beam-splitting operations [23, 215]) to maintain nonzero indistinguishability during the dynamics. In quantum optics, it is known that decoherence channels localized in the operational regions can be simulated. For example, amplitude damping can be realized via Sagnac-like interferometers for [258], while phase damping by either Fabry-Perot cavities [264] or quartz plates [154]. As long as particles are indistinguishable to the eyes of environments, entanglement protection by spatial indistinguishability holds until the projection measurement, namely sLOCC, is performed to start quantum information tasks. This is a general scenario, independent of specific implementations. The sLOCC procedure consists of local single-particle counting and coincidence measures, as already realized in recent experiments [23, 24].

Our results provide the theoretical background for a full characterization of open quantum systems dynamics with identical constituents, motivating analyses of non-Markovian system-environment interactions and generalizations to composite systems of larger size (many-qudit systems). They open the way to further studies investigating the effects of indistinguishability for other types of local environments, e.g. spin-like surroundings and classical noises, different classes of initial states and various figures of merit of quantumness.

A. sLOCC probability

In this appendix we provide the expressions of the the time dependent sLOCC probability for the three localized noise channels considered in the manuscript.

In general, the sLOCC measurement giving the distributed resource state $\rho_{LR}(t)$ of Eq. (4.12) comes with a cost, since it corresponds to the post-selection procedure to find one particle (qubit) in the region

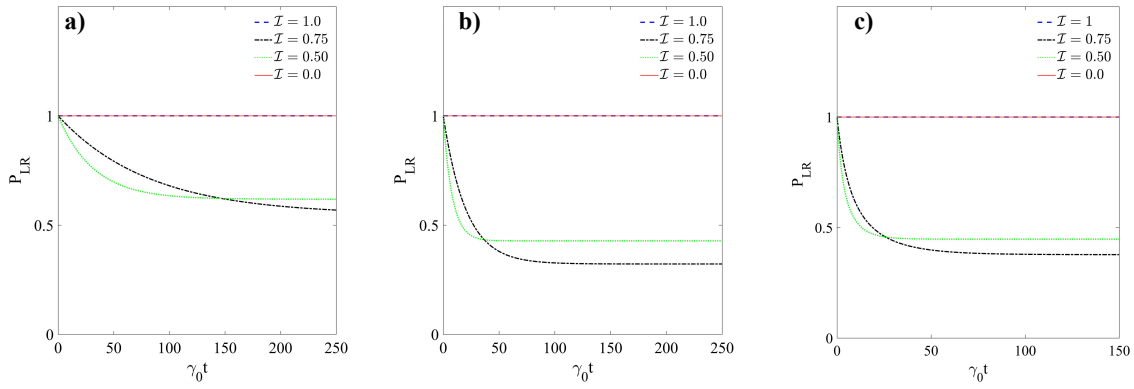

Figure 4.6: **sLOCC probability for bosons.** P_{LR} as a function of dimensionless time $\gamma_0 t$, starting from the initial state $|1_-\rangle$, fixing $l = r'$, under localized: **a)** phase damping noise, **b)** depolarizing noise, **c)** amplitude damping noise. The plots are given for different degrees of spatial indistinguishability: $\mathcal{I} = 1$ (blue dashed line), $\mathcal{I} = 0.75$ (black dot-dashed line), $\mathcal{I} = 0.5$ (green dotted line) and $\mathcal{I} = 0$ (red solid line).

L and the other one in the region R. This post-selection probability is given by the sLOCC probability

$$P_{LR}(t) = \mathrm{Tr}(\Pi_{LR}^{(2)} \rho_S(t), \tag{4.37}$$

where $\rho_S(t)$ is the two-qubit density matrix solution of the master equation of Eq. (4.9) for the given noise channel. As a result, the exploitable entanglement of $\rho_{LR}(t)$ is conditional in general. So, it is important that the value of $P_{LR}(t)$ remains high enough during the evolution to be of experimental relevance. Here we explicitly show that this is the case.

We consider the state $|1_-\rangle$ of Eq. (4.20) as initial state since it shows noise-free characteristics. In the main text, we have already reported that, for maximum spatial indistinguishability $\mathcal{I} = 1$ with $l = r'$ in the spatial wave functions of Eq. (4.15) (meaning $l = r = l' = r' = 1/\sqrt{2}$), $P_{LR}(t) = 1$ for bosons at any time for all the three types of local noise. This means that for bosonic qubits the maximum entanglement protection is even deterministic. The choice $l = r'$ is made such as to forbid that the sLOCC probability is zero and, at the same time, to maximize it when $\mathcal{I} = 1$.

Phase damping noise. For this kind of local system-environment interaction, the general expression for the sLOCC probability is

$$P_{LR}(t) = \frac{|l'r|^2 + |lr'|^2 - 2\eta l l' r r' e^{-\gamma_- t} \cos\theta}{1 - \eta e^{-\gamma_- t} \left(|l'l|^2 + |rr'|^2 + 2ll'rr' \cos\theta\right)}, \tag{4.38}$$

where γ_- is defined in Eq. (4.23). It is interesting to notice that, when $\mathcal{I} < 1$, that is $\gamma_- > 0$, the sLOCC probability at the stationary state ($t \to \infty$) is simply $P_{LR} = |l'r|^2 + |lr'|^2$. For maximal indistinguishability $\mathcal{I} = 1$ ($l = l'$ and $r = r'$), for which $\gamma_- = 0$, from Eq. (4.38) one has $P_{\mathrm{LR}}(t) = 1$ for bosons with $\theta = \pi$ and $P_{LR}(t) = 2l^2\left(1 - l^2\right)$ for fermions with $\theta = 0$ (the latter becomes $1/2$ when $l = r'$). In Figs. 4.5**a** and 4.6**a** we plot $P_{LR}(t)$ for the phase damping process, fixing $l = r'$, associated to fermions and bosons, respectively, considering different degrees of spatial indistinguishability.

Depolarizing noise. For a local depolarizing system-environment interaction, the general expression for the sLOCC probability is

$$P_{LR}(t) = \frac{2\left(l^2 r'^2 + l'^2 r^2 + \eta l r' r l' \cos\theta \left(1 - 3e^{-\gamma_- t}\right)\right)}{2 + \eta(1 - 3e^{-\gamma_- t})\left(l^2 l'^2 + r^2 r'^2 + 2ll'rr' \cos\theta\right)}. \tag{4.39}$$

For maximal indistinguishability $\mathcal{I} = 1$ ($l = l'$ and $r = r'$), for which $\gamma_- = 0$, from Eq. (4.39) with $l = r'$ we again find, as before, that $P_{\mathrm{LR}}(t) = 1$ for bosons with $\theta = \pi$ and $P_{LR}(t) = 1/2$ for fermions with $\theta = 0$. In Figs. 4.5**b** and 4.6**b** we plot $P_{LR}(t)$ for the depolarizing process, fixing $l = r'$, associated to fermions and bosons, respectively, for different values of $\mathcal{I}$.

Amplitude damping noise. For localized amplitude damping system-environment interaction, the general expression for the sLOCC probability is

$$P_{LR}(t)=\frac{l^2r'^2+l'^2r^2+2\eta lr'rl'\cos\theta\,(1-2e^{-\gamma_0(1-\xi)t})}{1+\eta(1-2e^{-\gamma_0(1-\xi)t})\,(l^2l'^2+r^2r'^2+2ll'rr'\cos\theta)}, \tag{4.40}$$

where $\xi=ll'+rr'$ is the spatial overlap parameter. For maximal indistinguishability $\mathcal{I}=1$ ($l=l'$ and $r=r'$), for which $\xi=1$, from Eq. (4.40) with $\theta=\pi/2$, we have that $P_{LR}(t)=1$ for bosons and $P_{LR}(t)=\frac{l^2(1-l^2)}{1-l^2(1-l^2)}$ for fermions (the latter becomes $P_{LR}(t)=1/3$ for $l=r'$). When $\mathcal{I}_{LR}<1$ ($\xi<1$), the sLOCC probability for the stationary ground state ($t\to\infty$) with $\theta=\pi/2$ and $l=r'$ is $P_{LR}=\frac{l^4+l'^4}{1+2\eta l^2l'^2}$. We display in Figs. 4.5**c** and 4.6**c** the time behavior of $P_{LR}(t)$ for the amplitude damping process, fixing $l=r'$, corresponding to fermions and bosons, respectively, for different values of $\mathcal{I}$.

The general conclusion of this detailed analysis is that the entanglement resource, shielded by indistinguishability from the noise, is efficiently exploited by sLOCC, since the sLOCC probabilities remains of experimental value during the dynamics. In particular, bosonic qubits admit a deterministic entanglement protection. We finally point out that for both the two extreme cases, $\mathcal{I}=1,0$, the sLOCC probability is time-independent.

B. Solution of the amplitude damping channel

From the master equation for the local amplitude damping channels acting on two spatially overlapping identical qubits, given in Eq. (4.33), we have obtained the differential equations of Eq. (4.35). These differential equations can be conveniently solved separately for the cases when $\mathcal{I}<1$ and for maximal spatial indistinguishability $\mathcal{I}=1$.

The solution for the case when the spatial indistinguishability is not maximum, $\mathcal{I}<1$, so that the spatial overlap parameter $0\leq\xi<1$,

$$\begin{aligned}
p_2(t)&=p_2(0)e^{-2\gamma_0 t},\\
p_{1_+}(t)&=p_{1_+}(0)e^{-(1+\xi)\gamma_0 t}+\left(\frac{1+\xi}{1-\xi}\right)p_2(0)\left(e^{-(1+\xi)\gamma_0 t}-e^{-2\gamma_0 t}\right),\\
p_{1_-}(t)&=p_{1_-}(0)e^{-(1-\xi)\gamma_0 t}+\left(\frac{1-\xi}{1+\xi}\right)p_2(0)\left(e^{-(1-\xi)\gamma_0 t}-e^{-2\gamma_0 t}\right),\\
p_0(t)&=1-p_{1_+}(t)-p_{1_-}(t)-p_2(t),
\end{aligned} \tag{4.41}$$

where $\xi=ll'+rr'$. The above equations clearly show that the system state eventually decays to the ground state $|0\rangle=|\psi_1\downarrow,\psi_2\downarrow\rangle$, where $|\psi_1\rangle$, $|\psi_2\rangle$ are defined in Eq. (4.15). In the special case when the two identical qubits are spatially separated, one in the site L and one in R, one has $l=r'=1$ or $l=r'=0$, leading to $\xi=0$ (distinguishable particles $\mathcal{I}=0$). In this case, the time-dependent populations given in Eq. (4.41) reduce to the usual decaying functions for the one-excitation Bell states $|1_\pm\rangle=(|L\uparrow,R\downarrow\rangle\pm|L\downarrow,R\uparrow\rangle)/\sqrt{2}$ and for the two-excitation state $|2\rangle=|L\uparrow,R\uparrow\rangle$.

When the qubits are maximally indistinguishable ($\mathcal{I}_{LR}=1$ and $\xi=1$), the time-dependent populations are

$$\begin{aligned}
p_{1_-}(t)&=p_{1_-}(0)\\
p_{1_+}(t)&=p_{1_+}(0)e^{-2\gamma_0 t}+2p_1(0)\gamma_0 te^{-2\gamma_0 t}\\
p_2(t)&=p_2(0)e^{-2\gamma_0 t},\\
p_0(t)&=1-p_{1_+}(t)-p_{1_-}(t)-p_2(t),
\end{aligned} \tag{4.42}$$

from which the system dynamics of an initial state being a mixture of the basis states $\mathcal{B}_1=\{|1_\pm\rangle,|2\rangle,|0\rangle\}$ can be completely determined.

Of course, different classes of initial states can be considered which will lead to different solutions. This is left to detailed investigations elsewhere.

Chapter 5

Indistinguishability-assisted two-qubit entanglement distillation

Abstract

Production of quantum states exhibiting a high degree of entanglement out of noisy conditions is one of the main goals of quantum information science. Here, we provide a conditional yet efficient entanglement distillation method which functions within the framework of spatially localized operations and classical communication. This method exploits indistinguishability effects due to the spatial overlap between two identical qubits in distinct sites and encompasses particle statistics imprint. We derive the general conditions for the maximum entanglement distillation out of mixed states. As applications, we give a thorough description of distilled entanglement and associated success probability starting from typical noisy states, such as thermal Gibbs states and Werner states. The influence of local temperatures and of noise parameter is discussed, respectively, in these two cases. The proposed scheme paves the way towards quantum repeaters in composite networks made of controllable identical quantum particles. This Chapter is related to Publication 4 in the List of Publications.

5.1 Introduction

Indistinguishability plays an important role in understanding systems made of identical quantum entities. Usually, this genuinely quantum trait arises from the unaddressability of individual particles of the same kind when particles themselves become spatially overlapping [1, 13, 2]. This property profoundly affects how these particles assemble to form composite quantum states of light and matter [103, 308]. Beyond these fundamental aspects, it is known that tailoring spatial overlap of identical particles allows controllable entanglement generation schemes [34, 16, 23, 24, 25, 35] and quantum information tasks, including teleportation [16, 23], quantum estimation [94, 31], and entanglement distribution between nodes of a quantum network [28, 26]. Also, bosonic bunching, a symptom of indistinguishability, can enhance the conversion of information and work [36, 37, 38]. Recently, it has been reported that bosonic indistinguishability leads to an efficiency at maximum power larger than the classical Curzon-Ahlborn limit [39].

Entanglement and quantum coherence are essential resources at the heart of quantum-enhanced technologies, including computation, secure communication [309], and sensing [310]. Nonetheless, noise and environmental interaction are inevitable, leading to decoherence and entanglement degradation [40, 41]. Hence, quantum information and computation science faces the challenge of preserving quantum resources within a given noise model. Many protection schemes have been proposed to preserve such quantum resources [150, 107, 109, 157, 264, 311, 152, 312, 313, 101, 100, 156, 156, 80, 79, 314, 154, 261]. However, instead of maintaining entangled pairs, a distillation protocol (also referred to purification) con-

verts mixed states to entangled states using local operations and classical operations (LOCC) performed by two local observers [42, 43]. As a result, many distillation techniques have been introduced, aiming at increasing entanglement in quantum states utilizing LOCC, local filtering [315], distillation protocols [153], noiseless linear amplification, and one-shot distillable entanglement [316]. Furthermore, entanglement distillation is a crucial feature of many proposals for quantum repeaters [317, 318, 319].

In this work we provide a probabilistic entanglement distillation procedure based on spatial overlap between identical particles in the context of spatially localized operations and classical communication (sLOCC). We identify the essential conditions for a nonzero success rate of entanglement distillation. Due to the probabilistic nature of the distillation protocol, there is an interesting trade-off between the degree of distilled entanglement and the probability of success. Hence, we optimize the success probability of distillation at the expense of a lower entanglement degree. As relevant applications, we present a thorough examination of the requirements for entanglement distillation starting from thermal and Werner input states. Our procedure only uses inherent properties of identical particles as elementary building blocks of composite quantum networks. Therefore, it is particularly suitable in quantum communication scenarios, allowing for the conversion of seemingly useless noisy states into operational resource states for transferring information.

This paper is structured as follows. In Sec. 5.2 we describe the distillation protocol, examine some general properties of the final state, and present some quantities useful to study the trade-off between the amount of distilled entanglement and the success probability of the protocol. In Sec. 5.3 and 5.4 we present our analysis of the protocol in the case of, respectively, thermal and Werner input states. Finally, in Sec. 5.5 we draw our conclusions and present some remarks, while some details of our analysis can be found in the Appendixes.

5.2 Distillation protocol

Before introducing the distillation protocol, let us briefly recall our primary framework for dealing with identical particles. We assume each particle to be endowed with an external and an internal degree of freedom, namely a spatial wave function and a pseudospin. In the no-label approach [2, 3], an elementary form of the two-particle state $|\Psi\rangle = |\Phi_1, \Phi_2\rangle$ is defined by single-particle state vectors $|\Phi_i\rangle = |\psi_i\, \sigma_i\rangle$ ($i = 1, 2$), where $|\psi_i\rangle$ is the spatial wave function and $|\sigma\rangle = \{|\uparrow\rangle, |\downarrow\rangle\}$ is the pseudospin.

As illustrated in Fig. 5.1, the indistinguishability-assisted distillation protocol involves two steps: (i) an unitary transformation of the spatial wave functions, which we call *spatial deformation* [159]; (ii) a postselection measurement typically involving classical communication between two observers (detectors) situated in separated regions L and R, which we name *activation*.

We assume that each qubit is initially in a diagonal state $\hat{\rho}_{\mathrm{X}} = \sum_{\sigma=\{\uparrow,\downarrow\}} \lambda_{\sigma}^{\mathrm{X}} |\mathrm{X}\, \sigma\rangle \langle \mathrm{X}\, \sigma|$ in the basis $\{|\mathrm{X}\, \sigma\rangle\}$, with $\mathrm{X} = \{\mathrm{L}, \mathrm{R}\}$ and $\sigma = \{\uparrow, \downarrow\}$, characterized by the probabilities of occurrence $\lambda_{\sigma}^{\mathrm{X}}$ ($\lambda_{\uparrow}^{\mathrm{X}} + \lambda_{\downarrow}^{\mathrm{X}} = 1$). Since the qubits are initially distinguishable in two distinct sites, they are individually addressable by their spatial modes. Thus, the initial two-particle state is separable and factorizable in the two spatial regions, that is $\hat{\rho}_{\mathrm{init}}^{\mathrm{LR}} = \hat{\rho}_{\mathrm{L}} \otimes \hat{\rho}_{\mathrm{R}}$. This state can be written as

$$\hat{\rho}_{\mathrm{init}}^{\mathrm{LR}} = \sum_{\sigma,\tau=\{\uparrow,\downarrow\}} \lambda_{\sigma,\tau}^{\mathrm{LR}} |\mathrm{L}\, \sigma, \mathrm{R}\, \tau\rangle \langle \mathrm{L}\, \sigma, \mathrm{R}\, \tau|\,, \tag{5.1}$$

where the probability coefficients are $\lambda_{\sigma,\tau}^{\mathrm{LR}} = \lambda_{\sigma}^{\mathrm{L}} \lambda_{\tau}^{\mathrm{R}}$. We show below how two observers located in two spatial distinct regions can accomplish entanglement distillation (purification), by performing spatially local particle counting on the shared pair of identical qubits, and coordinating their actions through classical messages if needed.

Step I: spatial deformation. The spatial deformation involves a transformation of the spatial wave functions which distributes them onto the two operational spatial sites L and R. In this way, the identical qubits can spatially overlap and are not localized anymore in their own respective regions. In an operational context, we consider the case of an input state experiencing a spatial deformation transformation,

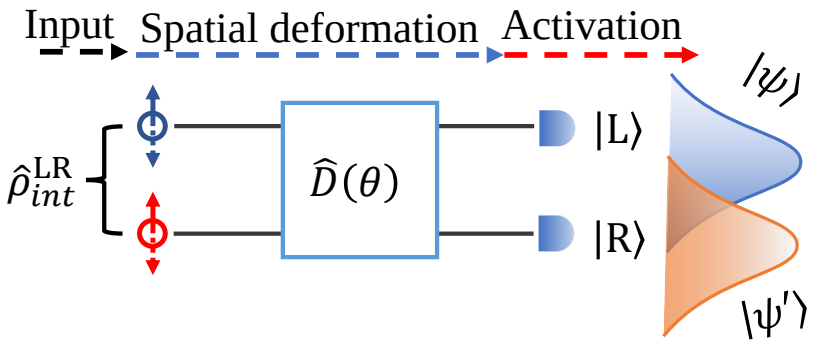

Figure 5.1: **Scheme of indistinguishability-assisted entanglement distillation**. As an input, each (spatially distinguishable) qubit is independently prepared, so that $\hat{\rho}_{\rm init}^{\rm LR} = \hat{\rho}_{\rm L} \otimes \hat{\rho}_{\rm R}$. *Step 1: spatial deformation*. An unitary spatial deformation $\hat{D}(\theta)$ is applied which allows the identical qubits to spatially overlap in the two distinct measurement regions. *Step 2: activation*. The postselection measurement $\Pi_{\rm LR}^{(2)}$ is performed and entanglement is thus distilled.

in which only the shapes of single-particle wave functions are altered, leaving the internal pseudospin degrees of freedom unchanged. To do so, we perturb the system by means of a spatial deformation Hamiltonian, defined as (hereafter we take $\hbar = 1$)

$$\hat{H}_D = \frac{\Omega_R}{2} \sum_{\sigma=\{\uparrow,\downarrow\}} \left(e^{\mathbf{i}\phi} \hat{L}_\sigma^\dagger \hat{R}_\sigma + e^{-\mathbf{i}\phi} \hat{L}_\sigma \hat{R}_\sigma^\dagger \right), \tag{5.2}$$

where Ω_R is the coupling strength and ϕ is an arbitrary phase. Here, $\hat{X}_\sigma^\dagger$ and $\hat{X}_\sigma$ ($\hat{X} = \{\hat{L}, \hat{R}\}$) are, respectively, the creation and the annihilation operators in the site $\mathrm{X} = \{\mathrm{L}, \mathrm{R}\}$, with the action of $\hat{X}_\sigma^\dagger$ on the vacuum state $|0\rangle$ given by $X_\sigma^\dagger |0\rangle = |\mathrm{X}\,\sigma\rangle$. These creation and annihilation operators obey standard anticommutation rules, $\{\hat{X}_\sigma^\dagger, \hat{X}_\sigma'^\dagger\} = \delta_{\sigma,\sigma'}$ for fermions, and commutation rules, $[\hat{X}_\sigma, \hat{X}_\sigma'^\dagger] = \delta_{\sigma,\sigma'}$ for bosons [132]. These rules make the two-particle state fulfil the standard phase change associated to a particle exchange, $|\mathrm{L}\,\sigma, \mathrm{R}\,\tau\rangle = \eta\,|\mathrm{R}\,\tau, \mathrm{L}\,\sigma\rangle$ with $\eta = 1(-1)$ for bosons (fermions), and, therefore, the Pauli exclusion principle for fermions [103]. The time-evolution operator associated to the spatial deformation is $\hat{D}(\theta) = \exp(-\mathbf{i}t\hat{H}_D)$, with $\theta = \Omega_R t$, so that the initial state evolves as $\hat{\rho}_D = \hat{D}(\theta)\hat{\rho}_{int}^{\rm LR}\hat{D}^\dagger(\theta)$. As a consequence, the deformed state has the form

$$\hat{\rho}_D = \sum_{\sigma,\tau=\{\uparrow,\downarrow\}} \lambda_{\sigma,\tau}^{\rm LR} \,|\psi\,\sigma, \psi'\,\tau\rangle\,\langle\psi\,\sigma, \psi'\,\tau|\,, \tag{5.3}$$

where $|\psi\rangle$ and $|\psi'\rangle$ are the deformed spatial wave functions defined as [see A. for the derivation of Eq. (5.3)]

$$\begin{aligned} |\psi\rangle &= \cos\left(\frac{\theta}{2}\right)|\mathrm{L}\rangle + \mathbf{i}e^{\mathbf{i}\phi}\sin\left(\frac{\theta}{2}\right)|\mathrm{R}\rangle\,, \\ |\psi'\rangle &= \mathbf{i}e^{-\mathbf{i}\phi}\sin\left(\frac{\theta}{2}\right)|\mathrm{L}\rangle + \cos\left(\frac{\theta}{2}\right)|\mathrm{R}\rangle\,. \end{aligned} \tag{5.4}$$

After this deformation, one may find each of the two particles in both regions, allowing them to spatial overlap. With spatial overlap we mean that the particles can be found in the same region of space with nonzero probability. It is worth mentioning that fermions with the same pseudospin are always forced to be in different sites due to the Pauli exclusion principle: the only accessible state in this case becomes, up to a global phase, $|\mathrm{L}\,\sigma, \mathrm{R}\,\sigma\rangle$.

Step II: activation. In the last step, the two observers in regions $\{\mathrm{L}, \mathrm{R}\}$ distillate or purify exploitable quantum states by selecting only one particle per spatial region, via particle projective measurements $\hat{\Pi}_{\rm LR}^{(2)} = \sum_{\sigma,\tau=\uparrow,\downarrow} |\mathrm{L}\,\sigma, \mathrm{R}\,\tau\rangle\,\langle\mathrm{L}\,\sigma, \mathrm{R}\,\tau|$ [16]. The procedure is probabilistic since it discards

the cases when both particles are detected in the same site. The action of projective measurements on the deformed state of Eq. (5.3), that is $\hat{\rho}_{\rm fin}^{\rm LR} = \hat{\Pi}_{\rm LR}^{(2)} \hat{\rho}_{\rm D} \hat{\Pi}_{\rm LR}^{(2)} / {\rm Tr}(\hat{\Pi}_{\rm LR}^{(2)} \hat{\rho}_{\rm D})$, gives

$$\hat{\rho}_{\rm fin}^{\rm LR} = \sum_{\sigma_1,\sigma_2,\tau_1,\tau_2=\{\uparrow,\downarrow\}} \Lambda_{\sigma_1,\tau_1}^{\sigma_2,\tau_2} \left|{\rm L}\,\sigma_1, {\rm R}\,\tau_1\right\rangle \left\langle {\rm L}\,\sigma_2, {\rm R}\,\tau_2\right| , \tag{5.5}$$

which is written in the computational basis $\mathcal{B}^{\rm LR} = \{|{\rm L}\ \uparrow, {\rm R}\ \uparrow\rangle, |{\rm L}\ \uparrow, {\rm R}\ \downarrow\rangle, |{\rm L}\ \downarrow, {\rm R}\ \uparrow\rangle, |{\rm L}\ \downarrow, {\rm R}\ \downarrow\rangle\}$. The coefficients $\Lambda_{\sigma_1,\tau_1}^{\sigma_2,\tau_2}$ of Eq. (5.5) depend on initial probabilities, spatial deformation, and both fermionic and bosonic statistics (see B. for a full description of the coefficients $\Lambda_{\sigma_1,\tau_1}^{\sigma_2,\tau_2}$). There is a success probability $P_{\rm LR} = {\rm Tr}(\hat{\Pi}_{\rm LR}^{(2)} \hat{\rho}_{\rm D})$ associated to the case when only one particle is found in a given region. The entanglement distillation protocol is thus conditional and encompasses the possibility of failure. We remark that classical communication between the two observers is typically involved in the protocol to check if each of them actually finds one particle per region. We also point out that the post-selected state is independent of the phase ϕ.

In general, indistinguishability depends on both the quantum state and the measurement performed on the system [17]. Since we are interested in the condition of spatial overlap between two identical qubits in two distinct regions, our goal is to determine whether the qubits are spatially distinguishable. To this aim, we can use the joint sLOCC measurement $\hat{\Pi}_{\rm LR}^{(2)}$, to evaluate the indistinguishability due to the spatial overlap of the particles within the state by means of the success probability $P_{\rm LR} = {\rm Tr}(\hat{\Pi}_{\rm LR}^{(2)} \hat{\rho}_{\rm D})$. If $P_{\rm LR} = 1$, indicating the presence of a single particle in each region with certainty, then the particles are considered spatially distinguishable with no spatial overlap. Conversely, if $P_{\rm LR} < 1$, the particles overlap in the two regions and are considered to be spatially indistinguishable. Once fixed the sLOCC measurement, the success probability depends in our setup on the initial state and on the parameter θ governing the spatial overlap.

Before considering specific input states from two different physical scenarios of interest, we examine some general properties of the final state of Eq. (5.5). We first observe that for equally deformed spatial wave functions in the case of bosons, i.e., for $\theta = \pi/2$ in Eq. (5.4) and $\eta = 1$, the output state reduces to a pure maximally entangled state in the singlet state form, $|\Psi_-^{\rm LR}\rangle = \left(|{\rm L}\ \uparrow, {\rm R}\ \downarrow\rangle - |{\rm L}\ \downarrow, {\rm R}\ \uparrow\rangle\right)/\sqrt{2}$, with a success probability given by

$$P_{\rm LR} = \frac{\lambda_{\uparrow,\downarrow}^{\rm LR} + \lambda_{\downarrow,\uparrow}^{\rm LR}}{2}. \tag{5.6}$$

The above expression implies that the occurrence of maximum entanglement distillation is conditional to the presence in the initial state of at least one term with opposite pseudospins. In fact, the success probability of Eq. (5.6) tells us that not every mixed state is distillable to a pure entangled singlet state, in line with previous observations [320]. Furthermore, the upper bound for the success probability of maximum entanglement distillation is $P_{\rm LR} = 1/2$ (when $\lambda_{\uparrow,\downarrow}^{\rm LR} + \lambda_{\downarrow,\uparrow}^{\rm LR} = 1$), independently of the purity of the input state. Interestingly, the same result does not apply to fermions, for which the degree of distilled entanglement depends on the input state. The general final state in the case of fermions is described by Eq. (5.16). Independently from the value of θ, the output state depends on the values of $\lambda_{\uparrow,\uparrow}^{\rm LR}$ and $\lambda_{\downarrow,\downarrow}^{\rm LR}$, which are connected to the initial state. Consequently, for example, in the case of an input state with nonzero values for at least one of these two coefficients, maximum entanglement distillation becomes unattainable.

More in general, there is a trade-off between the amount of distillable entanglement and the likelihood of success of the procedure. This aspect could be exploited in a practical scenario where the source is probabilistic and increasing the distillation success probability is demanding. In fact, one can optimize the success probability by distilling non-maximal entanglement: sacrificing perfect entanglement in favor of success probability can be strategical in many realistic scenarios.

We remark that the profound quantum property activating this entanglement distillation is the indistinguishability of the identical qubits stemming from their established spatial overlap in two distinct sites after spatial deformation of the wave functions.

Many ways can be employed to characterize the amount of distilled entanglement. For example, it can be quantified by the sLOCC-based concurrence, $C(\hat{\rho}^{\rm LR}) = \max\{0, \sqrt{\lambda_4} - \sqrt{\lambda_3} - \sqrt{\lambda_2} - \sqrt{\lambda_1}\}$, used

for identical particles [17], where λ_i are the eigenvalues in decreasing order of the operator $\hat{R} = \hat{\rho}^{\mathrm{LR}}\,\hat{\rho}^{\mathrm{LR}}$, being $\hat{\rho}^{\mathrm{LR}} = \hat{\sigma}_y^{\mathrm{L}} \otimes \hat{\sigma}_y^{\mathrm{R}} (\hat{\rho}^{\mathrm{LR}})^* \hat{\sigma}_y^{\mathrm{L}} \otimes \hat{\sigma}_y^{\mathrm{R}}$, with localized y-Pauli matrices $\hat{\sigma}_y^{\mathrm{X}} = |\mathrm{X}\rangle\langle\mathrm{X}| \otimes \hat{\sigma}_y$ ($\mathrm{X} = \mathrm{L}, \mathrm{R}$). Notice that this sLOCC-based concurrence is directly connected to the usual concurrence defined for distinguishable qubits [195].

Interestingly, one may want to ensure that the procedure will distillate enough entanglement to violate a Bell inequality. According to the Horodecki criterion for the CHSH-Bell inequality violation of a two-qubit density matrix [321], the expression of the maximum of the Bell function for the X-shape density matrix $\hat{\rho}_{\mathrm{fin}}^{\mathrm{LR}}$ can be written as $B_{\mathrm{LR}} = 2\sqrt{\mathcal{P}^2 + \mathcal{Q}^2}$ with $\mathcal{P} = \Lambda_{\uparrow,\uparrow}^{\uparrow,\uparrow} + \Lambda_{\downarrow,\downarrow}^{\downarrow,\downarrow} - \Lambda_{\uparrow,\downarrow}^{\uparrow,\downarrow} - \Lambda_{\downarrow,\uparrow}^{\downarrow,\uparrow}$ and $\mathcal{Q} = 2\Lambda_{\uparrow,\downarrow}^{\downarrow,\uparrow}$, where we used the fact that here $\Lambda_{\uparrow,\downarrow}^{\downarrow,\uparrow}$ is real and $\Lambda_{\uparrow,\uparrow}^{\downarrow,\downarrow} = \Lambda_{\downarrow,\downarrow}^{\uparrow,\uparrow} = 0$. In particular, the condition $B_{\mathrm{LR}} > 2$ is sufficient to perform quantum teleportation.

On the other hand, one may find a mixed bipartite state that does not violate any Bell inequality but is still useful for quantum teleportation [322]. A possible way to also include these cases is to characterize the amount of entanglement using the state's distance to an ideal one, such as the singlet state $|\Psi_-^{\mathrm{LR}}\rangle$, in terms of the fidelity $F_{\mathrm{LR}}(\hat{\rho}_{\mathrm{fin}}^{\mathrm{LR}}) = \langle\Psi_-^{\mathrm{LR}}|\,\hat{\rho}_{\mathrm{fin}}^{\mathrm{LR}}\,|\Psi_-^{\mathrm{LR}}\rangle$. For instance, for bosons when $\theta = \pi/2$ the fidelity is maximum, i.e., $F_{\mathrm{LR}} = 1$, and the success probability is given by Eq. (5.6). However, a fidelity $F_{\mathrm{LR}} > 2/3$ is enough for achieving quantum teleportation [323]. In such a case, one may prefer a higher probability of success at the expense of a lower fidelity.

As a result of the above considerations, the entanglement distillation analysis is a constrained optimization problem in which we seek to maximize the success probability with respect to θ, $P_{\mathrm{LR}}^{\max} = \max_{\theta}\left[\mathrm{Tr}(\hat{\Pi}_{\mathrm{LR}}^{(2)}\hat{\rho}_{\mathrm{D}})\right]$, with the constraint $B_{\mathrm{LR}}(\hat{\rho}_{\mathrm{fin}}^{\mathrm{LR}}) > 2$ (for the Bell inequality threshold) or $F_{\mathrm{LR}}(\hat{\rho}_{\mathrm{fin}}^{\mathrm{LR}}) > 2/3$ (for the fidelity threshold).

In the following sections, we shall analyze the performance of the indistinguishability-assisted entanglement distillation in the case of two well-known input states: a thermal state and a Werner state.

5.3 Application I: Thermal state

As a first example, we consider the distillation of thermal Gibbs states of two spatially separated identical qubits. From a resource theory point of view, a thermal state is a free state that one can generate and use at no cost. Therefore, one can interpret the distillation process as a quantum thermal machine that produces entanglement out of a thermal state.

To define the initial thermal state, we consider the bare system Hamiltonian $\hat{H}_0^{\mathrm{X}} = \frac{\omega}{2}\hat{\sigma}_z^{\mathrm{X}}$ ($X = \mathrm{L}, \mathrm{R}$), where $\hat{\sigma}_z^{\mathrm{X}} = \hat{\sigma}_z \otimes |X\rangle\langle X|$ is the localized z-Pauli matrix, and $\omega = \omega_\uparrow - \omega_\downarrow$ is the frequency spacing between the energy levels associated to the values of the pseudospin. Each qubit is initially coupled with its own local bosonic bath $\mathcal{B}_{\mathrm{X}}$ at inverse temperature $\beta_X = 1/T_{\mathrm{X}}$ (hereafter we take the Boltzmann's constant $k_B = 1$). Thus, each particle thermal state is in the Gibbs form $\hat{\rho}_{\mathrm{X}} = e^{-\beta_X \hat{H}_0^{\mathrm{X}}}/\mathcal{Z}(\beta_{\mathrm{X}})$, where $\mathcal{Z}(\beta_{\mathrm{X}}) = \mathrm{Tr}\left(e^{-\beta_X \hat{H}_0^{\mathrm{X}}}\right)$ is the partition function. Therefore, the initial two-particle state is factorizable in terms of single-particle states, $\hat{\rho}_{\mathrm{init}}^{\mathrm{LR}} = \hat{\rho}_{\mathrm{L}} \otimes \hat{\rho}_{\mathrm{R}}$.

For the sake of simplicity, in the next analytical considerations we limit ourselves to the case of equal temperature baths, that is $\beta = \beta_{\mathrm{L}} = \beta_{\mathrm{R}}$ (the case of different temperatures will be explicitly considered via a computational analysis shown in Fig. 5.3). After spatial deformation and projection, the activated output state of Eq. (5.5) becomes

$$\hat{G}_{\mathrm{fin}}^{\mathrm{LR}} = \sum_{i=\{0,1,\pm\}} \mathcal{Z}_{\mathrm{LR}}^{-1}\Lambda_i^{\mathrm{LR}}\,|\Psi_i^{\mathrm{LR}}\rangle\langle\Psi_i^{\mathrm{LR}}|\,, \tag{5.7}$$

which is written in the singlet-triplet basis $\mathcal{B}_{\mathrm{st}}^{\mathrm{LR}} = \{|\Psi_0^{\mathrm{LR}}\rangle, |\Psi_1^{\mathrm{LR}}\rangle, |\Psi_\pm^{\mathrm{LR}}\rangle\}$, where $|\Psi_0^{\mathrm{LR}}\rangle := |\mathrm{L}\downarrow, \mathrm{R}\downarrow\rangle$, $|\Psi_1^{\mathrm{LR}}\rangle := |\mathrm{L}\uparrow, \mathrm{R}\uparrow\rangle$, $|\Psi_\pm^{\mathrm{LR}}\rangle := (|\mathrm{L}\downarrow, \mathrm{R}\uparrow\rangle \pm |\mathrm{L}\uparrow, \mathrm{R}\downarrow\rangle)/\sqrt{2}$, and $\mathcal{Z}_{\mathrm{LR}} = \sum_{i=\{0,1,\pm\}}\Lambda_i^{\mathrm{LR}}$ [see B. for some details concerning the derivation of Eq. (5.7)]. The thermal coefficients for fermions are $\Lambda_0^{\mathrm{LR}} = e^{\beta\omega}$, $\Lambda_1^{\mathrm{LR}} = e^{-\beta\omega}$, $\Lambda_+^{\mathrm{LR}} = 1$, and $\Lambda_-^{\mathrm{LR}} = \cos^2(\theta)$. The thermal coefficients for bosons are $\Lambda_0^{\mathrm{LR}} = e^{\beta\omega}\cos^2(\theta)$, $\Lambda_+^{\mathrm{LR}} = \cos^2(\theta)$, and $\Lambda_-^{\mathrm{LR}} = 1$.

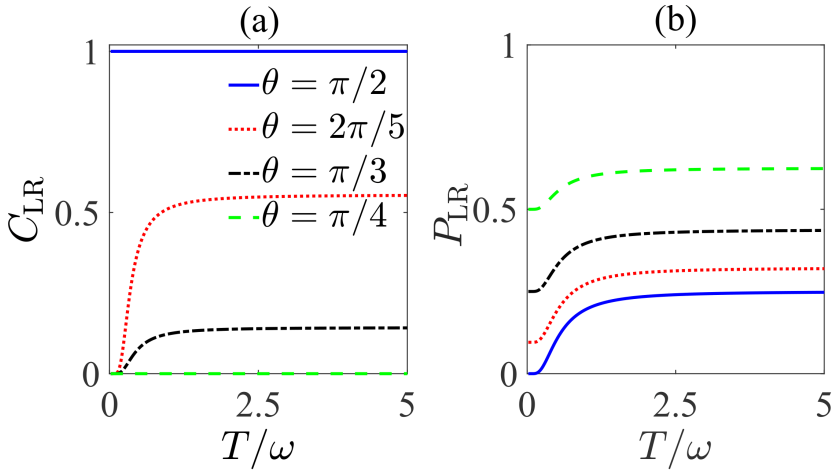

Figure 5.2: **Distilled entanglement and success probability for thermal input states with baths at the same temperature.** (a) Concurrence $C_{\rm LR} = C(\hat{G}^{\rm LR}_{\rm fin})$ and (b) success probability $P_{\rm LR}$ as functions of the baths' temperature T/ω for different values of θ, in the case of bosons.

We now provide some analytical results for both bosons and fermions. To quantify the amount of distilled entanglement out of the thermal state we use the concurrence C. For bosons ($\eta = 1$), one gets $C(\hat{G}^{\rm LR}_{\rm fin}) = \max\{0, \mathcal{C}\}$ with

$$\mathcal{C} = \frac{2 - 6\cos^2(\theta)}{4\cos^2(\theta)\cosh(\beta\omega) + \cos(2\theta) + 3}, \tag{5.8}$$

while the success probability is equal to

$$P_{\rm LR} = 1 - \left[\frac{1 + 2\cosh(\beta\omega)}{2 + 2\cosh(\beta\omega)}\right]\sin^2(\theta). \tag{5.9}$$

Both $\mathcal{C}$ and $P_{\rm LR}$ range in $[0, 1]$ and depend on the bath temperature and the spatial deformation parameter θ. Differently, it is possible to show that for fermions ($\eta = -1$), the entanglement amount is always zero, although the state is non-diagonal in the computational basis $\mathcal{B}^{\rm LR}$.

For spatially distinguishable qubits (i.e., for $\theta = 0$), the output is the separable state expressed in Eq. (5.1) for both bosons and fermions. For an equally weighted spatial deformation of the wave functions ($\theta = \pi/2$) in the case of bosons, the state of Eq. (5.7) reduces to the maximally entangled singlet state $|\Psi^{\rm LR}_-\rangle$, as previously observed, with a success probability $P_{\rm LR} = 1/[2 + 2\cosh(\beta\omega)]$, that ranges between 0 and $1/4$. For $\theta = \pi/2$ in the case of fermions, the singlet state is ruled out and the state of Eq. (5.7) becomes $\hat{G}^{\rm LR}_f = \sum_{i=\{0,1,+\}} \mathcal{Z}^{-1}_{\rm LR}\Lambda^{\rm LR}_i |\Psi^{\rm LR}_i\rangle\langle\Psi^{\rm LR}_i|$, with $\Lambda^{\rm LR}_0 = e^{\beta\omega}$, $\Lambda^{\rm LR}_1 = e^{-\beta\omega}$, and $\Lambda^{\rm LR}_+ = 1$.

Using Eqs. 5.8 and 5.9, valid for bosons, we display in Fig. 5.2 $C_{\rm LR} = C(\hat{G}^{\rm LR}_{\rm fin})$ [panel (a)] and $P_{\rm LR}$ [panel (b)] as functions of the bath temperature for some values of θ, i.e., for different settings of the spatial deformation of the wave functions. As commented above, for $\theta = \pi/2$ entanglement is always maximum irrespective of the bath temperature. For the other cases, contrarily to common expectations, the amount of entanglement increases with the temperature until it reaches a stationary value. This behavior can be explained with the fact that increasing the bath temperature leads to populating two-qubit states which exhibit quantum correlations arising from indistinguishability effects due to the spatial overlap. Instead, decreasing the temperature increases the likelihood of finding qubits in their ground state $|{\rm L}\downarrow, {\rm R}\downarrow\rangle$, which is a pure separable state from which entanglement cannot be distilled. The plot of the corresponding success probabilities shows that the process is ineffective for very low temperatures and that curves with smaller degrees of distilled entanglement are linked to curves with larger values of $P_{\rm LR}$.

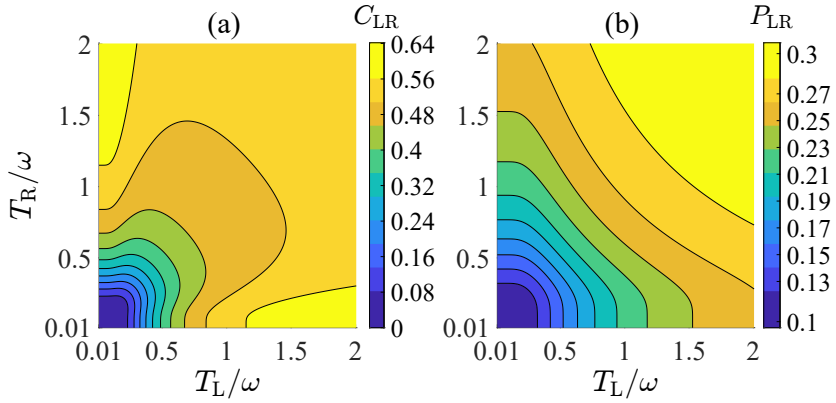

Figure 5.3: **Distilled entanglement and success probability for thermal input states with baths at different temperatures.** (a) Counter plot of the concurrence $C_{\rm LR}$ and (b) success probability $P_{\rm LR}$ as functions of the temperatures $T_{\rm L}/\omega$ and $T_{\rm R}/\omega$ for $\theta = 2\pi/5$, in the case of bosons.

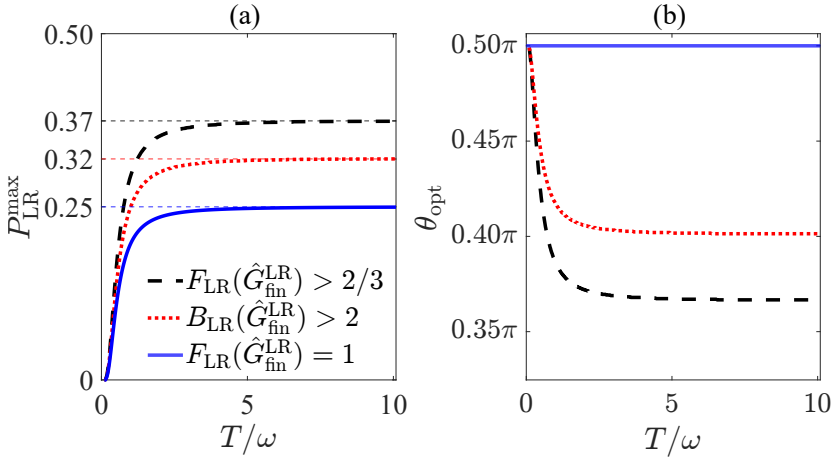

Figure 5.4: **Maximum success probability of entanglement distillation with thermal input states in baths at the same temperature.** (a) Maximum success probability $P_{\rm LR}^{\rm max}$ as a function of T/ω for bosons subject to the constraints $F_{\rm LR}(\hat{G}^{\rm LR}) > 2/3$ (blue solid line)) and $B_{\rm LR}(\hat{G}^{\rm LR}) > 2$ (red dotted line). The black dashed line shows the success probability in the case of perfect entanglement distillation. (b) The corresponding optimized spatial deformation parameters $\theta_{\rm opt}$ as a function of T/ω.

We have seen that the amount of the distilled entanglement depends on the baths' temperature $T = T_{\rm L} = T_{\rm R}$. However, it may be useful to understand how the indistinguishability-assisted entanglement distillation procedure works in the case when the two baths have different temperatures. Fig. 5.3 shows a contour plot of the distilled entanglement, quantified by the concurrence $C_{\rm LR}$, and its corresponding success probability $P_{\rm LR}$ in terms of two temperatures $T_{\rm L}$ and $T_{\rm R}$ in the case of a partial spatial deformation corresponding to $\theta = 2\pi/5$. As an interesting aspect, one can notice that by increasing the difference between the two temperatures it is possible to augment the degree of the distilled entanglement.

To conclude our study for the case of input thermal states, taking baths at the same temperature, we report in Fig. 5.4 the maximum success probability $P_{\rm LR}^{\rm max}$, obtained by maximizing Eq. (5.9) with respect to θ under the constraints $F_{\rm LR}(\hat{G}_{\rm fin}^{\rm LR}) > 2/3$ and $B_{\rm LR}(\hat{G}_{\rm fin}^{\rm LR}) > 2$, also considering the ideal case of maximum entanglement distillation when $F_{\rm LR}(\hat{G}_{\rm fin}^{\rm LR}) = 1$ [panel (a)]. We also plot the corresponding optimized spatial deformation parameter $\theta_{\rm opt}$ which maximizes the success probability for all the cases [panel (b)]. The fidelity between the output state of Eq. (5.7) and the singlet state is in particular given

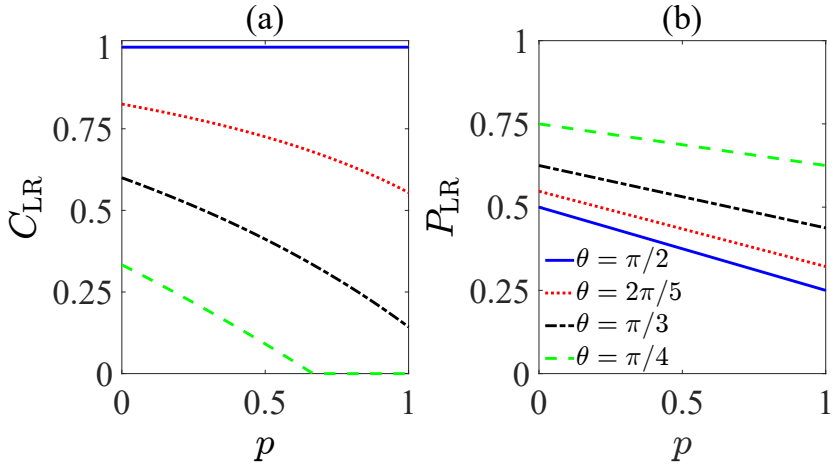

Figure 5.5: **Entanglement distillation and success probability for Werner input states.** (a) Concurrence $C_{\rm LR} = C(\hat{W}^{\rm LR}_{\rm fin})$ and (b) success probability $P_{\rm LR}$ as functions of the noise degree p for different values of θ, for bosons.

by

$$F_{\rm LR}(\hat{G}^{\rm LR}_{\rm fin}) = \frac{2}{3 + \cos(2\theta) + 4\cos^2(\theta)\cosh(\beta\omega)}. \tag{5.10}$$

When compared to the ideal case, the curve for the maximum success probability ensuring that the output state violates the Bell inequality shows that the success probability is increased. This result can be further improved considering that, as shown in Ref. [322], Bell inequality violation is a sufficient condition for nonclassical teleportation but is not necessary: in fact, some states fulfilling the necessary condition of $F_{\rm LR}(\hat{G}^{\rm LR}_{\rm fin}) > 2/3$ do not violate any Bell inequality but are still valuable for teleportation. The curve of $P^{\rm max}_{\rm LR}$ under the condition $F_{\rm LR}(\hat{G}^{\rm LR}_{\rm fin}) > 2/3$shows that even larger values of the success probability can be now achieved. The curves for the optimized spatial deformation parameters $\theta_{\rm opt}$ provide useful information to reproduce experimentally the above results.

5.4 Application II: Werner state

We now consider a Werner state [197] as input state, that is the experimentally relevant example of a pure state subject to the action of white noise. In the usual formulation, the Werner state is a mixture of a pure state and the maximally mixed state (white noise). It has been shown that simply bringing identical particles with opposite pseudospins, initially in the elementary state $|\Psi_{\rm LR}\rangle = |{\rm L}\uparrow, {\rm R}\downarrow\rangle$, to spatially overlap allows to access and generate entanglement by sLOCC measurements [16, 23]. However, in a realistic scenario this process might be subject to a certain extent of white noise, modeled by the maximally mixed state $\frac{1}{4}\mathbb{I}_{\rm LR} = \frac{1}{4}\sum_{\sigma,\tau=\{\uparrow,\downarrow\}} |{\rm L}\,\sigma, {\rm R}\,\tau\rangle\langle {\rm L}\,\sigma, {\rm R}\,\tau|$ with weight p. Under this condition, the input state has the form of the separable (unentangled) Werner state

$$\hat{W}^{\rm LR}_{\rm int} = (1-p)\,|\Psi_{\rm LR}\rangle\langle\Psi_{\rm LR}| + \frac{p}{4}\mathbb{I}_{\rm LR}. \tag{5.11}$$

Following the proposed procedure, we apply the spatial deformation followed by the postselection measurement to distillate the entanglement. The output state is given by $\hat{W}^{\rm LR}_{\rm fin} = \hat{\Pi}^{(2)}_{\rm LR}\hat{W}_{\rm D}\hat{\Pi}^{(2)}_{\rm LR}/{\rm Tr}(\hat{\Pi}^{(2)}_{\rm LR}\hat{W}_{\rm D})$, with the spatially deformed state $\hat{W}_{\rm D} = \hat{D}(t)\hat{W}^{\rm LR}_{\rm int}\hat{D}^\dagger(t)$. The corresponding success probability is given by $P_{\rm LR} = \frac{1}{8}\left[6 - p + (p+2)\cos(2\theta)\right]$. The explicit expression of the output state $\hat{W}^{\rm LR}_{\rm fin}$ can be straightforwardly obtained by using the general Eqs. 5.1 and 5.5, and the structure of the coefficients reported in Appendix B., where some indications to derive the output state are given.

For bosons, when $\theta = \pi/2$, the maximum entanglement distillation to the singlet state is possible for any noise degree with a success probability $P_{\rm LR} = \frac{2-p}{4}$ ranging from $1/4$ (maximum noise, $p = 1$)

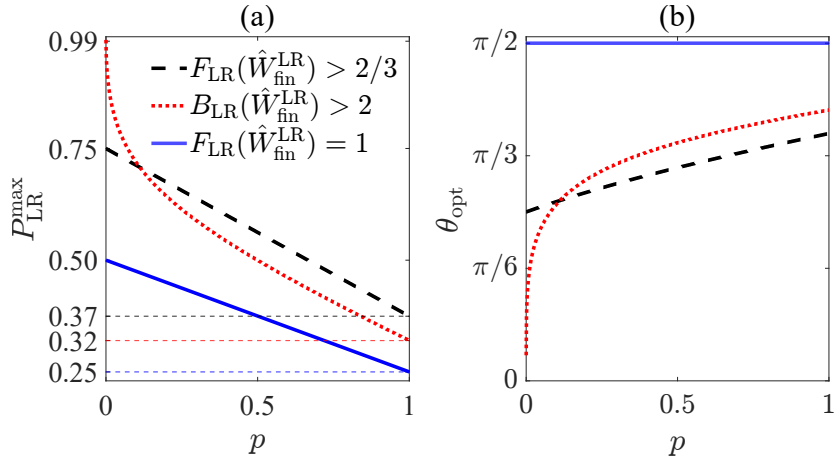

Figure 5.6: **Maximum success probability of entanglement distillation with Werner input states.** Maximum success probability $P_{\rm LR}^{\rm max}$ as a function of the noise degree p for bosons subject to the constraints $F_{\rm LR}(\hat{W}_{\rm fin}^{\rm LR}) > 2/3$ (blue solid line) and $B_{\rm LR}(\hat{W}_{\rm fin}^{\rm LR}) > 2$ (red dotted line). The black dashed line shows the success probability in the case of perfect entanglement distillation, $P_{\rm LR} = (2-p)/4$. (b) The corresponding optimized spatial deformation parameters $\theta_{\rm opt}$ as a function of p.

to $1/2$ (no noise, $p = 0$). Differently, for fermions, maximum entanglement distillation is only possible when there is no noise ($p = 0$), while generally the amount of distilled entanglement is noise dependent.

For the bosonic case, in Fig. 5.5 we plot the degree of distilled entanglement, quantified by the concurrence $C_{\rm LR}$ [panel (a)], and its corresponding success probability $P_{\rm LR}$ [panel (b)] as functions of the noise parameter p for different values of θ. We find that to distill a given degree of entanglement from a Werner state with a high amount of noise (e.g., $p > 0.5$), a spatial deformation more equally distributed onto the two sites (θ closer to $\pi/2$) may be required, leading to a larger spatial overlap. This property comes at the cost of a smaller success probability.

We now study the maximization of the success probability with respect to θ under the desired constraints $F_{\rm LR}(\hat{W}_{\rm fin}^{\rm LR}) > 2/3$ and $B_{\rm LR}(\hat{W}_{\rm fin}^{\rm LR}) > 2$. In particular, the expression for the fidelity between the output state $\hat{W}_{\rm fin}^{\rm LR}$ and the singlet state is

$$F_{\rm LR}(\hat{W}_{\rm fin}^{\rm LR}) = \frac{2(2-p)}{6-p+(p+2)\cos(2\theta)}. \tag{5.12}$$

In Fig. 5.6, we plot the maximum success probability $P_{\rm LR}^{\rm max}$ under the two desired conditions for fidelity and Bell inequality violation as a function of the noise parameter p, also considering the ideal case of maximum entanglement distillation when $F_{\rm LR}(\hat{G}_{\rm fin}^{\rm LR}) = 1$ [panel (a)]. We also display the optimized spatial deformation parameter $\theta_{\rm opt}$ which maximizes the success probability for all the cases [panel (b)]. We see how the distillation performance depends on the amount of noise in the initial state, pointing out that relatively high probabilities of success can be obtained even for large values of the noise parameter. Looking at the curve associated to the violation of the CHSH-Bell inequality, we point out that the maximum success probability $P_{\rm LR}^{\rm max}$ becomes very high for very low values of the noise degree ($p \to 0$), with the output state resulting close to a pure entangled state for $p \neq 0$, and being a pure non-maximally entangled Bell-like state for $p = 0$. This fact has a relevant operational consequence within the proposed indistinguishability-assisted entanglement distillation: under weak white noise, small spatial deformations ($\theta 0$), and thus small amounts of spatial overlap between the qubits, are sufficient to efficiently prepare an entangled state violating the Bell inequality (as one can see from the corresponding curve for the optimized spatial deformation parameter $\theta_{\rm opt}$). Such an observation is in line with the theorem that any pure Bell-like state violates a Bell inequality [324]. From Fig. 5.6 we also see that $P_{\rm LR}^{\rm max}$ reaches the minimum value of approximately 0.32 when the input state is a maximal mixture ($p = 1$). After comparing with to the ideal case ($F_{\rm LR}(\hat{W}_{\rm fin}^{\rm LR}) = 1$), one can clearly see how much we can increase the

success probability, yet guaranteeing that the distilled entangled state is a resource for quantum information processing such as teleportation. The curve of $P_{\mathrm{LR}}^{\max}$ under the condition $F_{\mathrm{LR}}(\hat{G}_{\mathrm{fin}}^{\mathrm{LR}}) > 2/3$ shows in particular that a minimum value of approximately 0.37 can be obtained for $p = 1$. Once again, the curves for the optimized spatial deformation parameters θ_{opt} can be useful from an experimental point of view.

5.5 Conclusions

In this work, we have introduced an entanglement distillation protocol enabled by indistinguishability effects originating from particle statistics and spatial overlap of two identical qubits. The spatial overlap is created by means of a spatial deformation of the wave functions which are distributed towards two distinct measurement sites. The protocol is characterized by a success probability, linked to postselecting the cases where only one particle is found at each site.

We have shown that maximum entanglement distillation is always possible for bosons provided that the initial input mixed state contains at least one term where the two qubits have opposite pseudospins, and determined the corresponding success probability. We have then studied the trade-off between the amount of distilled entanglement and the success probability of the procedure using for the initial configuration thermal Gibbs states and Werner states. We have maximized the success probability with respect to the spatial deformation parameter θ at the expense of a lower degree of entanglement which yet guarantees Bell inequality violation and teleportation usefulness. The latter is identified using a threshold based on the fidelity of the output state to the maximally entangled singlet state. This analysis is particularly relevant in practical scenarios where efficiency optimization is required.

For the case of initial thermal states we have found that increasing the common temperature of the two local baths is beneficial to the distillation protocol. In the case of different local temperatures, increasing their difference can be also exploited to augment the final entanglement. For the case of initial Werner states, we have found that entanglement distillation can be obtained also for any values of the noise parameter p by increasing the degree of indistinguishability at the expense of a lower success probability.

It is worth mentioning that our protocol is similar to a local filtering protocol [315] which allows entanglement distillation. However, we remark that the filtering process is here played by the controllable spatial overlap of identical particles and their statistical nature, that is by indistinguishability effects.

The proposed procedure is amenable to be implemented in the lab, especially in quantum optics platforms. In fact, several experimental tests have been recently realized which exploit the required indistinguishability effects via photons and optical devices [23, 24, 31, 26, 25, 133]. Based on the theoretical scheme of Fig. 5.1, the spatial deformation is a two-mode unitary gate produced by a conventional beamsplitter. Hence, the beamsplitter is why photon bunching, or Hong-Ou-Mandel effect [130], occurs when both photons are indistinguishable in all their degrees of freedom (polarization, temporal, and so on). Since photons are temporally indistinguishable, they simultaneously arrive at the detectors in the two separated regions, where we only postselect one photon in each region (by means of sLOCC) to generate the entanglement.

However, as demonstrated experimentally in Ref. [23], photons do not always need to cross paths at the same beamsplitter. Depending on the input state, a setup can be assembled where the optical paths of the photons remain detached along their travel until they reach the detection regions where the photons eventually spatially overlap. In such a scenario, two beamsplitters independently distribute each particle wave packet towards two remote operational sites [23, 133] according to the spatial deformations $\hat{D}_{\varphi}(\theta)\,|0\rangle \;=\; \cos\left(\frac{\theta}{2}\right)|\varphi_{\mathrm{L}}\rangle + \mathbf{i}e^{\mathbf{i}\phi}\sin\left(\frac{\theta}{2}\right)|\varphi_{\mathrm{R}}\rangle$ and $\hat{D}_{\chi}(\theta')\,|0\rangle \;=\; \mathbf{i}e^{\mathbf{i}\phi'}\sin\left(\frac{\theta'}{2}\right)|\chi_{\mathrm{L}}\rangle + \cos\left(\frac{\theta'}{2}\right)|\chi_{\mathrm{R}}\rangle$, where $|\varphi(\chi)\rangle_{\mathrm{L}}$ and $|\varphi(\chi)\rangle_{\mathrm{R}}$ are orthogonal spatial modes and $\hat{D}_{\varphi(\chi)}(\theta)$ is the corresponding spatial deformation operator. The particles are then indistinguishable for the final local detectors. The sLOCC is then performed and the entanglement gets distilled. These optical experimental settings can also simulate different particle statistics [325, 133], such as fermions and anyons. The above apparatuses are then well

suited to design experiments which realize the indistinguishability-assisted entanglement distillation not only for bosonic qubits via photons but also for simulated fermionic particles. Such achievements may open the way to developing quantum repeaters in quantum networks based on indistinguishability effects.

A. Details on the spatial deformation step

Let us consider a generic state with a qubit with pseudospin σ and another one with pseudospin τ respectively in regions L and R: $|\mathrm{L}\,\sigma,\mathrm{R}\,\tau\rangle = \hat{L}^\dagger_\sigma \hat{R}^\dagger_\tau |0\rangle$, where $\hat{L}^\dagger_\sigma$ ($\hat{R}^\dagger_\tau$) is qubit creation operator of with pseudospin σ (τ) in region L (R). In the step I of the procedure, each operator is spatially deformed as $\hat{L}^\dagger_\sigma(\theta) = \hat{D}(\theta)\hat{L}^\dagger_\sigma\hat{D}^\dagger(\theta)$ and $\hat{R}^\dagger_\tau(\theta) = \hat{D}(\theta)\hat{R}^\dagger_\tau\hat{D}^\dagger(\theta)$, resulting in

$$\begin{aligned}\hat{L}^\dagger_\sigma(\theta) &= \cos\left(\frac{\theta}{2}\right)L^\dagger_\sigma + \mathbf{i}e^{\mathbf{i}\phi}\sin\left(\frac{\theta}{2}\right)R^\dagger_\sigma,\\ \hat{R}^\dagger_\tau(\theta) &= \mathbf{i}e^{-\mathbf{i}\phi}\sin\left(\frac{\theta}{2}\right)L^\dagger_\tau + \cos\left(\frac{\theta}{2}\right)R^\dagger_\tau.\end{aligned} \tag{5.13}$$

Therefore, the single-particle states are $|\psi\,\sigma\rangle = \hat{L}^\dagger_\sigma(\theta)\,|0\rangle$ and $|\psi'\,\tau\rangle = \hat{R}^\dagger_\tau(\theta)\,|0\rangle$. Also, the elementary two-qubit states for different pseudospins ($\sigma \neq \tau$) are, for both fermions and bosons,

$$\begin{aligned}|\psi\,\sigma,\psi'\,\tau\rangle = \frac{\mathbf{i}}{2}\sin(\theta)\left(e^{-\mathbf{i}\phi}\,|\mathrm{L}\,\sigma,\mathrm{L}\,\tau\rangle + e^{\mathbf{i}\phi}\,|\mathrm{R}\,\sigma,\mathrm{R}\,\tau\rangle\right)\\ +\cos^2\left(\frac{\theta}{2}\right)|\mathrm{L}\,\sigma,\mathrm{R}\,\tau\rangle - \eta\sin^2\left(\frac{\theta}{2}\right)|\mathrm{L}\,\tau,\mathrm{R}\,\sigma\rangle\,,\end{aligned} \tag{5.14}$$

which satisfy particle exchange symmetry: $|\mathrm{L}\,\sigma,\mathrm{R}\,\tau\rangle = \eta\,|\mathrm{R}\,\tau,\mathrm{L}\,\sigma\rangle$. However, when qubits' pseudospins are identical ($\sigma = \tau$), the situation drastically changes depending on particle statistics. For example, when we have fermions the qubits anti-bunch in the state $\hat{L}^\dagger_\sigma(\theta)\hat{R}^\dagger_\sigma(\theta)\,|0\rangle = |\mathrm{L}\,\sigma,\mathrm{R}\,\sigma\rangle$, where each qubit resides in a different site. Differently, the elementary two-particle state for bosons becomes

$$\begin{aligned}|\psi\,\sigma,\psi'\,\sigma\rangle &= \frac{\mathbf{i}}{\sqrt{2}}\sin(\theta)\left(e^{-\mathbf{i}\phi}\,|\mathrm{L}\,\sigma,\mathrm{L}\,\sigma\rangle + e^{\mathbf{i}\phi}\,|\mathrm{R}\,\sigma,\mathrm{R}\,\sigma\rangle\right)\\ &\quad +\cos(\theta)\,|\mathrm{L}\,\sigma,\mathrm{R}\,\sigma\rangle\,,\end{aligned} \tag{5.15}$$

where bosonic bunching happens for $\theta = \pi/2$ since both particles are in the same regions. Taking into account these considerations allows for deriving every element of the deformed state in Eq. (5.3).

B. Details on the activation step

In the activation step (step II of the procedure), we select only one particle per region using the projective measurement $\hat{\Pi}^{(2)}_{\mathrm{LR}}$. The nonzero probability coefficients in Eq. (5.5) for fermions are

$$\begin{aligned}\Lambda^{\uparrow,\uparrow}_{\uparrow,\uparrow} &= \frac{1}{P_{\mathrm{LR}}}\lambda^{\mathrm{LR}}_{\uparrow,\uparrow}, \quad \Lambda^{\downarrow,\downarrow}_{\downarrow,\downarrow} = \frac{1}{P_{\mathrm{LR}}}\lambda^{\mathrm{LR}}_{\downarrow,\downarrow},\\ \Lambda^{\uparrow,\downarrow}_{\uparrow,\downarrow} &= \frac{1}{P_{\mathrm{LR}}}\left[\lambda^{\mathrm{LR}}_{\uparrow,\downarrow}\cos^4\left(\frac{\theta}{2}\right) + \lambda^{\mathrm{LR}}_{\downarrow,\uparrow}\sin^4\left(\frac{\theta}{2}\right)\right],\\ \Lambda^{\downarrow,\uparrow}_{\downarrow,\uparrow} &= \frac{1}{P_{\mathrm{LR}}}\left[\Lambda^{\mathrm{LR}}_{\downarrow,\uparrow}\cos^4\left(\frac{\theta}{2}\right) + \lambda^{\mathrm{LR}}_{\uparrow,\downarrow}\sin^4\left(\frac{\theta}{2}\right)\right],\\ \Lambda^{\downarrow,\uparrow}_{\uparrow,\downarrow} &= \frac{1}{4P_{\mathrm{LR}}}\left[\sin^2(\theta)\left(\lambda^{\mathrm{LR}}_{\uparrow,\downarrow} + \lambda^{\mathrm{LR}}_{\downarrow,\uparrow}\right)\right],\end{aligned} \tag{5.16}$$

with $\Lambda^{\downarrow,\uparrow}_{\uparrow,\downarrow} = \Lambda^{\uparrow,\downarrow}_{\downarrow,\uparrow}$ and the success probability is $P_{\mathrm{LR}} = 1 - \frac{1}{2}\sin^2(\theta)(\lambda^{\mathrm{LR}}_{\uparrow,\downarrow} + \lambda^{\mathrm{LR}}_{\downarrow,\uparrow})$.

On the other hand, the nonzero bosonic probability coefficients of Eq. (5.5) are

$$\begin{aligned}
\Lambda_{\uparrow,\uparrow}^{\uparrow,\uparrow} &= \frac{1}{P_{\rm LR}}\lambda_{\uparrow,\uparrow}^{\rm LR}\cos^2(\theta), \quad \Lambda_{\downarrow,\downarrow}^{\downarrow,\downarrow} = \frac{1}{P_{\rm LR}}\lambda_{\downarrow,\downarrow}^{\rm LR}\cos^2(\theta), \\
\Lambda_{\uparrow,\downarrow}^{\uparrow,\downarrow} &= \frac{1}{P_{\rm LR}}\left[\lambda_{\uparrow,\downarrow}^{\rm LR}\cos^4\left(\frac{\theta}{2}\right) + \lambda_{\downarrow,\uparrow}^{\rm LR}\sin^4\left(\frac{\theta}{2}\right)\right], \\
\Lambda_{\downarrow,\uparrow}^{\downarrow,\uparrow} &= \frac{1}{P_{\rm LR}}\left[\lambda_{\downarrow,\uparrow}^{\rm LR}\cos^4\left(\frac{\theta}{2}\right) + \lambda_{\uparrow,\downarrow}^{\rm LR}\sin^4\left(\frac{\theta}{2}\right)\right], \\
\Lambda_{\uparrow,\downarrow}^{\downarrow,\uparrow} &= \frac{-1}{4P_{\rm LR}}\left[\sin^2(\theta)\left(\lambda_{\uparrow,\downarrow}^{\rm LR} + \lambda_{\downarrow,\uparrow}^{\rm LR}\right)\right],
\end{aligned} \tag{5.17}$$

with $\Lambda_{\uparrow,\downarrow}^{\downarrow,\uparrow} = \Lambda_{\downarrow,\uparrow}^{\uparrow,\downarrow}$ and the success probability is $P_{\rm LR} = 1 - \frac{1}{2}\sin^2(\theta)\left(1 + \lambda_{\uparrow,\uparrow}^{\rm LR} + \lambda_{\downarrow,\downarrow}^{\rm LR}\right)$.

It is worth mentioning that the derivation of Eq. (5.7) involves substituting the following thermal coefficients in Eq. (5.16) and Eq. (5.17): $\lambda_{\uparrow,\uparrow}^{\rm LR} = e^{\beta\omega}$, $\lambda_{\uparrow,\downarrow}^{\rm LR} = 1$, and $\lambda_{\downarrow,\uparrow}^{\rm LR} = 1$, and $\lambda_{\downarrow,\downarrow}^{\rm LR} = e^{-\beta\omega}$. After diagonalization, Eq. (5.7) can be obtained. This approach is also applicable to the Werner state, where the substitutions $\lambda_{\uparrow,\uparrow}^{\rm LR} = p/4$, $\lambda_{\uparrow,\downarrow}^{\rm LR} = 1 - 3p/4$, and $\lambda_{\downarrow,\uparrow}^{\rm LR} = p/4$, and $\lambda_{\downarrow,\downarrow}^{\rm LR} = p/4$ lead to the final state for entanglement distillation.

Part II

Quantum walk for quantum information processing

Chapter 6

Introductory remarks II

In part II of my PhD thesis, I explore the application of quantum walks in quantum information processing. This part consists of chapters that are based on previously published papers in reputable scientific journals. However, before delving into the results, I provide a brief introduction to the background.

The concept of quantum random walk serves as the quantum counterpart to classical random walks and was initially introduced by Aharonov et al. in 1993 [44]. Quantum walks model the coherent evolution of quantum particles, and their most distinguished characteristic is the ability of the walker to exist in superposition states during propagation. This property leads to the emergence of interference effects, which significantly differentiate quantum walks from their classical counterparts. Quantum walks have demonstrated computational speed-up in various algorithms such as spatial search [45]. Over the past decade, they have evolved into a universal computational model and have been employed in the design of quantum computers [46, 47].

In general, quantum walk models can be categorized into two main types: discrete-time and continuous quantum walks. As the primary focus of this thesis is on the discrete-time quantum walk (DTQW), I provide a brief overview of discrete classical and quantum random walk models. Additionally, I will discuss the key properties of ordered and disordered quantum walks, emphasizing the aspects that are relevant to our investigation. Finally, I will review a background framework for utilizing quantum walks as generalized measurement devices, which will offer a clear perspective on our results concerning high-dimensional bi-photon interference on the coupled-fiber loop systems.

6.1 Classical random walk

A classical discrete random walk on a line is a specific type of stochastic process. In its simplest form, a classical random walk involves a particle, referred to as "the walker", making jumps to the left or right based on the outcomes of a probabilistic system known as "the coin", This coin system produces two mutually exclusive outcomes, which determine the particle's movement according to a probability distribution. Discrete random walks can be extended to higher-dimensional spaces or graphs, with classical random walks on graphs being understood as Markov chains.

Let us consider a stochastic process denoted as Z_k, which represents the path of a particle moving along an axis. The particle takes steps of one unit at time intervals, and each Z_k corresponds to the particle's position at time k [326]. At each step, the particle has a probability p of moving to the right and a probability $q = 1 - p$ of moving to the left. We introduce random variables, X_i, which indicate the direction taken by the particle at a particular step i. These variables are independent and identically distributed, taking the values of 1 or -1 based on the outcome of the aforementioned probabilistic event. Assuming an initial position $Z = 0$, the position at a certain step n is given by $Z_k = X_1 + X_2 + X_3 + \cdots + X_k$. A random variable Y_i is defined such that if it is zero, the walker will go right as $X_i = 1$, and if it is one, the walker will go left as $X_i = -1$. The random variable follows a binomial distribution.

Therefore, the probability of finding the walker at position X after k steps is given by

$$P(X,k) = \binom{k}{\frac{k+X}{2}} p^{\frac{k+X}{2}} (1-p)^{\frac{k-X}{2}}, \tag{6.1}$$

where $\binom{n}{k}$ represents the binomial coefficient. The expectation value of finding the particle at position X after k steps is $\langle X \rangle = k \cdot (2p-1)$. Additionally, the expectation value of $\langle X^2 \rangle = k \cdot (2p-1)^2$, one gets that the variance is given by

$$\mathrm{Var}(X) = 4kp(1-p). \tag{6.2}$$

Indeed, the variance (or, equivalently, the standard deviation) provides valuable information about the spread or deviation of the particle's positions from the mean value in the random walk. A larger variance indicates a greater dispersion of the particle's positions around the average value. In the case of a classical random walk, the variance is proportional to the number of steps taken, $\mathrm{Var}(X) \propto k$. This means that as the number of steps increases, the spread of the particle's positions also increases linearly. This linear spreading pattern is a characteristic feature of classical random walks.

6.2 Discrete-time quantum walk on a line

The quantum walk is a quantum counterpart of the classical random walk, taking advantage of quantum phenomena such as superposition, interference, and entanglement. In the following, I explain the key components of this model.

The state. A DTQW comprises several essential components: a walker, a coin, evolution operators that involve both the coin and shift, and a set of observables. The walker is a quantum system described by an infinite but countable dimensional Hilbert space denoted as $\mathcal{H}_\mathrm{p}$. Typically, the basis vectors of $\mathcal{H}_\mathrm{p}$ are used to represent the "position sites" of the walker, denoted as $|x\rangle \in \mathcal{H}_\mathrm{p}$.

In the case of the quantum walker moving on a line with discrete sites in the simplest scenario, the coin represents a quantum system residing in a 2-dimensional Hilbert space spanned by basis vectors $|0\rangle_\mathrm{c}$ and $|1\rangle_\mathrm{c}$, denoted as $\mathcal{H}_\mathrm{c}$. Therefore, the total state of the quantum walk is defined in the tensor product space $\mathcal{H} = \mathcal{H}_\mathrm{p} \otimes \mathcal{H}_\mathrm{c}$, encompassing both the position and coin aspects. Consequently, the elementary form of the quantum walker state is given by the joint state of the position and its corresponding coin, expressed as $|\psi\rangle = |x, c\rangle$.

The evolution. The evolution of the DTQW can be divided into two parts, which resemble the behavior of a classical random walk. Similar to the classical case, though, a coin will drive the system's evolution by going left or right based on the outcome of the quantum coin. In the quantum case, the role of the coin operator is to transform the coin state into a superposition, introducing quantum randomness into the evolution. Afterward, a conditional shift operator moves to the quantum system. The most general form of a 2-dimensional quantum coin operator, denoted as $\hat{C}$, is given by

$$\hat{C} = \begin{pmatrix} \sqrt{p} & e^{i\varphi_1}\sqrt{1-p} \\ e^{i\varphi_2}\sqrt{1-p} & -e^{i(\varphi_1+\varphi_2)}\sqrt{p} \end{pmatrix}, \tag{6.3}$$

where p is the bias controlling the probabilities of transitioning between the basis states $|0\rangle_\mathrm{c}$ and $|1\rangle_\mathrm{c}$, and φ_1 and φ_2 are the phase factors associated with the coin operator [327]. These phases introduce additional quantum interference effects in the evolution of the quantum walk and can influence the overall behavior of the system. If we set the bias $p = 1/2$ and $\varphi_1 = \varphi_2 = 0$, the general form reduces to the most commonly employed coin operator, the Hadamard operator:

$$\hat{H} = \frac{1}{\sqrt{2}} \begin{pmatrix} 1 & 1 \\ 1 & -1 \end{pmatrix}. \tag{6.4}$$

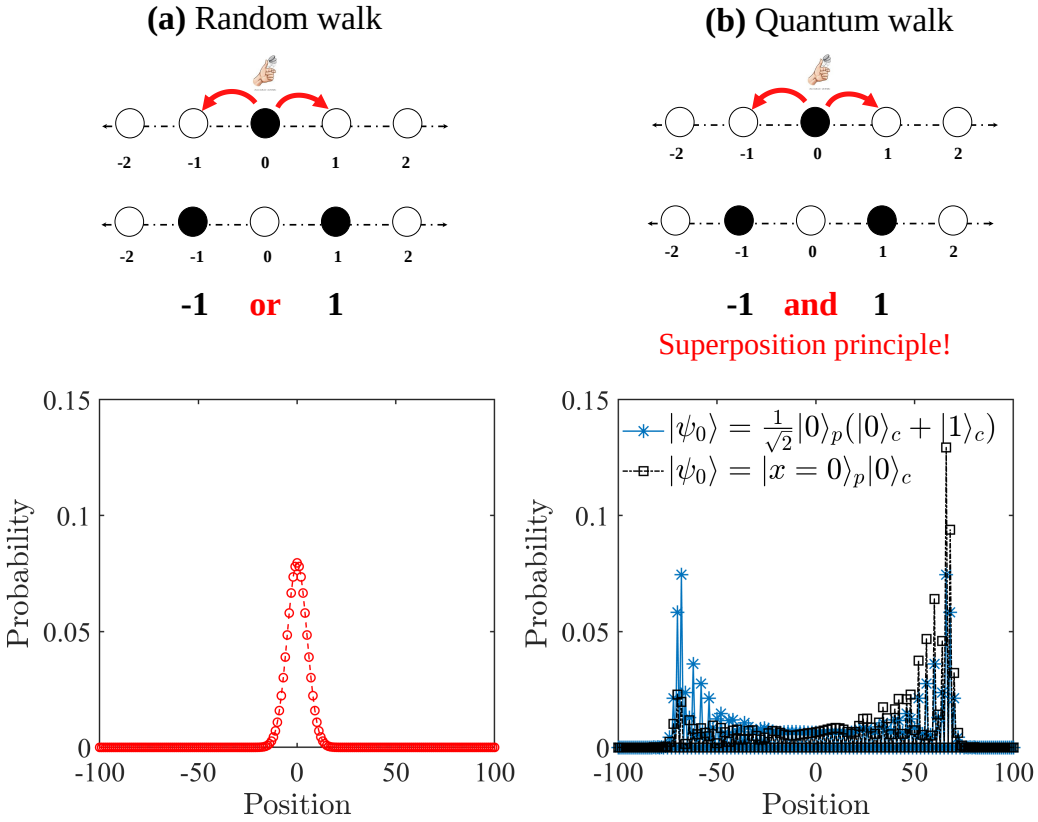

Figure 6.1: **Comparison between spatial distribution of quantum walk and Classical random Walk.** In the left, we report the spatial distribution of a classical random walker after 100 evolution steps: the probability of finding the walker is localized around the initial position ($x = 0$) and features the characteristic Gaussian shape. On the right, we see the completely different case of a quantum walker, which started its evolution at position $x = 0$, with two specific initial coin states.

The conditional shift operator is a unitary operator that determines the movement of the walker based on the state of the coin system, which can be expressed in the following form:

$$\hat{S} = |0\rangle_{\mathrm{c}} \langle 0|_{\mathrm{c}} \otimes \sum_x |x+1\rangle_{\mathrm{p}} \langle x|_{\mathrm{p}} + |1\rangle_{\mathrm{c}} \langle 1|_{\mathrm{c}} \otimes \sum_x |x-1\rangle_{\mathrm{p}} \langle x|_{\mathrm{p}} \,. \tag{6.5}$$

Specifically, if the coin system is in $|0\rangle_{\mathrm{c}}$, the walker will move one step forward. Conversely, if the coin state is in the other basis state, as $|1\rangle_{\mathrm{c}}$, the walker will move one step backward. The shift operator is performed in a coherent manner, preserving the quantum nature of the system. Thus, the unitary operator representing a single step of the DTQW $\hat{U} = \hat{S} \cdot (\mathbf{I} \otimes \mathcal{C})$ with $\mathbf{I}$ denoting the identity operator. To obtain the unitary evolution of a single quantum walker, one iteratively applies the coin and conditional shift operators for the desired number of steps, denoted as k. For instance, after k steps, the state of the walker can be expressed as:

$$|\psi_k\rangle = (\hat{S} \cdot \hat{\mathcal{C}})(\hat{S} \cdot \hat{\mathcal{C}}) \ldots (\hat{S} \cdot \hat{\mathcal{C}}) \, |\psi_0\rangle \,. \tag{6.6}$$

Here, $\hat{\mathcal{C}} = \sum_x |x\rangle \langle x| \otimes \hat{C}$ represents the time-position dependent coin operator. In the case of time-independence, the evolution simplifies to $|\psi_k\rangle = \hat{S}(\hat{\mathbf{I}} \otimes \hat{H})\hat{S}(\hat{\mathbf{I}} \otimes \hat{H}) \ldots (\hat{\mathbf{I}} \otimes \hat{H}) \, |\psi_0\rangle \,.$

Observables. Observables play a crucial role in quantum walks by extracting valuable information and showcasing advantages over classical random walks. One notable advantage arises from the interference effects that emerge after multiple applications of the evolution operator. Quantum entanglement between the walk' position and coin also contribute to these benefits. These advantages comes from the measurements or observable that we choose to employ to extract information from the composite quantum system.

Specifically, one might be interested in studying the average behavior of the quantum walk, such as the probability distribution in position, which can be represented by the operator $M_p = |x\rangle_{\mathrm{p}} \langle x|_{\mathrm{p}}$. In Fig. 6.1, an illustration is provided that showcases the comparison between a quantum walker dynamics and its classical counterpart. The probability distributions of the classical and quantum walks are numerically plotted. In the classical case, the probability of finding the walker is localized around the initial position ($x = 0$) and features the characteristic Gaussian shape. On the other hand, the quantum walker exhibits a distinct behavior. Depending on the initial coin state, which can be set as $|0\rangle_{\mathrm{c}}$ or $(|0\rangle_{\mathrm{c}} + |1\rangle_{\mathrm{c}})/\sqrt{2}$, the probability distribution focuses on a position far from the center. Additionally, one may wish to measure the spreading behavior of the DTQW and compare it with its classical counterpart. Similar to classical case The operator $\hat{X}$ that measures the walker position is the operator of interest, since the variance of the position operator provides a simple measure to quantify the spread of the walker

$$\sigma^2(\hat{X}) = \langle X^2 \rangle - \langle X \rangle^2, \tag{6.7}$$

as a function of the number of steps. In chapter VII and VIII, I will get back to this point.

6.3 The role of disorder

Disorder in DTQWs refers to the introduction of randomness or irregularity in the evolution of the walker. In a standard quantum walk, the evolution is determined by a fixed set of unitary operators, namely coin and shift operator. For an ordered quantum walk, we say the spreading behavior is ballistic since the variance measure of the position is proportional to a quadratic number of steps $\sigma^2(\hat{X}) \propto t^2$ compared to the classical case, which is linear. This means the quantum walker spreads quadratically faster in position space. However, when disorder is introduced, these rules exhibit variations. The role of disorder in DTQWs can have several effects on the behavior of the system. Here are some key aspects:

- **Localization.** The disorder can lead to a phenomenon called Anderson localization [48], where the walker becomes localized or confined to a particular region of the lattice. This contrasts with the spreading behavior observed in an ordered quantum walk. The reason is that a form of disorder, such as time-independent or static disorder, disrupts the interference patterns and can cause the probability distribution to become localized around specific positions. This effect applies to quantum walks and has been investigated using physical quantum walk platforms such as photonics [49, 50, 51, 52]. In Chapter VII, I will discuss how random time-independent or static disorder leads to disorder.

- **Decoherence.** Disorder can be introduced in the evolution of a quantum walk through random disorder, which is a physical phenomenon that typically arises from the interaction between quantum systems and their environment. In fact, with disorder, randomness disrupts constructive interference and leads to a loss of coherent evolution. However, there are cases in which decoherence can be considered useful, such as in the development of quantum algorithms [75]. Decoherence through measurement or free interaction with a classical environment provides a typical framework for studying the transition of quantum walks into classical random walks [72, 328]. Nevertheless, disorder can also be coherently imposed [56] or introduced through random disorder, which will be discussed in the next chapter.

- **Anomalous and normal diffusion.** The linear increase in the mean square displacement, as described in the previous sections, with respect to the number of steps, has become universally recognized as indicative of normal transport. Anomalous diffusion refers to any stochastic process that deviates from this linear growth trend. In particular, ordered quantum walks exhibit a ballistic spreading pattern in the absence of disorder. Processes that show a superlinear growth in the mean square displacement are called superdiffusive phenomena [329, 330, 331]. Superdiffusion

is observed in diverse transport or propagation processes, including complex biological environments [332, 74, 333], chaotic Hamiltonian systems [334, 335], transport in disordered systems [336, 337, 338], quantum optical systems [339], and single-molecule spectroscopy [340, 341].

On the other hand, disorder can lead to subdiffusion, where the spreading of the walker is slower than that observed in classical random walks. This occurs when random fluctuations introduced by disorder hinder the walker's efficient exploration of the entire lattice [342, 343, 344, 345, 346, 347].

In Chapter VII of my Ph.D. thesis [120], I propose a quantum probing protocol that utilizes quantum walks to investigate the spreading of quantum information. As an example, we employ the p-diluted model [348], which can be simulated using an optical setup. This model maintains the unitarity of the evolution and is characterized by spatial and temporal disorder. It allows for the exploration of transitional regimes and the manipulation of propagating quantum walkers.

- **Topological Effects.** Disorders in quantum walks can interact with the underlying topology of the lattice. Depending on the specific type of disorder and the lattice structure, the interplay between disorder and topology can give rise to interesting phenomena, such as topological Anderson insulators or the appearance of localized edge states [53, 54].

- **Non-classical enhancement.** While disorder is often considered a source of unwanted noise, it can actually be harnessed and manipulated to achieve specific goals in quantum information processing, quantum simulations, and other quantum technologies. In the context of quantum walks, disorder can lead to the generation of entanglement between the walker and coin states, as well as correlations between different parts of the system [55].

  Furthermore, in my Ph.D. thesis [56], as discussed in Chapter VIII, we demonstrate the optimization of disorder control to enhance the quantum correlation between two indistinguishable photons in separate modes of a quantum walk network. This research highlights the potential for utilizing and controlling disorder to achieve desired outcomes and advance the field of quantum information science

6.4 Discrete-time quantum walk as generalized measurement device

In addition to their role in quantum algorithms and simulations, DTQWs can also be viewed as generalized measurement devices [57]. In quantum mechanics, a measurement typically involves obtaining information about a quantum system by projecting it onto a specific basis state. Similarly, in a DTQW, the walker's position can be interpreted as a measurement outcome.

It has been shown that a DTQW can be used to implement a generalized measurement in terms of a positive operator value measure (POVM), where $\sum_i \hat{E}_i^\dagger \hat{E}i = \hat{\mathbf{I}}$ and $\hat{E}i$ represents the POVM elements. The evolution of a general quantum walk, denoted as $\hat{U} = \sum_i |i\rangle \langle \psi \text{in}|$, maps the initial state $|\psi \text{in}\rangle$ to the final state $|i\rangle$. Therefore, projective measurements $\hat{M} = |i\rangle \langle i|$ on the final state correspond to POVMs on the initial state.

For clarity, let me give an example to illustrate how a simple quantum walk can be interpreted as an unambiguous state discrimination protocol [15]. In this protocol, we consider a set of quantum states represented by density operators. These states are not necessarily orthogonal, meaning they may overlap in their quantum properties. The challenge is to design a measurement strategy that minimizes the probability of making an incorrect assignment while allowing for an inconclusive outcome when the states cannot be unambiguously distinguished.

Various measurement strategies have been developed to achieve unambiguous state discrimination, such as the Helstrom measurement and the minimum-error measurement. These strategies involve constructing a set of positive operator-valued measures (POVMs) that correspond to different measurement outcomes. The design of these POVMs aims to maximize the probability of correctly identifying each state while minimizing the probability of making an erroneous assignment. As an example, let us consider two non-orthogonal pure states:

$$|\psi_1\rangle = \cos\frac{\theta}{2}|0\rangle + \sin\frac{\theta}{2}|1\rangle\,,\ |\psi_2\rangle \quad = \cos\frac{\theta}{2}|0\rangle - \sin\frac{\theta}{2}|1\rangle\,. \tag{6.8}$$

The goal is to design an optimal measurement strategy to discriminate between these states. To do so, we can initialize the quantum walk with the particle located at the origin and in one of the two given states:

$$|\psi_\pm\rangle = \cos\frac{\theta}{2}|1\rangle_{\rm p}|1\rangle_{\rm c} \pm \sin\frac{\theta}{2}|1\rangle_{\rm p}|1\rangle_{\rm c}\,, \tag{6.9}$$

where $|1\rangle_{\rm p}$ and $|1\rangle_{\rm c}$ represent the position and coin states, respectively. The dynamic tunability of the coin's bias, as given by equation (6.10), is essential for performing the state discrimination protocol. In the next step, we perform two different coin operations at positions $x = 1$ and $x = -1$, respectively, as follows:

$$\hat{C}(x=1,1) = \begin{pmatrix} \sqrt{1-\tan^2\theta/2} & \sqrt{\tan^2\theta/2} \\ \sqrt{\tan^2\theta/2} & -\sqrt{1-\tan^2\theta/2} \end{pmatrix},\ \hat{C}(x=-1,1) = \begin{pmatrix} 0 & 1 \\ 1 & 0 \end{pmatrix}. \tag{6.10}$$

Therefore, the first step evolution can be represented as $\hat{U}_1 = \hat{S}\cdot\hat{C}(x=-1,1)\otimes|-1\rangle\langle-1| + \hat{S}\cdot\hat{C}(x=1,1)\otimes|1\rangle\langle1|$. After the first step, the evolved states are given by:

$$|\psi_\pm\rangle = \sqrt{\cos\theta}\,|2\rangle_{\rm p}|0\rangle_{\rm c} + \sin\frac{\theta}{2}|0\rangle_{\rm p}|1\rangle_{\rm c} \pm \sin\frac{\theta}{2}|0\rangle_{\rm p}|0\rangle_{\rm c}\,. \tag{6.11}$$

For the final step, we choose the coin operator to be the identity everywhere except at position $x = 0$, where we apply the Hadamard coin operator, (6.4). This results in the following expression:

$$|\psi_\pm\rangle = \sqrt{\cos\theta}\,|3\rangle_{\rm p}|0\rangle_{\rm c} \pm \sqrt{2}\sin\frac{\theta}{2}|\pm1\rangle_{\rm p}|0\rangle_{\rm c}\,. \tag{6.12}$$

As a consequence, if a particle is measured at position $x = 1$, it immediately reveals that the initial state was $|\psi_+\rangle$, whereas a measurement at position $x = -1$ indicates the initial state was $|\psi_-\rangle$. Indeed, as demonstrated in Ref. [57], it has been shown that any desired positive operator-valued measures (POVMs) can be constructed. Furthermore, experimental implementations of single-qubit generalized measurement scenarios have been achieved through a quantum walk model, utilizing the encoding of qubit states using single-photon polarization and optical paths [66, 67]. This technique has also been extended to enable generalized measurements on qudits [67]. Moreover, the application of this approach to two-qubit systems has allowed for the implementation of deterministic collective measurements on two identically prepared qubits using a controlled-quantum walk based on an optical mesh [68].

In Chapter X of my thesis, I revisit this topic and delve into these achievements once again. Specifically, I demonstrate how the DTQW model can be effectively utilized to perform high-dimensional bi-photon quantum interference and extract visibility in a coupled fiber-loop system.

6.5 Physical realization of discrete-time quantum walk

Numerous proposals and experimental realizations have been made for physically realizing different types of quantum walks using various optical and solid-state schemes. The implementation of DTQWs distinguishes itself by how it encodes the coin and position of the quantum walkers. Different physical platforms have been explored, including ion trap systems [58], cavity quantum electrodynamics systems [59], superconducting qubits [60], and ultra-cold atoms [61, 62]. In addition, quantum walks can also be implemented using single photons and linear optical elements [63, 64]. Surprisingly, it has been discovered that the quantum nature of light is not essential for the development of quantum walks. Classical optics can simulate quantum walks using an interferometric analogy [65]. For a more systematic review, please refer to Ref. [119]. However, since my thesis focuses on the DTQW implementation in quantum optics, I will review some previous implementations in the following paragraphs.

In the conventional approach in optical systems, optical paths are commonly used to encode the position, while polarization is employed to encode the quantum walker's coin state [63, 64]. This approach involves utilizing an optical mesh consisting of spatially separated optical elements, phase shifters, beam splitters, and other components to construct a quantum processor [66, 67, 67, 68]. Additionally, it enables extensions beyond ordered quantum walks by incorporating elements like disorder [348, 347, 56] or mesh topology [54].

However, these optical systems tend to be bulky, and the physical complexity increases, especially when dealing with a large number of steps. To overcome these challenges, one approach is to simulate quantum walks using a bulk-optics multipass double Sagnac interferometer. In my Ph.D. thesis, specifically in Chapter VIII [56], I will demonstrate the capability of this implementation to introduce controllable disorder, aiming to enhance the quantum correlation between two indistinguishable photons. Worth mentioning that, by utilizing an array of on-chip coupled waveguides [349, 212], it becomes feasible to implement quantum walks on chips, significantly reducing the system's size. This approach enables the simulation of various quantum phenomena, including bosonic bunching, fermionic anti-bunching [212], two-particle Anderson localization [52], and other related phenomena.

Additionally, orbital angular momentum (OAM) can serve as a positional attribute, functioning as a synthetic dimension for simulating the model [69, 70]. Such an implementation enables an increase in the dimensions of the quantum walk, including the position and coin space [350], providing controllability for the quantum coin for high-dimensional state transfer and engineering [351]. Another approach involves using an optical-fiber loop configuration that mimics the behavior of a synthetic photonic lattice to simulate the DTQW [71, 72]. This method leverages the time-bin degrees of freedom, where discrete-time modes offer advantages such as noise resilience and ease of manipulation using standard telecom-compatible components [352, 82, 83, 84]. This reduction in resource requirements enhances the practicality of photonic platforms for various quantum information tasks. Furthermore, the implementation of the synthetic photonic lattice offers excellent testbeds to simulate intriguing effects, including decoherence [72] and parity-time symmetry [85]. In chapter X of my thesis, I will present the implementation of a fully fiber-integrated coupled loop system. This system will be utilized for tasks such as bi-photon state preparation, manipulation, and the realization of time-bin two- and four-level interference between two photons.

Chapter 7

Readout of quantum information spreading using disordered quantum walk

Abstract

We design a quantum probing protocol using Quantum Walks to investigate the Quantum Information spreading pattern. We employ Quantum Fisher Information, as a figure of merit, to quantify extractable information about an unknown parameter encoded within the Quantum Walk evolution. Although the approach is universal, we focus on the coherent static and dynamic disorder to investigate anomalous and classical transport as well as Anderson localization. We provide a feasible experimental strategy to implement, in principle, the quantum probing protocol based on the quantum Fisher information using a Mach-Zehnder-like interferometric setup. Our results show that a Quantum Walk can be considered as a readout device of information about defects and perturbations occurring in complex networks, both classical and quantum. This Chapter is related to Publication 5 in the List of Publications.

7.1 Introduction

Quantum Walk (QW) is the quantum equivalent of a random walk, which benefits from quantum features such as quantum superposition, interference and entanglement [44, 353, 326, 354]. In contrast with a classical walker, the quantum walker spreads quadratically faster in position space [44, 353, 326, 354, 355]. This notion brings up a motivation to introduce algorithms for quantum computers that solve the problem exponentially faster than the best classical algorithm [46, 47]. On the other hand, QW provides a powerful model to describe energy transport phenomena in heterogeneous systems either biological, in the case of photosynthesis [74, 333], or solid state ones, in the case of Luttinger liquids [356]. Besides, nonclassical features play a substantial role in the dynamics of a quantum walker, as a sign for quantum coherence effects in biological systems [357, 358]. Finally, it is worth noting that the QW model is applicable to simulate a wide range of quantum phenomena such as topological phases [54, 359], neutrino oscillations [360, 361], and relativistic quantum dynamics [362, 363, 364].

A relevant quantity, useful to characterize the walk, is the Mean-Square Displacement (MSD) of the walker in absence of bias. The linear growth of the MSD as a function of the evolution time has become the universal identifier of what is known as normal transport. Any stochastic process that does not follow a linear growth trend with time is called anomalous. In particular, processes characterized by a superlinear growth of the MSD are usually addressed as superdiffusive [329, 330, 331]. There are several cases in which superdiffusion settles in transport or propagation processes, such as complex biological environments [332, 74, 333], chaotic Hamiltonian systems [334, 335], transport in disordered systems [336, 337, 338], quantum optical systems [339], single-molecule spectroscopy [340, 341]. On the other hand, numerical evidence has been notified for the existence of subdiffusive transport [342, 343, 344,

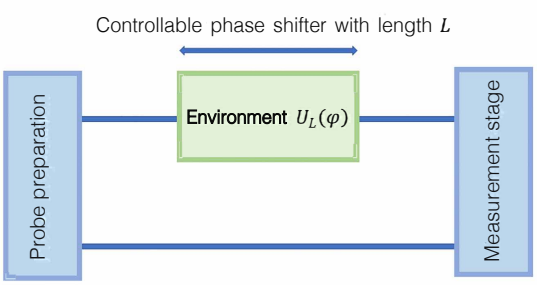

Figure 7.1: Typical representation of a quantum probing protocol using a Mach-Zehnder-like interferometer. A phase difference ϕ is applied between two paths which is acquired by the probe thanks to an adjustable path length L.

345, 346]. Also, an extremely slow process of matter-wave spreading, subdiffusion transport, has been experimentally implemented in Bose-Einstein condensates [365].

In recent years, there has been substantial interest in formulating QW models that can exhibit different transport behaviors with respect to the typical one, consisting in a MSD growing quadratically with time. The spreading behavior of quantum walkers can be modified by suitably tuning the evolution of a quantum walker through various types of disorder [52, 366, 348] and decoherence effects [72]. Due to the latter ones, it has been shown that the ballistic growth of the variance changes to a superdiffusive one, reaching the diffusive spread [348]. Moreover, by means of the same techniques, the subdiffusive region, between diffusive and Anderson localization regime [48], can be exploited [347]. On the contrary, there are few reports in which a QW in presence of evolution nonlinearities avoids complete trapping in a finite region of the lattice. In these cases, the spreading has to slow down to a subdiffusive case, but it does not converge, generating a phenomenon known as delocalization of the wave packet [367].

In the context of quantum probing strategies [368, 369, 370, 371, 372], one may characterize properties of a complex environment, such as fragile biological samples, by a small and controllable quantum probe that interacts with the bigger complex system. These features may be conveyed through error analyses of the quantum probe, having a natural connection with the theory of quantum parameter estimation [373, 374, 375, 376, 377, 310] where unknown parameters are inferred via repeated measurements on the system of interest. The quantum Fisher information (QFI), that depends on the kind of probe-environment interaction, is used to measure this error through the quantum Cramer-Rao bound.

Despite the high number of studies about transport features in a QW, as far as we know, investigations in a quantum probing fashion have remained elusive. The idea behind this work is to infer how much information about the features of the QW network can be extracted using quantum estimation merits from the characteristics of the quantum walker evolution. In quantum metrology, the extractable information about an unknown parameter, such as a phase ϕ, is usually given by the quantum Fisher information (QFI), which is also linked to the measurement accuracy of the estimation strategy. We take quantum Fisher information for granted to investigate the different transport regimes of information due to the properties of the quantum network. From another perspective, the growth pattern of QFI is a faithful indicator to describe defects and perturbations occurring in complex networks, both classical and quantum. We find that the disorder pattern plays a significant role in the spreading pattern of quantum information. The growth trend of QFI allows one to characterize the anomalous and normal spreading pattern, and also Anderson localization of the walker.

7.2 Discrete-time Quantum walk based quantum probe

7.2.1 State-of-art quantum probing scheme

Due to the sensitivity of the probe to the perturbations induced by the environment, quantum probes may effectively infer characteristics of the environment. One of the possible strategies is to send a quantum

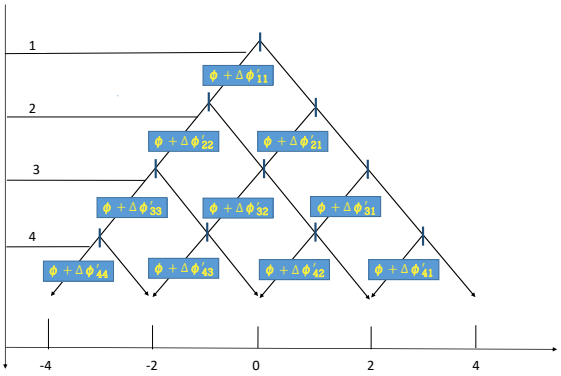

Figure 7.2: Typical representation of a quantum probing protocol using disordered quantum walk dynamics. A phase difference ϕ between coin (internal) states of the walker is applied after each step, including possible fluctuations $\Delta\phi'_{i,j}$ depending on step i (time) and position j within the circuit. This way, static and dynamic disorder can affect the quantum walk process.

probe through a Mach-Zehnder-like interferometer (MZI). As illustrated in Fig. 7.1, a MZI consists of a lower arm, the so-called reference path where the probe travels free, and of an upper arm, where the probe acquires a phase shift ϕ due to environmental action. Finally, at the probe is measured employing a suitable procedure to estimate environment properties of interest. Typically, the parameter ϕ is encoded in a unitary operator $U_L(\phi)$. Here, the phase shifter is length-dependent so that the probe is capable to capture the coding process with respect to the phase shift length. We aim to analyze the phase sensitivity in terms of controllable phase shift length.

In parameter estimation schemes [373, 378, 375, 376, 377], a parameter of interest, like ϕ, is estimated by processing the data by means of estimator observable outcomes $\hat{O} = \{o_1, o_2, \ldots, o_n\}$. The measurement sensitivity of the phase parameter is given by the Cramér-Rao inequality $\delta\phi \geq 1/\sqrt{M\mathcal{F}_\phi}$, where $\delta\phi$ is the mean square error in the measure of parameter ϕ, M is an asymptotically large number of independent measurements, and $\mathcal{F}_\phi$ is the QFI given by

$$\mathcal{F}_\phi = \int \mathrm{d}o\, p(\phi|o) \left(\frac{\partial}{\partial\phi} \ln p(\phi|o) \right)^2 . \tag{7.1}$$

In this equation, $p(\phi|o) = \mathrm{Tr}[\hat{M}_o\rho]$ is the conditional probability distribution that may gives information about parameter ϕ a result of the measurement outcome, where $\hat{M}$ is a set of positive operator-valued measurements (POVMs) [377] and ρ is the density operator. The optimal estimator is the one that saturates the Cramér-Rao inequality and maximizes the QFI. According to the Symmetric Logarithmic Derivative (SLD) approach, the QFI is $\mathcal{F}_\phi = \mathrm{Tr}[L_\phi^2\rho]$, where L_ϕ is the Symmetric Logarithmic Derivative (SLD) operator satisfying the equation $\mathrm{d}\rho/\mathrm{d}\phi = \{L, \rho\}/2$, with $\{\cdot,\cdot\}$ indicating the anticommutator. For a pure state $\rho^2 = \rho$, the SLD operator reduces to $L_\phi = 2\mathrm{d}\rho/\mathrm{d}\phi$. It is worth mentioning that QFI provides an upper bound to the sensitivity which is independent of the choice of measurement. Also, the set of optimal POVMs is given by the eigenstates of the SLD operator L_ϕ. However, in operational conditions, L_ϕ may not be the optimal observable that one tends to perform in the measurement setup, so optimization strategies, such as maximum likelihood method, have been suggested to supply an optimal estimator that saturates [377]. To the scope of this paper, we focus on the probing strategy in a discrete QW network to address maximum extractable information spreading pattern using QFI.

7.2.2 Discrete Quantum Walk as a quantum probe

Here, We design a quantum probing protocol to address the spreading behavior of a QW and the extractable information that the walker can assess, examining the problem by quantum estimation strategy. The discrete-time QW process is a multi-path interferometer setup, equivalent to a chain of Mach-Zehnder interferometers. A typical representation of a quantum walk network is displayed in Fig. 7.2 for

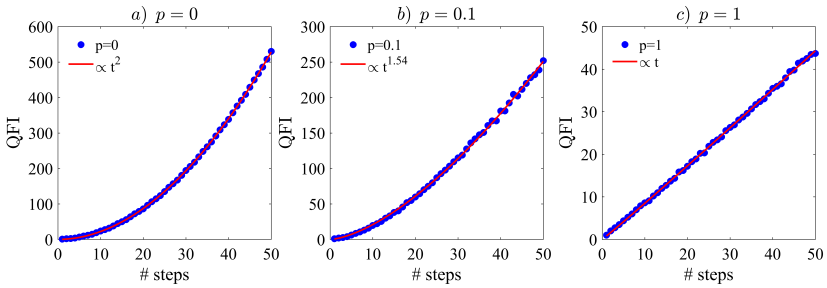

Figure 7.3: **Quantum Fisher information for a quantum walker.** Average QFI $\mathcal{F}$ of a quantum walker versus the number of steps t for static (top panels) and dynamic (bottom panels) disorder, at different degrees of disorder: **a)** $p = 0$, **b)** $p = 0.1$, **c)** $p = 1$. In all plots, the initial input is $|\Psi_0\rangle = |0\rangle_{\mathbf{p}} \otimes |\uparrow\rangle_{\mathbf{c}}$. The simulated data (blue dots) are plotted along with a power-law fitting function (red line).

four steps. Each line linking two different vertical bars corresponds to a mode along which the walker can travel. As can be seen in Fig. 7.2, the rightmost path is the reference path along which the quantum probe (walkers) travels freely. The length-dependent phase shifter is implemented by the sequence of (discrete) sites that the quantum walkers pass through along the multi-path dynamics. A measurement strategy is finally employed after each step to perform the optimal estimator and extract the information spreading about the phase. It is important to note that the probing continues until the relative error converges to the lowest value for the 99.9% confidence interval. Here, we numerically address the achievable bound QFI that one may tend to measure by a suitable and practical measurement strategy.

The dynamics of a Quantum Walker on a one-dimensional lattice is defined on the joint Hilbert space $\mathcal{H} = \mathcal{H}_{\mathbf{p}} \otimes \mathcal{H}_{\mathbf{c}}$ of position ($\mathcal{H}_{\mathbf{p}}$) and coin ($\mathcal{H}_{\mathbf{c}}$) subspaces of the walker [353, 326]. The coin basis states set is $\mathcal{B}_{\mathbf{c}} = \{\uparrow, \downarrow\}$, which can be seen as an internal degree of freedom of the walker, while the position space is spanned by the discrete set $\{|x\rangle_{\mathbf{p}}\}$, which represents the sites of the lattice. The evolution of the quantum walker is determined by the coin operator $\hat{\mathcal{C}} = \frac{1}{\sqrt{2}} \left(|\uparrow\rangle_{\mathbf{c}} \langle\uparrow|_{\mathbf{c}} + |\uparrow\rangle_{\mathbf{c}} \langle\downarrow|_{\mathbf{c}} + |\downarrow\rangle_{\mathbf{c}} \langle\uparrow|_{\mathbf{c}} - |\downarrow\rangle_{\mathbf{c}} \langle\downarrow|_{\mathbf{c}}\right)$ and the shift operator

$$\hat{S} = \sum_x |x+1\rangle_{\mathbf{p}} \langle x|_{\mathbf{p}} \otimes |\uparrow\rangle_{\mathbf{c}} \langle\uparrow|_{\mathbf{c}} + |x-1\rangle_{\mathbf{p}} \langle x|_{\mathbf{p}} \otimes |\downarrow\rangle_{\mathbf{c}} \langle\downarrow|_{\mathbf{c}} \,, \tag{7.2}$$

which moves the walker according to the coin state. Repeated action of the unitary operator $\hat{U} = \hat{S}(\hat{\mathcal{I}}_{\mathbf{p}} \otimes \hat{\mathcal{C}})$ defines a completely ordered QW evolution, where the coin operator is uniform in both space and time. However, in order to have a general nonuniform evolution structure, we need suitable phase maps [379]. Here, we consider the case in which ϕ is encoded in the QW process through the unitary operator $\hat{U}(\phi) = \hat{S}(\hat{\mathcal{I}}_{\mathbf{p}} \otimes \hat{\mathcal{C}})\hat{P}$, where $\hat{P}$ is a phase-shift operator defined as

$$\hat{P} = \sum_x |x\rangle_{\mathbf{p}} \langle x|_{\mathbf{p}} \otimes \left(|\downarrow\rangle_{\mathbf{c}} \langle\downarrow|_{\mathbf{c}} + e^{\mathbf{i}(\phi + \Delta\phi'(t,x))} |\uparrow\rangle_{\mathbf{c}} \langle\uparrow|_{\mathbf{c}}\right). \tag{7.3}$$

As can be seen in Fig. 7.2, the phase-shift operator $\hat{P}$ is ideally responsible for applying a phase difference ϕ between coin states $|\downarrow\rangle_{\mathbf{c}}$ and $|\uparrow\rangle_{\mathbf{c}}$ at each position. However, the encoding process might come with unwanted time-position-dependent fluctuations $\Delta\phi'(t,x)$ that coherently affect the evolution itself. For dynamic disorder, the walker state at step t is given by t repetitive action of step-dependent unitary operator is

$$|\Psi_t\rangle = \hat{U}_t \hat{U}_{t-1} \ldots \hat{U}_2 \hat{U}_1 |\Psi_0\rangle \,. \tag{7.4}$$

In addition, when phase fluctuations are frozen in time, therefore the quantum state at step t is $|\Psi_t\rangle = (\hat{U})^t |\Psi_0\rangle$. This way, static and dynamic disorder can affect the QW probability distribution (see appendix for further analysis).

The main aim of quantum estimation strategy is to evaluate the maximum extractable knowledge about an unknown parameter, which we call ϕ, from repeated measurements on the probe. One can

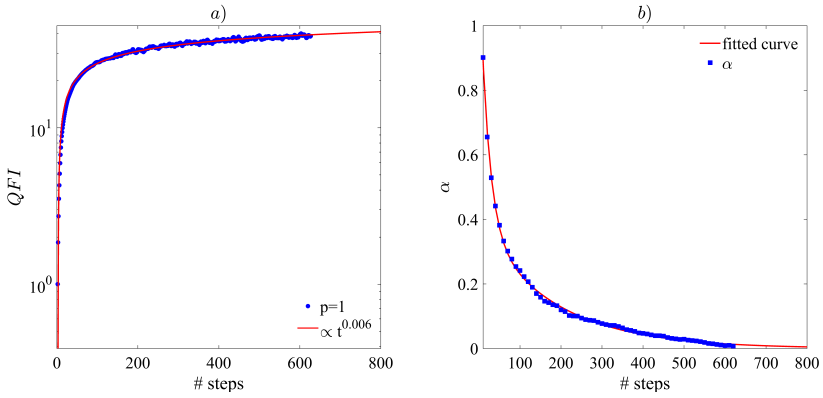

Figure 7.4: **a)** Logarithmic scale of average QFI $\mathcal{F}$ of a quantum walker and its fitted curve $\mathcal{F} \propto t^{\alpha}$ as a function of the number of steps t for complete static disordered $p = 1$. **b)** Step-dependent coefficient $\alpha(t)$ and its fitted curve as a function of the number of steps t. The simulated data (blue dots) are plotted along with a power-law fitting function (red line).

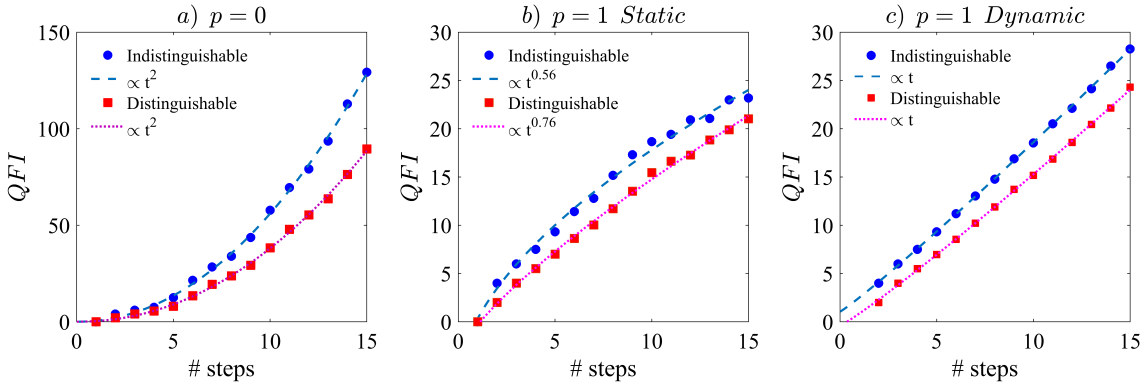

Figure 7.5: **Quantum Fisher information for two quantum walkers.** Average QFI $\mathcal{F}$ of a quantum walker versus the number of steps t for: **a)** ordered case ($p = 0$), **b)** complete static disorder ($p = 1$), and **c)** complete dynamic disorder ($p = 1$). In all plots, the blue circles and red squares represent, respectively, indistinguishable and distinguishable two-particle inputs. The simulated data (blue dots) are plotted along with a power-law fitting function (red line).

numerically obtain the QFI $\mathcal{F}_{\phi} = 4\mathrm{Tr}\,[L_{\phi}^{2}\rho]$ using the walker state at step t, $|\Psi_t\rangle = \hat{U}(\phi)\,|\Psi_{t-1}\rangle$, and its derivative with respect to parameter ϕ, which is

$$\left|\frac{\partial\Psi_t}{\partial\phi}\right\rangle = \frac{\partial\hat{U}(\phi)}{\partial\phi}\,|\Psi_{t-1}\rangle + \hat{U}(\phi)\left|\frac{\partial\Psi_{t-1}}{\partial\phi}\right\rangle. \tag{7.5}$$

Similar to earlier suggestions [380, 381], QW circuit is a multi-path interferometric arrangement where an input state is split into many beams by a chain of beamsplitters. In measurement stage of multi-path interferometer [380, 381], output modes are recombined and then are detected by M identical photodetectors to construct the probability distribution of detector i. This allows one to obtain the joint-probability distribution $p(\phi|x)$ using a POVM set given by

$$M_{kk'} = e^{\mathbf{i}(k(\phi)-k'(\phi))}\,|k\rangle\,\langle k'| + c.c, \tag{7.6}$$

satisfying the completeness condition $\sum_{k,k'} M_{kk'} = \mathcal{I}$ where $k \neq k'$, each mode $|k\rangle$ being defined by both position $|x\rangle$ and corresponding coin state $|\sigma\rangle$ ($\sigma = \{\uparrow,\downarrow\}$), namely $|k\rangle := |x\rangle\,|\sigma\rangle$. In Eq. 7.6, $k(\phi)$ is the phase that probe acquires at k mode.

7.3 Application: single probe and pair of probes

In the following, we study the case of both a single probe and a pair of probes sent into the quantum walk network under the effect of static and dynamical disorder. We limit our analysis to the case in which the random fluctuations $\Delta\phi'(t,x)$ can be only 0 or π. Afterwards, the degree of disorder p is defined as the percentage of random phases that the walker experiences during the evolution. This simply means that a p percentage of the random fluctuations $\Delta\phi'(t,x)$ are selected to have π value and to be randomly distributed in time and position. By iterating over enough random phase samples, it is possible to numerically calculate the QFI in presence of a given percentage of randomness p. A key point in the particle evolution is the type of disorder: static disorder, where the phase fluctuations are frozen in time, or dynamic disorder, where the imposed phase can change in both time and space, as happens in the p-Diluted model [348]. The degree of disorder p is directly connected to the time evolution of the probability distribution of the quantum walker (see SM for the probability distribution of a quantum walker corresponding to both cases of static and dynamic disorder).

7.3.1 Single Probe

Let us first consider the simplest instance where a particle starts the quantum walk in the position $|0\rangle_{\mathbf{p}}$ with the $|\uparrow\rangle_{\mathbf{c}}$ coin state, that is $|\Psi_0\rangle = |0\rangle_{\mathbf{p}} \otimes |\uparrow\rangle_{\mathbf{c}}$. For both static and dynamic disorder, we simulate the behavior of the average QFI for different degrees of disorder p. For each value of p, the simulation is performed by averaging over 10^4 different phase maps. The average QFI is plotted in Fig. 7.3 as a function of the step number t. As a result of the power-law fitting data, we find that the average QFI is $\mathcal{F} \propto t^{\alpha}$ where the range of α is $0 \leq \alpha \leq 2$ and $1 \leq \alpha \leq 2$ for the static disorder and the dynamic disorder, respectively. Without any disorder ($p = 0$), the QFI of the QW grows quadratically in time $\mathcal{F} \propto t^2$, analogously with a ballistic transport pattern, as displayed in Fig. 7.3**a**. Also, this means that the phase variance upper-bound is proportional to the inverse of the number of steps $\delta\phi \propto t^{-1}$. Similar to earlier studies, the phase sensitivity decreases with the number of available paths [380]. For static disorder (Fig. 7.3 (**I**)), the superdiffusive ($\alpha > 1$) to subdiffusive ($\alpha < 1$) transition is reachable by increasing the value of disorder p out of 50 steps. Therefore, the way information spreads in the quantum network can be determined as a result of the disorder strength. For dynamic disorder, we plot the average QFI in Fig. 7.3 (**II**). Here, we use the QFI to probe the transition from the ballistic regime with $p = 0$ (Fig. 7.3**a**), superdiffusive with $p = 0.1$ (Fig. 7.3**b**) and diffusive one with maximum degree of disorder $p = 1$ (Fig. 7.3**c**), analogous to the case of classical probe. This indicates that the output information, which is inferred trough measurements performed exclusively on the probe, shows a superdiffusive to classical transition in transport pattern. The observed fluctuation in the QFI value is due to the limited number of iterations which can be realized for each step number. Similarly to the variance of the position operator of the quantum walker [72, 348, 347] (see also SM), QFI provides a simple measure to quantify the transport pattern of the walker.

It is worth mentioning that the probing pattern depends on the number of steps that a walker takes. In the static disorder case, we find out that the QFI eventually tends to a given value. This is a clear signature of Anderson localization given by average upper-bound of QFI, as clearly seen in Fig. 7.4**a** where the growth trend declines until average QFI reaches a maximum value. As an additional clarification, the QFI is fitted with the power function $\mathcal{F} \propto t^{\alpha(t)}$, where $\alpha(t)$ is the step-dependent coefficient in a nonlinear fitting process. In Fig. 7.4**b**, $\alpha(t)$ is plotted by increasing the step number of the QW process. We observe how the growth trend depends on the step number t, and how it significantly declines for higher t. This property shows that information stops spreading within the quantum network as an indicator of particle localization.

7.3.2 Pair of Probes

To enrich the physics of the phenomenon, we now consider two input quantum walkers, either distinguishable or indistinguishable, in position $|0\rangle_{\mathbf{p}}$ with initial opposite coin states. When two identical

particles arrive at a beamsplitter with temporal delay, one in each input port, they are distinguishable in the eyes of the beamsplitter. For distinguishable particles (walkers) named 1 and 2, the input state is separable, that is

$$|\Psi_0^{\mathrm{s}}\rangle = |0\rangle_{\mathbf{1p}}\,|\uparrow\rangle_{\mathbf{1c}} \otimes |0\rangle_{\mathbf{2p}}\,|\downarrow\rangle_{\mathbf{2c}}\,. \tag{7.7}$$

For indistinguishable particles, the pair overlaps perfectly in time at beamsplitter [130]. Here, the input state is physically entangled in the coin states by virtue of complete spatial mode overlap [2, 14]: in the no-label approach [2, 3] this state is simply written as $|\Psi_0\rangle = |0_{\mathbf{p}}\uparrow_{\mathbf{c}}, 0_{\mathbf{p}}\downarrow_{\mathbf{c}}\rangle$, which in the first-quantization formalism with labels becomes the symmetrized state

$$|\Psi_0^{\pm}\rangle = |0\rangle_{\mathbf{1p}}\,|0\rangle_{\mathbf{2p}} \otimes \left(\frac{1}{\sqrt{2}}(|\uparrow\rangle_{\mathbf{1c}}\,|\downarrow\rangle_{\mathbf{2c}} \pm |\downarrow\rangle_{\mathbf{1c}}\,|\uparrow\rangle_{\mathbf{2c}})\right) \tag{7.8}$$

where $\pm$ being for bosons and fermions, respectively. The evolution can be studied by repeatedly applying the two-particle unitary operator $\hat{U}(\phi) \otimes \hat{U}(\phi)$ to the states above. We plot the average QFI versus the step number t in Fig. 7.5 for the ordered case $p = 0$ (**a**) and for the completely disordered one $p = 1$, with static (**b**) and dynamic (**c**) disorder. In general, the state of two indistinguishable particles exhibits a higher value of QFI compared to the distinguishable one. This property is explained by the fact that particle indistinguishability is an enriching resource for quantum information distribution within a composite system of identical particles [16, 17, 23]. Interestingly, we also notice that both input states follow the same spreading pattern. In the case of ordered case ($p = 0$), the growth pattern is ballistic, while for the completely disordered one ($p = 1$), the QFI follows a subdiffusive pattern (Fig. 7.5**b**) and a classical one (Fig. 7.5**c**) due to static and dynamic disorder, respectively. Notice that the QFI, as a spreading pattern indicator, is independent of the number of quantum walkers, in contrast with the position variance dimension which grows accordingly to the particle number [348].

7.4 Conclusion

In this work, we have proposed a quantum probing protocol using the quantum walk process to infer information about defects and perturbations occurring in both quantum and classical networks. This goal has been achieved by applying quantum metrology techniques to the QW process. We have exploited QFI to describe extractable information concerning an unknown phase ϕ that the quantum walker acquires at each step, plus random fluctuations, through the QW. Even though the framework is general, we have studied coherent static and dynamic disorder in the QW to describe the transport pattern of information about the unknown parameter ϕ. We have found that different disorder regimes, corresponding to a disorder percentage p in the QW process, lead to different spreading patterns, including ballistic, superdiffusive, classical, subdiffusive regimes, and Anderson localization. Quantum Fisher information, as a spreading pattern indicator, is independent of the number of quantum walkers, in contrast with the position variance dimension which grows accordingly to the particle number [348]. Ultimately, our results show that QW can play the role of a readout device of information about internal characteristics of complex networks.

Our results provide a general characterization of the spreading pattern using the quantum probing scheme of QFI bound. One may put the complex system in an interferometric scheme (like a MZI) to examine how a quantum probe interacts with the complex system. Also, we have applied the disordered quantum walk dynamics to explain the system-probe interaction. In Refs. [348, 347], it has been experimentally demonstrated the control over the parameter p by performing a selective random disorder for photons in a bulk optics scheme. Indeed, it is challenging to implement an optimal estimation strategy with accuracy associated with QFI bound [377]. Quantum Cramer-Rao bound needs available prior knowledge to adopt a local approach and the large number of experimental observations. Also, symmetric logarithmic derivative (SLD) operator itself may not represent the optimal observable to be measured. In fact, projection over eigenstates of SLD operator determines the POVM and not the estimator. If it is practically possible, one may try to perform the optimal measurement which are projections over the

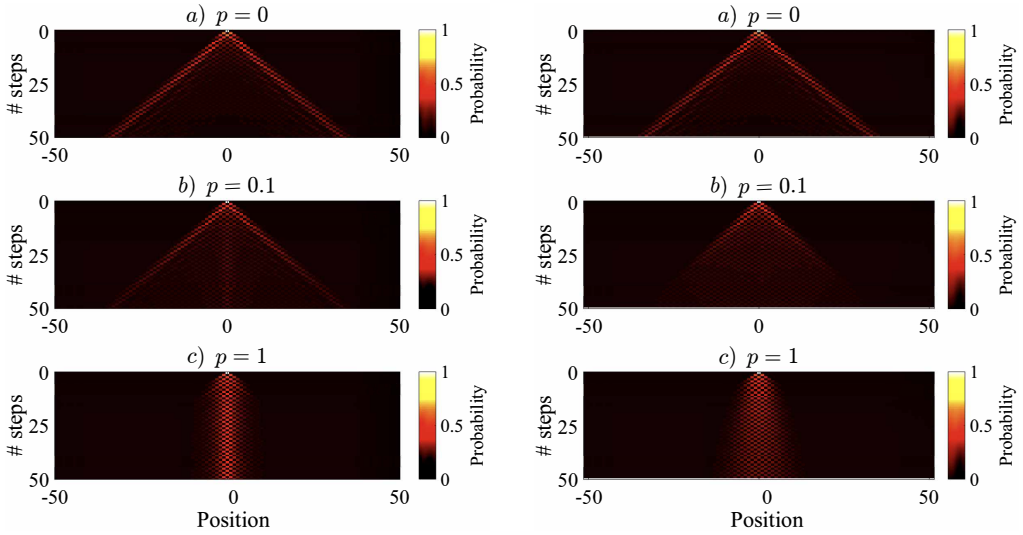

Figure 7.6: **Probability distribution.** Average probability distribution of an unbounded discrete QW on the line as a function of step number and position, for different values of disorder: **a)** $p = 0$ **b),** $p = 0.1$, **c)** $p = 1$, by averaging over 10^4 phase maps for both static (left panels) and dynamic (right panels) disorder. In all cases, the initial input state is $|\Psi_0\rangle = |0\rangle_p \otimes (|\uparrow\rangle_c + |\downarrow\rangle_c)/\sqrt{2}$.

eigenstates of the SLD operator. Moreover, one can compute the classical Fisher information (FI) by exploring all possible POVMs for a fixed input state. If the maximized FI reaches the QFI obtainable, we can conclude that the POVMs are optimal. This strategy is largely determined by how successful the POVMs can be implemented in each scheme. To saturate the Cramer-Rao bound, one may pursue the classical post-processing of data using maximum likelihood, which is known to provide an asymptotically efficient estimator [373]. In addition, the adaptive measurement strategy is employed to decrease the number of measurements [382]. Furthermore, machine learning might be a powerful tool to obtain the goal of interest [383, 384].

This protocol is on track to be experimentally implemented, and several platforms are likely candidates. An example of a potential candidate is a cascade of balanced beam splitters arranged in a network of Mach-Zehnder interferometers [52]. In this scheme, phase shifters are involved in implementing the randomized disorder to a certain degree. This experiment faces many challenges, but the most challenging one is probably utilizing phase-stable POVMs (possibly an optimal set or performing an optimization protocol, such as maximum likelihood method, to reach the quantum Cramer-Rao bound) along multiple paths. Indeed, the experiment also depends on measurement components that have low noise and phase stability. Our work is expected to motivate further studies such as: studying different types of disorder like the spatio-temporal correlated disorder [385], probing the QW on high-dimensional graph network [386], detecting memory effects of the environment on quantum walkers [387], assessing material characteristics of complex random media [388].

A. Further Analysis

In this Appendix, we address the probability distribution and the variance displacement of a single walker under the effect of different degrees of static and dynamic disorders. Let us consider a given initial state

$$|\Psi_0\rangle = \frac{1}{\sqrt{2}} |0\rangle_{\mathbf{p}} \otimes (|\uparrow\rangle_{\mathbf{c}} + |\downarrow\rangle_{\mathbf{c}}) , \tag{7.9}$$

to explore the probability distribution of a quantum walker in presence of both static and dynamic disorder. We limit our analysis in the case that a p percentage of phase fluctuations are selected out of 0 and π. We show the density plots of the evolution of single particles in Fig. 7.6, in terms of step number and

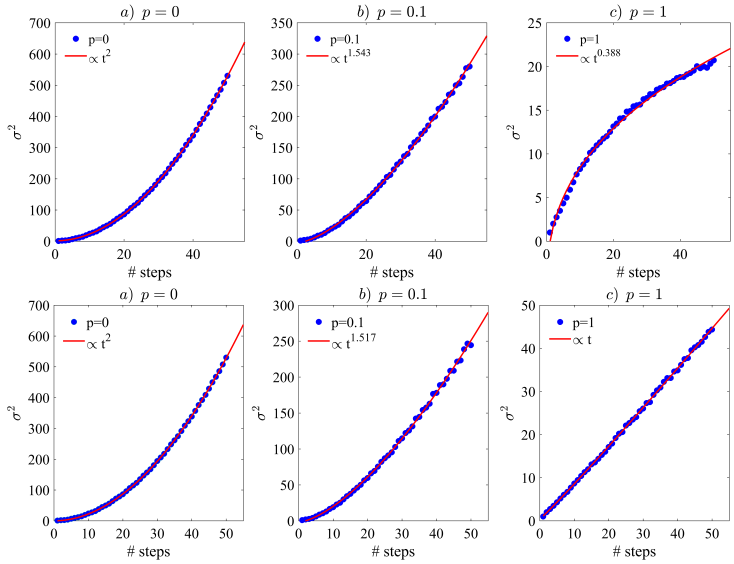

Figure 7.7: **Position variance.** Position variance σ^2 of a quantum walker on the line in terms of the step number t for different values of disorder **a**) $p = 0$ **b**), $p = 0.1$, and **c**) $p = 1$, by averaging over 10000 phase maps for both static disorder (top panels) and dynamic disorder (bottom panels). In all cases the initial input is $|\Psi_0\rangle = |0\rangle_p \otimes (|\uparrow\rangle_c + |\downarrow\rangle_c)/\sqrt{2}$. The simulated data (blue dots) are plotted along with a power-law fitting function (red line).

walker position. Here, both static disorder (Fig. 7.6(left panels)) and dynamic disorder (Fig. 7.6(right panels)) is realized with different degrees of disorder p: **a**) $p = 0$, which corresponds to a standard ordered QW; **b**) $p = 0.1$; **c**) $p = 1$ completely disordered QW. The horizontal axis denotes different positions that the walker can reach while the vertical one represents the step number t, increasing from top to bottom. We averaged the probability distributions over 10000 random phase maps realizations. As can be seen, the particle follows different transport pattern affected by static (Fig. 7.6(left panels) or dynamic disorder (Fig. 7.6(right panels)). Also, we show how the degree of disorder would affect the probability distribution of the quantum walker. It seems that the probability of finding a particle in the center raises by increasing the degree of disorder p.

In the QW problem, the operator $\hat{X}$ that measures the walker position is the operator of interest since the variance of the position operator provides a simple measure to quantify the spread of the walker [72]

$$\sigma^2(\hat{X}) = \langle \hat{X}^2 \rangle - \langle \hat{X} \rangle^2. \tag{7.10}$$

This measure has been proven to be particularly useful to compare the effects of different kinds of disorder on the spreading pattern of the walker(s). Generally, the variance of the position operator is given by $\sigma^2(\hat{X}) \propto t^\alpha$, where range $\alpha > 1$ is called superdiffusive and $\alpha < 1$ subdiffusive. For instance, an ordered QW presents a ballistic spread with $\sigma^2(\hat{X}) \propto t^2$, while the classical random walk is diffusive with $\sigma^2(\hat{X}) \propto t$.

As an example, we study the spreading behavior of a walker for the given input state $|\Psi_0\rangle$ of Eq. 7.9 with three different values of disorder. The position variance of a quantum walker generally depends on type of the disorder, degrees of disorder p and number of steps t. The variance of a single walker is plotted versus the number of steps for both static disorder (Fig. 7.6(top panels) and dynamic disorder (Fig. 7.6(bottom panels)). For an ordered QW, the walker shows a ballistic pattern, displayed in Fig. 7.7**a**. In static disorder, a super-diffusive pattern appears because of the increasing value of disorder degree to $p = 0.1$ (see Fig. 7.7(top panel (b)). Interestingly, in Fig. 7.7(top panel (c)), the subdiffusive pattern also can be simulated by increasing the value of the disorder degree to the maximum. In the dynamical disorder case, the quantum walker exhibits a transition from ballistic to superdiffusive behavior, and then a classical spreading pattern by increasing the degree of disorder to $p = 1$.

Chapter 8

Enhancing nonclassical bosonic correlations in a quantum walk network through experimental control of disorder

Abstract

The presence of disorder and inhomogeneities in quantum networks has often been unexpectedly beneficial for both quantum and classical resources. Here we experimentally realize a controllable inhomogenous quantum walk (QW) dynamics, which can be exploited to investigate the effect of coherent disorder on the quantum correlations between two indistinguishable photons. Through the imposition of suitable disorder configurations, we observe two-photon states that exhibit an enhancement in the quantum correlations between two selected modes of the network, compared to the case of an ordered QW. Different configurations of disorder can steer the system toward different realizations of such an enhancement, thus allowing spatial and temporal manipulation of quantum correlations between remote modes of QW networks. This Chapter is related to Publication 6 in the List of Publications.

8.1 Introduction

A thorough characterization of genuine quantum traits is crucial to understand the boundary between classical and quantum phenomena [253] and to perform quantum information tasks [15]. To this aim, several quantification methods have been introduced to faithfully identify the presence of quantum (nonclassical) resources such as entanglement [33], coherence [389], discord [390], joint measurability [391], steering [392], or thermal operations [393] in the case of composite systems.

Indistinguishability of quantum identical particles [222, 16] has also been revealed as a useful nonclassical resource. From an operational point of view, particles are so-called indistinguishable if they are in the same mode with respect to a characterization via two-particle interference [394]. From a broader perspective, the indistinguishability concept is related to a given set of quantum measurements [17]. In fact, indistinguishability plays a fundamental role in raising quantum processes, such as many-body interference [394, 17, 184], entanglement generation [222, 16, 10, 395, 24, 23], quantum teleportation [23], quantum metrology [396, 310], quantum coherence [397, 398, 94], quantumness protection [17, 32, 117], quantum key distribution [399, 400] and the high state complexity exploited by boson sampling algorithms [401, 402]

In this context, it is important to understand how quantum features based on indistinguishability behave in a dynamical framework, specifically in the case of bosons propagating through a nonhomogeneous system. For a large variety of systems, the disorder plays a detrimental role because it drives the system into decoherence [73]. Contrarily, for some systems, the disorder can enhance physical

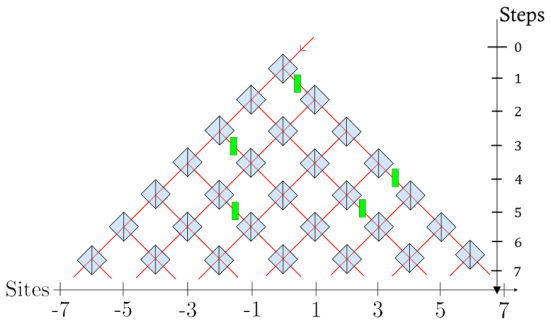

Figure 8.1: **Network representation of a disordered QW according to p-diluted model.** The green bars stand for the presence of π phases on the path which can be added to or removed from the network.

properties such as coherent transport [74], quantum algorithms speedup [75], and quantum correlations [76, 77, 78, 55]. These effects commonly appear due to the interaction with an external environment, though not always featuring a back-action mechanism [79, 80].

In this context, it is important to understand how quantum features based on indistinguishability behave in a dynamical framework, specifically in the case of bosons propagating through a non-homogeneous system. A suitable theoretical platform to perform such a study is represented by Quantum Walk (QW), which provides a very general coherent propagation model: at variance with classical Random Walks, QWs are able to preserve genuine nonclassical features such as superposition, interference, and entanglement [44, 403, 353]. QWs provide powerful models to describe energy transport phenomena in different types of systems like, photosynthetic complexes [74, 333], or solid state ones, as in the case of Luttinger Liquids [356].

It has been shown that adjustable disorder plays a significant role in the evolution of quantum walkers in which the ballistic growth can become anomalous, classical, or localized [72, 52, 366, 348] . The dynamics of a quantum walker is intimately connected to its nonclassical features. This has also highlighted the role of quantum coherence in biological systems [357, 358]. The way quantum-correlated walkers, realized by photon pairs, evolve in a homogeneous optical lattice has been studied, in which distinguishable or indistinguishable photons exhibit different behavior [404, 349, 405, 212, 406]. Moreover, the spreading pattern of the quantum walker(s) can be modified through various types of disorders [407, 52, 348, 347]. For a large variety of systems, the disorder plays a detrimental role in Quantum Walk dynamics because it drives the system into decoherence [73, 72]. Contrarily, for some systems, the disorder can enhance physical properties such as coherent transport [74], quantum algorithm speedup [75], and quantum correlations [76, 77, 78, 55]

At a variance with previous studies so far [55], it remains to find strategies via disorder control for enriching two-particle correlations in separated modes of a quantum walk network. Here we fill this gap by injecting two indistinguishable photons (biphoton) in a one-dimensional inhomogeneous Discrete Time Quantum Walk (1D DTQW) and experimentally adjusting specific disorder configurations, while keeping the system isolated. Moreover, we numerically show that averaging over randomized disorder configurations results in diminishing the initial biphoton quantum correlations (details are reported in the Supplementary Material (SM)). Our findings unambiguously prove that the presence of disorder assists in the dynamical enhancement of biphoton quantum correlations in a controllable fashion, paving the way to its potential employment in quantum information scenarios.

8.2 Theoretical framework

The 1D QW model consists of one or more walkers coherently moving along the discretized sites of a line [408]. In general, the state of the system can always be written as a superposition of the QW modes $|\Psi(t)\rangle = \sum_k \alpha_k(t)\,|k\rangle$, where each mode $|k\rangle := |x\rangle\,|\sigma\rangle$ is defined by both position $|x\rangle$ and its coin $|\sigma\rangle = \{|L\rangle, |R\rangle\}$, and amplitudes $\alpha_k(t)$ depend on the past evolution of the walker. Therefore, the

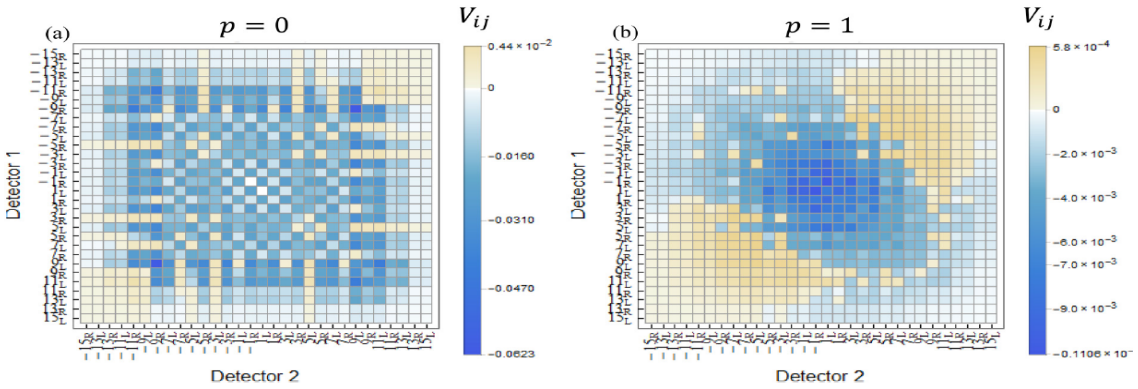

Figure 8.2: **Numerical simulation of violation matrices**. Step 15 matrices of the V_{ij} values of indistinguishable photons in the (a) ordered case ($p = 0$) and the (b) completely disordered one ($p = 1$). The disordered matrix has been computed by averaging over 10^4 disorder configurations

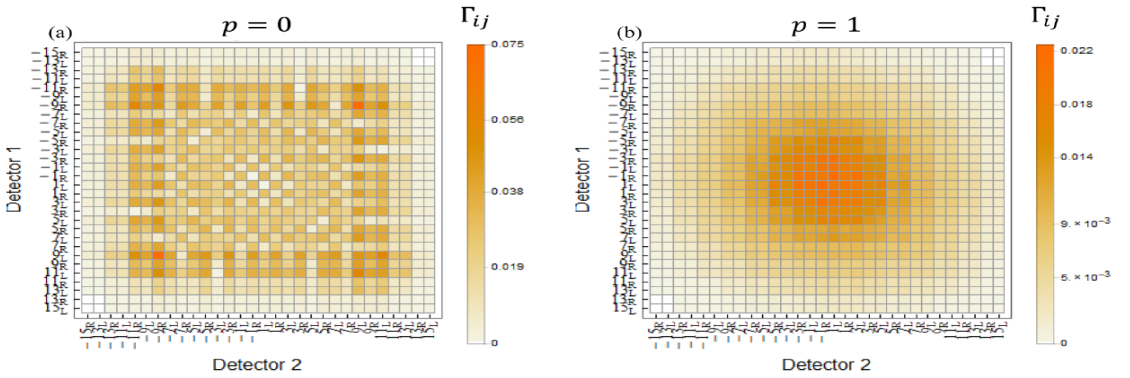

Figure 8.3: **Numerical simulation of coincidences matrices**. Step 15 matrices of output distributions of indistinguishable photons in the (a) ordered case ($p = 0$) and the (b) completely disordered one ($p = 1$). The disordered matrix has been computed by averaging over 10^4 disorder configurations

single step evolution can be written as $|\Psi(t+1)\rangle = \sum_k \hat{U}\alpha_k(t)\,|k\rangle$, where $\hat{U} = \hat{S}\cdot(\hat{I}\otimes\hat{C})$ is the one-step evolution operator on mode $|k\rangle$ with $\hat{S} = \sum_x |x+1\rangle\langle x|\otimes|L\rangle\langle L| + |x-1\rangle\langle x|\otimes|R\rangle\langle R|$ being the shift operator, that moves the walker according to the coin state, $\hat{I}$ the position identity operator and $\hat{C}$ is the coin operator, which in our case reads $\hat{C} = \frac{1}{\sqrt{2}}(|L\rangle\langle L| + i\,|L\rangle\langle R| + i\,|R\rangle\langle L| + |R\rangle\langle R|)$. We also allow for the presence of stepposition-dependent phases $\phi_k(t)$, which are responsible for the dynamical disorder that the quantum walker experiences, according to the so-called p-diluted model [348].

In this disorder framework, the single-step evolution of the quantum state of the system can be written as

$$|\Psi(t+1)\rangle = \sum_k e^{i\phi_k(t)}\hat{U}\alpha_k(t)\,|k\rangle\,, \tag{8.1}$$

where step-position-dependent phases $\phi_k(t)$ are chosen out of two choices 0 or π. Here we assume that the phases experienced by the quantum walker during its evolution are independently and randomly generated. In order to generate a random *phase map*, a Bernoulli process determines whether the phase shift at step t and position x is $\phi = 0$ [with a certain probability $1 - p/2$] or $\phi = \pi$ (with probability $p/2$). In the end, a phase map is a set of matrices $\{\Phi_p(t)\}_{t=0,\ldots,t_{max}}$. that describe all the phases imposed on the walker during the QW process with a given fixed p. This results in a network structure underlying the QW evolution, clearly represented by Fig. 8.1. On average, photons will experience a $p/2$ percentage of "flipped" phases during the quantum evolution. It is worth noting that the evolution stays coherent; in

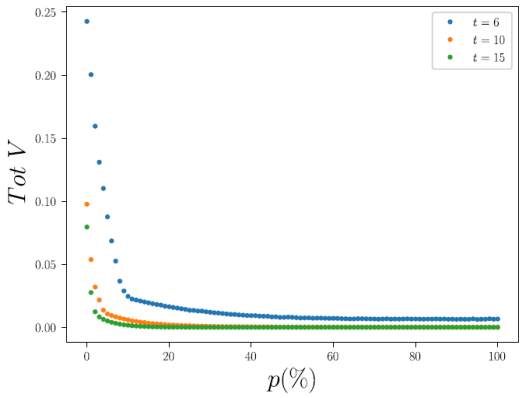

Figure 8.4: **Numerical simulation of total violation trends**. Step 15, step 10, and step 6 plot of the average total violation, computed over 10^4 disorder configurations, as a function of the disorder level p.

fact, there is no decoherence in this framework: If the initial state is pure, the final state stays so. In the following, we especially focus on the single phase maps that enhance the quantum correlation. between the walkers; in that case, the average level of disorder p is no more a relevant quantity.

In order to study the effect of disorder over nonclassical bosonic correlations in a QW dynamics, we consider two indistinguishable photon walkers as input. This choice is strategical since, unlike states of distinguishable photons, the state of an indistinguishable photon pair (biphoton) $|\Psi^{(2)}\rangle = |k_1, k_2\rangle$ ($|k_i\rangle = |x_i\rangle\,|\sigma_i\rangle$ exhibits intrinsic quantum correlations [2, 3]. The two-particle evolution is then obtained by applying $\hat{U} \otimes \hat{U}$ to the state expressed in the standard symmetrized first quantization formalism. Inspired by the classical intensity correlation of light, one way to measure the nonclassicality of the correlation between two detected outputs is by violating the Cauchy-Schwarz inequality [404, 349]

$$V_{ij} = \frac{2}{3}\sqrt{\Gamma_{ii}\Gamma_{jj}} - \Gamma_{ij} < 0, \tag{8.2}$$

where Γ_{ij} is the probability of finding a photon in mode i and the other one in j, namely the probability of measuring a coincidence between modes i and j. Inequality (8.5), in fact, stands for classically correlated light and its violation is assumed to witness the presence of quantum correlations and a sign of photon bunching [404, 349, 406]. In a discrete network, the violation of the inequality between two modes can be considered as evidence of quantum correlation which contains part of the total correlation information (see Appendix A for a detailed discussion of V_{ij} interpretation).

8.3 Numerical Results

Preliminary simulations were carried on in a ideal p-diluted framework: two indistinguishable photons travelling a bulk-optics 1D DTQW, provided with space-time disorder. We studied the average behavior of the violation matrix by averaging over many different evolution realizations with randomness p. The average probability distribution is used to obtain the output violation matrices. We show the violation matrix of an indistinguishable photon pair after 15 steps for the ordered case in Fig. 8.2 (a), corresponding to the disorder level $p = 0$ and the completely disordered one Fig. 8.2 (b), featured by maximal randomness$p = 1$. In this case, the disorder level p is a relevant quantity, since it indicates the average quantity of disorder imposed on the evolution. As can be seen, the violations are present both in the ordered and in the disordered case, though there is an evident migration of the violating values towards the matrix tails. In (Fig. 8.3), we report the values of probability Γ_{ij} of finding a coincidence between two photons emerging from mode i and j. Indeed, in the completely disordered case, a strong funneling of population toward central modes is present, while quantum correlations disappear in the central region. This phenomenon may nourish the idea that correlations specifically generated by the QW dynamics are

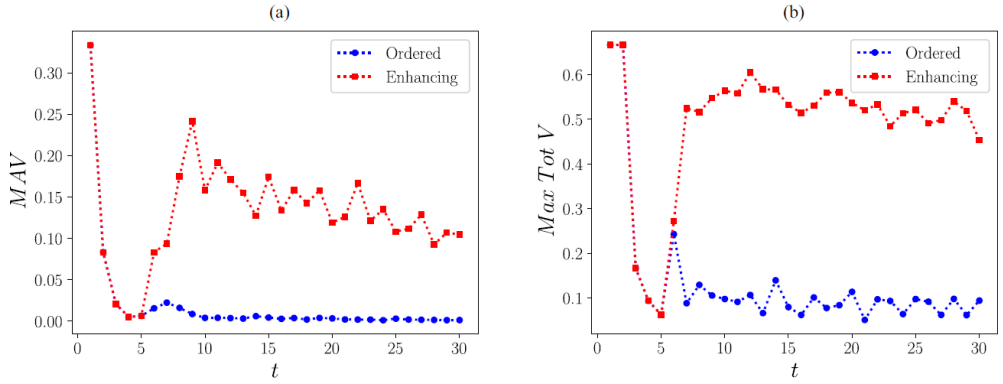

Figure 8.5: **Numerical simulation compression between ordered and enhancing disordered QW**. (a) MAV and (b) maximum achievable total violation versus the number of steps (discrete time) t for the ordered (blue circles) and enhancing disordered (red squares) QW.

classical and may even smother the underlying nonclassical correlations, especially in the completely disordered case, when the QW dynamics emulates the one of a classical random walk [409, 65]. Here, the dynamical average behavior of quantum correlation has been studied through total violation, defined as the sum of all the V_{ij} of the violating coincidences. It has been considered as a measure of the total quantum correlation present in the system. The normalized trend in function of the disorder level is reported in Fig 8.4 for different evolution time lengths. total violation has a decreasing trend as p increases, which can be seen as a consequence of the migration picture described above. Since violations are bound to appear only between scarcely populated modes, the global quantum correlations diminishes. In general, the average evolution appears naturally featured by a decrease of global nonclassicality in time. Nevertheless, this nonclassicality degradation can be challenged by specific single realizations of disorder. In order to find such phase maps, we adopt a random search protocol: We simulate the evolution with 10^4 4 different phase maps for each step number t up to 30 steps for a total amount 3×10^5 of explored configurations. These configurations are generated for a fixed level for disorder, but, since we focus on specific realizations, the average level of disorder becomes irrelevant. We compute the V_{ij} between each pair of output modes for each simulated probability distribution, obtaining the corresponding violation matrices. Then, the entire set of V_{ij} elements corresponding to any combination of i and j modes is reported. Now we can compare the values for any pair (i, j) and for each simulated phase map at a given step to find the maximum achievable violation (MAV), i.e., the maximum positive value of V_{ij} which could be achieved at that given step. In this way, it is also possible to recognize the specific phase maps enerating the MAVs, which can then be experimentally exploited. A more detailed numerical study about the conditions for emerging of MAVs is reported in Appendix B. Summarizing, for each configuration, the procedure consists of comparing maximum positive violations of inequality (2) at step t. This also allows to know where and when it is beneficial to apply the π phase shift within the QW network to identify and select enhancing phase maps. Simulation results are shown in Figs. 8.5 (a) and (b), respectively. We report the MAV as a function of the number of steps, and the stepwise trend of the maximum achievable total violation, defined as the sum of all the positive values V_{ij} of the considered violation matrix (named here as total quantum correlation). Since the explored configurations may not cover the entire set of possible disorder patterns, the results cannot be considered absolutely optimal, but rather enhancing in comparison with the ordered case. Nevertheless, the analysis highlights that disorder helps to retrieve quantum correlations after a specific step of QW, both for MAV and for total violation, suggesting that the two quantities are related although not bound to be maximized together. From numerical results, we can conclude that disorder, acting through mere interference, significantly modifies the evolution of the walker, not only reshaping the probability distribution but also affecting the amount of quantum correlation between the photons. As a consequence, disorder may enable enhancement of the quantum correlation of a bipartite system. It is worth noting that no violations are observed, whatever

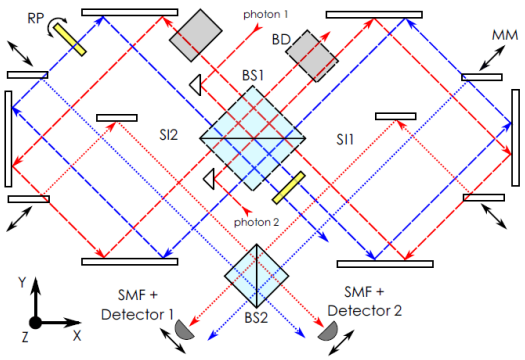

Figure 8.6: **The 2D sketch of the experimental setup**. BS, beam splitter; BD, beam displacer; RP, rotating glass plates; MM, moving mirror; S1, Sagnac interferometer 1; S2, Sagnac interferometer 2. Blue and red beams circulate in opposite directions and impinge on the BS1 in the same horizontal point but at different heights along the z direction, due to the effect of BDs.

the phase map, when a state of distinguishable photons is employed.

8.4 Experimental setup

The experimental setup, designed to test the theoretical predictions, consists of a bulk-optics multipass double Sagnac Interferometer (SI), already exploited in a previous experiment [348], in which inhomogeneities, described by the phases $\phi_k(t)$, can be addressed independently both in step number and evolution mode. The bulk-optics setup shown in Fig. 8.6 is analogous to a chain of intrinsically phase-stable Mach-Zehnder Interferometers (MZIs), each of them provided with an individually tunable phase shifting. The additional exploitation of the z direction allows to effectively realize a Beam Splitter (BS) network, which reproduces a 1D DTQW dynamics. Thanks to the particular geometry of the implementation, each propagation mode of the QW at the given step has a specific position in the plane transverse to the propagation direction. Therefore, the phase shifts can be independently addressed in each mesh of the QW by the simple insertion of Rotating Glass Plates (RP) along the propagation path. The output state can be measured through a set of Moving Mirrors (MMs), intercepting, and extracting from the setup only modes of the selected step t_j. Also, the previous propagation steps $t < t_j$ are not affected in any way by the measurement procedure. The extracted radiation is then coupled on a single-mode fiber and measured (for further details on the setup see Ref. [348, 347]). Using couplers to collect the extracted photons, we can measure coincidences between all possible modes at each step and experimentally reconstruct the two-photon probability distribution. The single-photon source is described in detail in Appendix B, together with further specifics of the experimental setup.

8.5 Experimental Results

To experimentally verify disorder-induced changes in the violation matrix, we measure both ordered and disordered evolution QW output distributions. In fact, based on the simulation study displayed in Fig. 5, the first quantum correlation enhancement, due to disorder, shall occur at the sixth step of QW. Therefore, the output violation matrices for optimal phase maps are measured up to the sixth step. Since there is no enhancement until the fifth step, the corresponding optimal phase maps can be considered equivalent to the ordered one, while for the sixth step it is possible to find many specific disorder configurations enhancing the nonclassicality in the correlation between two chosen output modes for both the ideal case and the accounting for experimental parameters. The phase map selected for the experimental implementation features phase shifters at step $t = 4$, position $x = -2$ with coin $\sigma = L$ and $x = 2$ with coin $\sigma = R$ are π, while all the others are left to zero; the corresponding experimental output

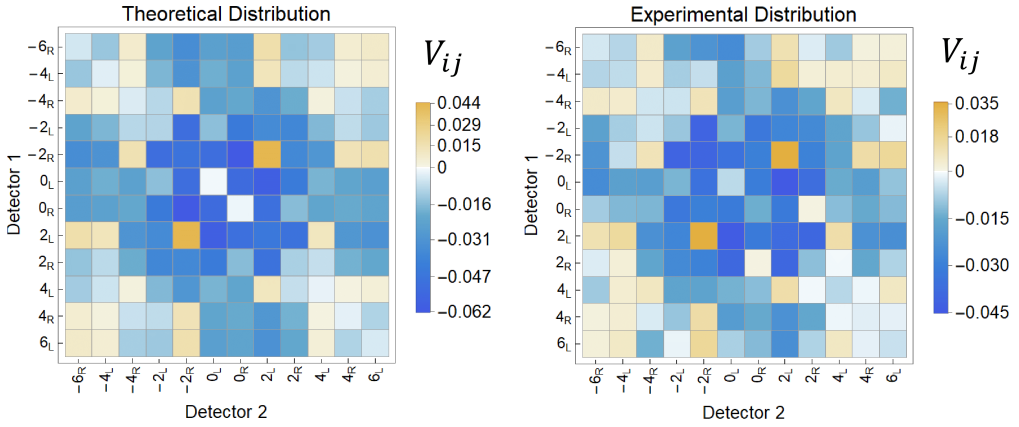

Figure 8.7: **Comparison between the theoretical and the experimental violation matrices at the sixth step for an enhancing disorder configuration.** Numerical simulations are performed taking into account experimental parameters. The expected peak in the value of V is experimentally found, while the measured output coincidence distributions reach globally a similarity value of 97.5 ($\pm$ 1.3)%

violation matrix is shown in Fig. 8.7 compared with the expected one, where the mode $|k\rangle = |x\rangle |\sigma\rangle$ is indicated by x_σ . A strong quantum correlation peak appears at modes $(2_L, -2_R)$ and $(-2_R, -2_L)$ confirming the expectation. As a further relevant result, the experimental stepwise trend for MAV is shown in Fig. 8.8 in comparison with the expected enhanced one obtained by numerical analysis, taking into account experimental constraints. They are plotted together with the ordered case trend to provide a clear display of the beneficial effect of the nonhomogeneous evolution. Theoretical patterns are shown up to the 10th step as a reference. The corresponding trends for the total violation computed over the same output distributions are also reported in Fig. 8.5. Simulations of the MAV values in the ordered case show that the quantum correlation spreads in a homogeneous network so that the values of V_{ij} and the total violation are going to decline as the propagation proceeds. However, as can be seen in Fig. 8.5, the inhomogeneity enriches the quantum correlation between two indistinguishable photons at the given modes. Experimental evidences, reported in Fig. 8.8, show that the very same configuration also enhances the total quantum correlation of the QW. Experimental errors are derived from the Poissonian statistics of the measured coincidences. Deviations from the expected results are mainly due to modest drops in photons indistinguishability along the evolution. Nevertheless, the indistinguishability decline slightly affects the exact violation values, while not changing the overall trend.

8.6 Conclusion

The presented numerical and experimental analysis demonstrates that two-mode quantum correlations due to particle indistinguishability, which disperse through the lattice and rapidly decay in an ordered evolution, can be retrieved after a minimum evolution time by inserting suitable inhomogeneity patterns in the system. By changing the disorder configurations, it is possible to tune the two-mode and total enhancement of nonclassicality in position and intensity; this corresponds to an adaptive network whose parameters evaluation determines the focusing of nonclassical resources in selected modes. These findings allow for enriching quantum correlation through controlling unitary evolution (effective Hamiltonian engineering) of the biphoton. Also, we show that the two-mode quantum correlation diminishes in the case of random-phase disorder in the system, which can be interpreted as a manifestation of detrimental classical noise. Nevertheless, this quantum correlation degradation can be challenged by single realizations of disorder. These results supply a conceptual and practical advance compared to previous studies limited to single-photon disorder-assisted quantum correlation enhancement between two degrees of freedom of the photon [55]. In fact, since violations of Eq.(8.5) indicate biphoton quantum correla-

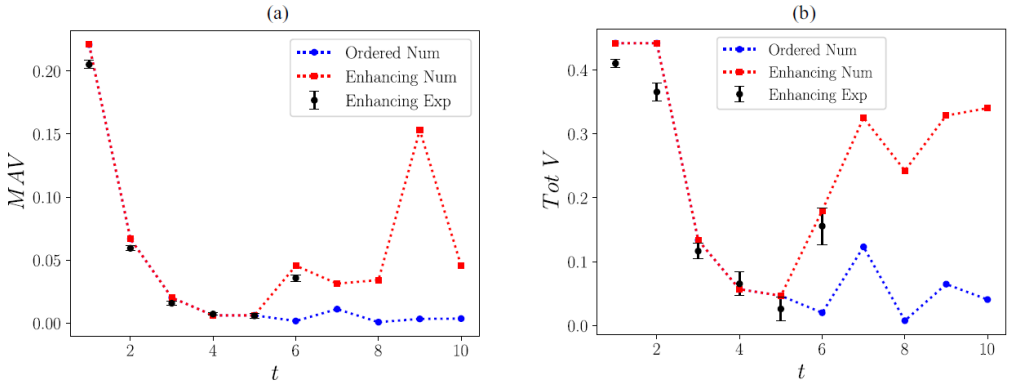

Figure 8.8: **Experimental results compression between the order and the enhancing disordered configuration QW**. Experimental results for (dark dot) (a) MAV and (b) corresponding total violation versus the number of steps. The trends are compared with the simulation for enhancing disorder (red squares) and ordered evolution (blue circles). The expected results are obtained by numerical simulations performed, accounting for experimental parameters and asymmetries, so that the theoretical trends show some discrepancies with respect to those in Fig. 8.4

tions between two modes, our method may also be interesting for quantum metrology issues. It is yet to be understood whether this enhancement procedure can be generalized to systems with $N > 2$ photons or not, which could result in a benchmarking outcome in the context of quantum resource theories.

A. Quantitative analysis of violation

The aim of this section is to provide a clearer interpretation of the quantity V_ij, which, in the main text, is exploited as a quantifier for nonclassicality in bosonic correlations. In particular, we focus on the relationship lying between this quantity and the two-particle boson bunching, the most simple and straightforward effect of bosonic indistinguishability; then, this relationship is extended to the network case, fitting the experimental implementation presented in the main text. As already described in the main text, the violation of the inequality:

$$\frac{2}{3}\sqrt{P_{i,i}P_{j,j}} - P_{i,j} < 0 \tag{8.3}$$

allows to point out the presence of non-classical correlations in photonic systems [404, 407, 405, 406]. The meaning of this simple relation can be traced back to the result of an elemental boson bunching phenomenon, i.e. the HOM effect [130], for the case of non perfectly indistinguishable photons. We consider a photon pair with a given probability q of being distinguishable, traveling through a supposedly balanced BS. After the BS, photons can be measured in three possible combinations of the two output modes and the probability of each combination depends on the probability of the photons being indistinguishable (which is $1 - q$). Therefore, inequality can be written as:

$$\frac{2}{3}(\frac{1}{2} - \frac{q}{4}) - \frac{q}{2} < 0 \tag{8.4}$$

which, in order to be violated, requires a value $q > \frac{1}{2}$, corresponding to photons which are more likely to be indistinguishable than distinguishable. Hence, the inequality 8.3 provides a straightforward quantifier of the effective indistinguishability of photons, in the operative context of boson bunching occurrence. In the general case of a BS network, such as the one exploited in the present work, a value of $V_{ij} > 0$ can be subject to multiple interpretations. In the general case for a pure initial state, after an n step propagation the system will be in a superposition state, which can be written considering the number of

photons traveling in the modes of interest:

$$|\Phi\rangle = \sqrt{1-\Pi}(...)+$$
$$+\sqrt{\Pi}(\alpha_{11}\,|2\rangle_1\,|0\rangle_2 + \alpha_{12}\,|1\rangle_1\,|1\rangle_2 + \alpha_{22}\,|0\rangle_1\,|2\rangle_2)$$

where Π is the overall probability of having both photons in the selected modes, which normalizes the α_{ij} coefficients. while $\{|k_1\rangle\,|k_2\rangle$ are the two output modes under observation, corresponding to combined states of position and coin of the form $|k\rangle =: |x\rangle\,|\sigma\rangle$. We do not consider contributions of other modes included in the first term (...). It is possible, obviously, to also have single-photon states of the two modes, but they would be invisible to coincidence like measurements. In this case, the amount of violation between modes $k1$ and $k2$ can be computed as:

$$V_{12} = \Pi * (\frac{2}{3}\sqrt{|\alpha_{11}|^2|\alpha_{22}|^2} - |\alpha_{12}|^2) \tag{8.5}$$

Therefore, the violation amount depends on two factors:

- The actual nonclassicality of the correlation determining a positive or negative value.
- The global probability of the selected output modes (given by Π)

The first factor is the one pointing out the form of a hypothetically postselected state of the two photons emerging from the considered modes. The higher this factor, the cleaner the distillation of $NOON$ states is by postselection, since it necessarily corresponds to a low $|\alpha_{k_1k_2}|^2$. The second factor is an amplification parameter, which gives the probability of actually finding two photons in the two-modes selected subsystem; hence, it gives the efficiency of the $NOON$ states distillation. In conclusion, the violation value provides an indication over the composite effect of the two parameters; hence, its maximization can be related to either one or the other. Hence, this aspect needs to be taken into account in a hypothetical application of this protocols. For instance, the most external output modes will provide the most pure $NOON$ states, since they are the mere propagation of the first HOM resulting state, but with a very low probability. On the other hand, by means of disorder, it is possible to manipulate the probability for central modes and get an higher efficiency, but at the cost of a nonzero chance of extracting a useless state.

B. Additional Numerical analysis

The highest MAV, besides the first step, is achieved at the output of the ninth step: The MAV for each modes pair (i, j) of the ninth step output distribution was computed by analyzing 10^6 6 different phase maps each. The resulting landscape in Fig. 8.9 shows that this maximum can be achieved in different positions, depending on the chosen enhancing disorder configuration. In particular, it suggests that the proper MAV can be achieved only in "central" modes pairs: The MAV can be induced between different mode pairs by imposing different (yet equally enhancing) phase maps, although that is not possible in modes that have not interfered enough. In fact, photons emerging from central modes will have the most interfering paths, becoming more affected by inhomogeneities along the evolution. This phenomenon is quite understandable considering the underlying network structure of the evolution (Fig. 8.1). Indeed, central modes are subjected to more complex interference phenomena with respect to those close to the boundaries, even more complex when their correlations are considered. This can be directly linked to the amount of MZIs jointly traveled by photons emerging from the two selected modes, i.e., the amount of phase shifts that are imposed over both photons. Therefore, regarding central modes, the manipulation of nonclassicality results is more powerful and effective.

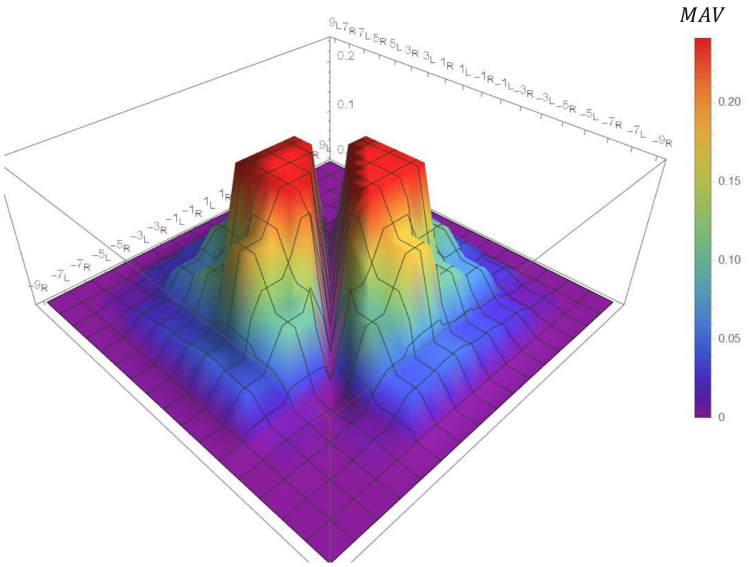

Figure 8.9: **Numerical simulation of** 9 **step MAV landscape**. Plot of the maximum violation achievable for each output modes pair at step 9 obtained by comparing 10^6 different disorder realizations.

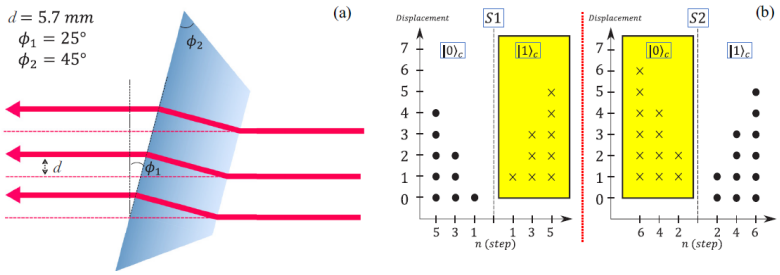

Figure 8.10: **BD and spatial structure of the QW**. (a) A sketch of the BD functioning, provided with relevant geometrical parameters. Through this device, it is possible to realize (b) a spatial structure featured by a distinct localization of each QW mode at any evolution step in the plane orthogonal to the propagation direction.

C. Experimental details

The exploitation of the z axis for the realization of the QW network relies on BDs Fig. 8.11 (a), implementing the unique spatial distribution of the network nodes Fig. 8.11 (b), essential to the actual realization of a space-time disorder. Photon pairs are generated by a high brilliance source realized according to the model described in Ref. [410]: A PPKTP crystal, embedded in a Sagnac interferometer, pumped by a CW laser radiation ($\lambda_p = 405\ nm$), which generates a collinear pair of photons (idler and signal) with opposite polarization at a wavelength of $\lambda_{i,s} = 2\lambda_p = 810\ nm$. They are coupled to a pair of optical fibers and experience an additional path through air before starting the actual QW evolution. They are made indistinguishable in all possible degrees of freedom such as polarization, wavelength, and propagation mode. In particular, we tuned the relative free-space path to get the best bunchin effect when they impinge on the bulk-optics BS (BS1 in Fig. 8.6) for the first time, corresponding to the first step of the QW. The unavoidable, critical free-space adjustment of beam superposition on the BS mainly limits the achieved visibility of HOM effect to an average $V \sim 89\%$.

It is also worth mentioning the experimental method of measurement of the autocorrelation term Γ_{ii} for each i: A BS (BS2 in Fig. 8.6) placed at the output of the setup allows to split two photons traveling the same mode with probability $2RT$ with R (T) being the reflectivity (transmissivity) of the BS. By

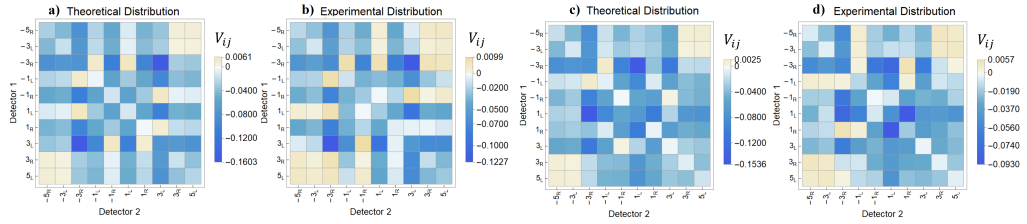

Figure 8.11: **Violation matrices at the fifth step**.Theoretical and experimental violation matrices at the fifth step for [(a) and (b)] ordered evolution and [(c) and (d)] disordered evolution. The disorder configuration has been chosen randomly.

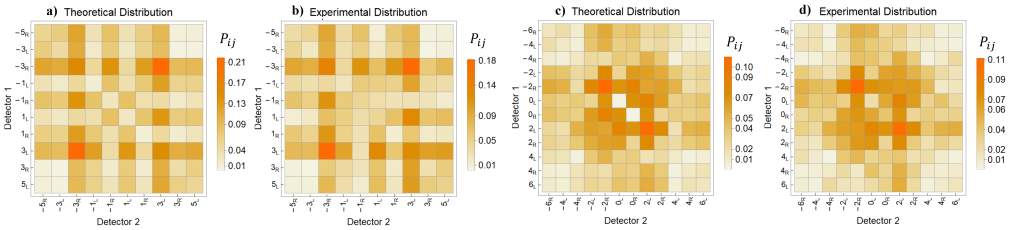

Figure 8.12: **Numerical and experimental coincidences matrices**.Fifth step (a) theoretical coincidences matrix and (b) corresponding experimental measurement output for the ordered QW. Sixth step (c) theoretical coincidences matrix and (d) corresponding experimental measurement output for the optimal disordered configuration. The similarities between theoretical and experimental coincidences distributions are 98 ($\pm$1)% for the fifth step case (a, b) and 97.5 ($\pm$1.3)% for the sixth step case (c, d). Errors are computed accounting for Poissonian statistics of measured coincidences.

carefully characterizing the BS2 we can weigh the measured coincidences in order to compare them with the values of Γ_{ij} for $i \neq j$. Our QW implementation is limited to a six-step evolution because of the internal losses in each unit passage (nearly 17%) and because of both the geometrical structure and the length of the QW that make it difficult to guarantee a high quality spatial overlap of the two photons at each passage of light through the BS1. On the other hand, the main advantages of the QW configuration consist of both phase stability and a flexible disorder configurability and also by the fact that the output distribution for any step of the QW is directly accessible and measurable. As a consequence, this QW platform is a powerful instrument for investigating the dynamical behavior of quantum features under any type of disorder. An evolution of six steps through this setup is enough to investigate on the photon correlation enhancement effect. Indeed, the numerical analysis reported in the main text indicates that a larger number of steps would not have brought any further physical insight into the experiment.

D. Additional Experimental results

The output violation distributions corresponding to the fifth step are shown in Fig. 8.11. They provide a preliminary demonstration of the dependence of quantum correlation distributions from the disorder pattern imposed on the evolution. It is useful to observe the corresponding coincidence matrices for the ordered fifth step and the optimal sixth step (Fig. 8.12). Disorder, as demonstrated in several previous works [72, 52, 348, 410], determines first an effect of spread hindering, also for multiparticle systems. This effect can be noticed even in the case of a single disorder configuration (Fig. 8.12). The manipulation of this localization effect can change the nonclassicality pattern in the output distribution in many different configurations, changing the probability of finding coincident photons between the output modes. Indeed, the corresponding experimental coincidence distributions result in good agreement with the expected ones.

Chapter 9

Generation and bi-photon quantum interference of high-dimensional entangled states via temporal photonic lattices

Abstract

Quantum walks [44] on photonic platforms represent a physics-rich framework for quantum measurement, simulation, and universal computing. Dynamic reconfigurability of photonic circuitry is the key to control the walk and retrieve its full operation potential. Universal quantum processing schemes based on robust gated fiber loops have been proposed but never demonstrated due to gate inefficiencies [89, 90, 91]. Here, we present a potentially scalable quantum walk processor by exploiting temporal photonic lattices based on a coupled fiber-loop system. We use such system to demonstrate critical operations, such as the generation and processing of two- and four-level discrete time-entangled photon pairs. Our scheme enables the realization of quantum interference measurements without post-selection for two-level entangled photons by controlling the quantum walk evolution. Our results introduce practical ways to utilize synthetic dimensions to efficiently perform quantum algorithms, such as quantum phase estimation or boson sampling. This Chapter is related to the Paper 7 (to be submitted) in the List of Publications. The task accomplished in the context of this thesis was to theoretically perform the d-level bi-photon quantum interference using quantum walk model.

9.1 Introduction

Photonic entanglement is a vital resource at the heart of quantum-enhanced technologies, including computation [149, 411, 412], secure communication [413, 414], and sensing [310, 415], owing to photons' noise resilience, ease of control at room temperature, and transmission in both free space and fiber infrastructures (e.g., satellite and fibers, respectively) [416]. Exploiting this resource requires phase-stable quantum circuitries delivering key operations, including entanglement generation, quantum state manipulation, and detection [417, 418, 419]. In conventional all-optical circuits [149, 415, 420], the light flow is controlled by optical paths (i.e., spatial modes) connected in a (real space) mesh intertwined with beam splitters. These devices usually require precise control over several spatially separated optical elements, which are resource heavy as well as increase the complexity of the circuit, especially when the number of operations or quantum modes grows [421]. Synthetic dimensions, created in complex lattices of interacting optical modes [422], promise a scalable solution. They offer resource-efficient quantum processing on large topologies, as they build on the intrinsic parallelism of optical operations at reduced device complexity [423, 424].

Discrete time modes (also known as time bins) have shown many benefits among photons' degrees

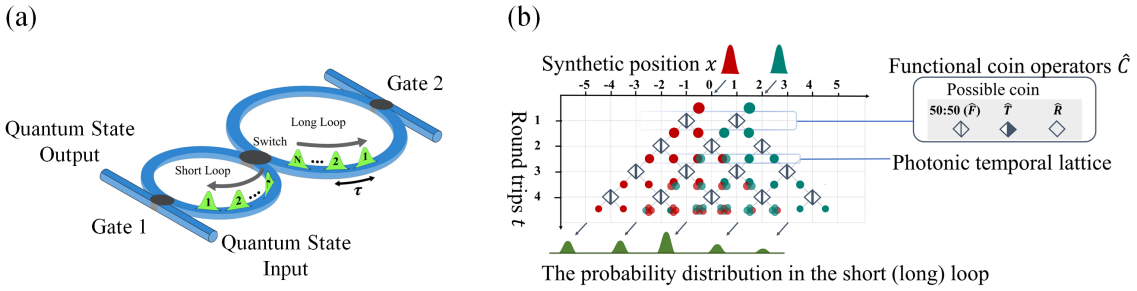

Figure 9.1: (a) The coupled fiber-loops system consists of long and short loops (shown by green and red colors, respectively) connected by an ultra-fast optical dynamical coupler and τ is the time delay among adjacent pulses. (b) The coupled fiber-loops system is mapped to a fully controllable discrete quantum walk network with the coin operator $\hat{C}(x,t)$ as a coupler (including, 50:50 $\hat{F}$, full transmission $\hat{T}$ and reflection $\hat{R}$), where the arrival of photons is a function of the discrete synthetic position x in the lattice and the number of round trips t.

of freedom, including noise resilience and easy manipulation with standard telecom-compatible components [81, 82, 83, 84]. In this regard, temporal photonic lattices (TPLs), in which time bins are realized via temporal delays between optical pulses, offer ideal platforms to create synthetic scalable dimensions. TPLs can straight-forwardly be implemented using accessible fiber technologies, as well as offer excellent testbeds to simulate intriguing effects, including parity-time symmetry [85, 86], superfluidity of light [87], and topological matters [88]. However, despite the multiple proposals to use TPLs for quantum processing [89, 90, 91, 92] experimental implementations are halted by inefficiency of current devices, such as low-error tolerance and gate inefficiencies.

In this work, we present a novel route towards employing TPLs for practical and scalable quantum information processing on discrete time-entangled photon states. We experimentally realize the TPL on a fully fiber-integrated coupled loop system and use it for bi-photon state preparation and interference based on the discrete-time quantum walk [44, 92]. Building on the dynamic control over the quantum circuitry, we can perform and optimize time-bin two-and four-level interference of two photons.

9.2 Result

In our experiment, we operate on a one-dimensional synthetic TPL created through an unbalanced fiber loop system with a $\delta l = 20\ m$ difference between the length of the two loops. Light can enter the system at defined modes (i.e., lattice grid points) in one loop and may dynamically couple to the other loop through an ultra-fast optical coupler that acts as a dynamic interconnect between the loops (See Methods). As pulses propagate through two loops, they arrive at the coupler at different times (see Fig. 9.1 (a)), delayed by $\tau = \delta l/v = 100\ ns$, where v is the speed of light in the fiber, and hop to their next-neighboring mode at the upcoming round trip. In other words, the delay between the pulses propagating within the two loops is equivalent to a transverse dimension in a conventional photonic mesh lattice resembling the spatial quantum walk model [44, 92], as illustrated in Fig. 9.1 (b). The quantum walker can be defined as $|\psi\rangle = \sum_n \alpha_n |n\rangle$ with probability amplitude α_n of finding the walker at mode $|n\rangle$. The mode $|n\rangle$ can be written as $|n\rangle = |x\rangle_{\mathrm{p}} |\sigma\rangle_{\mathrm{c}}$, where c and c label the position and the coin states, respectively. In our platform, the coin state $|\sigma\rangle_{\mathrm{c}} = \{|\mathrm{S}\rangle_{\mathrm{c}}, |\mathrm{L}\rangle_{\mathrm{c}}\}$ is given by the short ($|\mathrm{S}\rangle_{\mathrm{c}}$) and the long ($|\mathrm{S}\rangle_{\mathrm{c}}$) paths in the loop, while the synthetic position $|x\rangle_{\mathrm{p}}$ is given by the time bin. The whole evolution of a quantum walker can be attributed to the repetitive action of the unitary operator $\hat{U} = \hat{S} \cdot \hat{C}(x,t)$, which is the product of the shift $\hat{S}$ and the time-dependent coin $\hat{C}(x,t)$ operators. A unique feature of our all-fiber design is the dynamic tuneability of the coin's reflectance/transmittance ratio using an ultra-

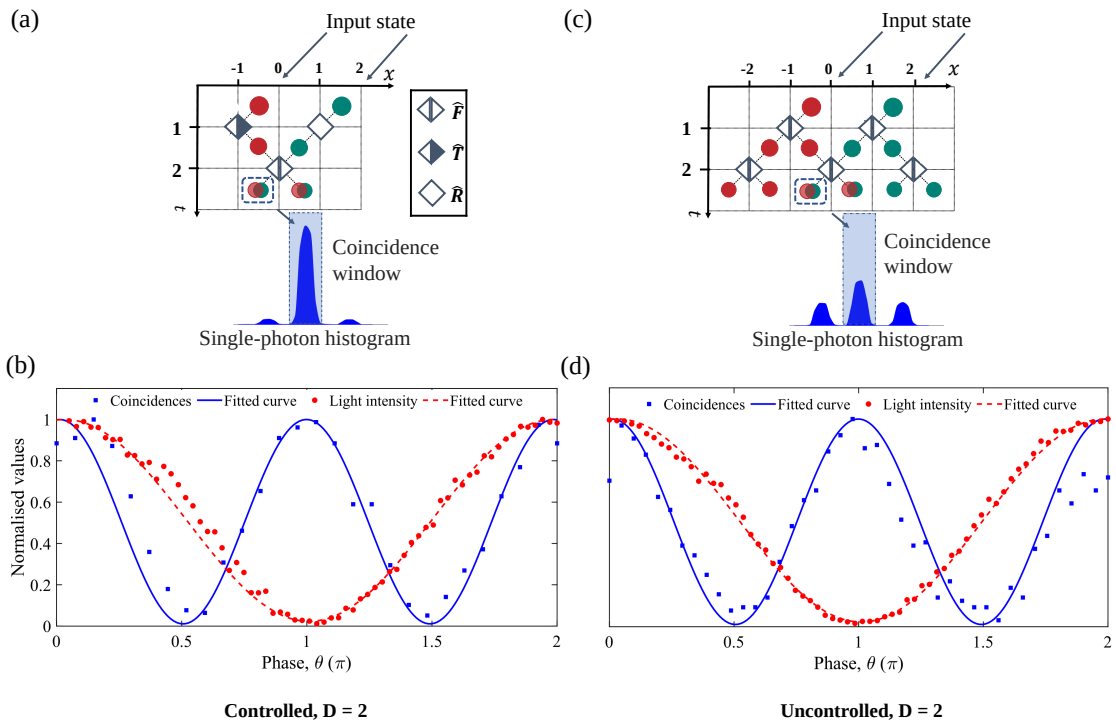

Figure 9.2: Schematic illustration of a different sequence of coin operations and quantum interferences of two-level bi-photon entangled states. We show two-photon coincidence counts (b) and (d) (in blue squares) of two-level bi-photon entangled states obtained based on controlled (a) and uncontrolled (c) schemes. Data are taken at a single site (marked by a dashed rectangle and light blue box in single photon histogram in (a) and (c)) for varying relative phase θ and show a raw visibilities of $V_{d=2} = 95.45\%$ in (b), $V'_{d=2} = 90.17\%$ (d). Classical intensities (in a solid red circle symbol) of two and four trains of pulses using different measurement strategies (a) and (d). Experimental data are fitted with the expected theoretical quantum interference in solid blue and red-dash lines for quantum and classical interference, respectively (See Methods).

fast coupler allowing for transitions from full transmission to equal splitting (i.e., 50:50 ratio) and full reflection within $50\ ns$ (i.e., half of the time bin spacing), See Methods for a detailed description. We have used the dynamic TPL to prepare discrete time entangled photon pairs (See Methods) and perform quantum interference measurements. In a typical measurement, we prepare two-photon states in the form $|\psi_d\rangle = \frac{1}{\sqrt{d}} \sum_{k=0}^{d-1} e^{2ik\theta} |k\rangle_s |k\rangle_i$, where $d = 2,\ 4$ and θ denotes the relative phase between different time bins. Here, the time width is typically $7\ ps$ ($150\ GHz$ bandwidth), while the temporal delay between the bins is given by τ. We thus inject the entangled state into the coupled loops and tune their evolution within the TPL. Finally, from the output of the coupled fiber loop, each photon is routed through a separate channel to a superconducting nanowire single-photon detector for coincidence counting [425]. Thus, we perform quantum interference measurements by realizing projections on product states of the form (See Methods) [425]:

$$|\psi_p\rangle = \frac{1}{d} \left(\sum_{k=0}^{d-1} e^{ik\theta} |k\rangle_s \right) \left(\sum_{k=0}^{d-1} e^{ik\theta} |k\rangle_i \right) \tag{9.1}$$

We first exploit the dynamic control over the quantum walk in the qubit case to perform post-selection-free quantum interference measurement (See Methods).

In a controlled scheme as illustrated in Fig. 9.2 (a), we inject the two-photon qubits $|\psi_2\rangle = \left(|-1\ \mathrm{S}\rangle_s |-1\ \mathrm{S}\rangle_i + e^{2i\theta} |1\ \mathrm{S}\rangle_s |1\ \mathrm{S}\rangle_i \right)/\sqrt{2}$ (indices s and i stand for signal and idler, respectively) into the short loop and optimize their evolution to perform direct interference measurement. As schematically illustrated in

Fig. 9.2 (a), this is realized by directing the photon(s) in the earlier time bin (position $x = -1$) into the long loop and by fully transmitting the photon(s) in the later time bin (position $x = 1$) into the short loop using the tuneable coupler. The delay experienced by the time bins in the second round-trip allows them to coherently interfere as both arriving at the coupler (now 50:50 ratio) simultaneously. Finally, we measure coincidences between the photons extracted from the short loop as a function of phase θ (see Fig. 9.2 (b)) across the entire gated time window (i.e., $550\ ns$) of the detectors, meaning that no post-selection is applied. Such a controlled strategy can precisely implement quantum interference without any noise subtraction with maximum detection efficiency $p_0 = 1$ (See Methods). Fitting the expected interference response to the data yields a raw visibility (i.e., including background noise) of $V_{d=2} = 90.17\%$, which exceeds the threshold of 70.71% required to violate the Bell inequality [425]. We also repeat the same measurement with classical light and compare the obtained normalized light intensity in Fig. 9.2 (b) with the quantum interference pattern (Fig. 9.2 (b)). The latter shows half of the period of classical light due to the nonclassicality of the sources. Our setup further allows a comparison between this scheme displayed in Fig. 9.2 (a) with that of an uncontrolled quantum walk (i.e., based on a fixed 50:50 coupling ratio), as illustrated in Fig. 9.2 (c).To this end, we let the photons propagate for two round trips. By post-selecting the coincidence events in the central mode of the short loop, we can measure quantum interference as shown in Fig. 9.2 (d), yielding a raw visibility of $V'_{d=2} = 95.45\%$. In our controlled scheme, negligible side peaks appear on sides as shown in the single-photon histogram in Fig. 9.2 (a), which implies that post-selection in the time bins is avoidable in that case. In addition, the uncontrolled quantum walk has significantly lowered the probability of detection to $p_0 = 1/4$ (See Methods). The guided evolution of the controlled quantum walk enhances the coincidence counts from 21 to 77 per minute and practically reduces the time needed in the post-selection-free configuration. It is worth mentioning that the lower visibility in the post-selection-free case is due to the imperfect behavior of the couplers.

Another unique feature of our TPL is its scalability to higher time modes. Increasing time-bin dimensionality typically requires the implementation of multiple-arm unbalanced interferometers to appropriately project the modes for quantum state processing. However, the stabilization of multiple-arm fiber interferometers is highly resourceful, time-consuming, and impractical, while our system bypasses the need for multiple-arm interferometers. Here, we demonstrate the scaling properties of TPLs by injecting four-level (i.e., $d = 4$) time-bin entangled photon pairs in the form $|\psi_4\rangle = \big(|-3\,\mathrm{S}\rangle_s |-3\,\mathrm{S}\rangle_i + e^{2i\theta} |-1\,\mathrm{S}\rangle_s |-1\,\mathrm{S}\rangle_i + e^{4i\theta} |1\,\mathrm{S}\rangle_s |1\,\mathrm{S}\rangle_i + e^{6i\theta} |3\,\mathrm{S}\rangle_s |3\,\mathrm{S}\rangle_i \big)/2$ into the loop system. We have performed quantum interference measurements on indeterministic quantum walk through the fiber loop system. However, we bi-photon quantum interference measurements are not possible with this scheme (see Suppl. Information for details). Hence, it was necessary to employ a deterministic quantum walk scheme. As a first controlled scheme in Fig. 9.3 (a), the coupler is set to 50:50 in the first two roundtrips and then to full reflection in the third roundtrip. Afterward, the coupler is assigned to 50:50 splitting during the last roundtrip to mix all four bins. Eventually, we measure coincidences between the photons at the central mode out of seven extracted from the short loop after evolution. Coincidences between photons are shown in Fig. 9.3 (b) for varying phase θ. This procedure results in a raw visibility of $V_{d=4} = 91.55\%$, which exceeds the threshold of 81.7% necessary to violate four-dimensional Bell's inequality [425], as well as in a coincidence detection efficiency of $p_0 = 1/4$. The second control pattern (maximally controlled) was employed to maximize the detection efficiency and directly operates on the quantum state by slicing it into two parts as illustrated in Fig. (9.3) (c).

Here, the coupler keeps the first two-time bins ($|1\,\mathrm{S}\rangle$ and $|1\,\mathrm{S}\rangle$) in the short loop and sends the other two ($|-1\,\mathrm{S}\rangle$ and $|-3\,\mathrm{S}\rangle$) into the long loop in the first roundtrip. Then, the pure reflection is carried out in the second roundtrip, followed by the 50:50 ratio in the last two roundtrips. After extracting the photons from the short loop, we post-select the central mode out of only three modes. Such an optimized control strategy leads to quantum interference with maximum probability for coincidence detection (i.e., $p_0 = 1$). The biphoton interference is shown in Fig. 9.3 (d) with raw visibility of $V'_{(d=4)} = 89.51\%$. Despite the increase in the coincidence counts from 4.5 to 8.3 per minute, the achieved visibility is lower due to the imperfect temporal response of the coupler.

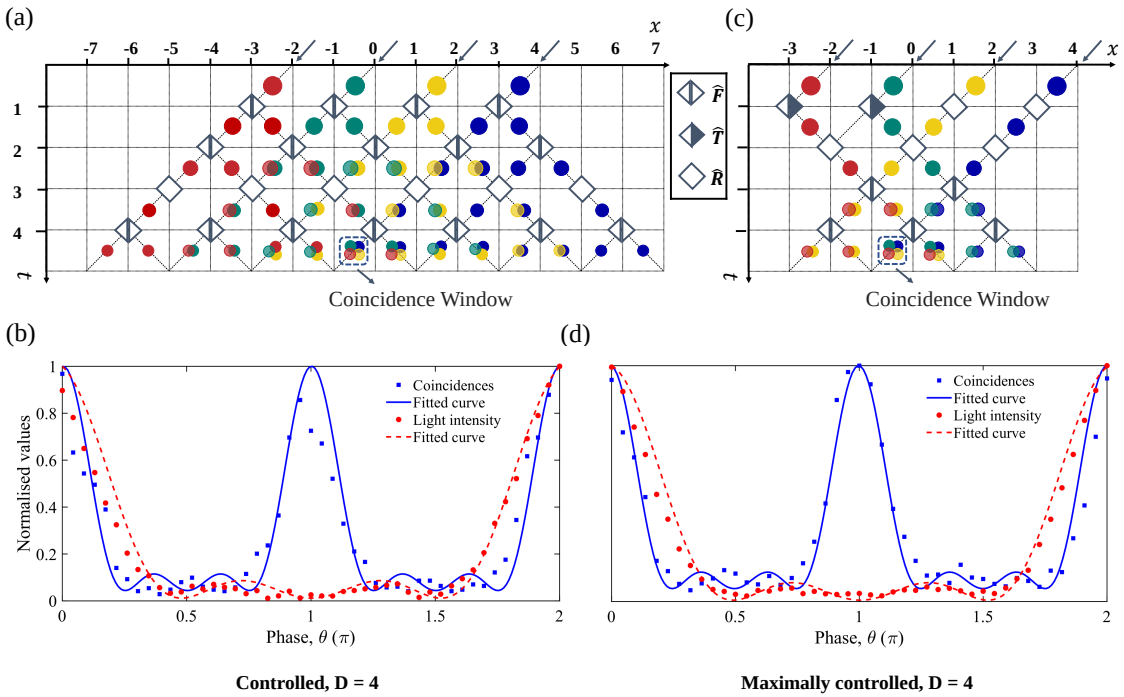

Figure 9.3: Quantum interference measurements of four-level bi-photon entangled states using two different controlled schemes of coin operations (a) and (c). Using these schemes, we show two-photon coincidence counts (b) and (d) (in blue squares) of four-level bi-photon entangled states by varying relative phase θ with raw visibilities of $V_{d=4} = 95.45\%$ in (b), $V'_{d=4} = 89.55\%$ in (d). The classical intensities of four trains of pulses with these two controlled schemes are shown by solid red circle symbols in (b) and (d).

9.3 Discussion

We provide a first proof-of-principle experiment demonstrating a TPL as a platform for the preparation, generation, and processing of high-dimensional time-bin entangled photon pairs based on a dynamically coupled fiber loop system. The versatility of our realization allows us controlling the walk of a biphoton state such that it results in a post-selection-free quantum interference measurement for two levels. It further allows the optimization of the quantum walk evolution for higher detection efficiency and coincidence counts potentially for any number of levels. Furthermore, our measurement strategy can be theoretically generalized to perform quantum interference for arbitrary d levels (See Methods). Hence, the proposed route may inspire new designs for engineering TPLs capable of generating and processing entangled modes higher than four and performing the biphoton quantum interference with maximum efficiencies. Controlled quantum walks along TPL offer a cost-effective, practical route towards complex state operations with considerably reduced instabilities and performance limitations of the numerous optical elements required to perform comparable operations in photonic devices based on path and OAM modes [66, 68, 93, 57]. We have shown that a dynamically coupled fiber loop can replace a cascade of unbalanced optical Mach-Zehnder interferometers without any fine adjustments of successive delays. Moreover, our entire implementation is fiber-integrated and compatible with telecom infrastructures, being hence cost-effective and practically applicable. However, faster optical couplers (e.g., 1 ns response time) with lower injection losses (i.e., < 1 dB) are pivotal to elevate the technological potential of our prototype. Yet, our results demonstrate how our TPL based on synthetic scalable dimensions can be used to perform a variety of quantum information protocols, such as quantum tomography, phase discrimination, and sensing.

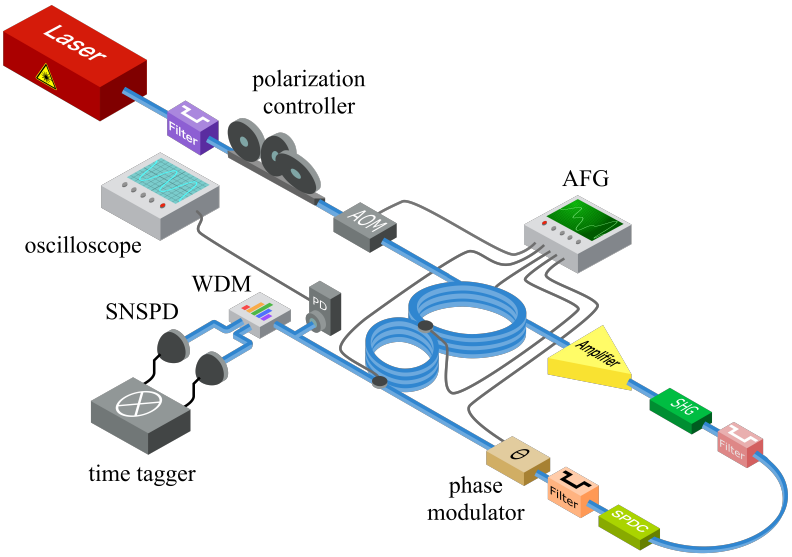

Figure 9.4: Experimental setup. A coupler connects two polarization-maintaining fiber loops of 120 m (600 ns) for the long loop and 100 m (500 ns) for the short loop. Arbitrary function generators (AFG) control the coupler's transmittance dynamically. The set-up also includes: a pulsed laser, periodically poled lithium niobate (PPLN) nonlinear crystals to generate photons through second harmonic generation (SHG) and spontaneous parametric down-conversion (SPDC), phase modulator, wavelength demultiplexer (WDM), oscilloscope, photodetector (PD), and two superconducting nanowire single photon detectors (SNSPDs). The oscilloscope and PDs are used in the classical part of the experiment.

9.4 Method

Experimental setup. The sketch of the experimental setup used to realize synthetic dimensions is presented in Fig 4. Our scheme has two main scopes, i.e., generating the time-entangled photon pairs and performing quantum state projections. For photon pair generation, a single pulse from a femtosecond fiber laser source (1550 nm wavelength, 10 MHz repetition rate, and timing jitter $< 1ps$) is sent into the fiber-loop system after its repetition rate and bandwidth are reduced to 181.8 kHz and 0.3 nm using an acousto-optic modulator (AOM) and a tunable filter, respectively. Due to the length of the fiber loops (220 m (1100 ns) combined), reducing the repetition rate is necessary to have enough time to complete the measurement procedure.

Afterward, the light pulse is injected into the longer loop to enter the fiber system through a dynamical coupler. The pulse is then split by the central coupler into two pulses, one circulating in the longer and the other in the shorter loop. Both couplers are precisely controlled by arbitrary function generators (AFGs). The pulses return to the coupler with a 100 ns time delay between them before they are split again by the dynamical (i.e., the central). Repeating this process in each round trip eventually leads to the generation of a pulse train. In the next step, the pulse train pumps a cascade of two periodically poled lithium niobate (PPLN) nonlinear waveguides. The first PPLN converts two pump photons into two one at 775 nm during the second harmonic generation (SHG) process. Residual pump photons are filtered out and a second PPLN splits the newly generated photon into two entangled photons at 1550 nm via spontaneous parametric down-conversion (SPDC). A time dependent phase is imprinted on the down converted photons to allow for quantum interference measurements. Finally, photon pairs are generated in a time bin entangled state of the form $|\psi_d\rangle = \frac{1}{\sqrt{d}} \sum_{k=0}^{d-1} e^{2ik\theta} |k\rangle_s |k\rangle_i$, where, in the cases analyzed here, $d = 2,\ 4$. These dimensionalities are given by the injection of two and four pulses after two and four roundtrips, respectively. This results in a two-photon entangled state, where each photon is in a superposition of two- and four-time modes, respectively. Those generated and phase modulated entangled photon pairs are reinserted into the loop for further interference measurements. After they have interfered, signal and idler are separated by a dense wavelength division multiplexer (DWDM) at 1553 nm

and $1547\ nm$, respectively, and then routed to two superconducting nanowire single-photon (SNSPD) detectors. A time tagger records timing events, which are used for coincidence measurements.

Uncontrolled operation: In the uncontrolled configuration, the central coupler was maintained at a fixed 50:50 ratio throughout the experiment. We used classical light for setup alignment and sent two or four pulses directly to the loop system without passing through a PPLN crystal cascade. After the required number of roundtrips, we obtained the data and transmitted it to classical detectors, repeating this procedure for a range of phase values. Subsequently, we performed quantum measurements by sending a prepared quantum state into the loop system. After the required number of roundtrips, we obtained the data and separated the signal and idle components. These components were then sent to separate channels of single photon detectors to generate single photon histograms. We identified different bins and measured coincidence counts within a specified window, repeating this procedure for a range of phase values. In the case of the two bins, the measurement of each phase point took of 3 minutes. Subsequently, we utilized Eq. (9.2) to perform curve fitting and determine the visibility, as demonstrated in Fig. 9.2 (d) of the main manuscript. In the four-bin case, the uncontrolled measurement scheme proved to be insufficient for performing measurements for the violation of the Bell inequality. Even under ideal conditions, 100% visibility is not possible with this configuration, as theoretical calculations showed, so controlled measurement schemes are used to obtain meaningful data.

Controlled operation: In the case of controlled operations, the measurement procedure resembled that of the uncontrolled case, with the exception that the central coupler was dynamically controlled instead of being statically fixed at 50:50. To achieve this, we utilized Matlab to generate precise waveforms for different schemes, which were then transferred to the variable coupler as per the desired application. Here also, prior to conducting quantum experiments, we carried out experiments using classical light for alignment. In the scenario with two bins, the controlled configuration led to a significant decrease in photon counts outside coincidence window compared to the uncontrolled scheme, as evidenced by the single-photon histograms presented in Fig. 9.2 (a and c) of the main manuscript. While no temporal filtering was required to measure the coincidence counts, the number of coincidences remained the same for a specific coincidence window and the entire round-trip window. Each phase point measurement had a duration of approximately 1 minute. Finally, we utilized Eq. (9.2) to fit the curve and determine visibility, with the results presented in Fig. 9.3 (b) of the main manuscript. For the scenario with four bins, it is necessary to conduct deterministic measurements in order to perform biphoton quantum interference. Two different schemes were investigated: one involving the distribution of photons across seven bins in each loop after four round trips, resulting in a low count in the coincidence window but still sufficient to draw conclusions; and another controlled scheme, where photons were maximally controlled, resulting in a lower number of bins (three in this case) after the same four round trips and a higher count in the coincidence window. Each phase point measurement took approximately 60 minutes, and curve fitting using Eq. (9.2) was performed to determine visibility. The results are presented in Fig. 9.3 (b and d) of the main text.

Theoretical aspect: Quantum interference measurement. We performed biphoton quantum measurements to extract the visibility associated with high dimensional states $|\psi_d\rangle = \frac{1}{\sqrt{d}}\sum_{k=0}^{d-1} e^{2ik\theta}|k\rangle_s|k\rangle_i$ with two $d = 2$ and four $d = 4$ dimensions. The intended quantum interference measurement is $E_p = |\psi_p\rangle\langle\psi_p|$ [425], result in Eq. (9.1). Thus, the expected ideal quantum interference is $P_d = |\langle\psi_p|\psi_d\rangle|^2$. We implemented the measurement by evolving the biphoton according to a controlled unitary evolution for t roundtrips, which is $|\psi_d(t)\rangle = \Pi_{n=1}^{t}\hat{\mathcal{U}}_n|\psi_d\rangle$, where $\hat{\mathcal{U}}_n$ is the controllable unitary evolution at roundtrip n. Ultimately, we choose a proper coincidence window between the idler and signal, and then the expected biphoton quantum inferences are given by

$$\begin{aligned} P_2(\epsilon_2) =& \frac{1}{4}\left(1+\epsilon_2\cos\left(2\theta\right)\right) \\ P_4(\epsilon_4) =& \frac{1}{2^6}\left(4+\epsilon_4\left(3\cos\left(2\theta\right)+2\cos\left(4\theta\right)+\cos\left(6\theta\right)\right)\right) \end{aligned} \tag{9.2}$$

where ϵ_2 and ϵ_4 are the result of a symmetric noise model [425], and depicts the decoherence process, a transition from a pure to a mixed state.

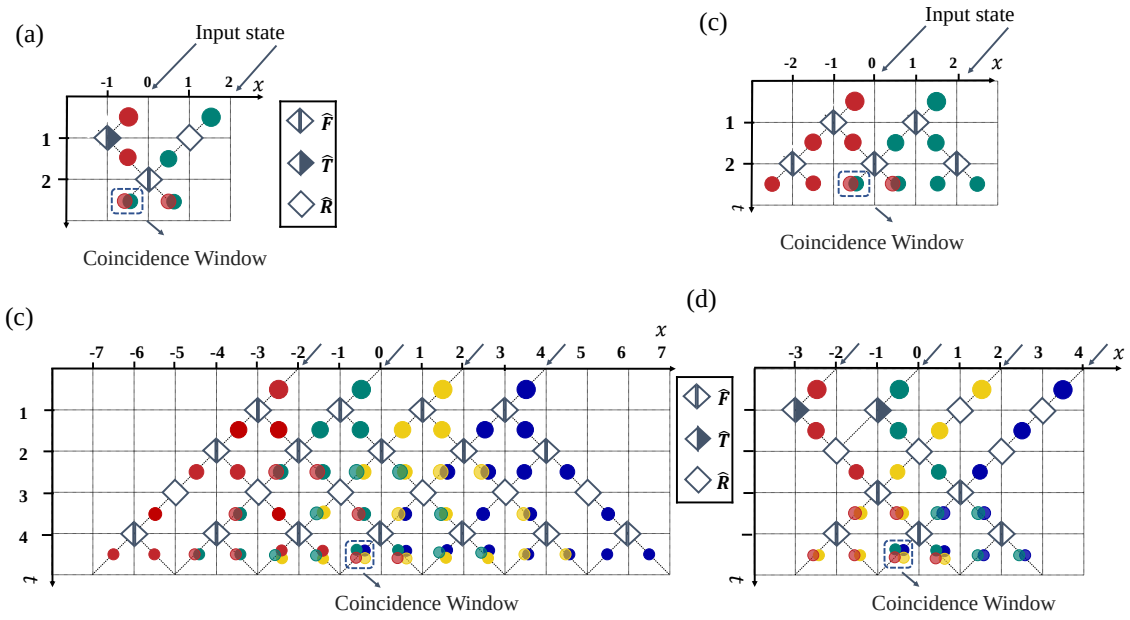

Figure 9.5: Schematic illustration of a different sequence of operations to implement quantum interference measurement: (a) controlled, (b) un-controlled quantum walk schemes for two-level biphoton interference, (c) controlled I, (d) controlled II quantum walk schemes for four-level biphoton interference.

Supplementary Information

1. Discrete-time quantum walk.

A discrete-time quantum walk (DTQW) on the line [353] describes the dynamics of photons on a one-dimensional temporal photonic lattices (TPLs). Many photonic platforms have been developed to implement DTQWs using different optical degrees of freedom to encode the coin operation and the position of the quantum walker [71, 328, 70]. Each mode of the discrete quantum walk, i.e., $|n\rangle = |x\rangle_{\mathrm{p}} |\sigma\rangle_{\mathrm{c}}$, comprises two degrees of freedom, i.e., the (synthetic) position $|x\rangle_{\mathrm{p}}$ and the coin state with basis $|\sigma\rangle_{\mathrm{c}} = \{|\mathrm{S}\rangle_{\mathrm{c}}, |\mathrm{L}\rangle_{\mathrm{c}}\}$ where $|\mathrm{S}\rangle_{\mathrm{c}}$ and $|\mathrm{L}\rangle_{\mathrm{c}}$ stand for the short and the long paths in the loops, respectively. The single-particle state can always be written as a superposition of the quantum walker modes $|\psi\rangle = \sum_n \alpha_n(t) |n\rangle$, where $\alpha_n(t)$ is the probability amplitude of finding the quantum walker at mode $|n\rangle$. The single-step quantum walk evolution $\hat{U} = \hat{S}.\hat{C}(x,t)$ is given by the product of the shift $\hat{S}$ and the time-dependent coin $\hat{C}(x,t)$ operators, where the latter acts on the coin state, and then the former moves the quantum walker according to its coin. The shift operator reads [353]

$$\hat{S} = \sum_x |x+1\rangle_{\mathrm{p}} |x\rangle_{\mathrm{p}} \otimes |\mathrm{L}\rangle_{\mathrm{c}} \langle \mathrm{L}|_{\mathrm{c}} + |x-1\rangle_{\mathrm{p}} |x\rangle_{\mathrm{p}} \otimes |\mathrm{S}\rangle_{\mathrm{c}} \langle \mathrm{S}|_{\mathrm{c}} \tag{9.3}$$

which mimics different delays that photons experience in different loops. The coin operator has the form $\hat{\mathcal{C}}(x,t) = \sum_x |x\rangle \langle x| \otimes \hat{C}$, which can be expressed in terms of matrix representation as

$$\hat{C}(x,t) = \begin{pmatrix} \cos\theta_{x,t} & \mathbf{i}\sin\theta_{x,t} \\ \mathbf{i}\sin\theta_{x,t} & \cos\theta_{x,t} \end{pmatrix} \tag{9.4}$$

when written in the coin bases $|\sigma\rangle_{\mathrm{c}} = \{|\mathrm{S}\rangle_{\mathrm{c}}, |\mathrm{L}\rangle_{\mathrm{c}}\}$. Here, the factor $\theta_(x,t)$ is responsible for the transmission and reflection coefficients. In our scheme, the coin operator is experimentally realized by an

ultra-fast optical dynamical coupler. The coin operator in Eq. (9.4) is not the most generic form for the quantum coin operator [327]. However, our optical dynamical coupler simulates various operations within different time bins and roundtrips with different transmission/reflection ratios. These include the transmission coin $T(x,t)$ (with $\theta_{x,t} = \pi/2$), which sends the walker from the short (long) to the long (short) loops, the Fourier coin $F(x,t)$ with 50:50 splitting ratios (with $\theta_(x,t) = \pi/4$), which puts the walker in the superposition of the two loops, as well as the reflection coin $R(x,t)$ (with $\theta_(x,t) = 0$) , which keeps the light in the short (long) loop. It is worth recalling that the single-step unitary evolution of two quantum walkers is given by $\hat{\mathcal{U}}_t = \hat{U}_t^s \otimes \hat{U}_t^i$, where the first operator acts on the signal and the latter acts on the idler [426]. The evolution of the quantum walker after the t-th step is given by $\hat{\mathcal{U}}_t = \Pi_{n=1}^t \hat{\mathcal{U}}_n$, which provides t repetitive actions of the independent single-step unitary evolution of two quantum walkers.

2. Discrete-Time quantum walk as a measurement device.

It has been shown that DTQW can be used to implement a generalized measurement in terms of a positive operator value measure (POVM), $\sum_i \hat{E}_i \hat{E}^\dagger = \mathbf{I}$ with $\mathbf{I}$ denoting the identity operator and ($\hat{E}_i$) representing POVMs. $\hat{U} = \sum_i |i\rangle \langle \psi_{\rm in}|$ maps maps the initial state $|\psi_{\rm in}\rangle$ into the final state $|i\rangle$. Therefore, projective measurements $\hat{M} = |i\rangle \langle i|$ on the final state corresponds to POVMs on the initial state. Also, the probability of measuring the ith POVM element on a quantum state density matrix ρ is $p_i = \mathrm{Tr}\,(E_i \rho)$ where Tr labels the trace. The intended POVM that leads to quantum interference measurement is $\hat{E}_p = |\psi_p\rangle \langle \psi_p|$ with

$$|\psi_p\rangle = \frac{1}{d} \left(\sum_{k=0}^{d-1} e^{ik\theta} |k\rangle_s \right) \left(\sum_{k=0}^{d-1} e^{ik\theta} |k\rangle_i \right) \tag{9.5}$$

Thus, the expected quantum interference is $P_d = |\langle \psi_p | \psi_d \rangle|^2$ which is given by

$$P_d = \frac{1}{d^3} \frac{\sin^2 d\theta}{\sin^2 \theta} \tag{9.6}$$

To perform the quantum interference pattern, we let the system evolve according to a controlled unitary evolution for t round-trips, which is $|\psi_d(t)\rangle = \Pi_{n=1}^t \hat{\mathcal{U}}_n |\psi_d\rangle$.Then, the projection measurement $\hat{M} = |-1\ \mathrm{S}\rangle_s |-1\ \mathrm{S}\rangle_i \langle -1\ \mathrm{S}|_s \langle -1\ \mathrm{S}|_i$ is applied, corresponding to the coincidence between the signal and idler photons at time slot -1 in the short loop corresponding to the mode $|-1\rangle_{\rm p} |\mathrm{S}\rangle_{\rm c}$. Therefore, the expected quantum interference can be rewritten as

$$P_d = \langle \psi_d(t)| \hat{M} |\psi_d(t)\rangle / p_0^d \tag{9.7}$$

where $p_0^d \in [0,1]$ is a constant factor ranging same as detection efficiency. The factor p_0 allows having different evolutions that provide the projection measurement with different detection efficiency. In other words, the quantum interference pattern, given by Eq. (9.6), can be realized with various evolutions of the two photons.

2..1 Controlled evolutions to perform two-and four-level biphoton quantum interference measurements.

We provide a theoretical framework for different evolution operators of the biphoton states to realize quantum interference measurements, as shown in the main text. As a first example, we design the scheme to measure the quantum interferences. After injecting the qubit state $|\psi_2\rangle = \big(|-1\ \mathrm{S}\rangle_s |-1\ \mathrm{S}\rangle_i + e^{2i\theta} |1\ \mathrm{S}\rangle_s |1\ \mathrm{S}\rangle_i \big)/\sqrt{2}$ into the short loop, we let it evolve with two independent unitary operators. The

unitary operation for the first step is

$$\begin{aligned}\hat{\mathcal{U}}_{TR} =&\hat{S}_s.\left(\sum_x |-x\rangle_{\mathrm{p}}\langle -x|_{\mathrm{p}}\otimes\hat{T}_s+\sum_x |x\rangle_{\mathrm{p}}\langle x|_{\mathrm{p}}\otimes\hat{R}_s\right)\\ &\otimes\hat{S}_i.\left(\sum_x |-x\rangle_{\mathrm{p}}\langle -x|_{\mathrm{p}}\otimes\hat{T}_i+\sum_x |x\rangle_{\mathrm{p}}\langle x|_{\mathrm{p}}\otimes\hat{R}_i\right)\end{aligned} \tag{9.8}$$

which sends the photons at the earlier time bin (position $x=-1$) into the long loop with the transmission coin $\hat{S}_{i(s)}$ and keeps those at the latter time bin (position $x=1$) into the short loop using $\hat{R}_{i(s)}$. In the next step, we let the photon interfere (at $x=0$) with the Fourier coin $\hat{F}_{i(s)}$ given by the unitary operator

$$\hat{\mathcal{U}}_F=\hat{S}_s\left(\mathbf{I}_{\mathrm{p}}\otimes\hat{F}_s\right)\otimes\hat{S}_i\left(\mathbf{I}_{\mathrm{p}}\otimes\hat{F}_i\right) \tag{9.9}$$

where $\mathbf{I}_{\mathrm{p}}$ is the identity operator over the position space. Thus, after these two steps, the evolved state is $|\psi_2(t=2)\rangle=\hat{\mathcal{U}}_F\cdot\hat{\mathcal{U}}_{TR}|\psi_2(t=0)\rangle$, as illustrated in Fig. 9.5 (a). Finally, the exact interference in Eq. (9.6) with $d=2$ is obtained by performing the projective measurement $\hat{M}$. However, the quantum system interacts inevitably with its surrounding environment [40]. Therefore, one can consider the symmetric noise model as [40] $\hat{\rho}=\epsilon|\psi_d(t)\rangle\langle\psi_d(t)|+\frac{1-\epsilon}{d}\hat{\mathbf{I}}$ where ϵ is the pureness of prepared state $|\psi_d(t)\rangle$, d is the state dimension. Ultimately, the quantum interference reads

$$P_2(\epsilon_2)=\frac{1}{4}\left(1+\epsilon_2\cos\left(2\theta\right)\right) \tag{9.10}$$

which is obtained by performing the projective measurement as $P_2(\epsilon_2)=\mathrm{Tr}\left(\hat{M}\hat{\rho}(t)\right)$. It is worth recalling that Fig. 9.2 (a) of the main text shows the experimental quantum interference. As mentioned in the main text, the same quantum interference pattern can be observed with the uncontrolled quantum walk (i.e., based on a fixed 50:50 coupling ratio, as shown in Fig. 9.5 (b)) for two round trips. Similarly, the expected interference Eq. (9.10) is obtained using the measurement outcome as $P_{d=2}=\langle\psi_2(t=2)|\hat{M}|\psi_2(t=2)\rangle/p_0^{d=2}$, where $p_0^{d=2}=1/4$ is the detection efficiency and $|\psi_2(t=2)\rangle=\hat{\mathcal{U}}_F\cdot\hat{\mathcal{U}}_F|\psi_2(t=0)\rangle$ is the evolved state. The slightly different visibilities measured in our experiment, i.e.,$V_{d=2}=90.17\%$ and $V'_{d=2}=95.45\%$ for controlled and uncontrolled cases, respectively can be justified as different noise amounts affecting the two evolution schemes due to the executions of different operations.

The scalability of our platform allows us to perform DTQW with high-dimensional discrete input states. Specifically, we could inject a 4-level entangled state of the form $|\psi_4\rangle=\left(|-3\,\mathrm{S}\rangle_s|-3\,\mathrm{S}\rangle_i+e^{2i\theta}|-1\,\mathrm{S}\rangle_s|-1\,\mathrm{S}\rangle_i+e^{4i\theta}|1\,\mathrm{S}\rangle_s|1\,\mathrm{S}\rangle_i+e^{6i\theta}|3\,\mathrm{S}\rangle_s|3\,\mathrm{S}\rangle_i\right)/2$ (i.e., $d=4$) into the loop system. Two different evolution strategies are designed to perform the measurement described by Eq. (9.5). As the first controlled scheme illustrated in Fig. 9.5 (c), we design the unitary evolution as $\hat{\mathcal{U}}_{d=4}=\hat{\mathcal{U}}_F\cdot\hat{\mathcal{U}}_R\cdot\hat{\mathcal{U}}_F\cdot\hat{\mathcal{U}}_F$ composed of two 50:50 splitting in the first two roundtrips, a pure reflection as

$$\hat{\mathcal{U}}_R=\hat{S}_s\left(\mathbf{I}_{\mathrm{p}}\otimes\hat{R}_s\right)\otimes\hat{S}_i\left(\mathbf{I}_{\mathrm{p}}\otimes\hat{R}_i\right) \tag{9.11}$$

in the third, and another 50:50 split at the last step. Quantum interference, given in Eq. (9.6) with $d=4$, is finally obtained by performing projections of the form $P_{d=4}=\langle\psi_4(t=4)|\hat{M}|\psi_4(t=4)\rangle/p_0^{d=4}$ where $|\psi_4(t=4)\rangle=\hat{\mathcal{U}}_{d=4}|\psi_4(t=0)\rangle$ is the evolved state and $p_0^{d=4}=1/4$. However, an optimal evolution can be designed to maximize the detection efficiency, meaning $p_0^{d=4}=1$. Thus, in the following scheme, as depicted in Fig. 9.5 (d), we devise the unitary operator as $\hat{\mathcal{U}}_{d=4}=\hat{\mathcal{U}}_F\cdot\hat{\mathcal{U}}_F\cdot\hat{\mathcal{U}}_R\cdot\hat{\mathcal{U}}_{TR}$, which keeps the first two time-bins ($|-3\,\mathrm{S}\rangle$ and $|-1\,\mathrm{S}\rangle$)in the long loop and sends the other two (($|1\,\mathrm{S}\rangle$ and $|3\,\mathrm{S}\rangle$)) into the short loop in the first roundtrip, followed by full reflection and 50:50 splitting operations at the two last steps. Finally, the exact expected quantum interference pattern is given by the projective measurement $P_{d=4}=\langle\psi'_4(t=4)|\hat{M}|\psi'_4(t=4)\rangle/p_0^{d=4}$, where $|\psi'_4(t=4)\rangle=\hat{\mathcal{U}}'_{d=4}|\psi_4(t=0)\rangle$ is the evolved state. The quantum interference pattern of a four-level input state is given by

$$P_4(\epsilon_4)=\frac{1}{2^6}\left(4+\epsilon_4\left(3\cos\left(2\theta\right)+2\cos\left(4\theta\right)+\cos\left(6\theta\right)\right)\right) \tag{9.12}$$

which is obtained by assuming the symmetric noise model introduced earlier. As shown in the main text, the imperfect behavior of the dynamical coupler increases the noise ratio. This affects the visibility, which declines from $V_{d=4} = 91.45\%$ to $V_{d=4} = 89.51\%$.

2..2 Biphoton quantum interference for arbitrary discrete dimensions using TPLs

As discussed in the main text, our realization can perform a sequence of time-position-dependent operators to serve a particular purpose. Although the experimental realization of the biphoton quantum interference measurement is limited to 4 levels, the measurement scheme can be generalized to more than four dimensions with $d = 2^n$ ($n = 1\ldots$). We assume that the process starts with sending the input state through one of the loops, then adjusting the coupler to implement the projection of Eq. 9.6. The first rule is that we need d roundtrips to verify two-photon quantum interference of the d-level input state. Specifically, d independent unitary operators $\hat{\mathcal{U}}_d = \Pi_{n=1}^{d}\hat{\mathcal{U}}_n$ are constructed to make the initial state evolve as $|\psi_d(t=d)\rangle = \hat{\mathcal{U}}_d\,|\psi_d(t=0)\rangle$. Then, the projection measurement $\hat{M}$ is applied to achieve the quantum interference of Eq. (9.6). We also divide the process into preparation and mixing stages, each of them being half the biphoton's evolution time. The preparation process begins with the unitary operator $\hat{U}_{TR}$ (given in Eq. (9.8)), and $d/2-1$ number of pure reflection operators (given in Eq. (9.11)). In the time-mode mixing stage, we let the photons evolve with different sequences of the 50:50 splitting and reflection operators. Finally, we take photons out from the short loop and performed coincidence measurements at position $x = -1$ for different values of θ, thus obtaining Eq. (9.6). As a summary, we write the sequence of operations per roundtrip for d-level two-photon quantum interference measurement:

$$\begin{aligned}
d=2,&\quad \hat{\mathcal{U}}_{d=2} = \hat{\mathcal{U}}_F\cdot\hat{\mathcal{U}}_{TR}\\
d=4,&\quad \hat{\mathcal{U}}_{d=4} = (\hat{\mathcal{U}}_F)^2\cdot\hat{\mathcal{U}}_R\cdot\hat{\mathcal{U}}_{TR}\\
d=8,&\quad \hat{\mathcal{U}}_{d=8} = \hat{\mathcal{U}}_F\cdot\hat{\mathcal{U}}_R\cdot(\hat{\mathcal{U}}_F)^2\cdot(\hat{\mathcal{U}}_R)^3\cdot\hat{\mathcal{U}}_{TR}\\
d=16,&\quad \hat{\mathcal{U}}_{d=16} = \hat{\mathcal{U}}_F\cdot(\hat{\mathcal{U}}_R)^2\cdot\hat{\mathcal{U}}_F\cdot\hat{\mathcal{U}}_R\cdot(\hat{\mathcal{U}}_F)^2\cdot(\hat{\mathcal{U}}_R)^3\cdot\hat{\mathcal{U}}_{TR}
\end{aligned} \tag{9.13}$$

Conclusive remarks

This ongoing doctoral dissertation introduces novel research that focuses on the characterization and preservation of quantum resources in composite quantum systems. Part I of the study primarily explores the concept of indistinguishability among identical particles, which is a pivotal resource for quantum information processing. Moving to Part II, the thesis delves deeply into the controllable dynamics of indistinguishable particles, specifically emphasizing photons, as they propagate through diverse quantum photonic configurations. In Part I, four chapters delved into various aspects of quantum information processing using the indistinguishability of identical particles. **Chapter II** introduced a novel entanglement measure for two identical qubits, showcasing the protection of non-local entanglement from preparation noise through spatial indistinguishability. In **Chapter III**, I discussed an experimental framework for remote entangling gates and performed quantum teleportation with fidelities surpassing classical thresholds. **Chapter IV** investigated the preservation of entanglement during open system dynamics under spatial indistinguishability. In **Chapter V**, an entanglement distillation method was presented, maximizing entanglement from mixed states through spatial overlap and examining the influence of noise parameters and temperatures. These chapters contributed to our understanding of quantum information processing using indistinguishability, offering valuable insights for practical applications.

In recent years, there has been growing research interest in the concept of spatially overlapping identical particles in different regions to utilize the effect of indistinguishability in quantum information processing. Previous studies have demonstrated that indistinguishability can be harnessed to perform various quantum information processing tasks, including teleportation [16, 23], quantum estimation [94, 31], and entanglement distribution between nodes of a quantum network [28, 26].

Numerous theoretical and experimental designs have been proposed to exploit indistinguishability for generating entanglement. These designs range from extending bipartite resource generation to multiple particles [25, 95], to utilizing graph theory approaches for generating complex multipartite states using linear quantum networks [96]. Building upon these studies, we have developed a general controllable scheme for generating a comprehensive class of multipartite entangled states, including W, Dicke, GHZ, and cluster states (this is a work in progress which is going to be submitted soon). Our scheme relies on spatially localized operations and classical communication. Furthermore, the entanglement concurrence based on sLOCC, as introduced in Ref. [17], has enabled researchers to investigate entanglement monogamy [97], study entanglement in anyonic systems [98, 99], and more. Additionally, we have provided an entanglement recovery protocol due to the indistinguishability effect [100, 101]. Recent developments have also motivated the robust engineering of maximally entangled states [35, 102]. However, experimental verification of entanglement preservation remains a major prospective area for our proposed schemes.

In the realm of quantum thermodynamics, it has been shown that indistinguishability can play a role as fuel in quantum engines to enhance the conversion of information and work [36, 37, 38], resulting in higher efficiency at maximum power beyond the classical Curzon-Ahlborn limit [39]. In a work in preparation, we propose an indistinguishability-based cyclic quantum cooling machine that can cool the system particles to a very low temperature.

As a comment on the entropic measure of spatial indistinguishability introduced in [17], we have

found that the measure is not general for any arbitrary input state. In general, the degree of indistinguishability depends on both the quantum state and the measurement performed on the system. To clarify this point, let me consider an example of two fermions with the same internal degrees of freedom, having elementary states of $|\mathrm{L}\sigma, \mathrm{R}\sigma\rangle$, where each can be found in different regions. In such a state, the two fermions are initially distinguishable and addressable by their spatial regions. Then, we spatially distribute the particles by unitarily modifying their single-particle wave functions. However, even though we modify the spatial wave functions in the two regions L and R, the two-particle state remains unchanged due to the Pauli exclusion principle or fermionic anti-bunching. Therefore, there is no change in spatial indistinguishability. Hence, the transformation may not always result in spatially indistinguishable output states. Instead, the entropic measure of spatial indistinguishability introduced in Ref. [17] quantifies the deformation settings or spatial distribution of particles in different regions. The same observation applies to the bosonic singlet state, given as $|\psi_1 \uparrow, \psi_2 \downarrow\rangle - |\psi_1 \downarrow, \psi_2 \uparrow\rangle$. If we substitute the general expressions of the single wave functions as $|\psi_1\rangle = \cos\left(\frac{\theta}{2}\right)|\mathrm{L}\rangle + \mathbf{i}e^{\mathbf{i}\phi}\sin\left(\frac{\theta}{2}\right)|\mathrm{R}\rangle$ and $|\psi_2\rangle = \mathbf{i}e^{-\mathbf{i}\phi}\sin\left(\frac{\theta}{2}\right)|\mathrm{L}\rangle + \cos\left(\frac{\theta}{2}\right)|\mathrm{R}\rangle$ with arbitrary values of θ and ϕ, the singlet bosonic state is $|\mathrm{L}\uparrow, \mathrm{R}\downarrow\rangle - |\mathrm{L}\downarrow, \mathrm{R}\uparrow\rangle$, which is a spatially distinguishable state.

Nevertheless, spatial indistinguishability or spatial overlap, as discussed in Chapter VI [118], is expected to be observed. We can assess spatial indistinguishability by measuring the probability of finding particles in each region. For example, if the probability of finding a particle in each region is one, then the two particles are spatially distinguishable. Quantifying such a measure is an immediate prospect.

In part II my thesis, three research papers were presented, each corresponding to a separate chapter and published or submitted in peer-reviewed journals. **Chapter VII** introduces a probing protocol based on discrete-time quantum walks, enabling the detection of coherent static and dynamic disorders, as well as the investigation of transport phenomena and Anderson localization. This protocol offers a feasible experimental strategy for quantum probing using the quantum Fisher information. **Chapter VIII** explores the controlled disorder's role in enhancing the quantum correlation between two identical photons. The results indicate that carefully imposed disorder configurations can enhance quantum correlations, surpassing those observed in ordered quantum walks. Finally, **Chapter IX** presents a scalable discrete-time quantum walk processor utilizing temporal photonic lattices. This processor allows for generating, manipulating, and testing high-dimensional time-bin entanglement. The experimental demonstration showcases the control of high-dimensional biphoton quantum interference and highlights the potential of temporal photonic lattices as reconfigurable quantum photonic circuits.

As an outlook, our research opens up several avenues for further exploration. Firstly, there is potential for studying different types of disorders, including spatiotemporally correlated disorders, to gain a deeper understanding of their effects on quantum systems. Additionally, investigating the role of disorder in quantum walks with fermions could provide valuable insights. Furthermore, whether disorder can enhance quantum correlations between more than two particles remains to be seen, which could have significant implications in quantum resource theories. Another exciting prospect is the potential for engineering synthetic photonic lattices that can generate and process entangled modes with dimensions higher than four. This would enable the efficient manipulation of biphoton quantum interference, leading to advancements in quantum tomography, phase discrimination, and sensing. Overall, our research opaves the way to the development of innovative designs and protocols in the field of quantum information processing.

In conclusion, this thesis highlights the significance of indistinguishability as a valuable resource for quantum information processing tasks. It also emphasizes the promising prospects for further advancements in this field. Moreover, the thesis demonstrates the versatility of the quantum walk model and its applicability in quantum optical platforms with different degrees of freedom. Throughout the thesis, we have thoroughly investigated and analyzed various topics of interest to the scientific community working in quantum science and technologies. The substantial impact of our work can be seen through the publications referenced in this text. However, the true value of this thesis lies not only in the knowledge acquired by exploring diverse topics in quantum information, but also in the practical experience gained

from working with different theoretical frameworks and from collaborating with many different research fellows.

References

Bibliography

[1] Asher Peres. *Quantum Theory: Concepts and Methods*. Springer, Dordrecht, The Netherlands, 1995.

[2] Rosario Lo Franco and Giuseppe Compagno. Quantum entanglement of identical particles by standard information-theoretic notions. *Sci. Rep.*, 6:20603, 2016.

[3] Giuseppe Compagno, Alessia Castellini, and Rosario Lo Franco. Dealing with indistinguishable particles and their entanglement. *Phil. Trans. R. Soc. A: Math. Phys. Eng. Sci.*, 376(2123):20170317, 2018.

[4] Fedor Herbut and Milan Vujicic. Irrelevance of the pauli principle in distant correlations between identical fermions. *J. Phys. A: Math. Gen.*, 20(16):5555–5563, 1987.

[5] Marek Kuś Maciej Lewenstein John Schliemann, J. Ignacio Cirac and Daniel Loss. Quantum correlations in two-fermion systems. *Phys. Rev. A*, 64:022303, 2001.

[6] Claude Cohen-Tannoudji, Bernard Diu, and Franck Laloe. *Quantum mechanics. Vol. 2*. Willey-VCH, Paris, France, 2005.

[7] K Eckert, John Schliemann, D Bruss, and M Lewenstein. Quantum correlations in systems of indistinguishable particles. *Ann. Phys.*, 299(1):88–127, 2002.

[8] Paolo Zanardi. Virtual quantum subsystems. *Phys. Rev. Lett.*, 87:077901, 2001.

[9] Howard Barnum, Emanuel Knill, Gerardo Ortiz, Rolando Somma, and Lorenza Viola. A subsystem-independent generalization of entanglement. *Phys. Rev. Lett.*, 92:107902, 2004.

[10] Fabio Benatti, Roberto Floreanini, Fabio Franchini, and Ugo Marzolino. Entanglement in indistinguishable particle systems. *Phys. Rep.*, 878:1, 2020.

[11] Ola Bratteli and Derek William Robinson. *Operator algebras and quantum statistical mechanics: Volume 1: C*-and W*-Algebras. Symmetry Groups. Decomposition of States*. Springer Science & Business Media, 2012.

[12] GianCarlo Ghirardi and Luca Marinatto. General criterion for the entanglement of two indistinguishable particles. *Phys. Rev. A*, 70:012109, 2004.

[13] Malte C Tichy, Florian Mintert, and Andreas Buchleitner. Essential entanglement for atomic and molecular physics. *J. Phys. B: At. Mol. Opt. Phys.*, 44(19):192001, 2011.

[14] Nathan Killoran, Marcus Cramer, and Martin B Plenio. Extracting entanglement from identical particles. *Phys. Rev. Lett.*, 112:150501, 2014.

[15] Isaac L. Chuang Michael A. Nielsen. *Quantum Computation and Quantum Information*. Cambridge University Press, Cambridge, 2010.

[16] Rosario Lo Franco and Giuseppe Compagno. Indistinguishability of elementary systems as a resource for quantum information processing. *Phys. Rev. Lett.*, 120:240403, 2018.

[17] Farzam Nosrati, Alessia Castellini, Giuseppe Compagno, and Rosario Lo Franco. Robust entanglement preparation against noise by controlling spatial indistinguishability. *npj Quant. Inf.*, 6(1):1–7, 2020.

[18] Paul G. Kwiat, Klaus Mattle, Harald Weinfurter, Anton Zeilinger, Alexander V. Sergienko, and Yanhua Shih. New high-intensity source of polarization-entangled photon pairs. *Phys. Rev. Lett.*, 75:4337–4341, 1995.

[19] Paul G. Kwiat, Edo Waks, Andrew G. White, Ian Appelbaum, and Philippe H. Eberhard. Ultrabright source of polarization-entangled photons. *Phys. Rev. A*, 60:R773–R776, 1999.

[20] Han-Sen Zhong, Yuan Li, Wei Li, Li-Chao Peng, Zu-En Su, Yi Hu, Yu-Ming He, Xing Ding, Weijun Zhang, Hao Li, Lu Zhang, Zhen Wang, Lixing You, Xi-Lin Wang, Xiao Jiang, Li Li, Yu-Ao Chen, Nai-Le Liu, Chao-Yang Lu, and Jian-Wei Pan. 12-photon entanglement and scalable scattershot boson sampling with optimal entangled-photon pairs from parametric down-conversion. *Phys. Rev. Lett.*, 121:250505, 2018.

[21] Jian-Wei Pan, Dik Bouwmeester, Harald Weinfurter, and Anton Zeilinger. Experimental entanglement swapping: entangling photons that never interacted. *Phys. Rev. Lett.*, 80(18):3891, 1998.

[22] Dik Bouwmeester, Jian-Wei Pan, Klaus Mattle, Manfred Eibl, Harald Weinfurter, and Anton Zeilinger. Experimental quantum teleportation. *Nature*, 390:575–579, 1997.

[23] Kai Sun, Yan Wang, Zheng-Hao Liu, Xiao-Ye Xu, Jin-Shi Xu, Chuan-Feng Li, Guang-Can Guo, Alessia Castellini, Farzam Nosrati, Giuseppe Compagno, and Rosario Lo Franco. Experimental quantum entanglement and teleportation by tuning remote spatial indistinguishability of independent photons. *Opt. Lett.*, 45(23):6410–6413, 2020.

[24] Mariana R. Barros, Seungbeom Chin, Tanumoy Pramanik, Hyang-Tag Lim, Young-Wook Cho, Joonsuk Huh, and Yong-Su Kim. Entangling bosons through particle indistinguishability and spatial overlap. *Opt. Express*, 28(25):38083–38092, 2020.

[25] Donghwa Lee, Tanumoy Pramanik, Seongjin Hong, Young-Wook Cho, Hyang-Tag Lim, Seungbeom Chin, and Yong-Su Kim. Entangling three identical particles via spatial overlap. *Opt. Express*, 30(17):30525–30535, 2022.

[26] Yan Wang, Ze-Yan Hao, Zheng-Hao Liu, Kai Sun, Jin-Shi Xu, Chuan-Feng Li, Guang-Can Guo, Alessia Castellini, Bruno Bellomo, Giuseppe Compagno, and Rosario Lo Franco. Remote entanglement distribution in a quantum network via multinode indistinguishability of photons. *Phys. Rev. A*, 106:032609, 2022.

[27] Stefano Pirandola and Samuel L Braunstein. Physics: Unite to build a quantum internet. *Nature*, 532(7598):169–171, 2016.

[28] Alessia Castellini, Bruno Bellomo, Giuseppe Compagno, and Rosario Lo Franco. Activating remote entanglement in a quantum network by local counting of identical particles. *Phys. Rev. A*, 99(6):062322, 2019.

[29] Carmine Napoli, Thomas R. Bromley, Marco Cianciaruso, Marco Piani, Nathaniel Johnston, and Gerardo Adesso. Robustness of coherence: An operational and observable measure of quantum coherence. *Phys. Rev. Lett.*, 116(15):150502, 2016.

[30] Martin Ringbauer, Thomas R Bromley, Marco Cianciaruso, Ludovico Lami, WY Sarah Lau, Gerardo Adesso, Andrew G White, Alessandro Fedrizzi, and Marco Piani. Certification and quantification of multilevel quantum coherence. *Phys. Rev. X*, 8, 2018.

[31] Kai Sun, Zheng-Hao Liu, Yan Wang, Ze-Yan Hao, Xiao-Ye Xu, Jin-Shi Xu, Chuan-Feng Li, Guang-Can Guo, Alessia Castellini, Ludovico Lami, Andreas Winter, Gerardo Adesso, Giuseppe Compagno, and Rosario Lo Franco. Activation of indistinguishability-based quantum coherence for enhanced metrological applications with particle statistics imprint. *PNAS*, 119:e2119765119, 2022.

[32] Armando Perez-Leija, Diego Guzmán-Silva, Roberto de J León-Montiel, Markus Gräfe, Matthias Heinrich, Hector Moya-Cessa, Kurt Busch, and Alexander Szameit. Endurance of quantum coherence due to particle indistinguishability in noisy quantum networks. *Npj Quantum Inf.*, 4(1):45, 2018.

[33] Paweł Horodecki Ryszard Horodecki, Michał Horodecki, and Karol Horodecki. Quantum entanglement. *Rev. Mod. Phys.*, 81(2):865–942, 2009.

[34] Bruno Bellomo, Rosario Lo Franco, and Giuseppe Compagno. N identical particles and one particle to entangle them all. *Phys. Rev. A*, 96(2):022319, 2017.

[35] Matteo Piccolini, Vittorio Giovannetti, and Rosario Lo Franco. Asymptotically-deterministic robust preparation of maximally entangled bosonic states. *arXiv:2303.11484*, 2023.

[36] J. Bengtsson, M. Nilsson Tengstrand, A. Wacker, P. Samuelsson, M. Ueda, H. Linke, and S. M. Reimann. Quantum szilard engine with attractively interacting bosons. *Phys. Rev. Lett.*, 120:100601, 2018.

[37] Gentaro Watanabe, B Prasanna Venkatesh, Peter Talkner, Myung-Joong Hwang, and Adolfo Del Campo. Quantum statistical enhancement of the collective performance of multiple bosonic engines. *Phys. Rev. Lett.*, 124(21):210603, 2020.

[38] Zoë Holmes, Janet Anders, and Florian Mintert. Enhanced energy transfer to an optomechanical piston from indistinguishable photons. *Phys. Rev. Lett.*, 124(21):210601, 2020.

[39] Nathan Myers, Francisco José Peña, Oscar Andrés Negrete, Patricio Vargas, Gabriele De Chiara, and Sebastian Deffner. Boosting engine performance with bose-einstein condensation. *New J. Phys.*, 24:025001, 2022.

[40] Heinz-Peter Breuer and Francesco Petruccione. *The theory of open quantum systems*. Oxford University Press, 2002.

[41] L. Aolita, F. de Melo, and L. Davidovich. Open-system dynamics of entanglement:a key issues review. *Rep. Prog. Phys.*, 78(4):042001, 2015.

[42] Charles H. Bennett, David P. DiVincenzo, John A. Smolin, and William K. Wootters. Mixed-state entanglement and quantum error correction. *Phys. Rev. A*, 54:3824–3851, 1996.

[43] M. Murao, M. B. Plenio, S. Popescu, V. Vedral, and P. L. Knight. Multiparticle entanglement purification protocols. *Phys. Rev. A*, 57:R4075, 1998.

[44] Yakir Aharonov, Luiz Davidovich, and Nicim Zagury. Quantum random walks. *Phys. Rev. A*, 48(2):1687, 1993.

[45] Andrew M. Childs and Jeffrey Goldstone. Spatial search by quantum walk. *Phys. Rev. A*, 70:022314, 2004.

[46] Andrew M. Childs. Universal computation by quantum walk. *Phys. Rev. Lett.*, 102:180501, 2009.

[47] Brendan L Douglas and Jingbo B Wang. A classical approach to the graph isomorphism problem using quantum walks. *J. Phys. A: Math. Theor.*, 41(7):075303, 2008.

[48] P. W. Anderson. Absence of diffusion in certain random lattices. *Phys. Rev.*, 109:1492–1505, 1958.

[49] Diederik S. Wiersma, Paolo Bartolini, Ad Lagendijk, and Roberto Righini. Localization of light in a disordered medium. *Nature*, 390(6661):671–673, 1997.

[50] Mordechai Segev, Yaron Silberberg, and Demetrios N Christodoulides. Anderson localization of light. *Nat. Photon.*, 7(3):197–204, 2013.

[51] Tal Schwartz, Guy Bartal, Shmuel Fishman, and Mordechai Segev. Transport and anderson localization in disordered two-dimensional photonic lattices. *Nature*, 446(7131):52–55, 2007.

[52] Andrea Crespi, Roberto Osellame, Roberta Ramponi, Vittorio Giovannetti, Rosario Fazio, Linda Sansoni, Francesco De Nicola, Fabio Sciarrino, and Paolo Mataloni. Anderson localization of entangled photons in an integrated quantum walk. *Nat. Photon.*, 7(4):322–328, 2013.

[53] Andrea Blanco-Redondo, Bryn Bell, Dikla Oren, Benjamin J. Eggleton, and Mordechai Segev. Topological protection of biphoton states. *Science*, 362:568–571, 2018.

[54] Hideaki Obuse and Norio Kawakami. Topological phases and delocalization of quantum walks in random environments. *Phys. Rev. B*, 84(19):195139, 2011.

[55] Qin-Qin Wang, Xiao-Ye Xu, Wei-Wei Pan, Kai Sun, Jin-Shi Xu, Geng Chen, Yong-Jian Han, Chuan-Feng Li, and Guang-Can Guo. Dynamic-disorder-induced enhancement of entanglement in photonic quantum walks. *Optica*, 5(9):1136–1140, 2018.

[56] Alessandro Laneve, Farzam Nosrati, Andrea Geraldi, Kobra Mahdavipour, Federico Pegoraro, Mahshid Khazaei Shadfar, Rosario Lo Franco, and Paolo Mataloni. Enhancing nonclassical bosonic correlations in a quantum walk network through experimental control of disorder. *Phys. Rev. Res.*, 3:033235, 2021.

[57] Paweł Kurzyński and Antoni Wójcik. Quantum walk as a generalized measuring device. *Phys. Rev. Lett.*, 110:200404, 2013.

[58] H. Schmitz, R. Matjeschk, Ch. Schneider, J. Glueckert, M. Enderlein, T. Huber, and T. Schaetz. Quantum walk of a trapped ion in phase space. *Phys. Rev. Lett.*, 103:090504, 2009.

[59] Peng Xue and Barry C Sanders. Quantum quincunx for walk on circles in phase space with indirect coin flip. *New J. Phys.*, 10(5):053025, 2008.

[60] Zhiguang Yan, Yu-Ran Zhang, Ming Gong, Yulin Wu, Yarui Zheng, Shaowei Li, Can Wang, Futian Liang, Jin Lin, Yu Xu, Cheng Guo, Lihua Sun, Cheng-Zhi Peng, Keyu Xia, Hui Deng, Hao Rong, J. Q. You, Franco Nori, Heng Fan, Xiaobo Zhu, and Jian-Wei Pan. Strongly correlated quantum walks with a 12-qubit superconducting processor. *Science*, 364(6442):753–756, 2019.

[61]

[62] Siamak Dadras, Alexander Gresch, Caspar Groiseau, Sandro Wimberger, and Gil S. Summy. Experimental realization of a momentum-space quantum walk. *Phys. Rev. A*, 99:043617, 2019.

[63] Peter L. Knight, Eugenio Roldán, and J. E. Sipe. Quantum walk on the line as an interference phenomenon. *Phys. Rev. A*, 68:020301, 2003.

[64] Optical cavity implementations of the quantum walk. *Opt. Commun.*, 227(1):147–157, 2003.

[65] Hyunseok Jeong, Mauro Paternostro, and Myungshik S Kim. Simulation of quantum random walks using the interference of a classical field. *Physical Review A*, 69(1):012310, 2004.

[66] Zhihao Bian, Jian Li, Hao Qin, Xiang Zhan, Rong Zhang, Barry C. Sanders, and Peng Xue. Realization of single-qubit positive-operator-valued measurement via a one-dimensional photonic quantum walk. *Phys. Rev. Lett.*, 114:203602, 2015.

[67] Zihao Li, Haoyu Zhang, and Huangjun Zhu. Implementation of generalized measurements on a qudit via quantum walks. *Phys. Rev. A*, 99:062342, 2019.

[68] Zhibo Hou, Jun-Feng Tang, Jiangwei Shang, Huangjun Zhu, Jian Li, Yuan Yuan, Kang-Da Wu, Guo-Yong Xiang, Chuan-Feng Li, and Guang-Can Guo. Deterministic realization of collective measurements via photonic quantum walks. *Nat. Commun.*, 9(1):1414, 2018.

[69] Pei Zhang, Xi-Feng Ren, Xu-Bo Zou, Bi-Heng Liu, Yun-Feng Huang, and Guang-Can Guo. Demonstration of one-dimensional quantum random walks using orbital angular momentum of photons. *Phys. Rev. A*, 75:052310, 2007.

[70] Filippo Cardano, Francesco Massa, Hammam Qassim, Ebrahim Karimi, Sergei Slussarenko, Domenico Paparo, Corrado de Lisio, Fabio Sciarrino, Enrico Santamato, Robert W. Boyd, and Lorenzo Marrucci. Quantum walks and wavepacket dynamics on a lattice with twisted photons. *Sci. Adv.*, 1(2):e1500087, 2015.

[71] A. Schreiber, K. N. Cassemiro, V. Potoček, A. Gábris, P. J. Mosley, E. Andersson, I. Jex, and Ch. Silberhorn. Photons walking the line: A quantum walk with adjustable coin operations. *Phys. Rev. Lett.*, 104:050502, 2010.

[72] A Schreiber, KN Cassemiro, V Potoček, A Gábris, I Jex, and Ch Silberhorn. Decoherence and disorder in quantum walks: from ballistic spread to localization. *Phys. Rev. Lett.*, 106(18):180403, 2011.

[73] Viv Kendon. Decoherence in quantum walks–a review. *Math. Struct. Comput. Sci.*, 17(6):1169–1220, 2007.

[74] Masoud Mohseni, Patrick Rebentrost, Seth Lloyd, and Alan Aspuru-Guzik. Environment-assisted quantum walks in photosynthetic energy transfer. *The J CHEM PHYS*, 129(17):11B603, 2008.

[75] Viv Kendon and Ben Tregenna. Decoherence can be useful in quantum walks. *Phys. Rev. A*, 67(4):042315, 2003.

[76] Rafael Vieira, Edgard PM Amorim, and Gustavo Rigolin. Dynamically disordered quantum walk as a maximal entanglement generator. *Phys. Rev. Lett.*, 111(18):180503, 2013.

[77] Rafael Vieira, Edgard PM Amorim, and Gustavo Rigolin. Entangling power of disordered quantum walks. *Phys. Rev. A*, 89(4):042307, 2014.

[78] Meng Zeng and Ee Hou Yong. Discrete-time quantum walk with phase disorder: localization and entanglement entropy. *Sci. Rep.*, 7(1):1–9, 2017.

[79] R. Lo Franco, B. Bellomo, E. Andersson, and G. Compagno. Revival of quantum correlations without system-environment back-action. *Phys. Rev. A*, 85:032318, 2012.

[80] Jin-Shi Xu, Kai Sun, Chuan-Feng Li, Xiao-Ye Xu, Guang-Can Guo, Erika Andersson, Rosario Lo Franco, and Giuseppe Compagno. Experimental recovery of quantum correlations in absence of system-environment back-action. *Nat. Commun.*, 4:2851, 2013.

[81] Alberto Politi, Martin J. Cryan, John G. Rarity, Siyuan Yu, and Jeremy L. O'Brien. Silica-on-silicon waveguide quantum circuits. *Science*, 320(5876):646–649, 2008.

[82] C. Reimer et al. Generation of multiphoton entangled quantum states by means of integrated frequency combs. *Science*, 351:1176–1180, 2016.

[83] Michael Kues, Christian Reimer, Piotr Roztocki, Luis Romero Cortés, Stefania Sciara, Benjamin Wetzel, Yanbing Zhang, Alfonso Cino, Sai T. Chu, Brent E. Little, David J. Moss, Lucia Caspani, José Azaña, and Roberto Morandotti. On-chip generation of high-dimensional entangled quantum states and their coherent control. *Nature*, 546(7660):622–626, 2017.

[84] Christian Reimer, Stefania Sciara, Piotr Roztocki, Mehedi Islam, Luis Romero Cortés, Yanbing Zhang, Bennet Fischer, Sébastien Loranger, Raman Kashyap, Alfonso Cino, Sai T. Chu, Brent E. Little, David J. Moss, Lucia Caspani, William J. Munro, José Azaña, Michael Kues, and Roberto Morandotti. High-dimensional one-way quantum processing implemented on d-level cluster states. *Nature Physics*, 15(2):148–153, 2019.

[85] Alois Regensburger, Christoph Bersch, Mohammad-Ali Miri, Georgy Onishchukov, Demetrios N Christodoulides, and Ulf Peschel. Parity-time synthetic photonic lattices. *Nature*, 488(7410):167–171, 2012.

[86] Ye-Long Xu, William S. Fegadolli, Lin Gan, Ming-Hui Lu, Xiao-Ping Liu, Zhi-Yuan Li, Axel Scherer, and Yan-Feng Chen. Experimental realization of bloch oscillations in a parity-time synthetic silicon photonic lattice. *Nature Communications*, 7(1):11319, 2016.

[87] Martin Wimmer, Monika Monika, Iacopo Carusotto, Ulf Peschel, and Hannah M. Price. Superfluidity of light and its breakdown in optical mesh lattices. *Phys. Rev. Lett.*, 127:163901, 2021.

[88] Tomoki Ozawa and Hannah M. Price. Topological quantum matter in synthetic dimensions. *Nature Reviews Physics*, 1(5):349–357, 2019.

[89] Peter P Rohde, Andreas Schreiber, Martin Štefaňák, Igor Jex, and Christine Silberhorn. Multi-walker discrete time quantum walks on arbitrary graphs, their properties and their photonic implementation. *New J. Phys.*, 13(1):013001, 2011.

[90] Keith R. Motes, Alexei Gilchrist, Jonathan P. Dowling, and Peter P. Rohde. Scalable boson sampling with time-bin encoding using a loop-based architecture. *Phys. Rev. Lett.*, 113:120501, 2014.

[91] Peter P. Rohde. Simple scheme for universal linear-optics quantum computing with constant experimental complexity using fiber loops. *Phys. Rev. A*, 91:012306, 2015.

[92] Ben Bartlett, Avik Dutt, and Shanhui Fan. Deterministic photonic quantum computation in a synthetic time dimension. *Optica*, 8(12):1515–1523, 2021.

[93] Xiao-Xiao Chen, Jia-Zhi Yang, Xu-Dan Chai, and An-Ning Zhang. Single-photon bell state measurement based on a quantum random walk. *Phys. Rev. A*, 100:042302, 2019.

[94] Alessia Castellini, Rosario Lo Franco, Ludovico Lami, Andreas Winter, Gerardo Adesso, and Giuseppe Compagno. Indistinguishability-enabled coherence for quantum metrology. *Phys. Rev. A*, 100:012308, 2019.

[95] Pawel Blasiak, Ewa Borsuk, and Marcin Markiewicz. Arbitrary entanglement of three qubits via linear optics. *Scientific Reports*, 12(1):21596, 2022.

[96] Seungbeom Chin, Yong-Su Kim, and Sangmin Lee. Graph picture of linear quantum networks and entanglement. *Quantum*, 5:611, 2021.

[97] Goutam Paul, Soumya Das, and Anindya Banerji. Maximum violation of monogamy of entanglement for indistinguishable particles by measures that are monogamous for distinguishable particles. *Phys. Rev. A*, 104:L010402, 2021.

[98] HS Mani, N Ramadas, and VV Sreedhar. Quantum entanglement in one-dimensional anyons. *Phys. Rev. A*, 101(2):022314, 2020.

[99] Ramadas N. and V.V. Sreedhar. Quantum entanglement in the one-dimensional anyonic hubbard model. *Annals of Physics*, 442:168908, 2022.

[100] Matteo Piccolini, Farzam Nosrati, Giuseppe Compagno, Patrizia Livreri, Roberto Morandotti, and Rosario Lo Franco. Entanglement robustness via spatial deformation of identical particle wave functions. *Entropy*, 23:708, 2021.

[101] Matteo Piccolini, Farzam Nosrati, Roberto Morandotti, and Rosario Lo Franco. Indistinguishability-enhanced entanglement recovery by spatially localized operations and classical communication. *Open Syst. Inf. Dyn.*, 28(04):2150020, 2021.

[102] Matteo Piccolini, Vittorio Giovannetti, and Rosario Lo Franco. Robust engineering of maximally entangled states by identical particle interferometry. *arXiv preprint arXiv:2305.14285*, 2023.

[103] Wolfgang Pauli. *General principles of quantum mechanics*. Springer Science & Business Media, 2012.

[104] Leandro Aolita, Fernando de Melo, and Luiz Davidovich. Open-system dynamics of entanglement: a key issues review. *Rep. Prog. Phys.*, 78(4):042001, 2015.

[105] B. Bellomo, R. Lo Franco, and G. Compagno. Non-markovian effects on the dynamics of entanglement. *Phys. Rev. Lett.*, 99(16):160502, 2007.

[106] Bruno Bellomo, Rosario Lo Franco, Sabrina Maniscalco, and Giuseppe Compagno. Entanglement trapping in structured environments. *Phys. Rev. A*, 78(6):060302, 2008.

[107] Paolo Zanardi and Mario Rasetti. Noiseless quantum codes. *Phys. Rev. Lett.*, 79(17):3306, 1997.

[108] Daniel A Lidar, Isaac L Chuang, and K Birgitta Whaley. Decoherence-free subspaces for quantum computation. *Phys. Rev. Lett.*, 81(12):2594, 1998.

[109] Lorenza Viola and Seth Lloyd. Dynamical suppression of decoherence in two-state quantum systems. *Phys. Rev. A*, 58:2733–2744, 1998.

[110] Lorenza Viola and Emanuel Knill. Random decoupling schemes for quantum dynamical control and error suppression. *Phys. Rev. Lett.*, 94(6):060502, 2005.

[111] Rosario Lo Franco, , Antonio D'Arrigo, Giuseppe Compagno, Giuseppe Falci, and Elisabetta Paladino. Preserving entanglement and nonlocality in solid-state qubits by dynamical decoupling. *Phys. Rev. B*, 90(5):054304, 2014.

[112] John Preskill. Reliable quantum computers. *Proc. R. Soc. London Series A*, 454(1969):385–410, 1998.

[113] Emanuel Knill. Quantum computing with realistically noisy devices. *Nature*, 434(7029):39, 2005.

[114] Peter W Shor. Scheme for reducing decoherence in quantum computer memory. *Phys. Rev. A*, 52(4):R2493, 1995.

[115] A Yu Kitaev. Fault-tolerant quantum computation by anyons. *Ann. Phys.*, 303(1):2–30, 2003.

[116] Michael Freedman, Alexei Kitaev, Michael Larsen, and Zhenghan Wang. Topological quantum computation. *Bull. Am. Math. Soc.*, 40(1):31–38, 2003.

[117] Farzam Nosrati, Alessia Castellini, Giuseppe Compagno, and Rosario Lo Franco. Dynamics of spatially indistinguishable particles and quantum entanglement protection. *Phys. Rev. A*, 102(6):062429, 2020.

[118] Farzam Nosrati, Bruno Bellomo, Gabriele De Chiara, Giuseppe Compagno, Roberto Morandotti, and Rosario Lo Franco. Indistinguishability-assisted two-qubit entanglement distillation. *arXiv preprint arXiv:2305.11964*, 2023.

[119] Karuna Kadian, Sunita Garhwal, and Ajay Kumar. Quantum walk and its application domains: A systematic review. *Comput. Sci. Rev.*, 41:100419, 2021.

[120] Farzam Nosrati, Alessandro Laneve, Mahshid Khazaei Shadfar, Andrea Geraldi, Kobra Mahdavipour, Federico Pegoraro, Paolo Mataloni, and Rosario Lo Franco. Readout of quantum information spreading using a disordered quantum walk. *J. Opt. Soc. Am. B*, 38(9):2570–2578, 2021.

[121] Adam Caulton. Discerning "indistinguishable" quantum systems. *Philosophy of Science*, 80(1):49–72, 2013.

[122] Steven French. Identity and individuality in classical and quantum physics. *Australasian Journal of Philosophy*, 67(4):432–446, 1989.

[123] Michael LG Redhead. Quantum field theory for philosophers. In *PSA: Proceedings of the biennial meeting of the Philosophy of Science Association*, volume 1982, pages 57–99. Philosophy of Science Association, 1982.

[124] Michael H Kolodrubetz and Jason R Petta. Coherent holes in a semiconductor quantum dot. *Science*, 325(5936):42–43, 2009.

[125] Z. B. Tan, D. Cox, T. Nieminen, P. Lähteenmäki, D. Golubev, G. B. Lesovik, and P. J. Hakonen. Cooper pair splitting by means of graphene quantum dots. *Phys. Rev. Lett.*, 114:096602, 2015.

[126] F. Martins et al. Noise suppression using symmetric exchange gates in spin qubits. *Phys. Rev. Lett.*, 116:116801, 2016.

[127] Frédéric Bouchard, Alicia Sit, Yingwen Zhang, Robert Fickler, Filippo M Miatto, Yuan Yao, Fabio Sciarrino, and Ebrahim Karimi. Two-photon interference: the hong–ou–mandel effect. *Rep. Prog. Phys.*, 84(1):012402, 2020.

[128] Sudhakar Prasad, Marlan O. Scully, and Werner Martienssen. A quantum description of the beam splitter. *Opt. Commun.*, 62(3):139–145, 1987.

[129] Heidi Fearn and R. Loudon. Quantum theory of the lossless beam splitter. *Opt. Commun.*, 64(6):485–490, 1987.

[130] Chong-Ki Hong, Zhe-Yu Ou, and Leonard Mandel. Measurement of subpicosecond time intervals between two photons by interference. *Phys. Rev. Lett.*, 59:2044–2046, 1987.

[131] Rosario Lo Franco. Directly proving the bosonic nature of photons. *Nat. Photon.*, 15(9):638–639, 2021.

[132] Claude Cohen-Tannoudji, Bernard Diu, Frank Laloe, and Bernard Dui. *Quantum Mechanics (2 vol. set)*. Wiley-Interscience, 2006.

[133] Yan Wang, Matteo Piccolini, Ze-Yan Hao, Zheng-Hao Liu, Kai Sun, Jin-Shi Xu, Chuan-Feng Li, Guang-Can Guo, Roberto Morandotti, Giuseppe Compagno, and Rosario Lo Franco. Proof-of-principle direct measurement of particle statistical phase. *Phys. Rev. Appl.*, 18:064024, 2022.

[134] Adam M. Kaufman, Brian J. Lester, Collin M. Reynolds, Michael L. Wall, M. Foss-Feig, K. R. A. Hazzard, A. M. Rey, and C. A. Regal. Two-particle quantum interference in tunnel-coupled optical tweezers. *Science*, 345(6194):306–309, 2014.

[135] Jonathan P. Dowling. Quantum optical metrology–the lowdown on high-n00n states. *Contemporary Physics*, 49(2):125–143, 2008.

[136] Artur Scherer, Barry C Sanders, and Wolfgang Tittel. Long-distance practical quantum key distribution by entanglement swapping. *Opt. Express*, 19(4):3004–3018, 2011.

[137] Tian-Yu Ye. Robust quantum dialogue based on the entanglement swapping between any two logical bell states and the shared auxiliary logical bell state. *Quant. Inform. Process.*, 14(4):1469–1486, 2015.

[138] Mosayeb Naseri. Revisiting quantum authentication scheme based on entanglement swapping. *Int. J. Theor. Phys.*, 55(5):2428–2435, 2016.

[139] Qi-Chao Sun, Ya-Li Mao, Yang-Fan Jiang, Qi Zhao, Si-Jing Chen, Wei Zhang, Wei-Jun Zhang, Xiao Jiang, Teng-Yun Chen, Li-Xing You, Li Li, Yi-Dong Huang, Xian-Feng Chen, Zhen Wang, Xiongfeng Ma, Qiang Zhang, and Jian-Wei Pan. Entanglement swapping with independent sources over an optical-fiber network. *Phys. Rev. A*, 95(3):032306, 2017.

[140] BC Jacobs, TB Pittman, and JD Franson. Quantum relays and noise suppression using linear optics. *Phys. Rev. A*, 66(5):052307, 2002.

[141] Nicolas Gisin and Rob Thew. Quantum communication. *Nat. Photon.*, 1(3):165, 2007.

[142] M. Zukowski, A. Zeilinger, M. A. Horne, and A. K Ekert. "event-ready-detectors" Bell experiment via entanglement swapping. *Phys. Rev. Lett.*, 71:4287–4290, 1993.

[143] T. Jennewein, G. Weihs, and A. Pan, J.-W.and Zeilinger. Experimental nonlocality proof of quantum teleportation and entanglement swapping. *Phys. Rev. Lett.*, 88:017903, 2001.

[144] Cyril Branciard, Nicolas Gisin, and Stefano Pironio. Characterizing the nonlocal correlations created via entanglement swapping. *Phys. Rev. Lett.*, 104(17):170401, 2010.

[145] Eric Chitambar, Debbie Leung, Laura Mančinska, Maris Ozols, and Andreas Winter. Everything you always wanted to know about locc (but were afraid to ask). *Communications in Mathematical Physics*, 328(1):303–326, 2014.

[146] Hugo Cable and Jonathan P. Dowling. Efficient generation of large number-path entanglement using only linear optics and feed-forward. *Phys. Rev. Lett.*, 99:163604, 2007.

[147] Itai Afek, Oron Ambar, and Yaron Silberberg. High-noon states by mixing quantum and classical light. *Science*, 328(5980):879–881, 2010.

[148] Morgan W Mitchell, Jeff S Lundeen, and Aephraem M Steinberg. Super-resolving phase measurements with a multiphoton entangled state. *Nature*, 429(6988):161–164, 2004.

[149] Emanuel Knill, Raymond Laflamme, and Gerald J Milburn. A scheme for efficient quantum computation with linear optics. *nature*, 409(6816):46–52, 2001.

[150] Sabrina Maniscalco, Francesco Francica, Rosa L. Zaffino, Nicola Lo Gullo, and Francesco Plastina. Protecting entanglement via the quantum Zeno effect. *Phys. Rev. Lett.*, 100(9):090503, 2008.

[151] Laura Mazzola, Sabrina Maniscalco, Jyrki Piilo, K-A Suominen, and Barry M Garraway. Sudden death and sudden birth of entanglement in common structured reservoirs. *Phys. Rev. A*, 79(4):042302, 2009.

[152] Zhong-Xiao Man, Yun-Jie Xia, and Rosario Lo Franco. Cavity-based architecture to preserve quantum coherence and entanglement. *Sci. Rep.*, 5:13843, 2015.

[153] Charles H. Bennett, Gilles Brassard, Sandu Popescu, Benjamin Schumacher, John A. Smolin, and William K. Wootters. Purification of noisy entanglement and faithful teleportation via noisy channels. *Phys. Rev. Lett.*, 76:722–725, 1996.

[154] Adeline Orieux, Antonio d'Arrigo, Giacomo Ferranti, Rosario Lo Franco, Giuliano Benenti, Elisabetta Paladino, Giuseppe Falci, Fabio Sciarrino, and Paolo Mataloni. Experimental on-demand recovery of entanglement by local operations within non-markovian dynamics. *Sci. Rep.*, 5(1):1–8, 2015.

[155] Sajeev Damodarakurup, Marco Lucamarini, Giovanni Di Giuseppe, David Vitali, and Paolo Tombesi. Experimental inhibition of decoherence on flying qubits via bang-bang control. *Phys. Rev. Lett.*, 103(4):040502, 2009.

[156] Álvaro Cuevas, Andrea Mari, Antonella De Pasquale, Adeline Orieux, Marcello Massaro, Fabio Sciarrino, Paolo Mataloni, and Vittorio Giovannetti. Cut-and-paste restoration of entanglement transmission. *Phys. Rev. A*, 96(1):012314, 2017.

[157] Ali Mortezapour and Rosario Lo Franco. Protecting quantum resources via frequency modulation of qubits in leaky cavities. *Sci. Rep.*, 8(1):14304, 2018.

[158] Dieter Suter and Gonzalo A. Álvarez. Colloquium: Protecting quantum information against environmental noise. *Rev. Mod. Phys.*, 88(4):041001, 2016.

[159] Matteo Piccolini, Farzam Nosrati, Gerardo Adesso, Roberto Morandotti, and Rosario Lo Franco. Generating indistinguishability within identical particle systems: spatial deformations as quantum resource activators. *arXiv preprint arXiv:2205.12136*, 2022.

[160] Andreas Trabesinger. Quantum computing: towards reality. *Nature*, 543(7646):S1–S1, 2017.

[161] Thaddeus D Ladd, Fedor Jelezko, Raymond Laflamme, Yasunobu Nakamura, Christopher Monroe, and Jeremy Lloyd O'Brien. Quantum computers. *Nature*, 464(7285):45, 2010.

[162] Vittorio Giovannetti, Seth Lloyd, and Lorenzo Maccone. Quantum metrology. *Phys. Rev. Lett.*, 96(1):010401, 2006.

[163] Artur K Ekert. Quantum cryptography based on Bell's theorem. *Phys. Rev. Lett.*, 67(6):661, 1991.

[164] Charles H. Bennett, Gilles Brassard, Claude Crépeau, Richard Jozsa, Asher Peres, and William K. Wootters. Teleporting an unknown quantum state via dual classical and Einstein-Podolsky-Rosen channels. *Phys. Rev. Lett.*, 70:1895–1899, 1993.

[165] Christian L Degen, Friedemann Reinhard, and Paola Cappellaro. Quantum sensing. *Rev. Mod. Phys.*, 89:035002, 2017.

[166] Jürgen Audretsch. *Entangled systems: new directions in quantum physics*. John Wiley & Sons, 2007.

[167] Rosario Lo Franco, Bruno Bellomo, Sabrina Maniscalco, and Giuseppe Compagno. Dynamics of quantum correlations in two-qubit systems within non-markovian environments. *Int. J. Mod. Phys. B*, 27:1345053, 2013.

[168] Immanuel Bloch, Jean Dalibard, and Wilhelm Zwerger. Many-body physics with ultracold gases. *Rev. Mod. Phys.*, 80(3):885–964, 2008.

[169] Marco Anderlini, Patricia J Lee, Benjamin L Brown, Jennifer Sebby-Strabley, William D Phillips, and James V Porto. Controlled exchange interaction between pairs of neutral atoms in an optical lattice. *Nature*, 448(7152):452, 2007.

[170] Xi-Lin Wang, Luo-Kan Chen, Wei Li, H-L Huang, Chang Liu, Chao Chen, Y-H Luo, Z-E Su, Dian Wu, Z-D Li, et al. Experimental ten-photon entanglement. *Phys. Rev. Lett.*, 117(21):210502, 2016.

[171] Alexander D. Cronin, Jörg Schmiedmayer, and David E. Pritchard. Optics and interferometry with atoms and molecules. *Rev. Mod. Phys.*, 81:1051–1129, Jul 2009.

[172] Andrea Crespi, Linda Sansoni, Giuseppe Della Valle, Alessio Ciamei, Roberta Ramponi, Fabio Sciarrino, Paolo Mataloni, Stefano Longhi, and Roberto Osellame. Particle statistics affects quantum decay and Fano interference. *Phys. Rev. Lett.*, 114(9):090201, 2015.

[173] Frederico Martins, Filip K. Malinowski, Peter D. Nissen, Edwin Barnes, Saeed Fallahi, Geoffrey C. Gardner, Michael J. Manfra, Charles M. Marcus, and Ferdinand Kuemmeth. Noise suppression using symmetric exchange gates in spin qubits. *Phys. Rev. Lett.*, 116:116801, 2016.

[174] Rami Barends, Lucas Lamata, Julian Kelly, L. García-Álvarez, Austin G. Fowler, Anthony Megrant, Evan Jeffre, T. C. White, D. Sank, J. Y. Mutus, B. Campbell, Yu Chen, Z. Chen, B. Chiaro, A. Dunsworth, I.-C. Hoi, C. Neill, P. J. J. O'Malley, C. Quintana, P. Roushan, A. Vainsencher, J. Wenner, E. Solano, and John M. Martinis. Digital quantum simulation of fermionic models with a superconducting circuit. *Nat. Commun.*, 6(1):7654, 2015.

[175] Daniel Braun, Gerardo Adesso, Fabio Benatti, Roberto Floreanini, Ugo Marzolino, Morgan W. Mitchell, and Stefano Pirandola. Quantum-enhanced measurements without entanglement. *Rev. Mod. Phys.*, 90:035006, 2018.

[176] Malte C. Tichy, Klaus Mayer, Andreas Buchleitner, and Klaus Mølmer. Stringent and efficient assessment of boson-sampling devices. *Phys. Rev. Lett.*, 113:020502, 2014.

[177] Leandro Aolita, Christian Gogolin, Martin Kliesch, and Jens Eisert. Reliable quantum certification of photonic state preparations. *Nat. Commun.*, 6:8498, 2015.

[178] Marco Bentivegna, Nicolò Spagnolo, and Fabio Sciarrino. Is my boson sampler working? *New J. Phys.*, 18(4):041001, 2016.

[179] Christoph Dittel, Robert Keil, and Gregor Weihs. Many-body quantum interference on hypercubes. *Quantum Science and Technology*, 2(1):015003, 2017.

[180] Nicolò Spagnolo, Chiara Vitelli, Marco Bentivegna, Daniel J. Brod, Andrea Crespi, Fulvio Flamini, Sandro Giacomini, Giorgio Milani, Roberta Ramponi, Paolo Mataloni, Roberto Osellame, Ernesto F. Galvão, and Fabio Sciarrino. Experimental validation of photonic boson sampling. *Nat. Photon.*, 8:615, 2014.

[181] Marco Bentivegna, Nicolò Spagnolo, Chiara Vitelli, Daniel J. Brod, Andrea Crespi, Fulvio Flamini, Roberta Ramponi, Paolo Mataloni, Roberto Osellame, Ernesto F. Galvão, and Fabio Sciarrino. Bayesian approach to boson sampling validation. *Int. J. Quant. Inform.*, 12:1560028, 2014.

[182] Andrea Crespi, Roberto Osellame, Roberta Ramponi, Marco Bentivegna, Fulvio Flamini, Nicolò Spagnolo, Niko Viggianiello, Luca Innocenti, Paolo Mataloni, and Fabio Sciarrino. Suppression law of quantum states in a 3D photonic fast Fourier transform chip. *Nat. Commun.*, 7:10469, 2016.

[183] Iris Agresti, Niko Viggianiello, Fulvio Flamini, Nicolò Spagnolo, Andrea Crespi, Roberto Osellame, Nathan Wiebe, and Fabio Sciarrino. Pattern recognition techniques for boson sampling validation. *Phys. Rev. X*, 9:011013, 2019.

[184] Taira Giordani, Fulvio Flamini, Matteo Pompili, Niko Viggianiello, Nicolò Spagnolo, Andrea Crespi, Roberto Osellame, Nathan Wiebe, Mattia Walschaers, Andreas Buchleitner, et al. Experimental statistical signature of many-body quantum interference. *Nat. Photon.*, 12(3):173, 2018.

[185] Sascha Agne, Thomas Kauten, Jeongwan Jin, Evan Meyer-Scott, Jeff Z. Salvail, Deny R. Hamel, Kevin J. Resch, Gregor Weihs, and Thomas Jennewein. Observation of genuine three-photon interference. *Phys. Rev. Lett.*, 118:153602, 2017.

[186] Adrian J. Menssen, Alex E. Jones, Benjamin J. Metcalf, Malte C. Tichy, Stefanie Barz, W. Steven Kolthammer, and Ian A. Walmsley. Distinguishability and many-particle interference. *Phys. Rev. Lett.*, 118:153603, 2017.

[187] Nikola Paunković, Yasser Omar, Sougato Bose, and Vlatko Vedral. Entanglement concentration using quantum statistics. *Phys. Rev. Lett.*, 88:187903, 2002.

[188] S. Bose, A. Ekert, Y. Omar, N. Paunković, and V. Vedral. Optimal state discrimination using particle statistics. *Phys. Rev. A*, 68:052309, 2003.

[189] Fabio Benatti, Sahar Alipour, and Alireza T. Rezakhani. Dissipative quantum metrology in many-body systems of identical particles. *New J. Phys.*, 16(1):015023, 2014.

[190] Daniel J. Brod, Ernesto F. Galvão, Niko Viggianiello, Fulvio Flamini, Nicolò Spagnolo, and Fabio Sciarrino. Witnessing genuine multiphoton indistinguishability. *Phys. Rev. Lett.*, 122:063602, 2019.

[191] S. Bose and D. Home. Duality in entanglement enabling a test of quantum indistinguishability unaffected by interactions. *Phys. Rev. Lett.*, 110(14):140404, 2013.

[192] AP Balachandran, TR Govindarajan, Amilcar R de Queiroz, and AF Reyes-Lega. Entanglement and particle identity: A unifying approach. *Phys. Rev. Lett.*, 110:080503, 2013.

[193] Fabio Benatti, Roberto Floreanini, Fabio Franchini, and Ugo Marzolino. Remarks on entanglement and identical particles. *Open Sys. Inform. Dyn.*, 24:1740004, 2017.

[194] Antônio C Lourenço, Tiago Debarba, and Eduardo I Duzzioni. Entanglement of indistinguishable particles: A comparative study. *Phys. Rev. A*, 99(1):012341, 2019.

[195] William K. Wootters. Entanglement of formation of an arbitrary state of two qubits. *Phys. Rev. Lett.*, 80:2245–2248, 1998.

[196] Scott Hill and William K. Wootters. Entanglement of a pair of quantum bits. *Phys. Rev. Lett.*, 78:5022–5025, 1997.

[197] Reinhard F Werner. Quantum states with Einstein-Podolsky-Rosen correlations admitting a hidden-variable model. *Phys. Rev. A*, 40(8):4277, 1989.

[198] Fabio Sciarrino, Giuseppe Vallone, Adán Cabello, and Paolo Mataloni. Bell experiments with random destination sources. *Phys. Rev. A*, 83:032112, 2011.

[199] Ryszard Horodecki, Pawel Horodecki, and Michal Horodecki. Violating Bell inequality by mixed spin-$1/2$ states: necessary and sufficient condition. *Phys. Lett. A*, 200(5):340–344, 1995.

[200] Hector Bombin and Miguel-Angel Martin-Delgado. Topological computation without braiding. *Phys. Rev. Lett.*, 98:160502, 2007.

[201] Daniel Nigg, Markus Mueller, Esteban A. Martinez, Markus Hennrich Philipp Schindler, Miguel A. Martin-Delgado Thomas Monz, and Rainer Blatt. Quantum computations on a topologically encoded qubit. *Science*, 345(6194):302–305, 2014.

[202] P. Milman, W. Maineult, S. Guibal, L. Guidoni, B. Douçot, L. Ioffe, and T. Coudreau. Topologically decoherence-protected qubits with trapped ions. *Phys. Rev. Lett.*, 99:020503, 2007.

[203] Sergey Gladchenko, David Olaya, Eva Dupont-Ferrier, Benoit Douçot, Lev B Ioffe, and Michael E Gershenson. Superconducting nanocircuits for topologically protected qubits. *Nat. Phys.*, 5(1):48, 2009.

[204] Sunil Mittal, Elizabeth A Goldschmidt, and Mohammad Hafezi. A topological source of quantum light. *Nature*, 561(7724):502, 2018.

[205] Yao Wang, Yong-Heng Lu, Jun Gao, Ruo-Jing Ren, Yi-Jun Chang, Zhi-Qiang Jiao, Zhe-Yong Zhang, and Xian-Min Jin. Topologically protected quantum entanglement. *Preprint at arXiv:1903.03015*, 2019.

[206] Daniel A. Lidar. Review of decoherence free subspaces, noiseless subsystems, and dynamical decoupling. *Adv. Chem. Phys.*, 154:295–354, 2014.

[207] Lorenza Viola, Emanuel Knill, and Seth Lloyd. Dynamical decoupling of open quantum systems. *Phys. Rev. Lett.*, 82(12):2417, 1999.

[208] L.-A. Wu, P. Zanardi, and D. A. Lidar. Holonomic quantum computation in decoherence-free subspaces. *Phys. Rev. Lett.*, 95:130501, 2005.

[209] Alois Mair, Alipasha Vaziri, Gregor Weihs, and Anton Zeilinger. Entanglement of the orbital angular momentum states of photons. *Nature*, 412(6844):313, 2001.

[210] Eleonora Nagali, Fabio Sciarrino, Francesco De Martini, Lorenzo Marrucci, Bruno Piccirillo, Ebrahim Karimi, and Enrico Santamato. Quantum information transfer from spin to orbital angular momentum of photons. *Phys. Rev. Lett.*, 103(1):013601, 2009.

[211] L. Aolita and S. P. Walborn. Quantum communication without alignment using multiple-qubit single-photon states. *Phys. Rev. Lett.*, 98(10):100501, 2007.

[212] Linda Sansoni, Fabio Sciarrino, Giuseppe Vallone, Paolo Mataloni, Andrea Crespi, Roberta Ramponi, and Roberto Osellame. Two-particle bosonic-fermionic quantum walk via integrated photonics. *Phys. Rev. Lett.*, 108(1):010502, 2012.

[213] Shi-Biao Zheng, You-Peng Zhong, Kai Xu, Qi-Jue Wang, H. Wang, Li-Tuo Shen, Chui-Ping Yang, John M. Martinis, A. N. Cleland, and Si-Yuan Han. Quantum delayed-choice experiment with a beam splitter in a quantum superposition. *Phys. Rev. Lett.*, 115:260403, 2015.

[214] Erwann Bocquillon, Vincent Freulon, J-M Berroir, Pascal Degiovanni, Bernard Plaçais, A Cavanna, Yong Jin, and Gwendal Fève. Coherence and indistinguishability of single electrons emitted by independent sources. *Science*, 339:1054, 2013.

[215] Mohammad Rashidi, Wyatt Vine, Thomas Dienel, Lucian Livadaru, Jacob Retallick, Taleana Huff, Konrad Walus, and Robert A. Wolkow. Initiating and monitoring the evolution of single electrons within atom-defined structures. *Phys. Rev. Lett.*, 121:166801, 2018.

[216] Christopher Bäuerle, D Christian Glattli, Tristan Meunier, Fabien Portier, Patrice Roche, Preden Roulleau, Shintaro Takada, and Xavier Waintal. Coherent control of single electrons: a review of current progress. *Rep. Prog. Phys.*, 81(5):056503, 2018.

[217] Bruno Bellomo, Rosario Lo Franco, and Giuseppe Compagno. Dynamics of non-classically-reproducible entanglement. *Phys. Rev. A*, 78:062309, 2008.

[218] H. Wang, J. Qin, X. Ding, M.-C. Chen, S. Chen, X. You, Y.-M. He, X. Jiang, L. You, Z. Wang, C. Schneider, J. J. Renema, S. Höfling, C.-Y. Lu, and J.-W. Pan. Boson sampling with 20 input photons and a 60-mode interferometer in a 10^{14}-dimensional hilbert space. *Phys. Rev. Lett.*, 123:250503, 2019.

[219] F. Arute et al. Quantum supremacy using a programmable superconducting processor. *Nature*, 574:505–510, 2019.

[220] Schmiedmayer Jörg Cronin, Alexander D. and David E. Pritchard. Optics and interferometry with atoms and molecules. *Rev. Mod. Phys.*, 81:1051–1129, 2009.

[221] F. Benatti, R. Floreanini, and K. Titimbo. Entanglement of identical particles. *Open Syst. Inf. Dyn.*, 21:1440003, 2014.

[222] H. M. Wiseman and John A. Vaccaro. Entanglement of indistinguishable particles shared between two parties. *Phys. Rev. Lett.*, 91:097902, 2003.

[223] Paolo Zanardi. Quantum entanglement in fermionic lattices. *Phys. Rev. A*, 65:042101, 2002.

[224] T. Sasaki, T. Ichikawa, and I. Tsutsui. Entanglement of indistinguishable particles. *Phys. Rev. A*, 83:012113, 2011.

[225] F. Buscemi, P. Bordone, and A. Bertoni. Linear entropy as an entanglement measure in two-fermion systems. *Phys. Rev. A*, 75:032301, 2007.

[226] S. Sciara, R. Lo Franco, and G. Compagno. Universality of Schmidt decomposition and particle identity. *Sci. Rep.*, 7:44675, 2017.

[227] S. Chin and J. Huh. Reduced density matrix of nonlocal identical particles, 2019.

[228] R. Hanbury Brown and R. Q. Twiss. A test of a new type of stellar interferometer on Sirius. *Nature*, 178:1046–1048, 1956.

[229] T. Qureshi and U. Rizwan. Hanbury Brown-Twiss effect with wave packets. *Quanta*, 6(1):61–69, 2017.

[230] S. Takeuchi. Beamlike twin-photon generation by use of type ii parametric downconversion. *Optics Lett.*, 26:843–845, 2001.

[231] C. E. Kuklewicz, M. Fiorentino, G. Messin, F. N. C. Wong, and J. H. Shapiro. High-flux source of polarization-entangled photons from a periodically poled ktiopo_4 parametric down-converter. *Phys. Rev. A*, 69:013807, 2004.

[232] N. Lütkenhaus, J. Calsamiglia, and K.-A. Suominen. Bell measurements for teleportation. *Phys. Rev. A*, 59:3295–3300, 1999.

[233] J. Calsamiglia and N. Lutkenhaus. Maximum efficiency of a linear-optical Bell-state analyzer. *App. Phys. B-Las. Opt.*, 72:67–71, 2001.

[234] S. Massar and S. Popescu. Optimal extraction of information from finite quantum ensembles. *Phys. Rev. Lett.*, 74:1259–1263, 1995.

[235] D. Cavalcanti, M. França Santos, M. O. Terra Cunha, C. Lunkes, and V. Vedral. Increasing identical particle entanglement by fuzzy measurements. *Phys. Rev. A*, 72:062307, 2005.

[236] J. L. O'Brien, G. J. Pryde, A. Gilchrist, D. F. V. James, N. K. Langford, T. C. Ralph, and A. G. White. Quantum process tomography of a controlled-not gate. *Phys. Rev. Lett.*, 93:080502, 2004.

[237] A. Reusch, J. Sperling, and W. Vogel. Entanglement witnesses for indistinguishable particles. *Phys. Rev. A*, 91:042324, 2015.

[238] Y. Shi. Quantum entanglement of identical particles. *Phys. Rev. A*, 67:024301, 2003.

[239] Y. S. Li, B. Zeng, X. S. Liu, and G. L. Long. Entanglement in a two-identical-particle system. *Phys. Rev. A*, 64:054302, 2001.

[240] R. Paskauskas and L. You. Quantum correlations in two-boson wave functions. *Phys. Rev. A*, 64:042310, 2001.

[241] M. C. Tichy, F. de Melo, M. Kus, F. Mintert, and A. Buchleitner. Entanglement of identical particles and the detection process. *Fortschr. Phys.*, 61:225, 2013.

[242] G. C. Ghirardi, L. Marinatto, and T. Weber. Entanglement and properties of composite quantum systems: a conceptual and mathematical analysis. *J. Stat. Phys.*, 108:49, 2002.

[243] F. Buscemi and P. Bordone. Measure of tripartite entanglement in bosonic and fermionic systems. *Phys. Rev. A*, 84:022303, 2011.

[244] Benjamin Morris, Benjamin Yadin, Matteo Fadel, Tilman Zibold, Philipp Treutlein, and Gerardo Adesso. Entanglement between identical particles is a useful and consistent resource. *Phys. Rev. X*, 10:041012, 2020.

[245] Seungbeom Chin and Joonsuk Huh. Entanglement of identical particles and coherence in the first quantization language. *Phys. Rev. A*, 99(5):052345, 2019.

[246] Y. Omar, N. Paunković, S. Bose, and V. Vedral. Spin-space entanglement transfer and quantum statistics. *Phys. Rev. A*, 65:062305, 2002.

[247] Yanna Li, Manuel Gessner, Weidong Li, and Augusto Smerzi. Hyper- and hybrid nonlocality. *Phys. Rev. Lett.*, 120:050404, 2018.

[248] Pawel Blasiak and Marcin Markiewicz. Entangling three qubits without ever touching. *Sci. Rep.*, 9(1):20131, 2019.

[249] Soumya Das, Goutam Paul, and Anindya Banerji. Hyper-hybrid entanglement, indistinguishability, and two-particle entanglement swapping. *Phys. Rev. A*, 102:052401, 2020.

[250] G. Argentieri, F. Benatti, R. Floreanini, and U. Marzolino. Entangled identical particles and noise. *Int. J. Quant. Inf.*, 9:1745, 2011.

[251] U. Marzolino. Entanglement in dissipative dynamics of identical particles. *EPL (Europhysics Letters)*, 104:40004, 2013.

[252] A. Beggi, F. Buscemi, and P. Bordone. Quantum correlations of identical particles subject to classical environmental noise. *Quantum Inf. Process.*, 15:3711, 2016.

[253] Wojciech Hubert Zurek. Decoherence, einselection, and the quantum origins of the classical. *Rev. Mod. Phys.*, 75:715–775, 2003.

[254] A. Peres. Stability of quantum motion in chaotic and regular systems. *Phys. Rev. A*, 30(4):1610, 1984.

[255] R. A. Jalabert and H. M. Pastawski. Environment-independent decoherence rate in classically chaotic systems. *Phys. Rev. Lett.*, 86:2490–2493, 2001.

[256] T. Yu and J. H. Eberly. Finite-time disentanglement via spontaneous emission. *Phys. Rev. Lett.*, 93(14):140404, 2004.

[257] Ting Yu and J. H. Eberly. Sudden death of entanglement. *Science*, 323:598–601, 2009.

[258] M. P. Almeida, F. de Melo, M. Hor-Meyll, A. Salles, S. P. Walborn, P. H. Souto Ribeiro, and L. Davidovich. Environment-induced sudden death of entanglement. *Science*, 316(5824):579–582, 2007.

[259] J. Laurat, K. S. Choi, H. Deng, C. W. Chou, and H. J. Kimble. Heralded entanglement between atomic ensembles: preparation, decoherence, and scaling. *Phys. Rev. Lett.*, 99(18):180504, 2007.

[260] R. Lo Franco and G. Compagno. *Overview on the Phenomenon of Two-Qubit Entanglement Revivals in Classical Environments*, pages 367–391. Springer, Cham, 2017.

[261] Antonio D'Arrigo, R Lo Franco, Giuliano Benenti, Elisabetta Paladino, and Giuseppe Falci. Recovering entanglement by local operations. *Ann. Phys.*, 350:211–224, 2014.

[262] J. Trapani, M. Bina, S. Maniscalco, and M. G. A. Paris. Collapse and revival of quantum coherence for a harmonic oscillator interacting with a classical fluctuating environment. *Phys. Rev. A*, 91:022113, 2015.

[263] Inés de Vega and Daniel Alonso. Dynamics of non-markovian open quantum systems. *Rev. Mod. Phys.*, 89:015001, 2017.

[264] J.-S. Xu, C.-F. Li, M. Gong, X.-B. Zou, C.-H. Shi, G. Chen, and G.-C. Guo. Experimental demonstration of photonic entanglement collapse and revival. *Phys. Rev. Lett.*, 104(10):100502, 2010.

[265] Luca Dellantonio, Sumanta Das, Jürgen Appel, and Anders S. Sørensen. Multipartite entanglement detection with nonsymmetric probing. *Phys. Rev. A*, 95:040301, 2017.

[266] Karl Kraus. *States, effects and operations: fundamental notions of quantum theory*. Springer, 1983.

[267] G. Lindblad. On the generators of quantum dynamical semigroups. *Commun. Math. Phys.*, 48(2):119–130, 1976.

[268] V. Gorini, A. Kossakowski, and E. C. G. Sudarshan. Completely positive dynamical semigroups of n-level systems. *J. Math. Phys.*, 17(5):821–825, 1976.

[269] M. Gross and S. Haroche. Superradiance: An essay on the theory of collective spontaneous emission. *Phys. Rep.*, 93(5):301–396, 1982.

[270] C. L. Latune, I. Sinayskiy, and F. Petruccione. Energetic and entropic effects of bath-induced coherences. *Phys. Rev. A*, 99:052105, 2019.

[271] Dong Zhou, Alex Lang, and Robert Joynt. Disentanglement and decoherence from classical non-markovian noise: random telegraph noise. *Quant. Inf. Proc.*, 9(6):727–747, 2010.

[272] R. Lo Franco, Antonio D'Arrigo, Giuseppe Falci, Giuseppe Compagno, and Elisabetta Paladino. Entanglement dynamics in superconducting qubits affected by local bistable impurities. *Phys. Scr.*, 2012(T147):014019, 2012.

[273] Paolo Bordone, Fabrizio Buscemi, and Claudia Benedetti. Effect of markov and non-markov classical noise on entanglement dynamics. *Fluc. Noise Lett.*, 11(03):1242003, 2012.

[274] B. Bellomo, R. Lo Franco, E. Andersson, J. D. Cresser, and G. Compagno. Dynamics of correlations due to a phase noisy laser. *Phys. Scr.*, T147:014004, 2012.

[275] X. Cai. Quantum dephasing induced by non-Markovian random telegraph noise. *Sci. Rep.*, 10:88, 2020.

[276] H. J. Wold, H. Brox, Y. M. Galperin, and J. Bergli. Decoherence of a qubit due to either a quantum fluctuator, or classical telegraph noise. *Phys. Rev. B*, 86:205404, 2012.

[277] E. Paladino, L. Faoro, G. Falci, and R. Fazio. Decoherence and $1/f$ noise in Josephson qubits. *Phys. Rev. Lett.*, 88:228304, 2002.

[278] G. Ithier, E. Collin, P. Joyez, P. J. Meeson, D. Vion, D. Esteve, F. Chiarello, A. Shnirman, Y. Makhlin, J. Schriefl, et al. Decoherence in a superconducting quantum bit circuit. *Phys. Rev. B*, 72(13):134519, 2005.

[279] J. Bylander, S. Gustavsson, F. Yan, F. Yoshihara, K. Harrabi, G. Fitch, D. G. Cory, Y. Nakamura, J.-S. Tsai, and W. D. Oliver. Noise spectroscopy through dynamical decoupling with a superconducting flux qubit. *Nat. Phys.*, 7(7):565, 2011.

[280] E. Paladino, Y. M. Galperin, G. Falci, and B. L. Altshuler. $1/f$ noise: Implications for solid-state quantum information. *Rev. Mod. Phys.*, 86:361–418, 2014.

[281] S. M. Anton, C. Müller, J. S. Birenbaum, S. R. O'Kelley, A. D. Fefferman, D. S. Golubev, G. C. Hilton, H.-M. Cho, K. D. Irwin, F. C. Wellstood, G. Schön, A. Shnirman, and J. Clarke. Pure dephasing in flux qubits due to flux noise with spectral density scaling as $1/f^{\alpha}$. *Phys. Rev. B*, 85:224505, 2012.

[282] B. Bellomo, G. Compagno, A. D'Arrigo, G. Falci, R. Lo Franco, and E. Paladino. Entanglement degradation in the solid state: Interplay of adiabatic and quantum noise. *Phys. Rev. A*, 81:062309, 2010.

[283] Benjamin Aaronson, Rosario Lo Franco, and Gerardo Adesso. Comparative investigation of the freezing phenomena for quantum correlations under nondissipative decoherence. *Phys. Rev. A*, 88:012120, 2013.

[284] Isabela A. Silva, Alexandre M. Souza, Thomas R. Bromley, Marco Cianciaruso, Raimund Marx, Roberto S. Sarthour, Ivan S. Oliveira, Rosario Lo Franco, Steffen J. Glaser, Eduardo R. deAzevedo, Diogo O. Soares-Pinto, and Gerardo Adesso. Observation of time-invariant coherence in a nuclear magnetic resonance quantum simulator. *Phys. Rev. Lett.*, 117:160402, 2016.

[285] W. Dür, M. Hein, J. I. Cirac, and H.-J. Briegel. Standard forms of noisy quantum operations via depolarization. *Phys. Rev. A*, 72:052326, 2005.

[286] A. B. Klimov and L. L. Sánchez-Soto. Depolarization for quantum channels with higher symmetries. *Phys. Scr.*, T140:014009, 2010.

[287] Y. Hamdouni and F. Petruccione. Time evolution and decoherence of a spin-$1/2$ particle coupled to a spin bath in thermal equilibrium. *Phys. Rev. B*, 76(17):174306, 2007.

[288] KM Fonseca Romero and R Lo Franco. Simple non-markovian microscopic models for the depolarizing channel of a single qubit. *Phys. Scr.*, 86(6):065004, 2012.

[289] A. Melikidze, V. V. Dobrovitski, H. A. De Raedt, M. I. Katsnelson, and B. N. Harmon. Parity effects in spin decoherence. *Phys. Rev. B*, 70(1):014435, 2004.

[290] A. Hutton and S. Bose. Mediated entanglement and correlations in a star network of interacting spins. *Phys. Rev. A*, 69:042312, 2004.

[291] T. Xin, S.-J. Wei, J. S. Pedernales, E. Solano, and G.-L. Long. Quantum simulation of quantum channels in nuclear magnetic resonance. *Phys. Rev. A*, 96(6):062303, 2017.

[292] C. A. Ryan, M. Laforest, and R. Laflamme. Randomized benchmarking of single-and multi-qubit control in liquid-state NMR quantum information processing. *New J. Phys.*, 11(1):013034, 2009.

[293] J. Kasprzak, M. Richard, S. Kundermann, A. Baas, P. Jeambrun, J. M. J. Keeling, F. M. Marchetti, M. H. Szymańska, R. André, J. L. Staehli, et al. Bose–Einstein condensation of exciton polaritons. *Nature*, 443(7110):409–414, 2006.

[294] C. Zipkes, S. Palzer, C. Sias, and M. Köhl. A trapped single ion inside a Bose–Einstein condensate. *Nature*, 464(7287):388–391, 2010.

[295] G. Puentes, D. Voigt, A. Aiello, and J. P. Woerdman. Experimental observation of universality in depolarized light scattering. *Optics Lett.*, 30(23):3216–3218, 2005.

[296] G. Puentes, A. Aiello, D. Voigt, and J. P. Woerdman. Entangled mixed-state generation by twin-photon scattering. *Phys. Rev. A*, 75(3):032319, 2007.

[297] A. Shaham and H. S. Eisenberg. Realizing controllable depolarization in photonic quantum-information channels. *Phys. Rev. A*, 83(2):022303, 2011.

[298] C. J. Myatt, B. E. King, Q. A. Turchette, C. A. Sackett, D. Kielpinski, W. M. Itano, C. Monroe, and D. J. Wineland. Decoherence of quantum superpositions through coupling to engineered reservoirs. *Nature*, 403:269, 2000.

[299] Philipp Schindler, Daniel Nigg, Thomas Monz, Julio T Barreiro, Esteban Martinez, Shannon X Wang, Stephan Quint, Matthias F Brandl, Volckmar Nebendahl, Christian F Roos, Michael Chwalla, Markus Hennrich, and Rainer Blatt. A quantum information processor with trapped ions. *New J. Phys.*, 15(12):123012, 2013.

[300] C. D. Bruzewicz, J. Chiaverini, R. McConnell, and J. M. Sage. Trapped-ion quantum computing: Progress and challenges. *Applied Phys. Rev.*, 6:021314, 2019.

[301] Alexandre Blais, Jay Gambetta, A. Wallraff, D. I. Schuster, S. M. Girvin, M. H. Devoret, and R. J. Schoelkopf. Quantum-information processing with circuit quantum electrodynamics. *Phys. Rev. A*, 75:032329, 2007.

[302] A. Blais, S. M. Girvin, and W. D. Oliver. Quantum information processing and quantum optics with circuit quantum electrodynamics. *Nat. Phys.*, 16:247, 2020.

[303] V. Giovannetti and R. Fazio. Information-capacity description of spin-chain correlations. *Phys. Rev. A*, 71:032314, 2005.

[304] S. Satoh, K. Susa, and I. Matsuyama. Simple method of measuring scattering losses in optical fibers. *Appl. Opt.*, 38:7080–7084, 1999.

[305] K. A. G. Fisher, R. Prevedel, R. Kaltenbaek, and K. J. Resch. Optimal linear optical implementation of a single-qubit damping channel. *New J. Phys.*, 14:033016, 2012.

[306] J. Campany and C. R. Fernández-Pousa. Linear-optics realization of the qubit amplitude-damping channel using phase modulation. In *IEEE Photonics Conference 2012*, pages 473–474, 2012.

[307] R.P.M.J.W. Notermans, R. J. Rengelink, and W. Vassen. Comparison of spectral linewidths for quantum degenerate bosons and fermions. *Phys. Rev. Lett.*, 117:213001, 2016.

[308] David J Griffiths and Darrell F Schroeter. *Introduction to quantum mechanics*. Cambridge University Press, 2018.

[309] Artur K. Ekert. *Quantum Cryptography and Bell's Theorem*, page 413. Springer US, Boston, MA, 1992.

[310] Vittorio Giovannetti, Seth Lloyd, and Lorenzo Maccone. Advances in quantum metrology. *Nat. Photon.*, 5(4):222, 2011.

[311] Bogna Bylicka, D Chruściński, and Sci Maniscalco. Non-markovianity and reservoir memory of quantum channels: a quantum information theory perspective. *Sci. Rep.*, 4(1):1–7, 2014.

[312] J. Tan, T. H. Kyaw, and Y. Yeo. Non-markovian environments and entanglement preservation. *Phys. Rev. A*, 81(6):062119, 2010.

[313] Q. J. Tong, J. H. An, H. G. Luo, and C. H. Oh. Mechanism of entanglement preservation. *Phys. Rev. A*, 81(5):052330, 2010.

[314] Paolo Facchi, DA Lidar, and S Pascazio. Unification of dynamical decoupling and the quantum zeno effect. *Phys. Rev. A*, 69(3):032314, 2004.

[315] N. Gisin. Hidden quantum nonlocality revealed by local filters. *Phys. Lett. A*, 210(3):151, 1996.

[316] Sebastian Ecker, Philipp Sohr, Lukas Bulla, Marcus Huber, Martin Bohmann, and Rupert Ursin. Experimental single-copy entanglement distillation. *Phys. Rev. Lett.*, 127:040506, 2021.

[317] H.-J. Briegel, W. Dür, J. I. Cirac, and P. Zoller. Quantum repeaters: the role of imperfect local operations in quantum communication. *Phys. Rev. Lett.*, 81:5932, 1998.

[318] Sylvia Bratzik, Silvestre Abruzzo, Hermann Kampermann, and Dagmar Bruß. Quantum repeaters and quantum key distribution: The impact of entanglement distillation on the secret key rate. *Phys. Rev. A*, 87:062335, 2013.

[319] Saikat Guha, Hari Krovi, Christopher A. Fuchs, Zachary Dutton, Joshua A. Slater, Christoph Simon, and Wolfgang Tittel. Rate-loss analysis of an efficient quantum repeater architecture. *Phys. Rev. A*, 92:022357, 2015.

[320] Michał Horodecki, Paweł Horodecki, and Ryszard Horodecki. Mixed-state entanglement and distillation: Is there a "bound" entanglement in nature? *Phys. Rev. Lett.*, 80:5239, 1998.

[321] R. Horodecki, P. Horodecki, and M. Horodecki. Violating bell inequality by mixed spin-12 states: necessary and sufficient condition. *Phys. Lett. A*, 200(5):340, 1995.

[322] Sandu Popescu. Bell's inequalities versus teleportation: What is nonlocality? *Phys. Rev. Lett.*, 72:797, 1994.

[323] Ming-Liang Hu. Relations between entanglement, bell-inequality violation and teleportation fidelity for the two-qubit x states. *Quant. Inf. Proc.*, 12(1):229, 2013.

[324] Nicolas Gisin. Bell's inequality holds for all non-product states. *Phys. Lett. A*, 154(5-6):201– 202, 1991.

[325] Konrad Tschernig, Chris Müller, Malte Smoor, Tim Kroh, Janik Wolters, Oliver Benson, Kurt Busch, and Armando Perez-Leija. Direct observation of the particle exchange phase of photons. *Nat. Photon.*, 15(9):671–675, 2021.

[326] Julia Kempe. Quantum random walks: an introductory overview. *Contemp. Phys.*, 44(4):307–327, 2003.

[327] Eric Bach, Susan Coppersmith, Marcel Paz Goldschen, Robert Joynt, and John Watrous. One-dimensional quantum walks with absorbing boundaries. *Journal of Computer and System Sciences*, 69(4):562–592, 2004.

[328] M. A. Broome, A. Fedrizzi, B. P. Lanyon, I. Kassal, A. Aspuru-Guzik, and A. G. White. Discrete single-photon quantum walks with tunable decoherence. *Phys. Rev. Lett.*, 104:153602, 2010.

[329] Ralf Metzler and Joseph Klafter. The random walk's guide to anomalous diffusion: a fractional dynamics approach. *Phys. Rep.*, 339(1):1–77, 2000.

[330] Ralf Metzler and Joseph Klafter. The restaurant at the end of the random walk: recent developments in the description of anomalous transport by fractional dynamics. *J. Phys. A: Math. Theor.*, 37(31):R161, 2004.

[331] Rainer Klages, Günter Radons, and Igor M Sokolov. *Anomalous transport: foundations and applications*. John Wiley & Sons, 2008.

[332] Gil Hornung, Brian Berkowitz, and Naama Barkai. Morphogen gradient formation in a complex environment: an anomalous diffusion model. *Phys. Rev. E*, 72(4):041916, 2005.

[333] M B Plenio and Susana F Huelga. Dephasing-assisted transport: quantum networks and biomolecules. *New J. Phys.*, 10(11):113019, 2008.

[334] Radu Balescu. Anomalous transport in turbulent plasmas and continuous time random walks. *Phys. Rev. E*, 51(5):4807, 1995.

[335] Michael F Shlesinger, George M Zaslavsky, and Joseph Klafter. Strange kinetics. *Nature*, 363(6424):31–37, 1993.

[336] Jean-Philippe Bouchaud and Antoine Georges. Anomalous diffusion in disordered media: statistical mechanisms, models and physical applications. *Phys. Rep.*, 195(4-5):127–293, 1990.

[337] Henk van Beijeren. Exact results for anomalous transport in one-dimensional hamiltonian systems. *Phys. Rev. Lett.*, 108:180601, 2012.

[338] Eunho Kim, Alejandro J Martínez, Sean E Phenisee, PG Kevrekidis, Mason A Porter, and Jinkyu Yang. Direct measurement of superdiffusive energy transport in disordered granular chains. *Nat. Comm.*, 9(1):1–6, 2018.

[339] Stefan Schaufler, Wolfgang P Schleich, and Valery P Yakovlev. Keyhole look at levy flights in subrecoil laser cooling. *Phys. Rev. Lett.*, 83(16):3162, 1999.

[340] G Zumofen and J Klafter. Spectral random walk of a single molecule. *Chem. Phys. Lett.*, 219(3-4):303–309, 1994.

[341] E Barkai and R Silbey. Distribution of single-molecule line widths. *Chem. Phys. Lett.*, 310(3-4):287–295, 1999.

[342] Yevgeny Bar Lev, Guy Cohen, and David R Reichman. Absence of diffusion in an interacting system of spinless fermions on a one-dimensional disordered lattice. *Phys. Rev. Lett.*, 114(10):100601, 2015.

[343] Kartiek Agarwal, Sarang Gopalakrishnan, Michael Knap, Markus Müller, and Eugene Demler. Anomalous diffusion and griffiths effects near the many-body localization transition. *Phys. Rev. Lett.*, 114(16):160401, 2015.

[344] Marko Žnidarič, Antonello Scardicchio, and Vipin Kerala Varma. Diffusive and subdiffusive spin transport in the ergodic phase of a many-body localizable system. *Phys. Rev. Lett.*, 117(4):040601, 2016.

[345] Maximilian Schulz, Scott Richard Taylor, Christpher Andrew Hooley, and Antonello Scardicchio. Energy transport in a disordered spin chain with broken u (1) symmetry: Diffusion, subdiffusion, and many-body localization. *Phys. Rev. B*, 98(18):180201, 2018.

[346] Juan Jose Mendoza-Arenas, M Žnidarič, Vipin Kerala Varma, John Goold, Stephen R Clark, and Antonello Scardicchio. Asymmetry in energy versus spin transport in certain interacting disordered systems. *Phys. Rev. B*, 99(9):094435, 2019.

[347] Andrea Geraldi, Syamsundar De, Alessandro Laneve, Sonja Barkhofen, Jan Sperling, Paolo Mataloni, and Christine Silberhorn. Transient subdiffusion via disordered quantum walks. *Phys. Rev. Res.*, 3:023052, 2021.

[348] Andrea Geraldi, Alessandro Laneve, Luis Diego Bonavena, Linda Sansoni, Jose Ferraz, Andrea Fratalocchi, Fabio Sciarrino, Álvaro Cuevas, and Paolo Mataloni. Experimental investigation of superdiffusion via coherent disordered quantum walks. *Phys. Rev. Lett.*, 123(14):140501, 2019.

[349] Alberto Peruzzo, Mirko Lobino, Jonathan CF Matthews, Nobuyuki Matsuda, Alberto Politi, Konstantinos Poulios, Xiao-Qi Zhou, Yoav Lahini, Nur Ismail, Kerstin Wörhoff, et al. Quantum walks of correlated photons. *Science*, 329(5998):1500–1503, 2010.

[350] Craig S Hamilton, Aurél Gábris, Igor Jex, and Stephen M Barnett. Quantum walk with a four-dimensional coin. *New J. Phys.*, 13(1):013015, 2011.

[351] Taira Giordani, Emanuele Polino, Sabrina Emiliani, Alessia Suprano, Luca Innocenti, Helena Majury, Lorenzo Marrucci, Mauro Paternostro, Alessandro Ferraro, Nicolò Spagnolo, and Fabio Sciarrino. Experimental engineering of arbitrary qudit states with discrete-time quantum walks. *Phys. Rev. Lett.*, 122:020503, 2019.

[352] Alberto Politi, Martin J. Cryan, John G. Rarity, Siyuan Yu, and Jeremy L. O'Brien. Silica-on-silicon waveguide quantum circuits. *Science*, 320(5876):646–649, 2008.

[353] Salvador Elías Venegas-Andraca. Quantum walks: a comprehensive review. *Quantum Information Processing*, 11(5):1015–1106, 2012.

[354] KR Parthasarathy. The passage from random walk to diffusion in quantum probability. *J. App. Prob.*, pages 151–166, 1988.

[355] Stephan Hoyer and David A Meyer. Faster transport with a directed quantum walk. *Phys. Rev. A*, 79(2):024307, 2009.

[356] Vir B Bulchandani, Christoph Karrasch, and Joel E Moore. Superdiffusive transport of energy in one-dimensional metals. *PNAS*, 117(23):12713–12718, 2020.

[357] Gregory S Engel, Tessa R Calhoun, Elizabeth L Read, Tae-Kyu Ahn, Tomáš Mančal, Yuan-Chung Cheng, Robert E Blankenship, and Graham R Fleming. Evidence for wavelike energy transfer through quantum coherence in photosynthetic systems. *Nature*, 446(7137):782–786, 2007.

[358] Neill Lambert, Yueh-Nan Chen, Yuan-Chung Cheng, Che-Ming Li, Guang-Yin Chen, and Franco Nori. Quantum biology. *Nature Physics*, 9(1):10–18, 2013.

[359] Takuya Kitagawa, Mark S Rudner, Erez Berg, and Eugene Demler. Exploring topological phases with quantum walks. *Phys. Rev. A*, 82(3):033429, 2010.

[360] Arindam Mallick, Sanjoy Mandal, and CM Chandrashekar. Neutrino oscillations in discrete-time quantum walk framework. *Eur. Phys. J. C*, 77(2):1–11, 2017.

[361] Giuseppe Di Molfetta and Armando Pérez. Quantum walks as simulators of neutrino oscillations in a vacuum and matter. *New J. Phys.*, 18(10):103038, 2016.

[362] Frederick W Strauch. Relativistic quantum walks. *Phys. Rev. A*, 73(5):054302, 2006.

[363] CM Chandrashekar, Subhashish Banerjee, and R Srikanth. Relationship between quantum walks and relativistic quantum mechanics. *Phys. Rev. A*, 81(6):062340, 2010.

[364] Giuseppe Di Molfetta, M. Brachet, and Fabrice Debbasch. Quantum walks as massless dirac fermions in curved space-time. *Phys. Rev. A*, 88:042301, 2013.

[365] E Lucioni, B Deissler, L Tanzi, G Roati, M Zaccanti, M Modugno, M Larcher, F Dalfovo, M Inguscio, and G Modugno. Observation of subdiffusion in a disordered interacting system. *Phys. Rev. Lett.*, 106(23):230403, 2011.

[366] Francesco De Nicola, Linda Sansoni, Andrea Crespi, Roberta Ramponi, Roberto Osellame, Vittorio Giovannetti, Rosario Fazio, Paolo Mataloni, and Fabio Sciarrino. Quantum simulation of bosonic-fermionic noninteracting particles in disordered systems via a quantum walk. *Phys. Rev. A*, 89(3):032322, 2014.

[367] Ihor Vakulchyk, Mikhail V Fistul, and Sergej Flach. Wave packet spreading with disordered nonlinear discrete-time quantum walks. *Phys. Rev. Lett.*, 122(4):040501, 2019.

[368] Claudia Benedetti and Matteo GA Paris. Characterization of classical gaussian processes using quantum probes. *Physics Letters A*, 378(34):2495–2500, 2014.

[369] Leigh M Norris, Gerardo A Paz-Silva, and Lorenza Viola. Qubit noise spectroscopy for non-gaussian dephasing environments. *Physical review letters*, 116(15):150503, 2016.

[370] Dario Tamascelli, Claudia Benedetti, Stefano Olivares, and Matteo GA Paris. Characterization of qubit chains by feynman probes. *Physical Review A*, 94(4):042129, 2016.

[371] Ayaka Usui, Berislav Buča, and Jordi Mur-Petit. Quantum probe spectroscopy for cold atomic systems. *New J. Phys.*, 20(10):103006, 2018.

[372] Claudia Benedetti, Fahimeh Salari Sehdaran, Mohammad H Zandi, and Matteo GA Paris. Quantum probes for the cutoff frequency of ohmic environments. *Physical Review A*, 97(1):012126, 2018.

[373] Carl Wilhelm Helstrom. *Quantum detection and estimation theory*. Academic press, 1976.

[374] A. s. Alicki. *Probabilistic and Statistical Aspects of Quantum Theory*. North-Holland, New York, 1976.

[375] Dénes Petz and Csaba Sudár. Geometries of quantum states. *J. Math. Phys.*, 37(6):2662–2673, 1996.

[376] Dénes Petz. Covariance and fisher information in quantum mechanics. *J. Phys. A: Math. Gen.*, 35(4):929, 2002.

[377] Matteo G. A. Paris. Quantum estimation for quantum technology. *Int. J. Quant. Inf.*, 7(supp01):125–137, 2009.

[378] Alexander S Holevo. *Probabilistic and statistical aspects of quantum theory*, volume 1. Springer Science & Business Media, 2011.

[379] Andre Ahlbrecht, Holger Vogts, Albert H Werner, and Reinhard F Werner. Asymptotic evolution of quantum walks with random coin. *J. Math. Phys.*, 52(4):042201, 2011.

[380] Giacomo M D'Ariano and Matteo GA Paris. Arbitrary precision in multipath interferometry. *Physical Review A*, 55(3):2267, 1997.

[381] GM D'Ariano, C Macchiavello, and MF Sacchi. On the general problem of quantum phase estimation. *Physics Letters A*, 248(2-4):103–108, 1998.

[382] Dominic W Berry and Howard M Wiseman. Optimal states and almost optimal adaptive measurements for quantum interferometry. *Physical review letters*, 85(24):5098, 2000.

[383] Alexander Hentschel and Barry C Sanders. Machine learning for precise quantum measurement. *Physical review letters*, 104(6):063603, 2010.

[384] Emanuele Polino, Mauro Valeri, Nicolò Spagnolo, and Fabio Sciarrino. Photonic quantum metrology. *AVS Quantum Science*, 2(2):024703, 2020.

[385] Andre Ahlbrecht, Christopher Cedzich, Robert Matjeschk, Volkher B Scholz, Albert H Werner, and Reinhard F Werner. Asymptotic behavior of quantum walks with spatio-temporal coin fluctuations. *Quantum Information Processing*, 11(5):1219–1249, 2012.

[386] Troy D Mackay, Stephen D Bartlett, Leigh T Stephenson, and Barry C Sanders. Quantum walks in higher dimensions. *Journal of Physics A: Mathematical and General*, 35(12):2745, 2002.

[387] Gunter M Schütz and Steffen Trimper. Elephants can always remember: Exact long-range memory effects in a non-markovian random walk. *Physical Review E*, 70(4):045101, 2004.

[388] Andreas Lubatsch and Regine Frank. Self-consistent quantum field theory for the characterization of complex random media by short laser pulses. *Physical Review Research*, 2(1):013324, 2020.

[389] Alexander Streltsov, Gerardo Adesso, and Martin B. Plenio. Colloquium: Quantum coherence as a resource. *Rev. Mod. Phys.*, 89:041003, 2017.

[390] Kavan Modi, Aharon Brodutch, Hugo Cable, Tomasz Paterek, and Vlatko Vedral. The classical-quantum boundary for correlations: Discord and related measures. *Rev. Mod. Phys.*, 84:1655–1707, 2012.

[391] Marco Túlio Quintino, Tamás Vértesi, and Nicolas Brunner. Joint measurability, einstein-podolsky-rosen steering, and bell nonlocality. *Phys. Rev. Lett.*, 113(16):160402, 2014.

[392] Howard M Wiseman, Steve James Jones, and Andrew C Doherty. Steering, entanglement, nonlocality, and the einstein-podolsky-rosen paradox. *Phys. Rev. Lett.*, 98(14):140402, 2007.

[393] Nelly Huei Ying Ng and Mischa Prebin Woods. Resource theory of quantum thermodynamics: Thermal operations and second laws. In *Thermodynamics in the Quantum Regime*, pages 625–650. Springer, 2018.

[394] ZY Ou, CK Hong, and L Mandel. Relation between input and output states for a beam splitter. *Opt. Commun*, 63(2):118–122, 1987.

[395] S Bose and D Home. Generic entanglement generation, quantum statistics, and complementarity. *Phys. Rev. Lett.*, 88(5):050401, 2002.

[396] Jonathan P Dowling. Quantum optical metrology–the lowdown on high-n00n states. *Contemporary physics*, 49(2):125–143, 2008.

[397] Leonard Mandel. Coherence and indistinguishability. *Opt. Lett*, 16(23):1882–1883, 1991.

[398] Jan Sperling, Armando Perez-Leija, Kurt Busch, and Ian A Walmsley. Quantum coherences of indistinguishable particles. *Phys. Rev. A*, 96(3):032334, 2017.

[399] Hoi-Kwong Lo, Marcos Curty, and Bing Qi. Measurement-device-independent quantum key distribution. *Phys. Rev. Lett.*, 108(13):130503, 2012.

[400] Yang Liu, Teng-Yun Chen, Liu-Jun Wang, Hao Liang, Guo-Liang Shentu, Jian Wang, Ke Cui, Hua-Lei Yin, Nai-Le Liu, Li Li, Xiongfeng Ma, Jason S. Pelc, M. M. Fejer, Cheng-Zhi Peng, Qiang Zhang, and Jian-Wei Pan. Experimental measurement-device-independent quantum key distribution. *Phys. Rev. Lett.*, 111:130502, 2013.

[401] Scott Aaronson and Alex Arkhipov. The computational complexity of linear optics. In *Proceedings of the forty-third annual ACM symposium on Theory of computing*, pages 333–342, 2011.

[402] Han-Sen Zhong, Hui Wang, Yu-Hao Deng, Ming-Cheng Chen, Li-Chao Peng, Yi-Han Luo, Jian Qin, Dian Wu, Xing Ding, Yi Hu, Peng Hu, Xiao-Yan Yang, Wei-Jun Zhang, Hao Li, Yuxuan Li, Xiao Jiang, Lin Gan, Guangwen Yang, Lixing You, Zhen Wang, Li Li, Nai-Le Liu, Chao-Yang Lu, and Jian-Wei Pan. Quantum computational advantage using photons. *Science*, 370(6523):1460–1463, 2020.

[403] Andris Ambainis, Eric Bach, Ashwin Nayak, Ashvin Vishwanath, and John Watrous. One-dimensional quantum walks. In *Proceedings of the thirty-third annual ACM symposium on Theory of computing*, pages 37–49, 2001.

[404] Yaron Bromberg, Yoav Lahini, Roberto Morandotti, and Yaron Silberberg. Quantum and classical correlations in waveguide lattices. *Phys. Rev. Lett.*, 102(25):253904, 2009.

[405] Yoav Lahini, Mor Verbin, Sebastian D Huber, Yaron Bromberg, Rami Pugatch, and Yaron Silberberg. Quantum walk of two interacting bosons. *Phys. Rev. A*, 86(1):011603, 2012.

[406] Konstantinos Poulios, Robert Keil, Daniel Fry, Jasmin DA Meinecke, Jonathan CF Matthews, Alberto Politi, Mirko Lobino, Markus Gräfe, Matthias Heinrich, Stefan Nolte, et al. Quantum walks of correlated photon pairs in two-dimensional waveguide arrays. *Phys. Rev. Lett.*, 112(14):143604, 2014.

[407] Yoav Lahini, Yaron Bromberg, Demetrios N Christodoulides, and Yaron Silberberg. Quantum correlations in two-particle anderson localization. *Phys. Rev. Lett.*, 105(16):163905, 2010.

[408] Andris Ambainis, Eric Bach, Ashwin Nayak, Ashvin Vishwanath, and John Watrous. One-dimensional quantum walks. In *Proceedings of the Thirty-Third Annual ACM Symposium on Theory of Computing*, STOC '01, page 37–49, New York, NY, USA, 2001. Association for Computing Machinery.

[409] Peter L Knight, Eugenio Roldán, and John E Sipe. Propagating quantum walks: the origin of interference structures. *journal of modern optics*, 51(12):1761–1777, 2004.

[410] Alessandro Fedrizzi, Thomas Herbst, Andreas Poppe, Thomas Jennewein, and Anton Zeilinger. A wavelength-tunable fiber-coupled source of narrowband entangled photons. *Opt. Express.*, 15(23):15377–15386, 2007.

[411] Pieter Kok, W. J. Munro, Kae Nemoto, T. C. Ralph, Jonathan P. Dowling, and G. J. Milburn. Linear optical quantum computing with photonic qubits. *Rev. Mod. Phys.*, 79:135–174, 2007.

[412] Jeremy L. O'Brien. Optical quantum computing. *Science*, 318(5856):1567–1570, 2007.

[413] Artur K. Ekert. Quantum cryptography based on bell's theorem. *Phys. Rev. Lett.*, 67:661–663, 1991.

[414] D. P. Nadlinger, P. Drmota, B. C. Nichol, G. Araneda, D. Main, R. Srinivas, D. M. Lucas, C. J. Ballance, K. Ivanov, E. Y.-Z. Tan, P. Sekatski, R. L. Urbanke, R. Renner, N. Sangouard, and J.-D. Bancal. Experimental quantum key distribution certified by bell's theorem. *Nature*, 607(7920):682–686, 2022.

[415] Sergei Slussarenko, Morgan M. Weston, Helen M. Chrzanowski, Lynden K. Shalm, Varun B. Verma, Sae Woo Nam, and Geoff J. Pryde. Unconditional violation of the shot-noise limit in photonic quantum metrology. *Nat. Photon.*, 11(11):700–703, 2017.

[416] J.-W. Pan, Z.-B. Chen, C.-Y. Lu, H. Weinfurter, A. Zeilinger, and M. Zukowski. Multiphoton entanglement and interferometry. *Rev. Mod. Phys.*, 84:777–838, 2012.

[417] Jeremy L. O'Brien, Akira Furusawa, and Jelena Vučković. Photonic quantum technologies. *Nat. Photon.*, 3(12):687–695, 2009.

[418] Jianwei Wang, Fabio Sciarrino, Anthony Laing, and Mark G. Thompson. Integrated photonic quantum technologies. *Nat. Photon.*, 14(5):273–284, 2020.

[419] Xiaojiong Chen, Zhaorong Fu, Qihuang Gong, and Jianwei Wang. Quantum entanglement on photonic chips: a review. *Advanced Photonics*, 3(6):064002–064002, 2021.

[420] Michael Reck, Anton Zeilinger, Herbert J. Bernstein, and Philip Bertani. Experimental realization of any discrete unitary operator. *Phys. Rev. Lett.*, 73:58–61, 1994.

[421] Wim Bogaerts, Daniel Pérez, José Capmany, David A. B. Miller, Joyce Poon, Dirk Englund, Francesco Morichetti, and Andrea Melloni. Programmable photonic circuits. *Nature*, 586(7828):207–216, 2020.

[422] Luqi Yuan, Qian Lin, Meng Xiao, and Shanhui Fan. Synthetic dimension in photonics. *Optica*, 5(11):1396–1405, 2018.

[423] Max Ehrhardt, Robert Keil, Lukas J. Maczewsky, Christoph Dittel, Matthias Heinrich, and Alexander Szameit. Exploring complex graphs using three-dimensional quantum walks of correlated photons. *Science Advances*, 7(9):eabc5266, 2021.

[424] Siddharth Buddhiraju, Avik Dutt, Momchil Minkov, Ian A. D. Williamson, and Shanhui Fan. Arbitrary linear transformations for photons in the frequency synthetic dimension. *Nature Communications*, 12(1):2401, 2021.

[425] D. Collins, N. Gisin, N. Linden, S. Massar, and S. Popescu. Bell inequalities for arbitrarily high-dimensional systems. *Phys. Rev. Lett.*, 88:040404, 2002.

[426] Y. Omar, N. Paunković, L. Sheridan, and S. Bose. Quantum walk on a line with two entangled particles. *Phys. Rev. A*, 74:042304, 2006.